TESE DE DOUTORAMENTO

NEW LIGANDS AND PHARMACOLOGICAL TOOLS FOR THE STUDY OF G PROTEIN-COUPLED RECEPTORS USING MULTICOMPONENT REACTIONS

Ana Mallo Abreu

ESCOLA DE DOUTORAMENTO INTERNACIONAL DA UNIVERSIDADE DE SANTIAGO DE COMPOSTELA

PROGRAMA DE DOUTORAMENTO EN INVESTIGACIÓN E DESENVOLVEMENTO DE MEDICAMENTOS

SANTIAGO DE COMPOSTELA

2021

USC
UNIVERSIDADE
DE SANTIAGO
DE COMPOSTELA

DECLARACIÓN DO AUTOR/A DA TESE

D./Dna. **Ana Mallo Abreu**

Título da tese: **New Ligands and Pharmacological Tools for the Study of G Protein-Coupled Receptors Using Multicomponent Reactions**

Presento a miña tese, seguindo o procedemento axeitado ao Regulamento, e declaro que:

1) A tese abarca os resultados da elaboración do meu traballo.
2) De ser o caso, na tese faise referencia ás colaboracións que tivo este traballo.
3) Confirmo que a tese non incorre en ningún tipo de plaxio doutros autores nin de traballos presentados por min para a obtención doutros títulos.
4) A tese é a versión definitiva presentada para a súa defensa e coincide a versión impresa coa presentada en formato electrónico

E comprométome a presentar o Compromiso Documental de Supervisión no caso de que o orixinal non estea na Escola.

En , **de** **de 2021**.

Sinatura electrónica

USC
UNIVERSIDADE
DE SANTIAGO
DE COMPOSTELA

AUTORIZACIÓN DO DIRECTOR DA TESE

New Ligands and Pharmacological Tools for the Study of G Protein-Coupled Receptors Using Multicomponent Reactions

D. **Eddy Sotelo Pérez**

INFORMA:

Que a presente tese, correspóndese co traballo realizado por Dna. **Ana Mallo Abreu**, baixo a miña dirección, e autorizo a súa presentación, considerando que reúne os requisitos esixidos no Regulamento de Estudos de Doutoramento da USC, e que como director desta non incorre nas causas de abstención establecidas na Lei 40/2015.

De acordo co indicado no Regulamento de Estudos de Doutoramento, declara tamén que a presente tese de doutoramento é idónea para ser defendida en base á modalidade de COMPENDIO DE PUBLICACIÓNS, nos que a participación da doutoranda foi decisiva para a súa elaboración e as publicacións se axustan ao Plan de Investigación.

En , de de 2021

USC
UNIVERSIDADE
DE SANTIAGO
DE COMPOSTELA

Acknowledgments

Han pasado cinco años desde que comencé esta etapa y finalmente, con este libro se materializa lo que tanto he luchado por conseguir. Durante este tiempo me he apoyado en muchas personas, algunas viejas amistades y otras nuevas, sin las cuales no sé si hubiera sido posible completar este proyecto.

Lo primero, agradecer al Prof. **Eddy Sotelo** las oportunidades que me ha brindado y por enseñarme la profesión de investigadora, incluidas alguna de las principales cualidades que todo buen investigador debe cultivar: “creatividad, curiosidad y desconfianza”.

Depois, agradecer ao Professor Doutor **Rui Moreira** pela oportunidade de trabalhar no seu laboratório com uma curta antecedência, e por me permitir aprender com todos os membros do laboratório.

Al Dr. **Jhonny Azuaje** por enseñarme la forma adecuada de trabajar dentro de un laboratorio y por sus consejos para tomar decisiones acertadas en el ámbito de la química experimental.

Durante el desarrollo de esta tesis ha sido crucial tanto el laboratorio de computacional de la Universidad de Upssala, más concretamente el Prof. **Hugo Gutiérrez de Terán** y el Dr. **Willem Jespers**; como el laboratorio de farmacología da Universidade de Santiago de Compostela, dirigido por la Prof. **María Isabel Loza**, y el laboratorio de farmacología de la Universidad de Barcelona, dirigido por la Prof. **Gemma Brugal**. El trabajo de estos equipos ha contribuido a incrementar el valor científico de lo expuesto en las siguientes páginas.

Agradezco a la Dra. **Luz Escalante** todos sus consejos, sus amables explicaciones y todos los buenos momentos que hemos pasado durante esta etapa.

A **Xosé González**, técnico del Laboratorio de Química Orgánica de la Facultad de Farmacia por su constante dedicación y preocupación a la hora de solventar las necesidades del día a día y, a la **Unidade de Raios X** da Univesidade de Santiago de Compostela por su ayuda y apoyo en el desarrollo del primer artículo.

A **Alba Salgado**, amiga y compañera a quien he conocido en el laboratorio, antes incluso de comenzar la etapa doctoral, y con la que cuento tanto en los buenos como en los malos momentos.

Uma das pessoas que o meu estágio na Faculdade de Farmácia de ULisboa me deu é a **Rita Félix**, que me ajudou desde o início e ainda hoje me apoia. Amiga que encontrei para a vida e que, como sabe, vou sempre estar perto para tudo o que precisar porque amizades como estas acontecem muito poucas vezes.

No me olvido de mis compañeros de ComBioMed, los que están y los que han pasado por el grupo de investigación en el que me he formado: Dr. **Rodrigo Bernárdez**, Dra. **Maria Majellaro**, **Carmen Fernández**, **Antonio Sánchez**, **Adrián Monteiro**, **Carlos Carbajales**, **Carmen Velando**, **Miguel Parada**, **Carlos Rodríguez**, **Rubén Prieto**, y una larga lista.

Também não posso esquecer a todos os amigos e colegas com que partilhei o laboratório 106, Dra. **Ana Ressurreição**, Dr **Pedro Florindo**, Dr. **Luís Carvalho, André Campaniço**, **Jorge Grilo**, **Claúdia Braga**, **Andreia Figueiredo**, **Sofia Domingos**, **Lara Fidalgo**, **Diogo Silva** e a todos os membros do laboratório. Também agradecer a minha inestimável amiga do laboratório 104, **Elizabeth Lopes**, e a todos os colegas dos laboratórios da computacional e dos produtos naturais.

No quiero olvidarme del Módulo 7 da Facultade de Matemáticas da Univesidade de Santiago de Compostela donde me he colado en numerosas ocasiones, conociendo así a personas excepcionales como la Prof. **Rosana Rodríguez**, cuyos consejos me han ayudado a mantener la motivación y superar las dificultades. También al Dr. **Daniel Cao**, **Óscar Otero** y todos los compañeros y amigos que me han apoyado y con los que he pasado buenos momentos.

Agradecer también a todo mi grupo de amigos forjado en el C. M. U. Gelmírez: **Álvaro Rueda**, **Estela Moretón**, **María Ortega**, **Javier Freire**, **Abel Facal**, **Laura Feijóo**, **Laura Cabral**, **Luis Domínguez**, **Iago Couso**, **Miguel Díaz**, **Zaila Giráldez** y una larga lista de personas con las que he compartido risas y cañas que han sido vitales para la finalización de este gran proyecto.

A mi compañero de aventuras al que podría incluir en muchos de los anteriores agradecimientos, **Sebastián Buedo**, sin el cual no sé si hubiese tenido el valor para embarcarme en este proyecto.

A mi familia, por los valores que me han inculcado, por esos momentos de preocupación y de felicidad, por el constante apoyo que son, por ser las personas más importantes. Por eso agradecer a mis padres, mi hermana y mis abuelos. Por el "cuándo lees" que tanto se repetía en las comidas, porque finalmente, después de todo lo que hemos pasado, aquí está. El esfuerzo ha dado sus frutos y podemos dar gracias por celebrarlo todos juntos.

Finalmente, agradecer a la **Deputación da Coruña** (Expediente: 2019000011466) por la financiación aportada y a la empresa **Oncostellae** por depositar su confianza en mí y permitirme desempeñar el trabajo de investigador compatibilizándolo con la finalización de esta tesis.

USC
UNIVERSIDADE
DE SANTIAGO
DE COMPOSTELA

A mis yeyos,

mis padres, Conchi y Juan,

y a mi hermana Cris

USC
UNIVERSIDADE
DE SANTIAGO
DE COMPOSTELA

INDEX

PHD PUBLICATIONS LIST

1- **A. Mallo-Abreu**, M. Majellaro, W. Jespers, J. Azuaje, O. Caamaño, X. García-Mera, J. M. Brea, M. I. Loza, H. Gutiérrez-de-Terán, E. Sotelo. Trifluorinated Pyrimidine-Based A_{2B} Antagonists: Optimization and Evidence of Stereospecific Recognition, *J. Med. Chem.* **2019**, *62* (20), 9315–9330. I. F.: 6,205. ISSN: 1520-4804.

2- **A. Mallo-Abreu**, R. Prieto-Díaz, W. Jespers, J. Azuaje, M. Majellaro, C. Velando, X. García-Mera, O. Caamaño, J. Brea, M. I. Loza, H. Gutiérrez-de-Terán, E. Sotelo. Nitrogen-Walk Approach to Explore Bioisosteric Replacements in a Series of Potent A_{2B} Adenosine Receptor Antagonists. *J. Med. Chem*. **2020**, *63* (14), 7721–7739. I. F.: 7,446. ISSN: 1520-4804.

3- **A. Mallo-Abreu**, I. Reyes-Resina, J. Azuaje, R. Franco, A. García-Rey, M. Majellaro, D. Miranda-Pastoriza, X. García-Mera, W. Jespers, H. Gutiérrez-de-Terán, G. Navarro, E. Sotelo. Potent and Subtype-Selective Dopamine D_2 Receptor Biased Partial Agonists Discovered Via an Ugi-Based Approach. *J. Med. Chem*. **2021**, *64*, (12), 8710-8726. I. F.: 7,446. ISSN: 1520-4804.

USC
UNIVERSIDADE
DE SANTIAGO
DE COMPOSTELA

ABBREVIATIONS INDEX

A_1AR	A_1 adenosine receptor
A_{2A}AR	A_{2A} adenosine receptor
A_{2B}AR	A_{2B} adenosine receptor
A_3AR	A_3 adenosine receptor
ABPs	Activity-based probes
AC	Adenylate cyclase
Acb	Nucleus accumbent
ADA	Adenosine deamination
ADP	Adenosine diphosphate
AML	Acute myeloid leukaemia
AMP	Adenosine monophosphate
APCI	Atmospheric-pressure chemical ionization
APD	Antipsychotic drug
AR	Adenosine receptor
AT_1R	Angiotensin II type 1 receptor
ATP	Adenosine triphosphate
BAR	Bennett acceptance ratio
BFI	Bond-forming-index
BrAAP	Branched chain amino acid preferring
bs	Broad singlet
cAB40	Carboxy acid blue 40
CCDC	Cambridge Crystallographic Data Centre
CD	Circular dichroism
CHO	Chinese hamster ovary
CI	Chemical ionization
CKD	Chronic kidney disease
C-L	Caspase-like
CNS	Central nervous system
CP	Cortical plate
CP	Core particle
Cpds	Compounds

CRD	Cysteine-rich domain
CT-L	Chymotrypsin-like
CuAAC	Copper(I)-Catalysed Azide-Alkyne Cycloaddition
Cx	Cerebral cortex
Cy5	Cyanine 5
CYP	Cytochrome P450
Cyp	Cyclopentyl
d	Doublet
DA	Dopamine
DAG	Diacylglycerol
DAR	Dopamine receptor
DBF	Dibenzylfluorescein
DC	Dendritic cell
dd	Doublet of doublets
Dec.	Decomposition
DHPM	3,4-dihydropyrimidin-2(1*H*)-one
DMEM	Dulbecco's modified medium
DMSO	Dimethyl sulfoxide
DNA	Deoxyribonucleic acid
DPCPX	Dipropylcyclopentylxanthine
DR	Death receptors
DRD_1	Dopamine D_1 receptor
DRD_2	Dopamine D_2 receptor
DRD_{2L}	Dopamine D_2-long receptor
DRD_{2S}	Dopamine D_2-short receptor
DRD_3	Dopamine D_3 receptor
DRD_4	Dopamine D_4 receptor
DRD_5	Dopamine D_5 receptor
E/S	Enzyme/substrate
EBD	Extended binding domain
EC_{50}	Half maximal effective concentration
EL	Extracellular loop
EPS	Extrapyramidal symptoms

ESI	Electrospray ionization
Et	Ethyl
F	Fluorescence donor
FAD	Flavin adenine dinucleotide
FCS	Fetal calf serum
FDA	Food and Drug Administration
FEP	Free energy perturbation
FGA	First generation antipsychotic
FPR	Formyl peptide receptor
FSI	Fast-spiking interneurons
FZD1–10	Frizzled receptors
GA	Genetic algorithm
GDP	Guanosine diphosphate
GEF	Guanine nucleotide exchange factor
GHSR	Growth hormone secretagogues receptor
GLP1R, GLP2R	Glucagon-like peptide receptors
Glu	Glutamate
GNRHRs	Gonadotropin-releasing hormone receptors
GPCRs	G protein-coupled receptors
GRK	G protein-coupled receptor kinase
GTP	Guanosine triphosphate
GTPase	Guanosine triphosphatase
***h*A$_1$AR**	Human A_1 adenosine receptor
***h*A$_{2A}$AR**	Human A_{2A} adenosine receptor
***h*A$_{2B}$AR**	Human A_{2B} adenosine receptor
***h*A$_3$AR**	Human A_3 adenosine receptor
HEK-293	Human embryonic kidney
HeLa	Human cervix carcinoma
HIV	Human immunodeficiency virus
HPLC	High performance liquid chromatography
HPT	Hyperparathyroidism
HRMS	High Resolution Mass Spectrometry
IC_{50}	Half-maximum inhibitory concentration

IL	Intracellular loop
INF-γ	Interferon-γ
IP_3	Inositol triphosphate
***i*-Pr**	Isopropyl
J	Coupling constant
K_B	Affinity exhibited by the antagonist for the receptor
K_i	Inhibition constant
LD	Linker domain
LHS	Left-hand side
LRMS	Low Resolution Mass Spectrometry
m	Multiplet
mAChR	Muscarinic acetylcholine receptor
MAE	Mean absolute error
MAE	Mean absolute error
MCH	Melanin-concentrating hormone
MCL	Mantle cell lymphoma
MCR	Multicomponent reaction
MD	Molecular dynamic simulation
MDSCs	Myeloid-derived suppressor cells
MECA	Melanocortin/EDG/Cannabinoid/Adenosine
MHC-I	Major histocompatibility complex class one
MM	Multiple myeloma
MOR	μ-opioid receptor
Mp	Melting point
MPLC	Medium pressure liquid chromatography
MSN	Medium spiny neuron
NAD^+	Nicotinamide adenine dinucleotide
NAM	Negative allosteric modulator
NBD	Nitrobenzoxadiazole
NC-IUPHAR	International Union of Pharmacology, Committee on Receptor Nomenclature and Classification
NECA	5'-*N*-Ethylcarboxamidoadenosine
NF-κB	Nuclear factor κB

NMDAR	N-methyl-D-aspartate receptors
NMR	Nuclear magnetic resonance
OT	Olfactory tubercle
P2Y	Nucleotide receptor
PAINS	Promiscuous assay-interfering compounds
PAM	Positive allosteric modulator
PBC	Periodic boundary conditions
PEI	Polyethyleneimine
PET	Positron emission tomography
PFC	Prefrontal cortex
PLS	Parallel reaction synthesizer
POPC	1-palmitoyl-2-oleoyl phosphatidylcholine
PTHR1, PTHR2	Parathyroid hormone receptors
PYR	Pyramidal neuron
Q	Quencher
q	Quartet
qABP	Quenched activity-based probe
qd	Quartet of doublets
RHS	Right-hand side
RNA	Ribonucleic acid
s	Singlet
SAM	Silent allosteric modulator
SAR	Structure-activity relationship
SCAAS	Surface constrained all-atom solvent
SD	Standard deviation
SFSR	Structure functional selectivity relationship
SGA	Second generation antipsychotic
SMO	The smoothened receptor
SN	*Subtantia nigra pars compacta*
SNAAP	Small neutral amino acid preferring
SOG	Somatostatin/Opioid/Galanin and neuropeptide W
TD	Tardive dyskinesia
TDI	Time-dependent inhibition profiles

TGA	Third generation antipsychotic
T-L	Threonine-like
TLC	Thin-layer chromatography
TM	Transmembrane domains
TM	Transmembrane
TNBC	Triple negative breast cancer
TNF-*α*	Tumor necrosis factor-*α*
t_R	Retention time
TsOH	*p*-toluenesulfonic acid
Ub	Ubiquitine
UDC	Ugi-deprotection-cyclization
UPP	Ubiquitin proteasome pathway
VEGF	Vascular endothelial growth
VFP	Venus Flytrap
VTA	Ventral tegmental area
XAC	Xanthine amine congener

SUMMARY

The present Doctoral Thesis describes the design, synthesis, pharmacological evaluation, structure-activity relationships, and molecular modeling of new potent and selective ligands for the A_{2B} adenosine ($A_{2B}AR$) and D_2 dopamine (DRD_2) receptors. The developed work, which is organized into three main areas (**Chapters 3.1-3.2**), is presented as a compendium of publications addressing relevant topics and advanced concepts in the Medicinal and Chemical Biology of these membrane receptors. Furthermore, the results described in this thesis are part of a methodological project, which demonstrates the competitive advantages of multicomponent reactions in Medicinal Chemistry.

The first chapter of the thesis (**Chapter 3.1**) published in the Journal of Medicinal Chemistry (*J. Med. Chem.* **2019**, *62* (20), 9315-9330), describes the optimization of fluorinated antagonists of the adenosine A_{2B} receptors. Since the clinical introduction of the first drug incorporating a fluorine atom, fludrocortisone, the number of fluorine containing compounds included within the therapeutic arsenal has rapidly risen to approximately 25% of drugs. The unique nature of the fluorine atom and the remarkable properties of the carbon−fluorine bond are now well documented and extensively exploited in medicinal chemistry. The replacement of hydrogen atoms by fluorine at active prototypes can exert a significant effect on diverse structural, pharmacodynamic, and pharmacokinetic parameters, leading to improved metabolic stability or optimized ligand efficiency. Moreover, fluorinated ligands have become highly appreciated molecular probes during research programs employing positron emission tomography (PET).

Several studies have shown that the A_{2B} adenosine receptor is a low-affinity receptor that requires micromolar concentrations of adenosine to generate productive functional signaling. As a consequence, this receptor remains silent when extracellular adenosine concentrations are low, a situation that changes under serious pathophysiological conditions in which the adenosine concentration increases dramatically (hypoxia, inflammation), leading to the activation of signaling pathways mediated by the A_{2B} adenosine receptor. Recent evidence shows that the A_{2B} adenosine receptor is transcriptionally regulated by factors involved in inflammatory hypoxia. Furthermore, the $A_{2B}AR$ is a key factor in the regulation of biological processes such as

cardiac contractility, glucose homeostasis, angiogenesis, lung inflammation, inflammatory response, cancer, and pain. Consequently, the development of drugs which selectively block this target is a novel approach for the treatment of serious diseases such as cancer, diabetes or obstructive pulmonary disease (COPD).

Considering the aforementioned aspects, we investigated the effect of fluorination in the A_{2B}AR affinity of two prototypes previously developed by the ComBioMed group. For this project we chose as model ligands compounds **ISAM-140** and **SYAF080**, synthesizing novel compounds that incorporate -CF_3 groups in different positions using the Biginelli reaction as a synthetic tool. The design of the compounds, and the interpretation of the resulting structure-activity relationship (SAR), were assisted by a receptor-driven molecular modeling including the results of free energy perturbation (FEP) simulations. The three most attractive trifluorinated A_{2B}AR antagonists identified were separated into their single stereoisomers (enantiomers or diastereomers) and evaluated.

It is important to highlight that, like reference ligands (**ISAM-140** and **SYAF080**), all the compounds obtained in this chapter contain a stereocenter at position four of the heterocyclic nucleus. Additionally, some of them contain another chiral center at the alkyl residue of the ester group. Ligands which contain a single stereocenter were isolated and evaluated pharmacologically as racemic mixtures. Otherwise, compounds obtained using a racemic *β*-ketoester mixture during the Biginelli reaction were isolated and evaluated as mixtures of diastereomers. The joint rationalization of the structural and binding data (K_i) as well as molecular modeling studies provide solid evidence of stereospecific interaction of the ligands documented in this chapter with the A_{2B} adenosine receptor.

Column chromatography separation enabled us to isolate the fluorinated analogues of the ligand **SYAF080** with two chiral centers as diastereomers pairs, although we were not able to assign the nature of the stereocenters on each of them. Unfortunately, all attempts of separation in diastereomeric pairs for the tricyclic series containing two chiral centers (fluorinated analogues of **ISAM-140**) failed.

Once the pharmacological evaluation had been carried out, and due to the promising affinity (low nanomolar range) shown by the mixture of the four diastereomers of one fluorinated analogue of **ISAM-140**, the separation by chiral HPLC

was performed. However, even after extensive exploration of various chiral stationary phases, mobile phases, or other experimental conditions, the separation was not successful. Furthermore, the unequivocal assignment of the exocyclic chiral center configuration is not feasible by circular dichroism spectroscopy, which motivated the design of a diastereoselective synthetic pathway for these compounds. The enantiopure forms of the trifluorinated *β*-ketoesters were used in this synthetic approach. The subsequent Biginelli reaction with these intermediates has provided the target derivatives as pairs of diastereomers containing the pre-established stereochemistry at the alkoxy residue of the ester group. The resulting two pairs of diastereomers were successfully resolved into individual diastereomers, with excellent stereochemical purity (97-99%), using semipreparative chiral HPLC.

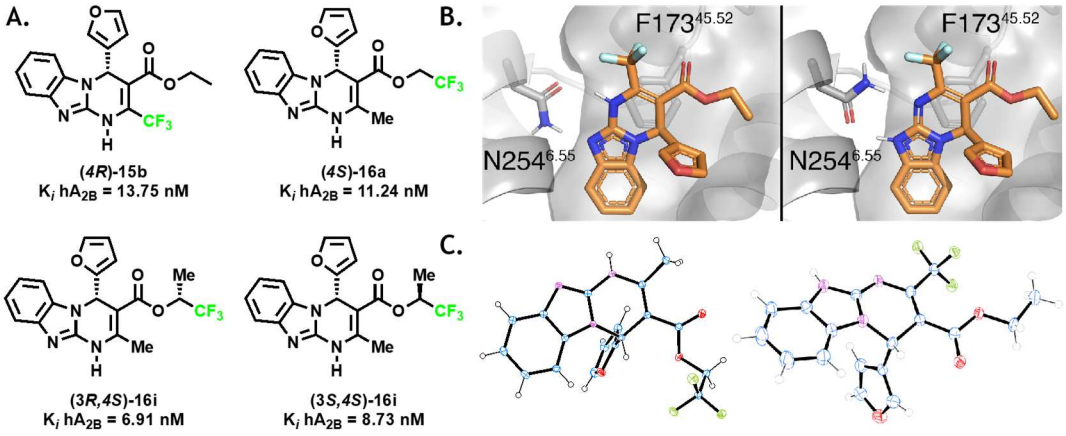

Figure 1: A. Most interesting ligands synthesized in this chapter. B. Theoretical model of receptor binding mode. C. Structure obtained by X-ray crystallography of two of the most active ligands in our study.

In this chapter we have documented the first examples of fluorinated A_{2B} adenosine receptor antagonists that combine excellent $A_{2B}AR$ affinity (K_i <15 nM) and remarkable selectivity toward the other adenosine receptors ($A_{1A}R$, $A_{2A}AR$, A_3AR). A combination of chiral HPLC, circular dichroism, diastereoselective synthesis, and X-ray crystallography enabled us to obtain experimental evidence supporting the modeled stereospecific interaction between representative trifluorinated stereoisomers and the $A_{2B}AR$ (Figure 1).

These results represent a step forward in the identification and optimization of non-xanthine $A_{2B}AR$ antagonists, which are metabolically more stable and exemplify the stereospecific interaction between representative trifluorinated stereoisomers and the

A_{2B}AR receptor. Ligands shown in Figure 1 are currently being studied within the framework of our research project aimed at exploring the potential of blocking the A_{2B}AR receptor in cancer (immuno) therapy.

The second chapter of this Doctoral Thesis, **Chapter 3.2**, was published in the Journal of Medicinal Chemistry (*J. Med. Chem.* **2020**, *63* (14), 7721–7739). This study addresses the development of more metabolically stable ligands for the adenosine A_{2B} receptor using **ISAM-140** as a model ligand. Specifically, we focus on the exploration of bioisosteric substitutions for the furan and thiophene rings at position 4 of the 1,4-dihydrobenzo[4,5]imidazo[1,2-*a*]pyrimidine ring using a bioisosteric criteria in pentagonal rings, by application of the nitrogen-walk approach.

Recent advances in the study of the immunosuppressive effect of adenosine; the pro-tumorigenic effect of A_{2B}AR; and also the antiproliferative, antiangiogenic, and antimetastatic properties documented for A_{2B}AR antagonists reinforce the interest in A_{2B}AR as an emerging target for cancer (immuno)therapy. The renewed interest in A_{2B}AR has fueled the exploration of novel facets of its signaling and function, particularly its capability to form homo- and heteromeric complexes. Different techniques have shown that, like other adenosine receptors, A_{2B}AR forms homomeric assemblies and stable heteromeric complexes (*e.g.*, A_{1A}R-A_{2B}AR and A_{2A}AR-A_{2B}AR) in cells and tissues that co-express these receptor subtypes. Remarkably, these studies confirmed that, when activated, A_{2B}AR becomes the dominant receptor. As such, A_{2B}AR is able to downregulate A_{2A}AR-mediated responses as well as the ligand binding and signaling of A_{2A}AR through the formation of stable heteromers.

The structural similarity between the ribose moiety of the endogenous ligand (adenosine) and the pentagonal heterocyclic cores such as the furan and thiophene rings, has led to the latter being common motifs in the structure of adenosine receptor antagonists (especially A_{2A}R and A_{2B}AR). The electron-rich nature of the heterocyclic core means that some of these rings can be classified as structural alerts. Therefore, early identification of structural elements with the potential to become structural alerts is a key issue during early drug discovery. In this context, the relevance of these groups in terms of target engagement should be examined and their potential metabolic liabilities experimentally evaluated to identify alternative groups that could replace the elusive structural alerts. Since five-membered heteroarenes are ubiquitous scaffolds in

the structures of adenosine antagonists (particularly for A_{2A}AR and A_{2B}AR), a comprehensive study has been made to identify heterocyclic cores that can replace them in diverse pharmacophores.

General strategies for reducing metabolic liabilities include blocking potential reactive sites with substituents, introducing nitrogen atoms, or replacing the pentagonal core with hexagonal heterocycles. However, the survey of aryl or heteroaryl analogues for bioisosteric replacements remains poorly explored, and available examples have shown a pronounced decline in the affinity and selectivity profiles. Therefore, the replacement of these critical pharmacophoric groups remains a major challenge.

In the context of our ongoing project aimed at identifying non xanthine A_{2B}AR antagonists, we have documented novel families of mono-, bi-, and tricyclic pyrimidine derivatives that combine high affinity and exquisite selectivity profiles. The experimental and computational data for these series have contributed to the rationalization and quantification of the contribution of the different structural elements and have systematically highlighted the critical role of the pentagonal residues to preserve strong A_{2B}AR binding. Of particular importance was the specific stereo disposition of the pentagonal ring in an enantiospecific binding orientation, which was validated by the synthesis and evaluation of the different stereoisomers of compounds in some of our series.

The diversity space at position 4 of the tricyclic system remains poorly explored and some of the rings introduced at this position could be responsible for toxic effects. With this background, the second chapter of the Doctoral Thesis presents an exhaustive study of the effect of the substituent at position 4, particularly heterocyclic five-membered cores, with the aim of identifying optimal rings for this position in a series that used **ISAM-140** as reference ligand. The study included the synthesis and evaluation of 42 novel ligands that contain 18 different heterocyclic combinations, which were proposed according to bioisosteric replacement criteria. The design and the interpretation of the observed SAR were supported by a receptor-driven molecular model of the synthesized compounds. This model was used as a basis to perform a series of free-energy perturbation (FEP) simulations of the whole series, to sustain the interpretation of the SAR in terms of receptor−ligand interactions.

Using the Biginelli reaction as the main synthetic tool, we have prepared a first subset designed to expand the diversity elements at position 4 of the reference series containing the **ISAM-140** ligand. This series has been used to evaluate the importance of the pentagonal core, and to facilitate an exhaustive exploration of the effect of nitrogen introduction. The new series were designed according to bioisosteric replacement criteria, by application of the nitrogen-walk approach, that is, systematically introducing a nitrogen atom in the different positions of the pentagonal core in the parent series. This approach is widely recognized as a classical bioisosteric change, in which the replacement of a CH group by a nitrogen atom in heteroaromatic systems usually has significant consequences during multiparametric optimization. Although the effects of such apparently trivial modifications on basicity, lipophilicity, polar surface area, and hydrogen-bonding capacity are relatively predictable, their impact on receptor recognition and binding affinity, solubility, active transport, and metabolic stability can be more difficult to analyze.

The nitrogen-walk approach has been applied to explore bioisosteric replacements for the furan and thiophene cores in a series of potent A_{2B}AR antagonists. Several novel ligands that combine remarkable affinity (K_i < 30 nM) and exceptional selectivity were identified by introducing 18 different pentagonal heterocyclic frameworks at position 4 of the tricyclic ring (Figure 2).

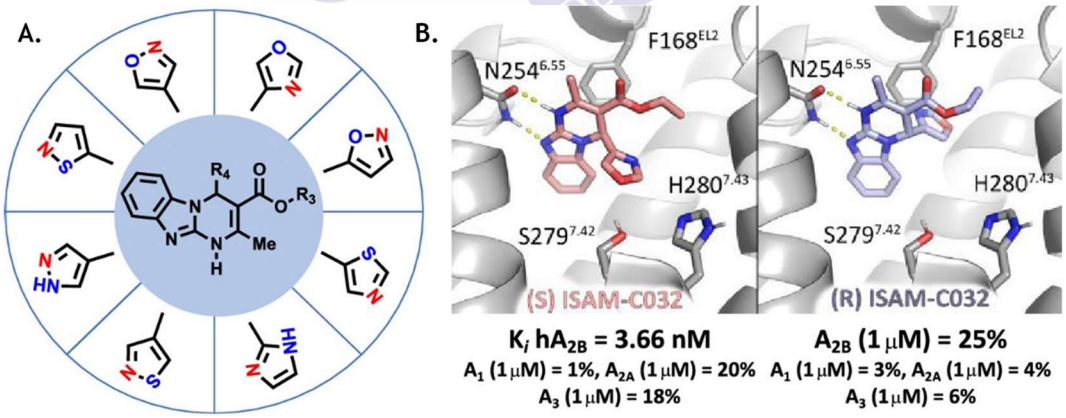

Figure 2: A. Outline of the most relevant modifications made for R_4. B. Theoretical model of receptor binding mode with the most active ligand enantiomers obtained.

A preliminary exploration of the *in vitro* inhibitory profile of the selected ligands on the cytochromes CYP3A4 and CYP2D6 was also carried out, as well as a more complete *in vitro* absorption, distribution, metabolism, and excretion (ADME)

characterization of the best identified ligand, as racemic mixture, determining its microsomal stability and solubility.

Finally, the most potent ligand was separated in its enantiomers by semi-preparative chiral HPLC and pharmacologically evaluated at the four adenosine receptors. The affinity results confirmed the enantiospecific recognition by the A_{2B}AR, in line with the previous studies of this project. The antagonistic behavior of the lead compound identified in the context of this work and its eutomer was corroborated through functional cAMP experiments, and joint analysis of the current and previous series allowed a comprehensive understanding of the SARs and the binding mode within the series using computational models.

Preliminary characterization of selected ligands evidenced a negligible inhibitory activity at CYP3A4 and CYP2D6 cytochromes. The first is the most important cytochrome in the metabolization of drugs and the second is the most frequently involved in the metabolization of drugs containing basic nitrogen atoms. Furthermore, these studies enabled us to verify the excellent microsomal stability of the lead compound synthesized. A combination of chiral HPLC and circular dichroism provided experimental support to the modeled stereospecific interaction between the most attractive novel antagonist and the human A_{2B}AR. This work represents a step forward in the identification of novel structurally diverse and metabolically stable (non-furan-based) pyrimidine derivatives that are able to antagonize human A_{2B}AR in a stereospecific manner.

The third chapter of the thesis (**Chapter 3.3**) has been published in the Journal of Medicinal Chemistry (*J. Med. Chem.* **2021**, *64* (12), 8710-8726). The work documents the discovery of biased partial agonists of the D_2 dopamine receptor (activating the cAMP or *β*-arrestin pathways) that show excellent potency and selectivity profiles.

The discovery and study of new GPCR signaling pathways (other than the canonical pathway: the dissociation of the G protein heterotrimer) has led to a paradigm shift that allows a better understanding of the functioning and regulation of GPCRs. The unequivocal confirmation that the activation of GPCRs can trigger more subtle signaling processes, and much less studied, opens up new research horizons, as well as the possibility of a better understanding on the effects of known drugs and the development of new more effective and safe ligands that regulate alternative signaling

pathways. One of those signaling downstream is the *β*-arrestin pathway, a component of the internalization and desensitization machinery of GPCRs. The process by which GPCRs ligands differentially modulate the G protein and/or *β*-arrestin pathway to mediate specific signal transduction routes is a phenomenon known as functional selectivity or biased agonism. The concept of biased agonism has progressively reshaped our understanding of GPCR signaling and shifted the paradigm of GPCR drug discovery. However, the molecular mechanisms behind biased signaling remain largely unknown, with the study of the functional contributions of G protein and the *β*-arrestin signaling pathways of endogenous/exogenous ligands is still challenging.

Biased ligands can trigger the specific pathway responsible for the therapeutic effect without activating the pathways that are involved in side effects. These ligands are extremely useful in elucidating the key structural contributors to signal transduction pathways and they also have significant potential to develop therapeutic agents with fewer side effects.

The DRD_2 is a GPCR in which the exploration of the biased agonism concept is becoming the new paradigm to provide better drugs. This receptor is a critical target of antipsychotic and antiparkinsonian agents, but it is also a receptor implicated in the mechanism of action of several drugs associated with abuse and addiction. This chapter focuses on the optimization of ligands for the treatment of schizophrenia. Current therapies, using typical and atypical antipsychotics, are characterized by alleviating symptoms while presenting significant side effects. The discovery of aripiprazole and cariprazine, prototypes of a new generation of atypical antipsychotics and recently approved by the FDA for the treatment of schizophrenia, manic/mixed bipolar I episodes and depressive disorder, changed the view of antipsychotic action on the dopamine signaling.

Inspired by the unique antipsychotic profile of aripiprazole, a new series of DRD_2 biased agonists has been developed. All compounds were designed using these drugs as models. They contain three well-defined regions: (1) the primary pharmacophore (PP), which consists of a mono- or disubstituted phenyl-piperazine residue (commonly known as the left-hand segment (LHS) or head group); (2) the central linker, which is variable in length and nature, and can be acyclic or cyclic; and (3) the secondary (or allosteric)

pharmacophore (SP), which generally consists of a heterocyclic core (commonly referred to as the right-hand segment (RHS) fragment or tail group).

In this study, it was decided to retain the pharmacophore in the LHS segment, using the 1-(2,3-dichlorophenyl)piperazine moiety (which is present in aripiprazole), and a linear linker of four atoms, shorter than usual. Six different and previously unexplored groups in the RHS moiety were also proposed to examine the effect of these structural modifications on subtype selectivity, and also their effect on the DRD_2 functional selectivity profile. The selected RHS frameworks provide novel topologies, physicochemical features and alternative binding modes that should enable the capture of diverse conformational states within the receptor. In addition to the heterocyclic and functional diversity introduced, some of the proposed RHS fragments bear a chiral center within the RHS heterocyclic framework, thus introducing stereochemical diversity that would enable the future investigation of previously unexplored stereoselective interactions within the RHS region.

In this chapter, we discuss the design, synthesis, and pharmacological evaluation of several series of DRD_2 partial agonists that exhibit either G protein or β-arrestin biased signaling profiles uniquely combined with exquisite subtype selectivity. These new families were designed and assembled using a highly versatile multicomponent approach based on the Ugi reaction. The experimental data provided SAR and structure-functional selectivity relationship (SFSR) trends that were consistent with the proposed binding modes, as defined in a receptor-driven docking model. The overall results of the study represent a successful proof of concept of an unexplored strategy for the rapid identification of novel structurally diverse and functionally selective dopamine D_2 receptor ligands. Therefore, this chapter documents a versatile, efficient, and previously unexplored multicomponent approach that enables the rapid generation of novel receptor-biased and subtype-selective DRD_2 ligands.

This strategy exemplifies the search for diverse and previously unexplored RHS fragments, but also highlights their critical role in modulating the functional selectivity profile. The pharmacological characterization of the new series of compounds enabled the identification of several ligands that elicit excellent DRD_2 selectivity and remarkable functional selectivity through cAMP or β-arrestin signaling pathways

(Figure 3). These results can be explained to some extent by the molecular modeling of these ligands using the recent DRD_2 crystal structure.

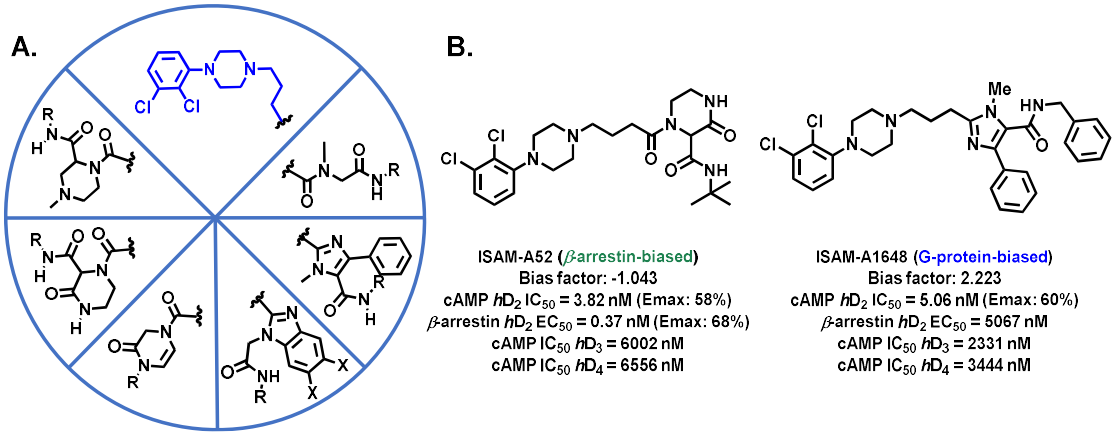

Figure 3: A. Substitution patterns performed in our study. B. The most active and subtype-selective biased compounds synthesized in this chapter.

Further studies are now in progress in our laboratory to expand the diversity of the moieties and linkers, to explore in detail the SAR and SSR around the most promising ligands developed, and to establish the role of stereochemistry in the observed biological profiles.

Taken together, the results documented in this Doctoral Thesis highlight the synthetic potential of multicomponent reactions to accelerate the discovery, optimization, and profiling of new prototypes in Medicinal Chemistry.

RESUMO

A presente tese de doutoramento describe o deseño, síntese, avaliación farmacolóxica, relación estrutura-actividade e modelaxe molecular de novos ligandos potentes e selectivos para os receptores A_{2B} de adenosina e D_2 de dopamina. O traballo realizado, que se organiza en tres grandes áreas (**Capítulos 3.1-3.3**), preséntase en forma de compendio de publicacións abordando temas relevantes e conceptos avanzados da Química Médica e Biolóxica deses receptores de membrana. Ademais da contribución ao descubrimento de novos ligandos e ferramentas farmacolóxicas, os resultados descritos nesta tese forman parte dun proxecto metodolóxico encamiñado a demostrar as vantaxes competitivas das reaccións multicompoñente en Química Médica.

O primeiro capítulo da tese de doutoramento (**Capítulo 3.1**), publicado na revista *Journal of Medicinal Chemistry* (*J. Med. Chem*. **2019**, *62* (20), 9315-9330), describe a optimización de antagonistas fluorados para os receptores A_{2B} de adenosina. Desde a introdución clínica do primeiro ligando que incorpora un átomo de flúor, a fludrocortisona, o número de compostos que conteñen flúor incluídos no arsenal terapéutico aumentou rapidamente ata aproximadamente o 25% dos ligandos. A natureza única do átomo de flúor e as singulares propiedades do enlace carbono-flúor, están a día de hoxe ben documentadas e amplamente explotadas en química médica.

Substituír átomos de hidróxeno por flúor en prototipos activos pode exercer un efecto significativo sobre diversos parámetros estruturais , farmacodinámicos e farmacocinéticos. Dita modificación, xeralmente, tradúcese nunha maior estabilidade metabólica, mellor biodistribución e maior afinidade do ligando polo seu receptor. Ademais, os ligandos fluorados convertéronse en sondas moleculares moi apreciadas polos programas de investigación que empregan tomografía por emisión de positróns (PET).

Diversos estudos demostraron que o receptor A_{2B} é un receptor de baixa afinidade, que require concentracións de adenosina de rango micromolar para a súa activación funcional. Como consecuencia, este receptor permanece silente cando as concentracións extracelulares de adenosina son baixas, situación que cambia baixo condicións fisiopatolóxicas graves nas que a concentración de adenosina aumenta drasticamente (hipoxia, inflamación), conducindo á activación das vías de sinalización mediadas polo receptor A_{2B}. Evidencias recentes mostran que o receptor A_{2B} de adenosina está

transcricionalmente regulado por factores implicados na hipoxia inflamatoria. Ademais, o receptor A_{2B} é un actor chave na regulación de procesos biolóxicos como a contractilidade cardíaca, a homeostase da glucosa, a anxioxénese, a inflamación pulmonar, a resposta inflamatoria, cancro e a dor. En consecuencia, o desenvolvemento de ligandos capaces de bloquear esta diana de forma selectiva é unha aproximación novedosa para o tratamento de patoloxías graves como o cancro, a diabetes ou a enfermidade pulmonar obstrutiva crónica (EPOC).

Tendo en conta os aspectos anteriormente apuntados, investigamos o efecto da introdución de grupos trifluorometilo na afinidade A_{2B} de dous prototipos desenvolvidos anteriormente no grupo ComBioMed. Para iso, eliximos como ligandos modelo os compostos **ISAM-140** e **SYAF080**. Neste proxecto sintetizamos novos compostos que incorporan grupos $-CF_3$ en diferentes posicións utilizando a reacción de Biginelli como estratexia sintética. O deseño dos compostos e a interpretación da relación estrutura-actividade (SAR) resultante foron apoiadas por ferramentas computacionais que incluíron os resultados das simulacións de perturbación da enerxía libre (FEP). Posteriormente, separáronse os tres mellores antagonistas fluorados identificados nos seus estereoisómeros (enantiómeros ou diastereómeros) para a súa avaliación.

É importante resaltar que, do mesmo xeito que os ligandos de referencia (**ISAM-140** e **SYAF080**), todos os ligandos obtidos neste capítulo conteñen un estereocentro na posición catro do núcleo heterocíclico. Adicionalmente, algúns derivados conteñen outro centro quiral no residuo alquílico do grupo éster. Os derivados que conteñen un único estereocentro illáronse e avaliáronse farmacoloxicamente como mesturas racémicas. Pola súa banda, os compostos obtidos empregando un *β*-cetoéster racémico durante a reacción de Biginelli illáronse e avaliáronse como mesturas de diastereoisómeros. A avaliación conxunta dos datos estruturais e de afinidade (K_i), así como os estudos de modelaxe molecular, proporcionaron unha evidencia sólida da interacción estereoespecífica dos ligandos documentados neste capítulo co receptor A_{2B} de adenosina.

A separación por cromatografía en columna permitiunos illar os análogos fluorados do ligando **SYAF080** con dous centros quirales como pares de diastereoisómeros, aínda que non se puideron asignar de forma inequívoca a natureza dos estereocentros en cada

un deles. Desafortunadamente, todos os intentos de separación en pares de diastereoisómeros para a serie tricíclica que conteñen dous centros quirales (análogos fluorados do **ISAM-140**) fallaron. Por conseguinte, os compostos desta serie illáronse e ensaiáronse como unha mestura dos catro diastereómeros.

Unha vez realizada a avaliación farmacolóxica, e debido á prometedora afinidade (do rango de nanomolar baixo) mostrada pola mestura dos catro diastereoisómeros dun análogo fluorado do **ISAM-140**, realizouse a separación por HPLC quiral. Con todo, ata despois dunha extensa exploración de diversas fases estacionarias quirais, fases móbiles, ou outras condicións experimentais, a separación non tivo éxito. Ademais, a asignación inequívoca da configuración do centro quiral exocíclico non é factible mediante espectroscopía de dicroísmo circular, o que motivou ao deseño dunha ruta sintética diastereoselectiva para estes compostos. Neste enfoque sintético empregáronse as formas enantiopuras dos *β*-cetoésteres trifluorados. A posterior reacción de Biginelli con estes precursores proporcionou os derivados diana como pares de diastereoisómeros que conteñen a estereoquímica preestablecida no residuo alcoxi do grupo éster. Os dous pares de diastereoisómeros resultantes resolvéronse con éxito en diastereómeros individuais, cunha pureza estereoquímica excelente (97-99%), utilizando HPLC quiral semipreparativo.

Neste capítulo documentamos os primeiros exemplos de antagonistas do receptor A_{2B} de adenosina fluorados que combinan unha excelente afinidade A_{2B} (K_i <15 nM) e unha notable selectividade fronte aos outros receptores de adenosina (A_1, A_{2A}, A_3). O uso combinado de HPLC quiral, dicroísmo circular, síntese diastereoselectiva e cristalografía de raios X permitiu obter evidencias experimentais inequívocas da interacción estereoespecífica dos nosos estereoisómeros trifluorados co receptor A_{2B} (Figura 1).

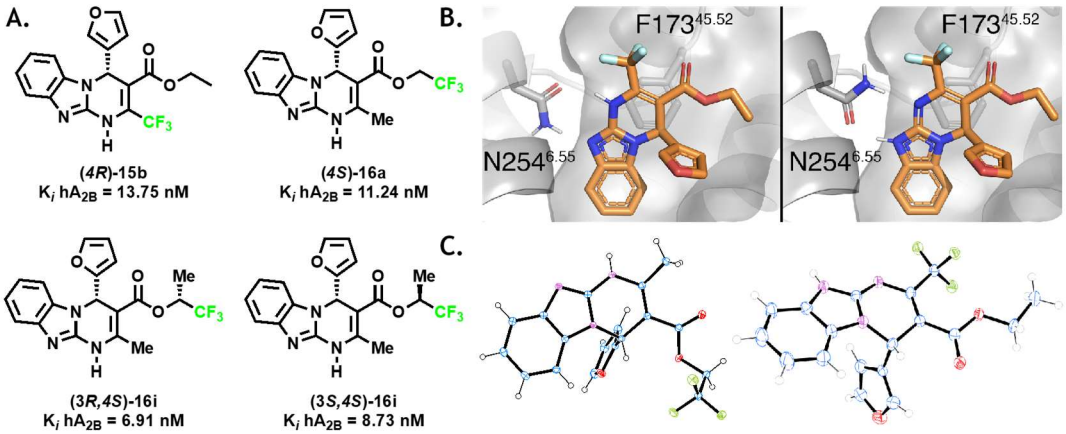

Figura 1: A. Ligandos máis interesantes sintetizados neste capítulo. B. Modelo teórico de unión ao receptor. C. Estrutura obtida por cristalografía de raios X de dous dos ligandos máis activos do noso estudo.

Estes resultados representan un paso adiante na identificación e optimización de antagonistas A_{2B} non xantínicos, metabolicamente máis estables e que exemplifican a modulación estereoselectiva do receptor A_{2B}. Os ligandos mostrados na Figura 1 están sendo estudados actualmente no marco do noso proxecto de investigación, encamiñado a explorar o potencial do bloqueo do receptor A_{2B} na (inmuno)terapia contra o cancro.

O segundo capítulo desta tese de doutoramento, o **Capítulo 3.2**, foi publicado na revista *Journal of Medicinal Chemistry* (*J. Med. Chem.* **2020**, *63* (14), 7721-7739). Neste traballo abordamos o desenvolvemento de ligandos para o receptor A_{2B} de adenosina máis estables metabolicamente usando **ISAM-140** como ligando modelo. Concretamente, centrámonos na exploración de substitucións bioisostéricas para os aneis de furano e tiofeno na posición 4 do anel 1,4-dihidrobenzo[4,5]imidazo[1,2-*a*]pirimidina usando criterios de bioisostería en aneis pentagonais (*Nitrogen-walk approach*).

Os avances recentes no estudo do efecto inmunosupresor da adenosina; así como do efecto pro-tumorixénico validado para o receptor A_{2B} e das propiedades anti-proliferativas, anti-anxioxénicas e anti-metastásicas documentadas para varios antagonistas A_{2B} reforzan o interese por este receptor como unha diana emerxente na (inmuno)terapia contra o cancro. O renovado interese polo receptor A_{2B} impulsou a exploración de novas facetas na súa sinalización e función, en particular, da súa capacidade para formar complexos homo- e heteroméricos. Diferentes técnicas demostraron que, do mesmo xeito que outros receptores de adenosina, o receptor A_{2B}

forma complexos homo- e heteroméricos estables (por exemplo, complexos A_1-A_{2B} e A_{2A}-A_{2B}) en células e tecidos que coexpresan estes subtipos de receptores. Sorprendentemente, estes estudos confirmaron que, ao activarse o receptor A_{2B}, este convértese no receptor dominante e, como tal, é capaz de regular negativamente as respostas mediadas polo receptor A_{2A}, así como a unión do ligando e a sinalización do devandito receptor a través da formación de heterómeros estables.

A similitude estrutural entre o fragmento da ribosa do ligando endóxeno (adenosina) e os núcleos heterocíclicos pentagonais como os aneis de furano e tiofeno, propiciou que estes últimos sexan residuos comúns nas estruturas dos antagonistas dos receptores de adenosina (especialmente dos receptores A_{2A} e A_{2B}). A natureza rica en electróns do núcleo heterocíclico implica que algúns destes aneis poden clasificarse como alertas estruturais. Polo tanto, a identificación temperá de elementos estruturais co potencial de converterse en alertas estruturais constitúe un tema chave durante o descubrimento cedo de ligandos. Neste contexto, débese examinar a relevancia destes grupos e avaliar experimentalmente os seus posibles efectos metabólicos para identificar grupos alternativos que poderían substituir esas alertas estruturais. Dado que os heteroarenos de cinco membros son aneis ubicuos nas estruturas dos antagonistas de adenosina (en particular, para os receptores A_{2A} e A_{2B}), realizamos un estudo exhaustivo para identificar núcleos heterocíclicos que poidan substituílos por diversos farmacóforos.

As estratexias xerais para reducir a inestabilidade metabólica inclúen bloquear os potenciais lugares reactivos con substitutivos, introducir átomos de nitróxeno ou substituír o núcleo pentagonal con heterociclos hexagonais. Con todo, o estudo dos análogos de arilo ou heteroarilo para substitucións bioisostéricas segue estando pouco explorado e os exemplos dispoñibles mostraron unha diminución pronunciada nos perfís de afinidade e selectividade. Xa que logo, a substitución destes grupos farmacofóricos críticos segue sendo un gran desafío.

No contexto do proxecto que se está levando a cabo no noso laboratorio, destinado a identificar antagonistas nonxantínicos do receptor A_{2B}, documentamos novas familias de derivados da pirimidina (mono, bi e tricíclicas) que combinan perfís de afinidade e selectividade. Os datos experimentais e computacionais destas series contribuíron a racionalizar e cuantificar a contribución dos diferentes elementos estruturais e

destacaron sistematicamente o papel crítico dos residuos pentagonais para preservar a unión forte polo receptor A_{2B}. En particular, destaca a importancia da estereodisposición do anel pentagonal nunha orientación de unión enantioespecífica, que foi validada pola síntese e avaliación dos diferentes estereoisómeros de compostos nalgunhas das series avaliadas.

O espazo de diversidade na posición catro do sistema tricíclico segue estando pouco explorado e algúns dos aneis introducidos nesta posición poderían ser responsables de efectos tóxicos. Con estes antecedentes, o segundo capítulo da tese de doutoramento presenta un estudo exhaustivo do efecto do substitutivo na posición catro, particularmente núcleos heterocíclicos de cinco membros, co obxectivo de identificar aneis óptimos para esta posición nunha serie que usa o **ISAM-140** como ligando de referencia. O estudo incluíu a síntese e avaliación de 42 novos ligandos que conteñen 18 combinacións heterocíclicas diferentes propostas segundo criterios de substitución bioisostérica. O deseño e a interpretación da SAR observada foron apoiados por modelos computacionais que se utilizaron como base para realizar unha serie de simulacións da FEP de toda a serie, para sustentar a interpretación da SAR en termos de interaccións receptor-ligando.

Utilizando a reacción de Biginelli como principal ferramenta sintética, preparamos un primeiro subconxunto concibido para ampliar os elementos de diversidade na posición catro da serie usada como referencia que contén o ligando **ISAM-140**. Esta serie empregouse co obxectivo avaliar a importancia do núcleo pentagonal e facilitar unha exploración e análise exhaustiva do efecto da introdución de nitróxeno. As novas series deseñáronse de acordo cos criterios de substitución bioisostérica, mediante o *Nitrogen-walk approach*, é dicir, introducindo sistematicamente un átomo de nitróxeno nas diferentes posicións da matriz do núcleo pentagonal. Esta aproximación é amplamente recoñecida como un cambio bioisostérico clásico, na que a substitución dun grupo CH por un átomo de nitróxeno en sistemas heteroaromáticos xeralmente ten consecuencias significativas durante a optimización multiparamétrica. Aínda que os efectos destas modificacións aparentemente triviais sobre a basicidade, a lipofilicidade, a área de superficie polar e a capacidade de enlace de hidróxeno son relativamente predicibles, o seu impacto no recoñecemento do receptor e a afinidade de unión, solubilidade, actividade de transporte e estabilidade metabólica poden ser máis difíciles de analizar a priori.

O *Nitrogen-walk approach* aplicouse para explorar substitucións bioisostéricas para os aneis de furano e tiofeno nunha serie de potentes antagonistas do receptor A_{2B}. Identificáronse varios ligandos novos que combinan unha afinidade notable (K_i <30 nM) e unha selectividade excepcional mediante a introdución de 18 estruturas heterocíclicas pentagonais diferentes na posición catro do anel tricíclico (Figura 2).

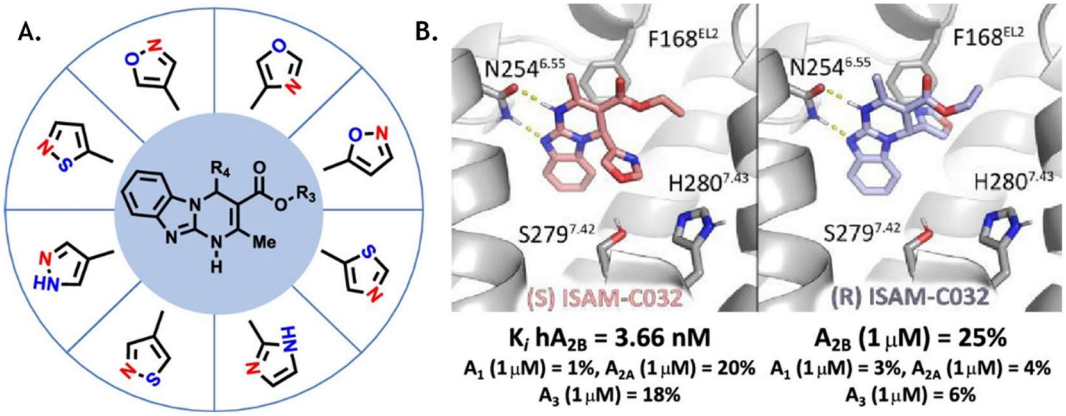

Figura 2: A. Esquema das modificacións máis relevantes realizadas sobre R_4. B. Modelo teórico da unión ao receptor cos enantiómeros do ligando máis activo obtido.

Tamén se levou a cabo unha exploración preliminar do perfil inhibitorio *in vitro* dos ligandos seleccionados nos citocromos CYP3A4 e CYP2D6, así como unha caracterización *in vitro* máis completa da absorción, distribución, metabolismo e excreción (ADME) do mellor ligando identificado como mestura racémica, determinando a súa estabilidade microsomal e solubilidade.

Finalmente, os enantiómeros de este ligando foron separados por HPLC quiral semipreparativo e avaliados farmacoloxicamente nos catro receptores de adenosina. Os resultados de afinidade confirmaron o recoñecemento enantioespecífico polo receptor A_{2B}, en liña cos estudos previos deste proxecto.

O efecto antagonista do mellor ligando identificado no contexto deste traballo e o seu eutómero corroborouse mediante experimentos de funcionais (AMPc). Pola súa banda, a análise conxunta da serie actual e dos datos de series anteriores facilitaron o entendemento das relacións estrutura-actividade e dos modos de unión da serie empregando ferramentas computacionais.

A caracterización preliminar dos ligandos seleccionados evidenciou unha actividade inhibidora practicamente insignificante nos citocromos CYP3A4 e CYP2D6.

O primeiro é o principal citocromo na metabolización de fármacos e o segundo é o máis frecuentemente involucrado na metabolización de fármacos que conteñen átomos de nitróxeno de natureza básica. Adicionalmente, eses estudos permitiron verificar a excelente estabilidade microsomal do mellor composto sintetizado. Unha combinación de HPLC quiral e dicroísmo circular proporcionou apoio experimental á interacción estereoespecífica modelada entre o antagonista novidoso máis atractivo e o receptor A_{2B} de adenosina humano. Este traballo representa un paso adiante na identificación de novos derivados de pirimidina estruturalmente diversos e metabolicamente estables (sen núcleos de furano) que son capaces de antagonizar o receptor A_{2B} humano dun xeito estereoespecífico .

O terceiro capítulo da tese (**Capítulo 3.3**) foi publicado na revista *Journal of Medicinal Chemistry* (*J. Med. Chem*. **2021**, *64* (12), 8710-8726). O traballo documenta o descubrimento de agonistas parciais nesgados do receptor D_2 (activando a vía do AMPc ou das *β*-arrestinas) que mostran excelentes perfís de potencia e selectividade.

O descubrimento e estudo de novas vías de sinalización dos GPCR (distintas da disociación do heterotrímero da proteína G) supuxo un cambio de paradigma que permite entender mellor o funcionamento e regulación dos GPCRs. A confirmación inequívoca de que a activación dos GPCRs pode desencadear procesos de sinalización máis sutís, e moito menos estudados, abre novos horizontes de investigación, así como a posibilidade de entender mellor os efectos de fármacos coñecidos e o desenvolvemento de novos ligandos máis eficaces e seguros que regulen vías de sinalización alternativas. Unha desas cascadas de sinalización é a vía das *β*-arrestinas, un compoñente da maquinaria de internalización e desensibilización dos GPCRs. O proceso mediante o cal os ligandos dos GPCRs modulan diferencialmente a vía da proteína G e/ou a vía da *β*-arrestina para mediar en rutas específicas de transdución de sinais é un fenómeno coñecido como selectividade funcional ou agonismo nesgado.

O concepto de agonismo nesgado modificou progresivamente nosa comprensión da sinalización dos GPCRs e cambiou o paradigma do descubrimento de ligandos para os mesmos. Con todo, os mecanismos moleculares detrás da sinalización nesgada seguen sendo unha gran incógnita, xa que o estudo das contribucións funcionais da proteína G e as vías de sinalización pola *β* -arrestina dos ligandos endóxenos/exóxenos aínda constitúe un desafío. Os ligandos nesgados son capaces desencadear a vía específica

responsable do efecto terapéutico sen activar as vías que están implicadas nos efectos secundarios. Estes ligandos son extremadamente útiles para dilucidar as claves que contribúen á transdución de sinais e tamén teñen un potencial terapéutico significativo para desenvolver potenciais axentes farmacolóxicos con menores efectos secundarios.

O receptor D_2 de dopamina é un GPCR no que a exploración do concepto de agonismo nesgado estase convertendo no novo paradigma para proporcionar mellores ligandos. Este receptor é o obxectivo principal dos axentes antipsicóticos e antiparkinsonianos, pero tamén está implicado no mecanismo de acción de varias drogas asociadas co abuso e a adicción. Este capítulo céntrase na optimización de ligandos para o tratamento da esquizofrenia. As terapias actuais, baseadas no uso de antipsicóticos típicos e atípicos, caracterízanse por paliar a sintomatoloxía, presentando importantes efectos secundarios. O descubrimento do aripiprazol e a cariprazina, prototipos dunha nova xeración de antipsicóticos atípicos e recentemente aprobados pola FDA para o tratamento da esquizofrenia, os episodios maníacos/mixtos bipolares I e o trastorno depresivo, cambiaron a visión da acción antipsicótica sobre a sinalización da dopamina.

Inspirados polo perfil antipsicótico único de aripiprazol, desenvolvemos unha nova serie de agonistas nesgados para o receptor D_2. Todos os compostos foron deseñados tomando como referencia estes dous ligandos que conteñen tres rexións ben definidas: (1) o farmacóforo primario (PP), que consiste nun residuo de fenil-piperazina mono ou disustituido (comunmente coñecido como fragmento ao lado esquerdo (*left hand segment*, LHS), ou grupo de cabeza); (2) o espallador central, que é variable en lonxitude e natureza, podendo ser acíclico ou cíclico; e (3) o farmacóforo secundario (ou alostérico) (SP), que xeralmente consiste nun núcleo heterocíclico (comunmente denominado fragmento ao lado dereito (*right hand segment*, RHS) ou grupo de cola).

Neste estudo decidiuse manter na rexión LHS o farmacóforo, utilizando o residuo 1-(2,3-diclorofenil)piperazina (presente no aripiprazol), e un espallador lineal de catro átomos, máis curto do habitual. Tamén se propuxeron seis grupos diferentes e previamente inexplorados na rexión RHS para examinar o efecto destas modificacións estruturais na selectividade e no perfil de selectividade funcional sobre o receptor D_2. Os fragmentos RHS seleccionados proporcionan topoloxías novidosas, características fisicoquímicas e modos de unión alternativos que deberían permitir a captura de diversos estados conformacionais dentro do receptor. Ademais da diversidade

heterocíclica e funcional introducida, algúns dos fragmentos de RHS propostos teñen un centro quiral dentro de devandito fragmento, introducindo así diversidade estereoquímica que permitiría a investigación futura de interaccións estereoselectivas previamente inexploradas dentro da rexión RHS.

Neste capítulo abordamos o deseño, síntese e caracterización farmacolóxica de varias series de agonistas parciais do receptor D_2 que exhiben perfís de sinalización nesgados pola proteína G ou a β-arrestina e unha exquisita selectividade polo receptor D_2. Estas novas familias foron deseñadas e ensambladas utilizando un enfoque multicompoñente altamente versátil baseado na reacción de Ugi. Os datos experimentais proporcionaron tendencias da SAR e a relación estrutura-selectividade funcional (SFSR) que eran coherentes cos modos de unión propostos, como se define na modelaxe molecular.

Os resultados xerais do estudo supoñen unha proba de concepto dunha estratexia inexplorada para a rápida identificación de novos ligandos para o receptor D_2 estruturalmente diversos e funcionalmente selectivos. Polo tanto, este capítulo documenta un método multicompoñente versátil, eficiente e previamente inexplorado que permite a xeración rápida de novos ligandos nesgados para o receptor D_2 e con selectividade de subtipo.

Esta estratexia exemplifica a procura de fragmentos RHS diversos e previamente inexplorados, pero tamén destaca o seu papel fundamental na modulación do perfil de selectividade funcional. A caracterización farmacolóxica da nova serie de compostos permitiu a identificación de varios ligandos que provocan unha excelente selectividade para o receptor D_2 e unha notable selectividade funcional mediante as vías de sinalización polo cAMP ou a β-arrestina (Figura 3). Estes resultados poden explicarse en certa medida pola modelaxe molecular destes ligandos utilizando a estrutura cristalina recente do receptor D_2.

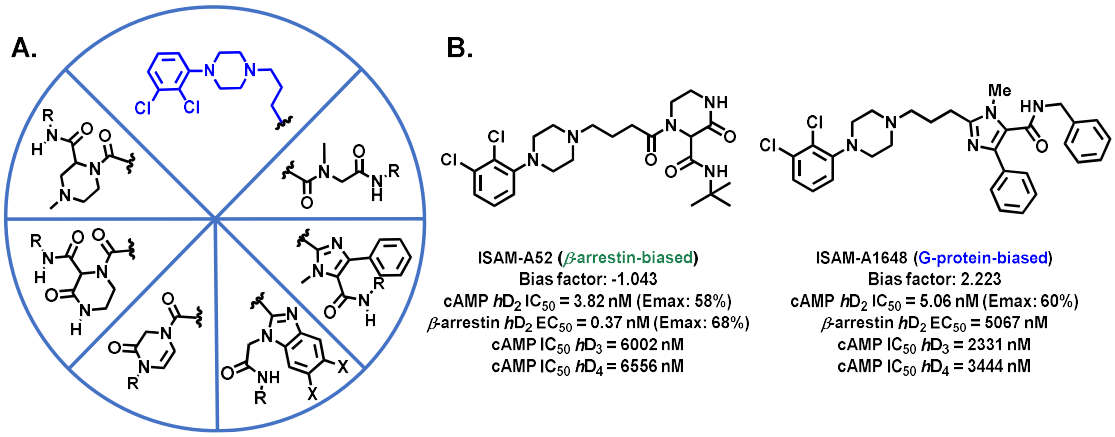

Figura 3: A. Patróns de substitución realizados no noso estudo. B. Compostos nesgados máis activos e con selectividade subtipo sintetizados neste capítulo.

Actualmente, estanse realizando máis estudos no noso laboratorio para expandir a diversidade dos residuos e os espalladores que conforman os compostos. Deste xeito, pódese explorar en detalle a SAR e a relación estrutura-selectividade ao redor dos ligandos máis prometedores desenvolvidos neste capítulo da tese de doutoramento e, establecer o papel da estereoquímica nos perfís biolóxicos observados.

En conxunto, os resultados aquí documentados destacan o potencial sintético das reaccións multicompoñente para acelerar o descubrimento, a optimización e a elaboración de perfís de novos prototipos en Química Médica.

USC
UNIVERSIDADE
DE SANTIAGO
DE COMPOSTELA

RESUMEN

La presente tesis doctoral describe el diseño, síntesis, evaluación farmacológica, relación estructura-actividad y modelización molecular de nuevos ligandos potentes y selectivos para los receptores A_{2B} de adenosina y D_2 de dopamina. El trabajo realizado, que se organiza en tres grandes áreas (**Capítulos 3.1-3.3**), se presenta en forma de compendio de publicaciones abordando temas relevantes y conceptos avanzados de la Química Médica y Biológica de esos receptores de membrana. Además de la contribución al descubrimiento de nuevos ligandos y herramientas farmacológicas, los resultados descritos en esta tesis forman parte de un proyecto metodológico encaminado a demostrar las ventajas competitivas de las reacciones multicomponente en Química Médica.

El primer capítulo de la tesis doctoral (**Capítulo 3.1**), publicado en la revista *Journal of Medicinal Chemistry* (*J. Med. Chem.* **2019**, *62* (20), 9315−9330), describe la optimización de antagonistas fluorados para los receptores A_{2B} de adenosina. Desde la introducción clínica del primer ligando que incorpora un átomo de flúor, la fludrocortisona, el número de compuestos que contienen flúor incluidos en el arsenal terapéutico ha aumentado rápidamente hasta aproximadamente el 25% de los ligandos. La naturaleza única del átomo de flúor, y las singulares propiedades del enlace carbono-flúor, están a día de hoy bien documentadas y ampliamente explotadas en química médica.

Reemplazar átomos de hidrógeno por flúor en prototipos activos puede ejercer un efecto significativo sobre diversos parámetros estructurales, farmacodinámicos y farmacocinéticos. Dicha modificación, generalmente, se traduce en una mayor estabilidad metabólica, mejor biodistribución y mayor afinidad del ligando por su receptor. Además, los ligandos fluorados se han convertido en sondas moleculares muy apreciadas por los programas de investigación que emplean tomografía por emisión de positrones (PET).

Diversos estudios han demostrado que el receptor A_{2B} es un receptor de baja afinidad, que requiere concentraciones de adenosina de rango micromolar para su activación funcional. Como consecuencia, este receptor permanece silente cuando las concentraciones extracelulares de adenosina son bajas, situación que cambia bajo algunas condiciones fisiopatológicas graves en las que la concentración de adenosina

aumenta drásticamente (hipoxia, inflamación), conduciendo a la activación de las vías de señalización mediadas por el receptor A_{2B}. Evidencias recientes muestran que el receptor A_{2B} de adenosina está transcripcionalmente regulado por factores implicados en la hipoxia inflamatoria. Además, el receptor A_{2B} es un actor clave en la regulación de procesos biológicos como la contractilidad cardíaca, la homeostasis de la glucosa, la angiogénesis, la inflamación pulmonar, la respuesta inflamatoria, el cáncer y el dolor. En consecuencia, el desarrollo de ligandos capaces de bloquear esta diana de forma selectiva es una aproximación novedosa para el tratamiento de patologías graves como el cáncer, la diabetes o la enfermedad pulmonar obstructiva crónica (EPOC).

Tomando en cuenta los aspectos anteriormente reseñados, investigamos el efecto de la introducción de grupos trifluorometilo en la afinidad A_{2B} de dos prototipos desarrollados anteriormente en el grupo ComBioMed. Para ello elegimos como ligandos modelo los compuestos **ISAM-140** y **SYAF080**. En este proyecto sintetizamos nuevos compuestos que incorporan grupos $-CF_3$ en diferentes posiciones utilizando la reacción de Biginelli como herramienta sintética.

El diseño de los compuestos, y la interpretación de la relación estructura-actividad (SAR) resultante, fueron apoyados por herramientas computacionales que incluyeron los resultados de las simulaciones de perturbación de la energía libre (FEP). Posteriormente se separaron los tres mejores antagonistas fluorados identificados en sus estereoisómeros (enantiómeros o diastereómeros) para su evaluación.

Es importante resaltar que, al igual que ligandos de referencia (**ISAM-140** y **SYAF080**), todos los ligandos obtenidos en este capítulo contienen un estereocentro en la posición cuatro del núcleo heterocíclico. Adicionalmente, algunos derivados contienen otro centro quiral en el residuo alquílico del grupo éster. Los derivados que contienen un único estereocentro se aislaron y evaluaron farmacológicamente como mezclas racémicas. Por su parte, los compuestos obtenidos empleando un *β*-cetoéster racémico durante la reacción de Biginelli se aislaron y evaluaron como mezclas de diastereoisómeros. La evaluación conjunta de los datos estructurales y de afinidad (K_i), así como los estudios de modelado molecular, proporcionaron una evidencia sólida de la interacción estereoespecífica de los ligandos documentados en este capítulo con el receptor A_{2B} de adenosina.

La separación por cromatografía en columna nos permitió aislar los análogos fluorados del ligando **SYAF080** con dos centros quirales como pares de diastereoisómeros, aunque no se pudieron asignar de forma inequívoca la naturaleza de los estereocentros en cada uno de ellos. Desafortunadamente, todos los intentos de separación en pares de diastereoisómeros para la serie tricíclica que contienen dos centros quirales (análogos fluorados del **ISAM-140**) fallaron. Por consiguiente, los compuestos de esta serie se aislaron y ensayaron como una mezcla de los cuatro diastereómeros.

Una vez realizada la evaluación farmacológica y, debido a la prometedora afinidad (del rango de nanomolar bajo) mostrada por la mezcla de los cuatro diastereoisómeros de un análogo fluorado del **ISAM-140**, se realizó la separación por HPLC quiral. Sin embargo, incluso después de una extensa exploración de diversas fases estacionarias quirales, fases móviles, u otras condiciones experimentales la separación no tuvo éxito. Además, la asignación inequívoca de la configuración del centro quiral exocíclico no es factible mediante espectroscopía de dicroísmo circular, lo que motivó al diseño de una ruta sintética diastereoselectiva para estos compuestos. En este enfoque sintético se emplearon las formas enantiopuras de los *β*-cetoésteres trifluorados. La posterior reacción de Biginelli con estos precursores ha proporcionado los derivados diana como pares de diastereoisómeros que contienen la estereoquímica preestablecida en el residuo alcoxi del grupo éster. Los dos pares de diastereoisómeros resultantes se resolvieron con éxito en diastereómeros individuales, con una pureza estereoquímica excelente (97-99%), utilizando HPLC quiral semipreparativo.

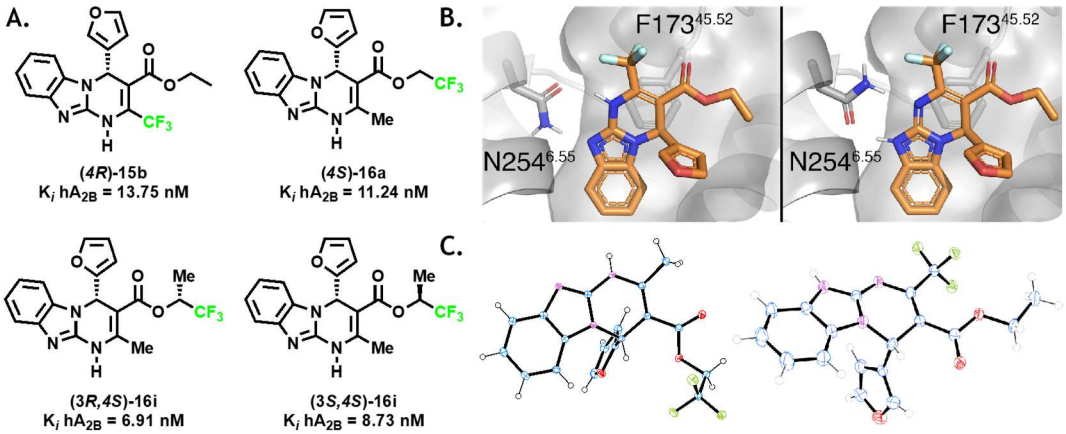

Figura 1: A. Ligandos más interesantes sintetizados en este capítulo. B. Modelo teórico de unión al receptor. C. Estructura obtenida por cristalografía de rayos X de dos de los ligandos más activos de nuestro estudio.

En este capítulo hemos documentado los primeros ejemplos de antagonistas del receptor A_{2B} de adenosina fluorados que combinan una excelente afinidad A_{2B} (Ki <15 nM) y una notable selectividad frente a los otros receptores de adenosina (A_1, A_{2A}, A_3). El uso combinado de HPLC quiral, dicroísmo circular, síntesis diastereoselectiva y cristalografía de rayos X permitió obtener evidencias experimentales inequívocas de la interacción estereoespecífica de nuestros estereoisómeros trifluorados con el receptor A_{2B} (Figura 1).

Estos resultados representan un paso adelante en la identificación y optimización de antagonistas A_{2B} no xantínicos, metabólicamente más estables y que ejemplifican la modulación estereoselectiva del receptor A_{2B}. Los ligandos mostrados en la Figura 1 están siendo estudiados actualmente en el marco de nuestro proyecto de investigación encaminado a explorar el potencial del bloqueo del receptor A_{2B} en la (inmuno)terapia contra el cáncer.

El segundo capítulo de esta tesis doctoral, **Capítulo 3.2**, fue publicado en la revista *Journal of Medicinal Chemistry* (*J. Med. Chem.* **2020**, *63* (14), 7721–7739). En este trabajo abordamos el desarrollo de ligandos para el receptor A_{2B} de adenosina más estables metabólicamente usando **ISAM-140** como ligando modelo. Concretamente, nos centramos en la exploración de sustituciones bioisostéricas para los anillos de furano y tiofeno en la posición 4 del anillo 1,4-dihidrobenzo[4,5]imidazo[1,2-*a*]pirimidina usando criterios de bioisostería en anillos pentagonales (*Nitrogen-walk approach*).

Los avances recientes en el estudio del efecto inmunosupresor de la adenosina; así como del efecto pro-tumorigénico validado para el receptor A_{2B} y de las propiedades anti-proliferativas, anti-angiogénicas y anti-metastásicas documentadas para varios antagonistas A_{2B} refuerzan el interés por este receptor como una diana emergente en la (inmuno)terapia contra el cáncer. El renovado interés por el receptor A_{2B} ha impulsado la exploración de nuevas facetas en su señalización y función, en particular de su capacidad para formar complejos homo- y heteroméricos. Diferentes técnicas han demostrado que, al igual que otros receptores de adenosina, el receptor A_{2B} forma complejos homo-méricos y hetero-méricos estables (por ejemplo, complejos A_1-A_{2B} y A_{2A}-A_{2B}) en células y tejidos que coexpresan estos subtipos de receptores. Sorprendentemente, estos estudios confirmaron que al activarse el receptor A_{2B} este se convierte en el receptor dominante y, como tal, es capaz de regular negativamente las respuestas mediadas por el receptor A_{2A}, así como la unión del ligando y la señalización de dicho receptor a través de la formación de heterómeros estables.

La similitud estructural entre el fragmento de ribosa del ligando endógeno (adenosina) y los núcleos heterocíclicos pentagonales como los anillos de furano y tiofeno, ha propiciado que estos últimos sean residuos comunes en las estructuras de los antagonistas de los receptores de adenosina (especialmente de los receptores A_{2A} y A_{2B}). La naturaleza rica en electrones del núcleo heterocíclico implica que algunos de estos anillos pueden clasificarse como alertas estructurales. Por lo tanto, la identificación temprana de elementos estructurales con el potencial de convertirse en alertas estructurales constituye un tema clave durante el descubrimiento temprano de ligandos. En este contexto, se debe examinar la relevancia de estos grupos y evaluar experimentalmente sus posibles efectos metabólicos para identificar grupos alternativos que podrían reemplazar esas alertas estructurales. Dado que los heteroarenos de cinco miembros son anillos ubicuos en las estructuras de los antagonistas de adenosina (en particular para los receptores A_{2A} y A_{2B}), hemos realizado un estudio exhaustivo para identificar núcleos heterocíclicos que puedan reemplazarlos por diversos farmacóforos.

Las estrategias generales para reducir la inestabilidad metabólica incluyen bloquear los potenciales lugares reactivos con sustituyentes, introducir átomos de nitrógeno o reemplazar el núcleo pentagonal con heterociclos hexagonales. Sin embargo, el estudio de los análogos de arilo o heteroarilo para reemplazos bioisostéricos sigue estando poco explorado, y los ejemplos disponibles han mostrado una disminución pronunciada en

los perfiles de afinidad y selectividad. Por tanto, la sustitución de estos grupos farmacofóricos críticos sigue siendo un gran desafío.

En el contexto del proyecto que se está llevando a cabo en nuestro laboratorio, destinado a identificar antagonistas no-xantínicos del receptor A_{2B}, hemos documentado nuevas familias de derivados de la pirimidina (mono, bi y tricíclicas) que combinan excelentes perfiles de afinidad y selectividad. Los datos experimentales y computacionales de estas series han contribuido a racionalizar y cuantificar la contribución de los diferentes elementos estructurales y han destacado sistemáticamente el papel crítico de los residuos pentagonales para preservar la unión fuerte por el receptor A_{2B}. En particular, destaca la importancia de la estereodisposición del anillo pentagonal en una orientación de unión enantioespecífica, que fue validada por la síntesis y evaluación de los diferentes estereoisómeros de compuestos en algunas de las series evaluadas.

El espacio de diversidad en la posición cuatro del sistema tricíclico sigue estando poco explorado y algunos de los anillos introducidos en esta posición podrían ser responsables de efectos tóxicos. Con estos antecedentes, el segundo capítulo de la tesis doctoral presenta un estudio exhaustivo del efecto del sustituyente en la posición cuatro, particularmente núcleos heterocíclicos de cinco miembros, con el objetivo de identificar anillos óptimos para esta posición en una serie que emplea el **ISAM-140** como ligando de referencia. El estudio incluyó la síntesis y evaluación de 42 nuevos ligandos que contienen 18 combinaciones heterocíclicas diferentes propuestas según criterios de reemplazo bioisostérico. El diseño y la interpretación de la SAR observada fueron respaldados por modelos computacionales que se utilizaron como base para realizar una serie de simulaciones de la FEP de toda la serie, para sustentar la interpretación del SAR en términos de interacciones receptor-ligando.

Utilizando la reacción de Biginelli como principal herramienta sintética, hemos preparado un primer subconjunto concebido para ampliar los elementos de diversidad en la posición cuatro de la serie usada como referencia que contiene el ligando **ISAM-140**. Esta serie se ha empleado con el objetivo evaluar la importancia del núcleo pentagonal y facilitar una exploración y análisis exhaustivo del efecto de la introducción de nitrógeno. Las nuevas series se diseñaron de acuerdo con los criterios de reemplazo bioisostérico, mediante el *Nitrogen-walk approach*, es decir, introduciendo

sistemáticamente un átomo de nitrógeno en las diferentes posiciones de la matriz del núcleo pentagonal. Esta aproximación es ampliamente reconocida como un cambio bioisostérico clásico, en la que el reemplazo de un grupo CH por un átomo de nitrógeno en sistemas heteroaromáticos generalmente tiene consecuencias significativas durante la optimización multiparamétrica. Aunque los efectos de estas modificaciones aparentemente triviales sobre la basicidad, la lipofilicidad, el área de superficie polar y la capacidad de enlace de hidrógeno son relativamente predecibles, su impacto en el reconocimiento del receptor y la afinidad de unión, solubilidad, actividad de transporte y estabilidad metabólica pueden ser más difíciles de analizar *a priori*.

El *Nitrogen-walk approach* se ha aplicado para explorar reemplazos bioisostéricos para los anillos de furano y tiofeno en una serie de potentes antagonistas del receptor A_{2B}. Se identificaron varios ligandos nuevos que combinan una afinidad notable (K_i <30 nM) y una selectividad excepcional mediante la introducción de 18 estructuras heterocíclicas pentagonales diferentes en la posición cuatro del anillo tricíclico (Figura 2).

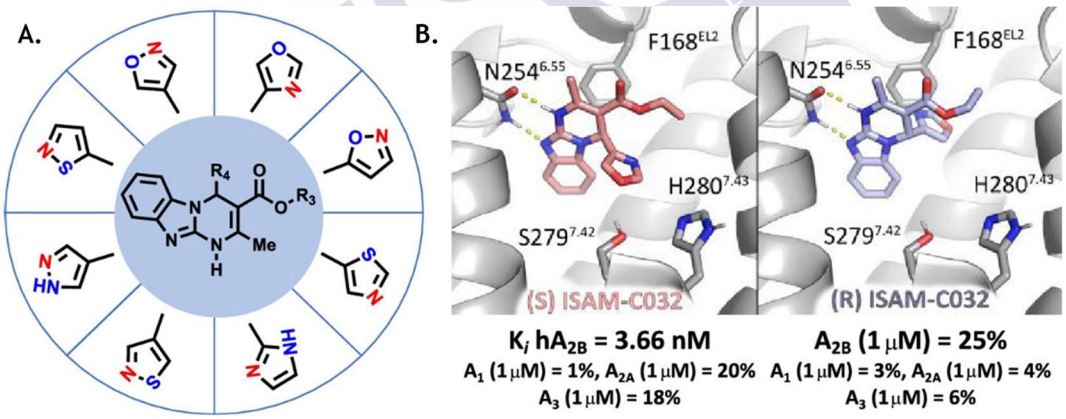

Figura 2: A. Esquema de las modificaciones más relevantes realizadas sobre R_4. B. Modelo teórico de la unión al receptor con los enantiómeros del ligando más activo obtenido.

También se llevó a cabo una exploración preliminar del perfil inhibitorio *in vitro* de los ligandos seleccionados en los citocromos CYP3A4 y CYP2D6, así como una caracterización *in vitro* más completa de la absorción, distribución, metabolismo y excreción (ADME) del mejor ligando identificado, como mezcla racémica, determinando su estabilidad microsomal y solubilidad.

Finalmente, los enantiómeros de este ligando fueron separados por HPLC quiral semipreparativo y evaluados farmacológicamente en los cuatro receptores de adenosina.

Los resultados de afinidad confirmaron el reconocimiento enantioespecífico por el receptor A_{2B}, en línea con los estudios previos de este proyecto.

La actividad funcional (AMPc) del mejor ligando racémico de este estudio y su eutómero fue estudiada, confirmando el efecto antagonista de ambos. Por su parte, el análisis conjunto de la serie actual y los datos de series anteriores facilitaron el entendimiento de las relaciones estructura-actividad y los modos de unión de la serie empleando herramientas computacionales.

La caracterización preliminar de los ligandos seleccionados ha evidenciado una actividad inhibidora prácticamente insignificante en los citocromos CYP3A4 y CYP2D6. El primero es el principal citocromo implicado en la metabolización de fármacos y el segundo el más involucrado en la metabolizción de fármacos que contienen nitrógenos de naturaleza básica. Adicionalmente, esos estudios permitieron verificar la excelente estabilidad microsomal del mejor compuesto sintetizado en este capítulo. Una combinación de HPLC quiral y dicroísmo circular permitió demostrar de forma experimental la interacción estereoespecífica predicha durante la intervención de nuestros antagonistas y el receptor A_{2B} de adenosina humano. Este trabajo representa un paso adelante en la identificación de nuevos derivados de pirimidina estructuralmente diversos y metabólicamente estables (sin núcleos de furano) que son capaces de antagonizar el receptor A_{2B} humano de una manera estereoespecífica.

El tercer capítulo de la tesis (**Capítulo 3.3**) ha sido publicado en la revista *Journal of Medicinal Chemistry* (*J. Med. Chem.* **2021**, *64* (12), 8710-8726). El trabajo documenta el descubrimiento de agonistas parciales sesgados del receptor D_2 (activando la vía del AMPc o las *β*-arrestinas) que muestran excelentes perfiles de potencia y selectividad.

El descubrimiento y estudio de nuevas vías de señalización de los GPCR (distintas de la disociación del heterotrímero de la proteína G) ha supuesto un cambio de paradigma que permite entender mejor el funcionamiento y regulación de los GPCRs. La confirmación inequívoca de que la activación de los GPCRs puede desencadenar procesos de señalización más sutiles, y mucho menos estudiados, abre nuevos horizontes de investigación, así como la posibilidad de entender mejor los efectos de fármacos conocidos y el desarrollo de nuevos ligandos más eficaces y seguros que regulen vías de señalización alternativas. Una de esas cascadas de señalización es la vía

de las β-arrestinas, un componente de la maquinaria de internalización y desensibilización de los GPCRs. El proceso mediante el cual los ligandos de los GPCRs modulan diferencialmente la vía de la proteína G y/o la vía de la β-arrestina para mediar en rutas específicas de transducción de señales es un fenómeno conocido como selectividad funcional o agonismo sesgado. El concepto de agonismo sesgado ha modificado progresivamente nuestra comprensión de la señalización de los GPCRs y ha cambiado el paradigma del descubrimiento de ligandos para los mismos. Sin embargo, los mecanismos moleculares detrás de la señalización sesgada siguen siendo una gran incógnita, ya que el estudio de las contribuciones funcionales de la proteína G y las vías de señalización por la β-arrestina de los ligandos endógenos/exógenos todavía constituye un desafío. Los ligandos sesgados son capaces desencadenar la vía específica responsable del efecto terapéutico sin activar las vías que están implicadas en los efectos secundarios. Estos ligandos son extremadamente útiles para dilucidar las claves que contribuyen a la transducción de señales y también tienen un potencial terapéutico significativo para desarrollar potenciales agentes farmacológicos con menores efectos secundarios.

El receptor D_2 de dopamina es un GPCR en el que la exploración del concepto de agonismo sesgado se está convirtiendo en el nuevo paradigma para proporcionar mejores ligandos. Este receptor es el objetivo principal de los agentes antipsicóticos y antiparkinsonianos, pero también está implicado en el mecanismo de acción de varias sustancias asociadas con el abuso y la adicción. Este capítulo se centra en la optimización de ligandos para el tratamiento de la esquizofrenia. Las terapias actuales, mediante antipsicóticos típicos y atípicos, se caracterizan por paliar la sintomatología, presentando importantes efectos secundarios. El descubrimiento del aripiprazol y la cariprazina, prototipos de una nueva generación de antipsicóticos atípicos y recientemente aprobados por la FDA para el tratamiento de la esquizofrenia, los episodios maníacos/mixtos bipolares I y el trastorno depresivo, cambiaron la visión de la acción antipsicótica sobre la señalización de la dopamina.

Inspirados por el perfil antipsicótico único de aripiprazol, hemos desarrollado una nueva serie de agonistas sesgados para el receptor D_2. Todos los compuestos fueron diseñados tomando como referencia estos dos ligandos que contienen tres regiones bien definidas: (1) el farmacóforo primario (PP), que consiste en un residuo de fenil-piperazina mono o disustituido (comúnmente conocido como el fragmento del lado

izquierdo (*left hand segment*, LHS) o grupo de cabeza); (2) el espaciador central, que es variable en longitud y naturaleza, pudiendo ser acíclico o cíclico; y (3)) el farmacóforo secundario (ou alostérico) (SP), que generalmente consiste en un núcleo heterocíclico (comúnmente denominado fragmento del lado derecho (*right hand segment*, RHS) o grupo de cola).

En este estudio se decidió mantener inalterada la región LHS el farmacóforo, utilizando el residuo 1-(2,3-diclorofenil)piperazina (presente en el aripiprazol), y un espaciador lineal de cuatro átomos, más corto de lo habitual. También se propusieron seis grupos diferentes y previamente inexplorados en la región RHS para examinar el efecto de estas modificaciones estructurales en la selectividad y en el perfil de selectividad funcional sobre el receptor D_2. Los fragmentos RHS seleccionados proporcionan topologías novedosas, características fisicoquímicas y modos de unión alternativos, que deberían permitir la captura de diversos estados conformacionales dentro del receptor. Además de la diversidad heterocíclica y funcional introducida, algunos de los fragmentos de RHS propuestos tienen un centro quiral dentro de dicho fragmento, introduciendo así diversidad estereoquímica que permitiría la investigación futura de interacciones estereoselectivas previamente inexploradas dentro de la región RHS.

En este capítulo abordamos el diseño, síntesis y caracterización farmacológica de varias series de agonistas parciales del receptor D_2 que exhiben perfiles de señalización sesgados por la proteína G o la β-arrestina y una exquisita selectividad por el receptor D_2. Estas nuevas familias fueron diseñadas y ensambladas utilizando un enfoque multicomponente altamente versátil, basada en la reacción de Ugi. Los datos experimentales proporcionaron tendencias de la SAR y la relación estructura-selectividad funcional (SFSR) que eran coherentes con los modos de unión propuestos, como se define en el modelado molecular.

Los resultados generales del estudio suponen una prueba de concepto exitosa de una estrategia inexplorada para la rápida identificación de nuevos ligandos para el receptor D_2 estructuralmente diversos y funcionalmente selectivos. Por lo tanto, este capítulo documenta un método multicomponente versátil, eficiente y previamente inexplorado que permite la generación rápida de nuevos ligandos sesgados para el receptor D_2 y con selectividad de subtipo.

Esta estrategia ejemplifica la búsqueda de fragmentos RHS diversos y previamente inexplorados, pero también destaca su papel fundamental en la modulación del perfil de selectividad funcional. La caracterización farmacológica de la nueva serie de compuestos permitió la identificación de varios ligandos que provocan una excelente selectividad para el receptor D_2 y una notable selectividad funcional mediante las vías de señalización por el cAMP o la β-arrestina (Figura 3). Estos resultados pueden explicarse por el modelado molecular de estos ligandos utilizando la estructura cristalina reciente del receptor D_2.

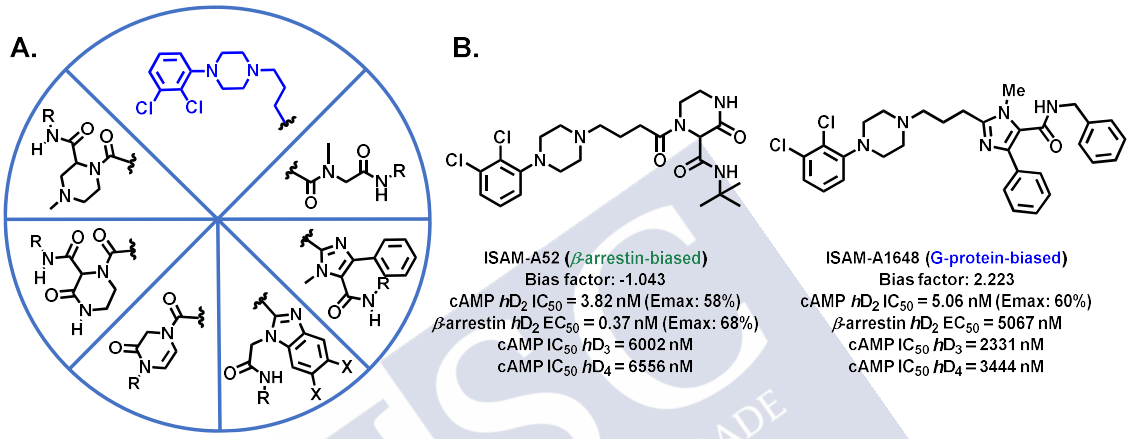

Figura 3: A. Patrones de sustitución realizados en nuestro estudio. B. Compuestos sesgados más activos y con selectividad subtipo sintetizados en este capítulo.

Actualmente se están realizando más estudios en nuestro laboratorio para expandir la diversidad de los residuos y los espaciadores que conforman los compuestos. De esta manera se puede explorar en detalle la SAR y la relación estructura-selectividad alrededor de los ligandos más prometedores desarrollados en este capítulo de la tesis doctoral y, establecer el papel de la estereoquímica en los perfiles biológicos observados.

En conjunto, los resultados aquí documentados destacan el potencial sintético de las reacciones multicomponente para acelerar el descubrimiento, la optimización y la elaboración de perfiles de nuevos prototipos en Química Médica.

USC
UNIVERSIDADE
DE SANTIAGO
DE COMPOSTELA

1. INTRODUCTION

USC
UNIVERSIDADE
DE SANTIAGO
DE COMPOSTELA

1.1 G PROTEIN-COUPLED RECEPTORS, GPCRS

G protein-coupled receptors (GPCRs) belong to one of the largest families of proteins in the mammalian genome and they are crucial for nearly every physiological process.[1] To date, more than 800 individual GPCRs have been identified and these represent 4% of the whole human genome.[2]

Members of this receptor superfamily act as nanomachines that are involved in signal transduction of a wide array of extracellular stimuli, including proteins, neurotransmitters, hormones, small molecules, ions, and light from the extracellular to the intracellular side of the cell.[3] Moreover, GPCRs constitute the largest class of drug targets and approximately one-third of all drugs on the market act by binding to GPCRs and modifying their intracellular signalling profile.[4]

At the most basic level, all GPCRs are characterized by seven α-helical transmembrane domains (TM) and these consist of an extracellular N-terminal end, three intra- and extracellular loops that act as interhelical linkers, and an intracellular C-terminal tail.[5]

1.1.1 GPCR classification

The most recent classification of GPCRs was made by Fredriksson *et al*. in 2003. They proposed five main families attending to their phylogenetic relationships: Glutamate, rhodopsin, adhesion, frizzled/taste 2, and secretin. This division is referred to as the GRAFS families or GRAFS classification, based on the initials of the family names.[6] The GRAFS classification will be described below along with the A–F classification system of Kolakowski since this method is also used by the International Union of Pharmacology, Committee on Receptor Nomenclature and Classification (NC-IUPHAR) with a slight modification related to frizzled receptors (Figure 1.1).[7]

- The **Rhodopsin Receptor Family or Class A**: This is the largest of the five GPCR families and it has around 701 members.[8] This family is highly heterogeneous when GPCR primary structure and ligand preference are taken into consideration. The diversity does not concern the N-terminal domain, where nearly all of the receptors have a short end, but it is related to the TM region.[9] The rhodopsin family is subdivided into four main groups[10]:

- The *α*-Group of Rhodopsin Receptors, which includes five main clusters: prostaglandin receptors, amine receptors (serotonin, dopamine, muscarinic, histamine, and adrenergic receptors, amongst others), opsin receptors, melatonin receptors, and MECA (Melanocortin/EDG/Cannabinoid/Adenosine) receptors.
- The *β*-Group of Rhodopsin Receptors: This group is formed by 36 receptors such as gonadotropin-releasing hormone receptors (GNRHRs) and the growth hormone secretagogues receptor (GHSR).
- The *γ*-Group of Rhodopsin Receptors is formed by three main branches: The SOG (Somatostatin/Opioid/Galanin and neuropeptide W) receptor cluster, the MCH (melanin-concentrating hormone) receptor cluster, and the chemokine receptor cluster.
- The *δ*-Group of Rhodopsin Receptors is composed of four main branches: The Mas-related receptor cluster, glycoprotein receptor cluster, purine receptor cluster (formyl peptide receptors (FPRs) and nucleotide receptors (P2Y)), and the olfactory receptor cluster, which is the largest cluster of all members.

- The **Secretin Receptor Family or Class B1**: This is a 15-membered family in which all GPCRs have a large extracellular hormone-binding domain, and bind peptide hormones.[11] They have in common between 21% and 67% sequence identity, and nearly all of their diversity is in the N-terminal region. Nevertheless, a disulphide pattern between cysteine residues at the N-terminal site is a common feature of all family members.[12,13] Several examples of the Secretin family are parathyroid hormone receptors (PTHR1, PTHR2) and the glucagon-like peptide receptors (GLP1R, GLP2R).

- The **Adhesion Receptor Family or Class B2**: This is the second largest family and it has 33 members. These receptors are characterized by large C-terminal and N-terminal residues. However, the N-terminal end of most adhesion receptors contains, in a variable number, diverse types of protein domains associated with adhesive functions.[14]

- The **Glutamate Receptor Family or Class C**: This family contains 22 human proteins, including metabotropic glutamate receptors (mGluRs) and taste receptors. These family members are dimeric allosteric multidomain proteins that have a

characteristic extracellular domain. This domain is formed by a cysteine-rich domain (CRD) and bilobate proteins called Venus Flytrap (VFP). CRD is not always present in the N-terminal region.[15]

- The **Frizzled/Taste 2 Family**: Initially, this family was part of the O (Other) family in the A–F classification system, but in the GRAFS classification, it forms a separate family.[9] The main characteristic of this type of receptors is in the N-terminal domain, where they have a cysteine-rich domain (CRD) followed by a hydrophobic linker domain (LD).[16] The ten frizzled receptors (FZD1–10), the smoothened receptor (SMO), and the taste 2 subfamily of taste receptors comprise this group.

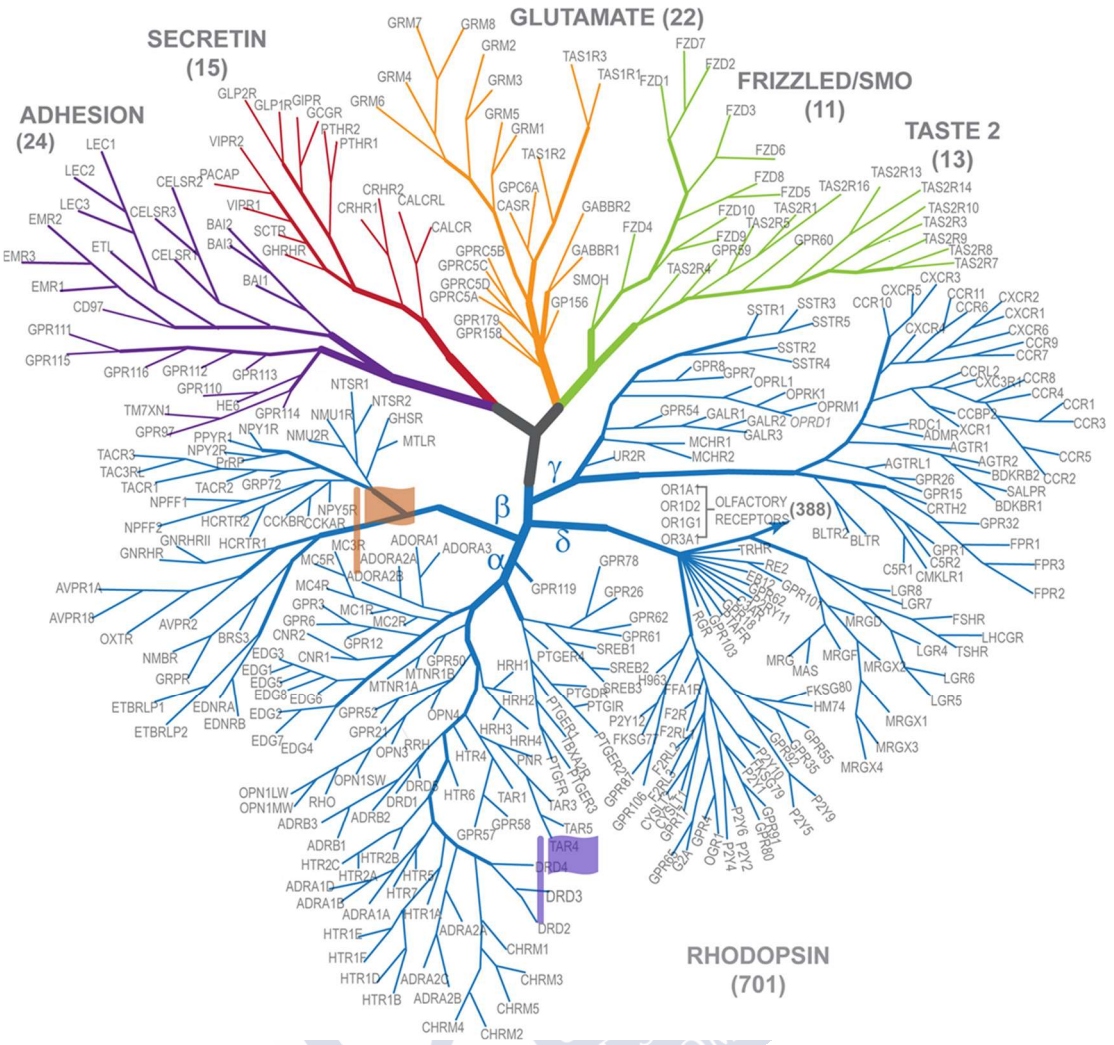

Figure 1.1: GPCR phylogenetic tree. The orange flag indicates the Adenosine A_{2B} receptor (ADORA2B) and the purple flag highlights the dopamine D_2 receptor (DRD2). Both receptors will be discussed in the following sections. Adapted with permission from J. Med. Chem. 2018, 61, 9841−9878. © 2018 American Chemical Society.

1.1.2 GPCR structure

Palczewski *et al.* solved the first GPCR structure in 2000 and this was the crystal structure of bovine rhodopsin from bovine retinal disc membranes (Figure 1.2).[17] The rhodopsin crystal structure revealed a highly organized heptahelical transmembrane bundle bound to 11-*cis*-retinal as a key cofactor in an inactive state. The subsequent GPCR crystal structures obtained also correspond to the dark (inactive) state of rhodopsin.[18] Bearing these two points in mind, subsequent studies employed restrained molecular dynamics to generate two main conformational models (the inactive and active states), which are often referred to as the R and R* states, respectively.[19]

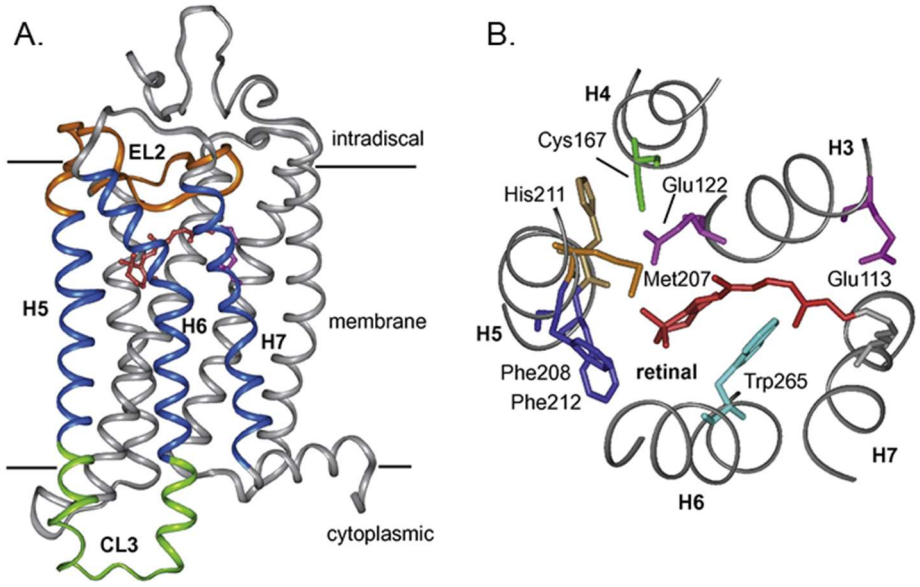

Figure 1.2: Crystal structure of rhodopsin. The first view (A) is through the transmembrane of the bilayer, and the second (B) is an extracellular view of the surface receptor bound to 11-cis-retinal. Reprinted with permission from Elsevier: Elsevier, Progress in Nuclear Magnetic Resonance Spectroscopy 57 (2010) 159–180, © 2010.[20]

However, since the discovery of biased agonism, the classical 'two-state' receptor theory (described above) has been evolving into a multistate dynamic behaviour and it is postulated that GPCRs could generate multiple conformations in response to different ligands. X-ray crystallography may not be an optimal tool to study this new understanding since it only provides a static picture of the ligand-receptor complex. Therefore, Kahsai *et al.* developed a quantitative mass spectrometry strategy to explore conformational changes and dynamics induced by different ligands, with multiple-ligand specific conformations observed.[21]

All GPCRs have an important region for the recognition of their endogenous ligand and this is called the orthosteric site. This is the primary binding site recognized by the endogenous GPCR agonist frequently located in the middle of the seven-transmembrane helical bundle, between the middle plane of the membrane and the extracellular loops, and it has a different shape depending on the nature of the ligand.[22]

Moreover, an allosteric interaction occurs when both the orthosteric site and any additional conformation linked site are occupied by ligands. Allosteric modulators are ligands that interact with a GPCR allosteric site and lead the modulation of the orthosteric site by binding and/or signalling properties.[23]

1.1.3 GPCR signalling

The canonical GPCR signalling was first described as a heterotrimeric G protein structure by Alfred G. Gilman[24] and Martin Rodbell,[25] who shared the 1994 Nobel Prize in Physiology or Medicine for their discovery of 'G proteins and the role of these proteins in signal transduction in cells'. G proteins consist of G_{α}, G_{β}, and G_{γ} subunits that are associated with each other and are bound to the intracellular part of the membrane, where they predominantly relay the receptor activation.[26] The G_{α} subunit contains an inherent guanosine triphosphatase (GTPase) domain implicated in the hydrolysis and binding of the GTP as well as interactions with the other subunits. The G_{β} subunit consists of seven β-propeller structures that have seven WD40 protein sequence repeats. The C-terminus end of the G_{γ} subunit binds to the G_{β} subunit through the fifth and sixth blades, and both subunit N-terminus tails adopt a coiled-coin α-helical conformation. The G_{β} and G_{γ} subunits can only be dissociated under denaturing conditions.[27]

Originally, each GPCR was thought to signal through the dissociation of the G protein heterotrimer. Due to the binding of an agonist to the extracellular site or transmembrane domains of GPCRs, these receptors would act as a guanine nucleotide exchange factor (GEF), and, catalyse the exchange of guanosine diphosphate (GDP) by guanosine triphosphate (GTP), thus allowing both the G_{α} subunit bound to GTP and free $G_{\beta/\gamma}$ complexes to send signals to second-messenger effectors such as cyclic adenosine monophosphate (cAMP), inositol triphosphate (IP_3), and diacylglycerol (DAG).[26,28] The cycle would be completed when the inherent GTPase hydrolysed the G_{α} subunit-GTP bond to trigger the heterotrimer rearrangement.

Nevertheless, since the appearance of concepts such as 'functional selectivity', 'biased agonism' and 'stimulus trafficking', amongst others, pluridimensional signalling efficacy emerged as the main explanation for the GPCR signalling model.[29,30] In this case, there is not only the possibility of multiple receptor active states but there is also a chance of ligand-driven receptor stimulus traffic.[31] Ligand binding results in the inhibition or activation of multiple GPCR-mediated effectors that are often involved in distinct phases of G protein, G protein-coupled receptor kinase (GRK) and β-arrestin signalling.[32]

In other words, the main paradigm of binary GPCR signalling 'on' or 'off' was transformed into the theory that GPCRs act as microprocessors, since they can act by stabilizing a unique, ligand-selective conformation according to the ligand to which they bind to provide various propensities to participate in different transduction pathways.[32,33]

1.1.4 GPCR signal modulation

Once GPCRs had been cloned and expressed *in vitro*, it was perceived that they displayed varying degrees of constitutive or basal activity and could generate active signalling states in the absence of ligands.[22] Endogenous **agonists** (such as hormones or neurotransmitters, and their synthetic analogues) are usually considered to be full agonists. These agonists are ligands that induce 100% of the activity. Compounds that induce agonism, but not at the maximum level of efficacy, are considered as partial agonists.

Antagonists are compounds that block the receptor signal. In relation to the basal activity there are two types of antagonism: neutral antagonists, which maintain the constitutive activity and only block the agonist effect, and inverse agonists which block and decrease the basal activity of the receptor.

All of the above types of compounds bind to the orthosteric site of the receptor and were defined without regard to the functional selectivity or biased signalling. This new insight leads to the possibility of developing novel drugs that target the orthosteric site to enhance the therapeutic effects while decreasing side effects.

Biased signalling refers to the phenomenon in which GPCRs can act to stabilize a certain conformation depending on the ligand to which they bind, thus leading to the beneficial pathway.[32] This phenomenon can be divided into three different cases (Figure 1.3): ligand bias, receptor bias, and system bias.[34]

- Ligand bias signalling: This concept refers to a situation where diverse compounds bind to the orthosteric binding site of the same receptor and induce different signalling pathways between them (Figure 1.3B).

- Receptor bias signalling: In this case the same ligand causes different responses to several receptors (Figure 1.3C).

- System bias: This is also referred to as 'tissue bias' or 'cell bias'. This concept describes the phenomenon where a ligand for a given receptor activates different pathways in a specific manner depending on the species, the tissue, or the cell (Figure 1.3D).

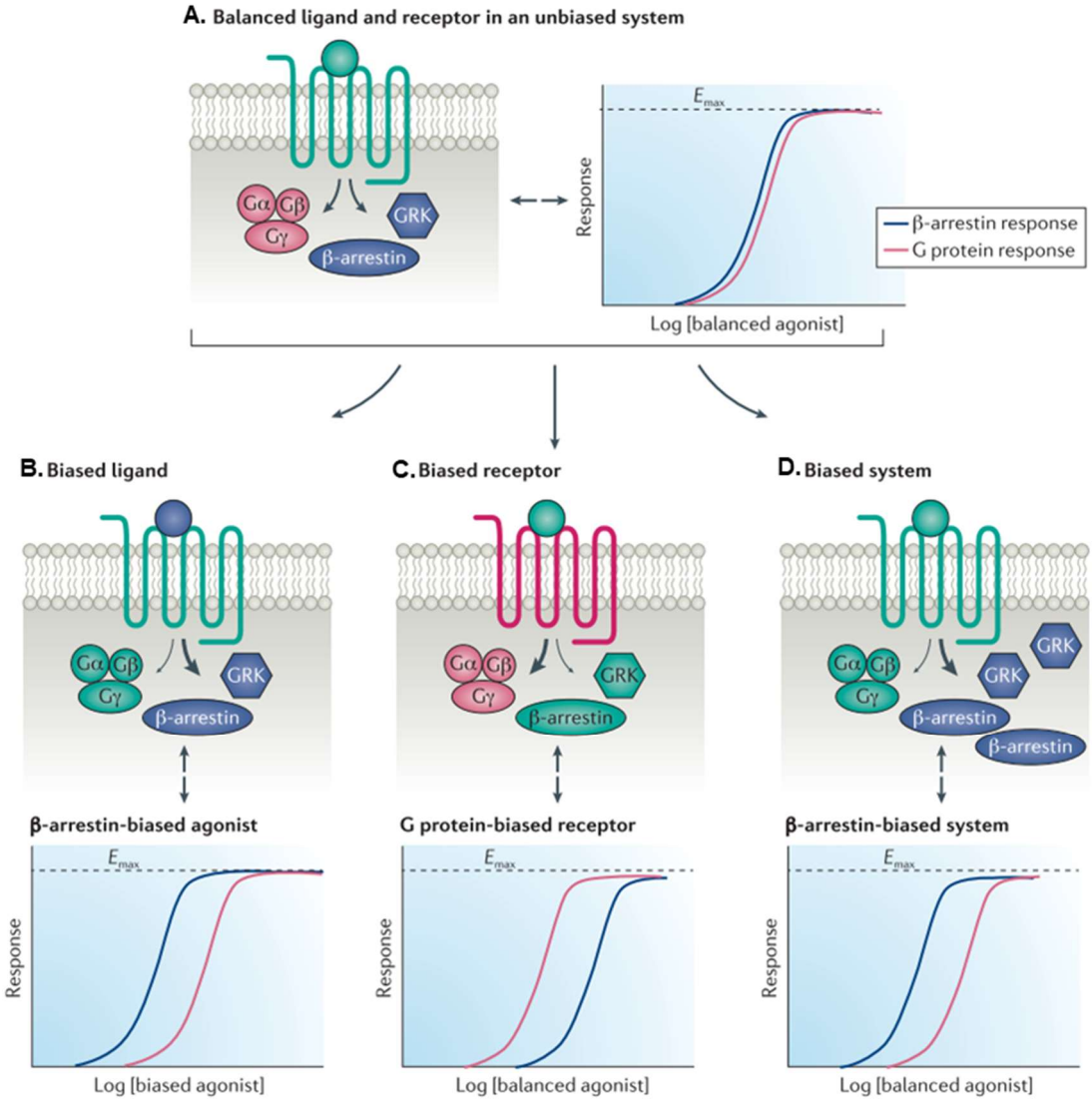

Figure 1.3: A. Balanced ligand and receptor in an unbiased system. This agonist may produce equivalent responses by two different pathways, such as *β*-arrestin and G protein. B. Biased ligand. The ligand-receptor-effector complex generates a certain conformation that preferentially signals by a certain pathway (*β*-arrestin-biased) related to other pathways (G protein biased). C. Biased receptor. The lack of certain receptor sites, such as the C-terminal phosphorylation site necessary for *β*-arrestin recruitment, signal preferentially through one pathway, in this case G protein-biased signalling. D. Biased system. This may be due to differential expression of signalling effectors or other cofactors. Reprinted with permission from Elsevier: Elsevier, Nature Reviews Drug Discovery 17 (2018) 243-260, © 2018.

A prototypic example of a biased compound is TRV027 (Figure 1.4), a biased ligand of the angiotensin II type 1 receptor (AT_1R), which antagonizes the angiotensin-stimulated G protein activation pathway while stimulating the β-arrestin pathway.[35] This compound is under clinical trials for the treatment of acute heart failure. Theoretically, this ligand would provide beneficial effects on the renin-angiotensin-aldosterone system blockade while avoiding potentially adverse effects on cardiac performance.[35]

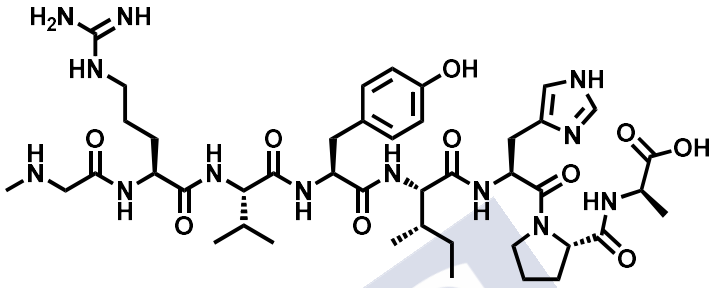

Figure 1.4: Structure of TRV027

After the discovery of diverse receptor sites that are topographically distinct from the orthosteric pocket (*e.g.*, allosteric sites), allosterism has quickly become an emerging paradigm in the development of new drugs. An allosteric interaction is defined as an interaction between two topographically distinct binding sites on the same receptor.[36]

At the most basic level, allosteric modulators can be classified as follows (Figure 1.5):[37]

- Positive allosteric modulators (PAMs): These compounds can considerably enhance the potency of the endogenous ligand when they bind to the orthosteric site by promoting its binding or reducing the energy barrier involved in the shift to the receptor active state.[38]

- Negative allosteric modulators (NAMs): These ligands can decrease the efficacy or potency of the endogenous agonist. Two different mechanisms can be involved: These compounds (i) might stabilize a lower affinity receptor conformation by triggering a decrease in the agonist affinity and (ii) they can raise the energy barrier for a transition to the receptor active conformation, or both.[38]

- Silent allosteric modulators (SAMs): These compounds bind to the allosteric site of the receptor but fail to modulate the subsequent signal transduction. Nonetheless, these modulators can perform as competitive inhibitors by blocking the same allosteric site at which PAM and NAM act. Even though SAMs are not very useful for a therapeutic standpoint, they can be valuable tools to reveal whether the presumed PAM or NAM effects are receptor-mediated.[39]

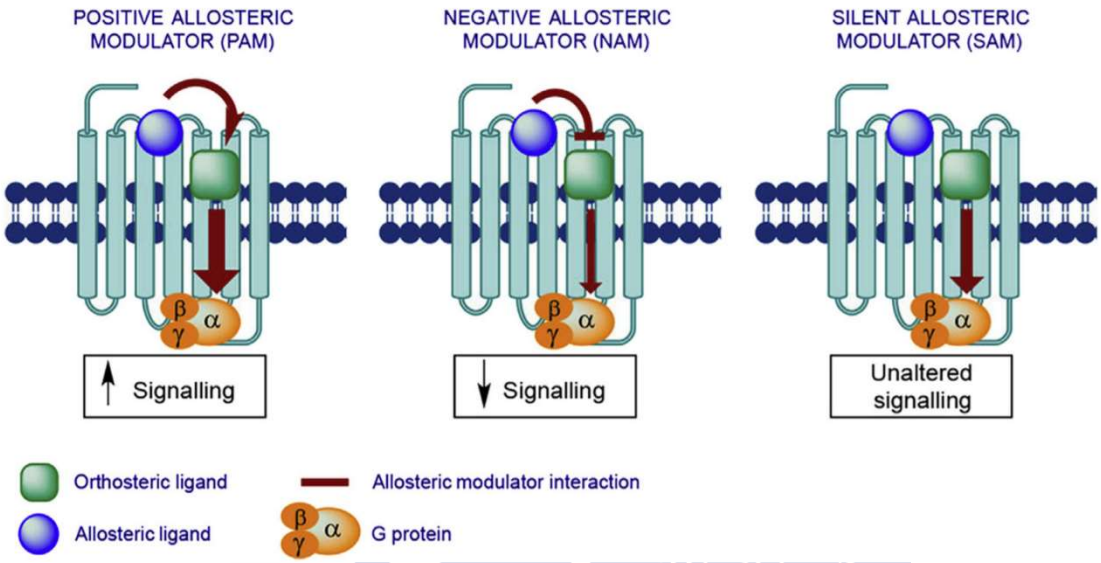

Figure 1.5: Different types of allosteric modulators. Reprinted with permission from Elsevier: Elsevier Books GPCRS: Structure, Function, and Drug Discovery (Chapter 11) by López-Rodríguez, M. L., Benhamú, B., Vázquez-Villa, H., © 2020.[40]

The major disadvantage of all of these modulators is that they do not have any effect in the absence of an orthosteric ligand (endogenous or exogenous). Currently, only three allosteric modulators have been approved for their commercial distribution, although there are many examples under clinical trials. One is a PAM, cinacalcet, and two are NAMs, maraviroc and plerixafor (Figure 1.6). Cinacalcet is an orally bioavailable positive allosteric modulator of the calcium-sensing GPCR receptor approved by the FDA and marketed in the USA since 2004. Cinacalcet is indicated for the treatment of secondary hyperparathyroidism (HPT) in patients with chronic kidney disease (CKD) who are on dialysis, and for the treatment of hypercalcaemia in patients with parathyroid carcinoma.[41] Maraviroc is an orally bioavailable negative allosteric modulator approved in 2007 as the first-in-class chemokine GPCR CCR5 receptor antagonist by the FDA for use in human immunodeficiency virus (HIV) treatment-experienced patients.[42] Finally, plerixafor was approved in 2008 by the FDA in

combination with granulocyte colony-stimulating factor. These compounds act by mobilizing haematopoietic stem cells to the peripheral blood for their collection and subsequent autologous transplantation in patients with multiple myeloma and non-Hodgkin's lymphoma.[43]

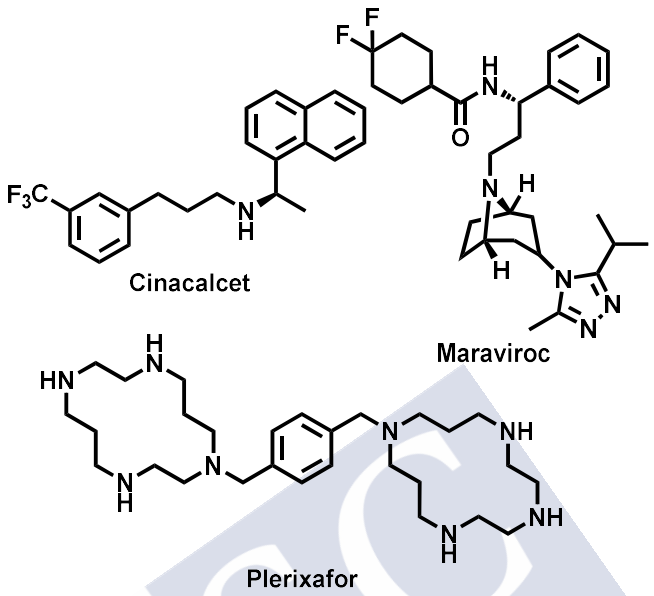

Figure 1.6: Allosteric modulators in clinical use.

Compounds that bind simultaneously to both orthosteric and allosteric sites, were subsequently developed and these were named as '**bitopic**' or '**dualsteric' ligands**. This concept is derived from Schwyzer's 'message-address' concept published in 1977.[44] Initially these ligands consisted of two parts connected by a linker: the 'message' part that binds to the receptor activation site, and the 'address' part that guides the compound to the interested receptor or receptor subtype. If the message part is the pharmacophore that binds to the orthosteric site of the receptor, and the address part is a molecule that can interact with the allosteric binding pocket, these ligands can be referred to as orthosteric/allosteric compounds or, in short, as dualsteric or bitopic ligands. In this case, the orthosteric receptor activation is modulated by the allosteric moiety triggering a novel quality of signal (Figure 1.7).[45]

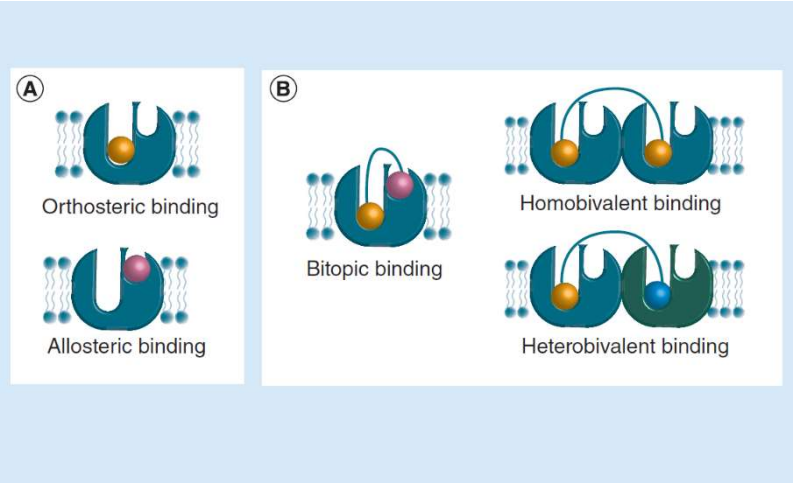

Figure 1.7: Different types of binding mode. A. Classical binding mode with orthosteric and allosteric ligands. B. Multivalent ligand mode with a single receptor (bitopic ligands) or with dimers (homobivalent ligands for two identical receptors or heterobivalent binding for two different receptors). Republished with permission of Future Science Ltd, from Kopinathan A, Scammells PJ, Lane JR, Capuano B. Multivalent approaches and beyond: novel tools for the investigation of dopamine D_2 receptor pharmacology. Future Med Chem. 2016;8(11):1349-1372; permission conveyed through Copyright Clearance Center, Inc.

However, variations in the bitopic binding mode can also be expected, such as a situation wherein ligand binding occurs only with the orthosteric pocket or with an allosteric site. This type of attachment mechanism is called 'flip-flop' and it is virtually indistinguishable from a single compound that will bind to both pockets.[46] Another possibility is a cooperative binding wherein the compound adopts two simultaneous poses at the same receptor, although one might expect to see evidence of this mechanism under suitable experimental conditions.[46] All of these mechanisms should be taken into account for the design and validation of novel bitopic ligands (Figure 1.8).

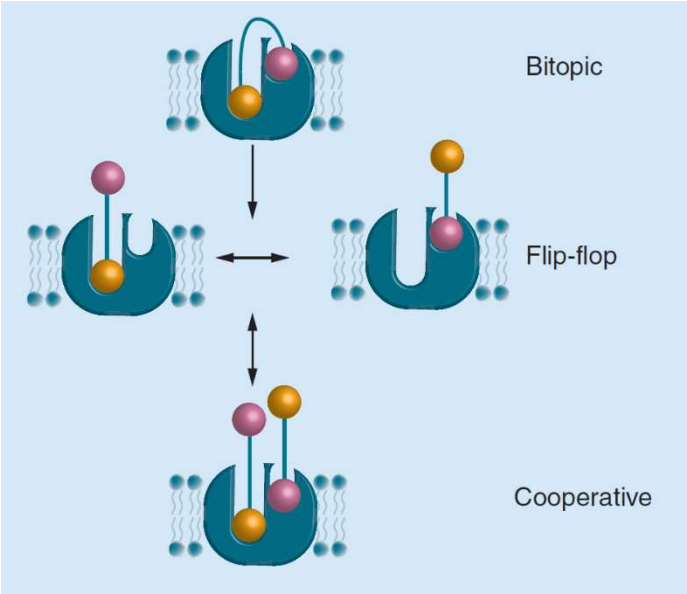

Figure 1.8: Variations in the bitopic binding mode. Republished with permission of Future Science Ltd, from Kopinathan A, Scammells PJ, Lane JR, Capuano B. Multivalent approaches and beyond: novel tools for the investigation of dopamine D_2 receptor pharmacology. Future Med Chem. 2016;8(11):1349-1372; permission conveyed through Copyright Clearance Center, Inc.

One of the first examples of bitopic ligand was discovered by Christopoulos *et al.*,[47] who developed a series of truncated McN-A-343 analogues, including a muscarinic acetylcholine receptor (mAChR) partial agonist that can also interact allosterically at the M_2 mAChR (Figure 1.9). The analogues contain minimal residues of 3-chlorophenylcarbamate (DDBL-4 and DDBL-5), and they were identified as pure allosteric modulators (Figure 1.9).[47] This new information allowed the authors to identify McN-A-343 as a bitopic ligand.

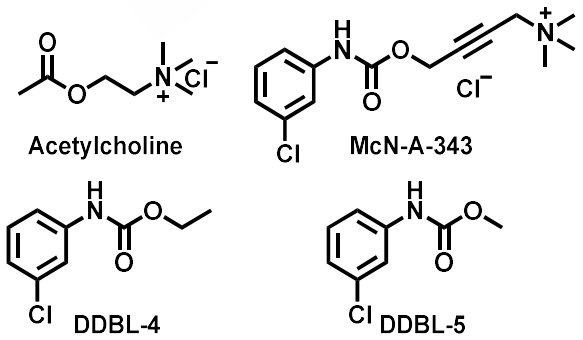

Figure 1.9: The endogenous ligand acetylcholine with the bitopic ligand McN-A-343 and its derivatives synthetised in the laboratory of Chistopoulos *et al.*

Moreover, it is now widely accepted that several GPCRs can form oligomers with receptor conformational rearrangements that can influence their signalling thus, opening

a new possibility for the development of novel drug candidates with increased efficacy and selectivity.[48]

These compounds are known as 'bivalent' ligands and are composed of two pharmacophoric moieties connected through a linker. If both pharmacophores are identical, which means that they will target two identical receptors, the compounds are termed 'homobivalent' ligands. If the target GPCRs are different, they are called 'heterobivalent' ligands.[49] The main problem with this type of compound is their large size, the consequence of which is that the molecular weight reduces their bioavailability and limits their performance in studies *in vivo*. Although these limitations are not insurmountable and several bivalent ligands have shown interesting *in vivo* pharmacological activities, *e.g.*, MDAN-21[50] or SR141716,[51] none of these compounds have entered a clinical trial (Figure 1.10).[49]

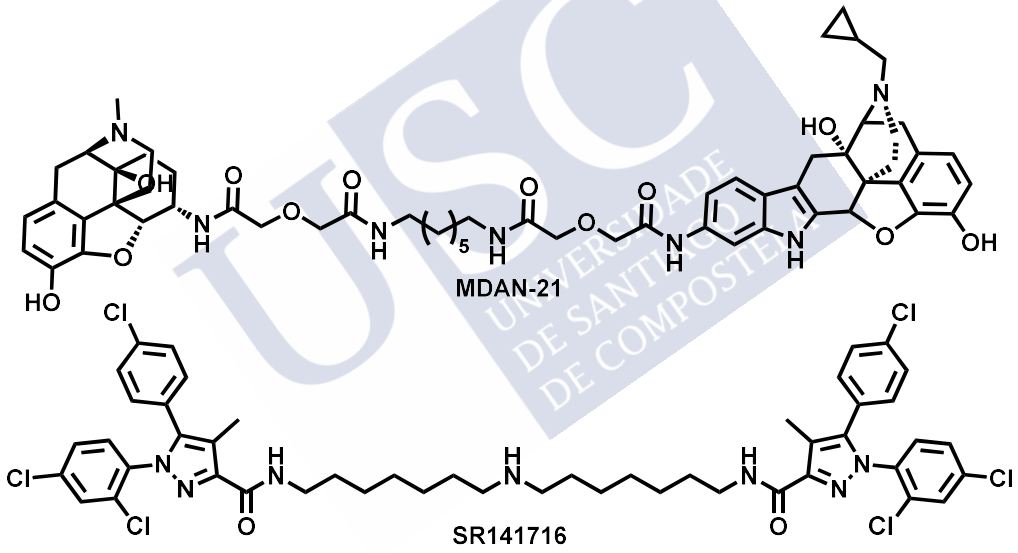

Figure 1.10: Examples of bivalent ligands.[50,51]

1.1.5 Development of novel ligands

Despite improvements in the understanding of GPCR signalling, as well as in the development of innovative and promising ligands, novel, faster, and more efficient synthetic strategies are needed. Most of the current approaches lack an important feature, namely the ability to produce ligands in a sustainable and affordable way.[52]

Medicinal Chemistry strategies are generally, multistage, tedious, highly wasteful processes, and often involve the use of toxic materials. The development of promising ligands is systematically becoming more and more cost- and resource-inefficient and

environmentally unfriendly, while novel commercial drugs are continually decreasing in number.[52]

The rapid development of novel ligands is essential to overcome the issues outlined above. Synthetic strategies such as multicomponent or click reactions allow for the facile, automatic, and high throughput production of diverse libraries of small organic compounds.[53]

Multicomponent reactions (MCRs) are defined as convergent synthetic reactions in which three or more reactants are combined in one step to yield a single product that contains most of the atoms (preferably all) from the starting materials (Figure 1.11).[54]

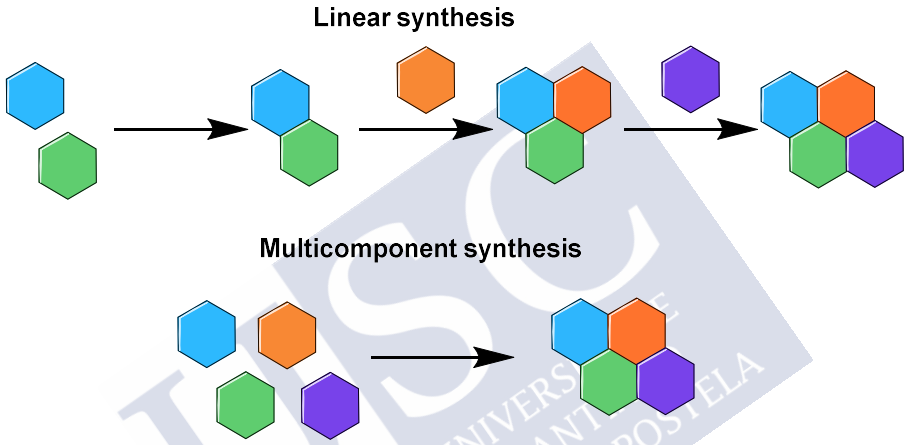

Figure 1.11: General schemes for the linear and multicomponent syntheses.

In view of the current standard guidelines for the green pharmaceutical production defined in 1998 by Anastas and Warner as the Twelve Principles of Green Chemistry,[55] MCRs are generally very favourable. By definition, MCRs have an excellent atom economy and this means that these types of reactions are designed to maximize the incorporation of all of the molecules used in the process into the final compound. Less dangerous reagents are chosen for MCRs to generate substances that have little or no toxicity to the environment and human health. Besides, these processes have a very high bond-forming-index (BFI), for example, several non-hydrogen atom bonds are formed in one synthetic transformation.[56] MCRs provide step economy and, as a consequence, fewer solvents and auxiliary substances are required and, the number of reactions and purification steps is minimised.[57] Furthermore, MCRs can be carried out with a wide range of solvents (often safer and renewable, such as water), they are performed at room

temperature, and they involve the simultaneous formation of several new bonds in just one synthetic step.[57]

Many basic MCRs are classical named reactions such as Strecker,[58] Mannich,[59] Hantzsch,[60] Petasis,[61] and Passerini,[62] amongst others (Figure 1.12), but this thesis is focused on Biginelli[63] and Ugi[64] reactions.

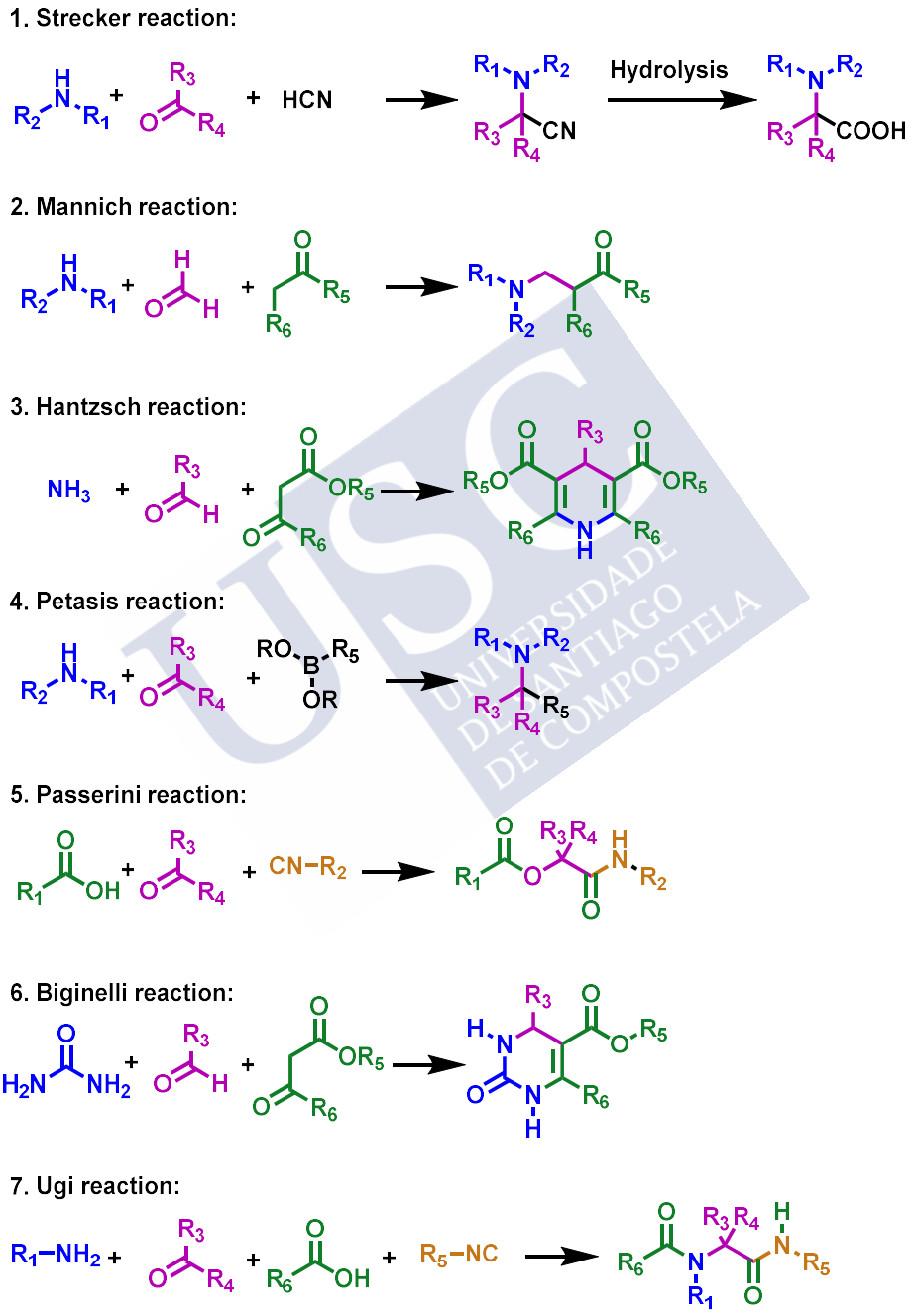

Figure 1.12: Several examples of MCRs.

The **Biginelli reaction** was discovered by Pietro Biginelli in 1893[63] and originally involved the reaction of ethyl acetoacetate and urea in the presence of benzaldehyde in

ethanol with a catalytic amount of hydrochloric acid under reflux conditions. The product of this reaction, which was precipitated by cooling the reaction mixture, was identified as 3,4-dihydropyrimidin-2(1*H*)-one (DHPM).[65]

Diverse proposed mechanisms for the Biginelli reaction have been discussed in several reports (both experimental and theoretical). Three main mechanisms that involve protonated intermediates have been proposed (Scheme 1.1).

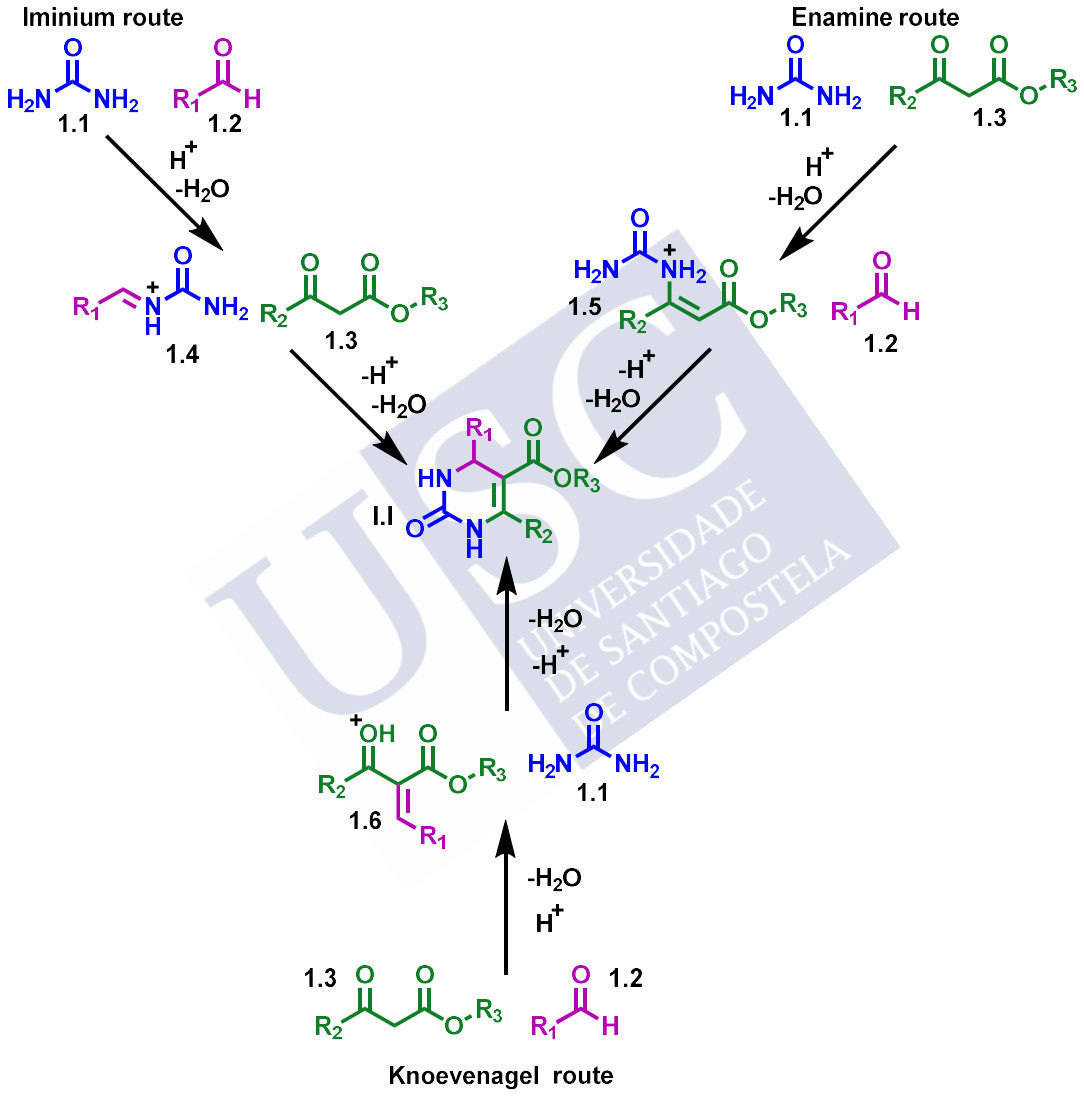

Scheme 1.1: The three possible mechanisms described for Biginelli reactions.

The first mechanism is called the 'iminium route' and involves a condensation between urea and aldehyde to give an iminium intermediate (**1.4**), which undergoes a nucleophilic addition with a *β*-ketoester to form the Biginelli adduct (**I.I**).[66] The second mechanism, the 'enamine route', begins with condensation between a *β*-ketoester and urea to give a protonated enamine intermediate (**1.5**), which reacts with aldehyde to

form DHPM. [66] The third mechanism proceeds through the Knovenagel pathway, in which a carbenium ion intermediate (**1.6**) is formed by the reaction between an aldehyde and *β*-ketoester, which reacts with urea to give DHPM.[66]

Several catalysts such as Lewis/Brønsted acids, ionic liquids, biocatalysts or organocatalyst can be used to enhance the Biginelli reaction yield.[67]

Even though the Biginelli reaction was formerly associated with DHMP, which is the most representative scaffold, variations of all building blocks can create large Biginelli compound libraries and give rise to a wide variety of scaffolds (Scheme 1.2), which were shown to exhibit a broad spectrum of biological activities such as antihypertensive, antibacterial, antimalarial or antitumour activity, amongst others.[66,68]

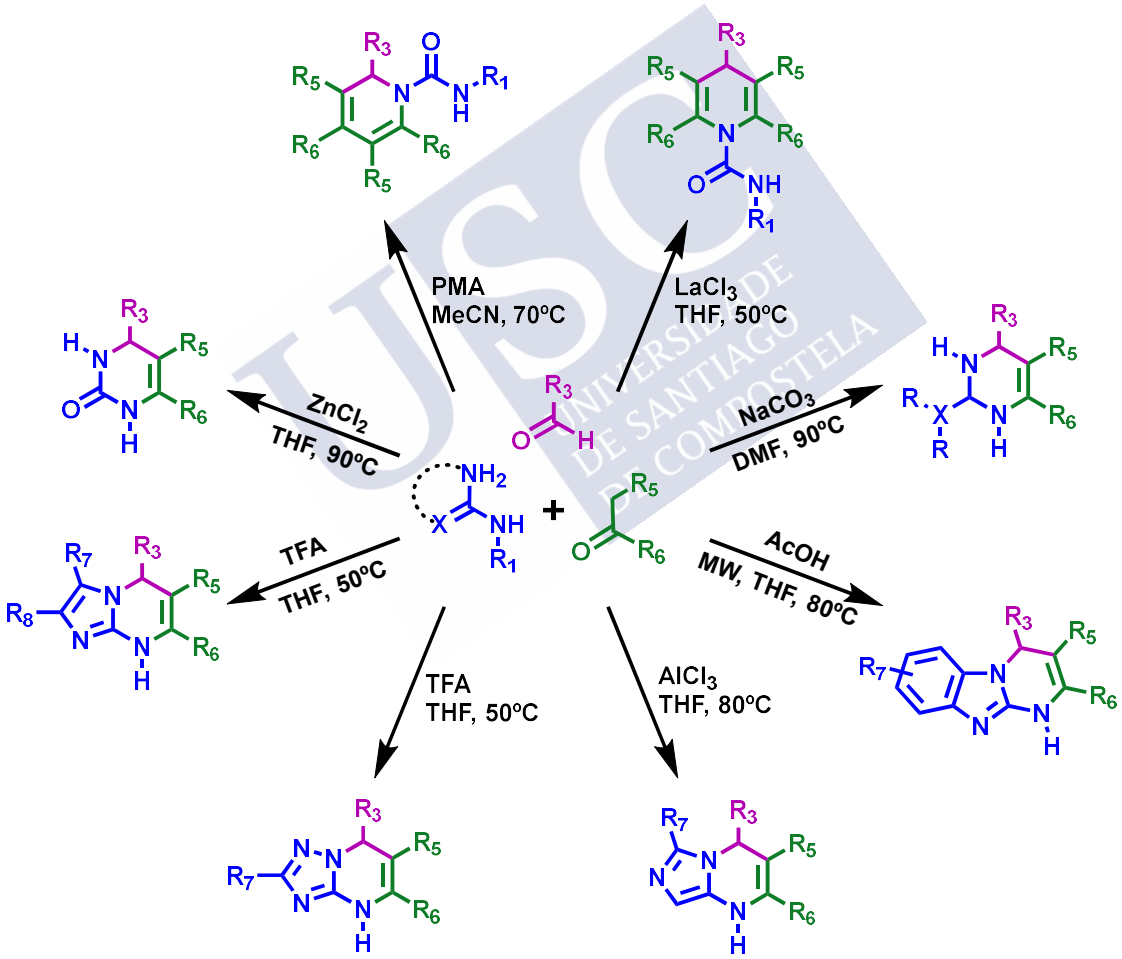

Scheme 1.2: Examples of multiple scaffolds produced by the Biginelli reaction.

The **Ugi reaction** was discovered by Ivar Ugi in 1959.[64] The classical reaction involves the condensation of a primary amine, a carbonyl compound (aldehyde or ketone), an isocyanide and a carboxylic acid to give *α*-acylamino amides.[69]

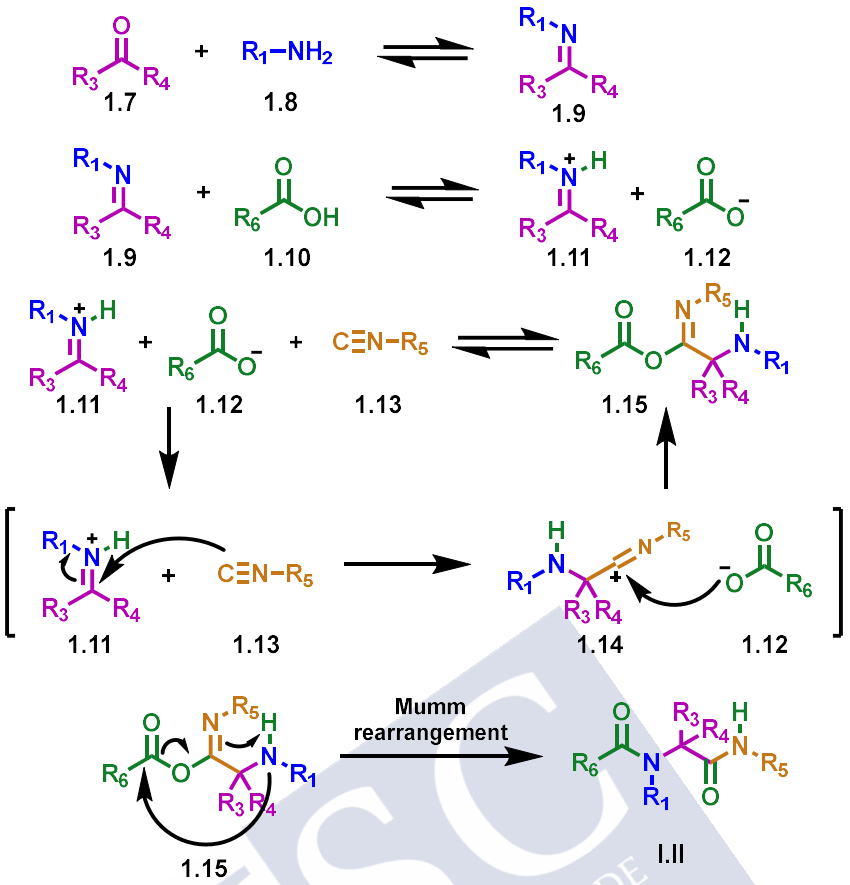

Scheme 1.3: The mechanism of the Ugi reaction.

The most widely accepted mechanism for this reaction (Scheme 1.3) begins with the formation of the imine from the condensation of the carbonyl compound and the amine. In the next step the nitrogen atom of the imine is protonated by the carboxylic acid to give an iminium ion and, thus increasing the electrophilicity of the C=N bond. The iminium ion is then attacked by the isonitrile to generate an α-adduct (**1.14**) that contains a highly electrophilic centre (nitrilium ion) and this is simultaneously attacked by the carboxylate ion. The structural analogy between the α-adduct (**1.15**) and acid anhydrides (one of the oxygen atoms has been replaced by an N–R group) explains their behaviour in the reaction medium. Anhydrides are acylating agents, along with their nitrogenous analogues and the closest acylable atom is the nitrogen in the amine.[70] Finally, intramolecular acylation and hydroxylamine-amide tautomerism generate the Ugi product (**I.II**). This last acylation is known as the Mumm rearrangement.[71]

It is revealing to follow the changes in the nucleophilicity and electrophilicity of the different components and intermediates during this MCR. Initially, the C=N bond of the imine behaves as a base against the acid component. Subsequently, the protonated

Schiff base (**1.11**) functions as the electrophile and the acid anion as the nucleophile in the α-addition reaction. As a consequence of the isonitrile α-addition, a highly electrophilic nitrilium ion (**1.14**) is generated while the nitrogen atom of the amine recovers its nucleophilic character, thus making the transfer of the acyl group viable.[70]

All steps in this sequence of reactions are in balance. However, the Mumm rearrangement gives rise to a very stable α-acylamino amide (**I.II**), which irreversibly displaces the reaction equilibrium toward product formation.[70]

The Ugi reaction is probably the most important of the MCRs.[71] Due to its broad range of modifications and variations, it is widely used in the pharmaceutical industry to prepare collections of compounds (Scheme 1.4A).[72–74] As an example, this approach could allow the formation of local anaesthetics, such as lidocaine and its derivatives (Scheme 1.4B).[75]

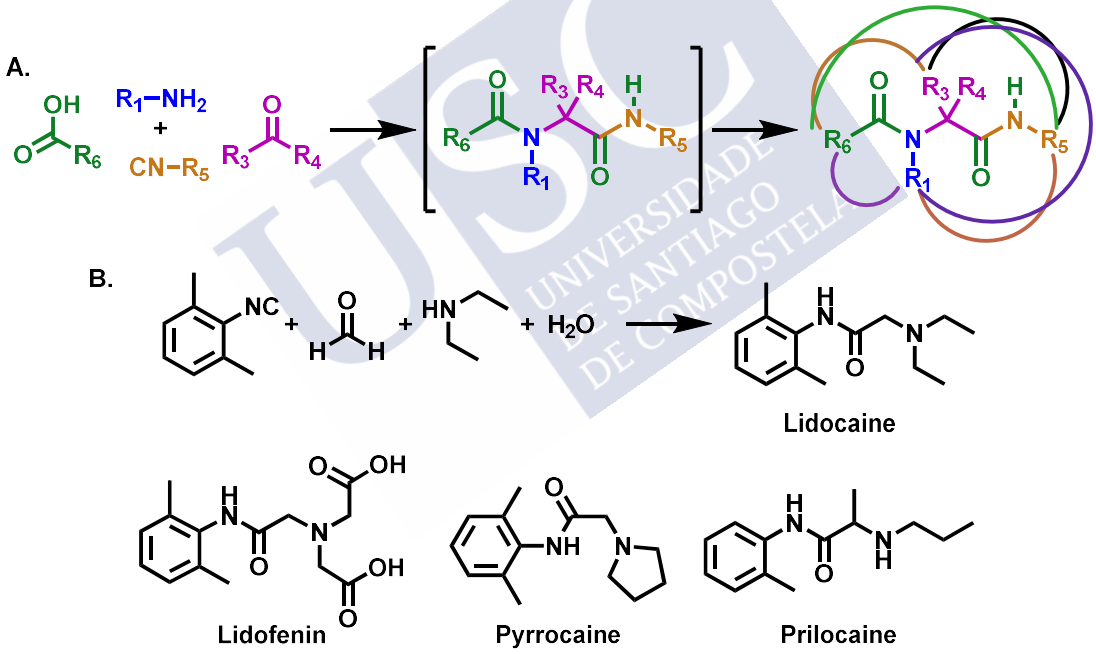

Scheme 1.4: A. Possible ways for diversification for the Ugi reaction. B. Synthesis of local anaesthetics using the Ugi reaction.

Prior to briefly explain adenosine and dopamine receptors, it is also worth highlighting the role of click reactions in the acceleration of synthetic processes. This reaction was the main synthetic tool used during my research stay in Research Institute for Medicines, at Universidade de Lisboa (iMed.Ulisboa) (**Appendix 1**). Click chemistry, particularly the 1,3-dipolar cycloaddition, has been attracting considerable attention in recent years. In the context of the identification of novel, efficient, rapid,

and environmentally friendly synthetic approaches, it includes powerful reactions to develop heteroatom linkages (carbon-heteroatom-carbon bonds) in an aqueous environment to give rise to 1,4-disubstituted or 1,5-disubstituted 1,2,3-triazoles as a regioselective synthesis depending on whether the reactions were catalysed by copper or ruthenium, respectively (Scheme 1.5).[76]

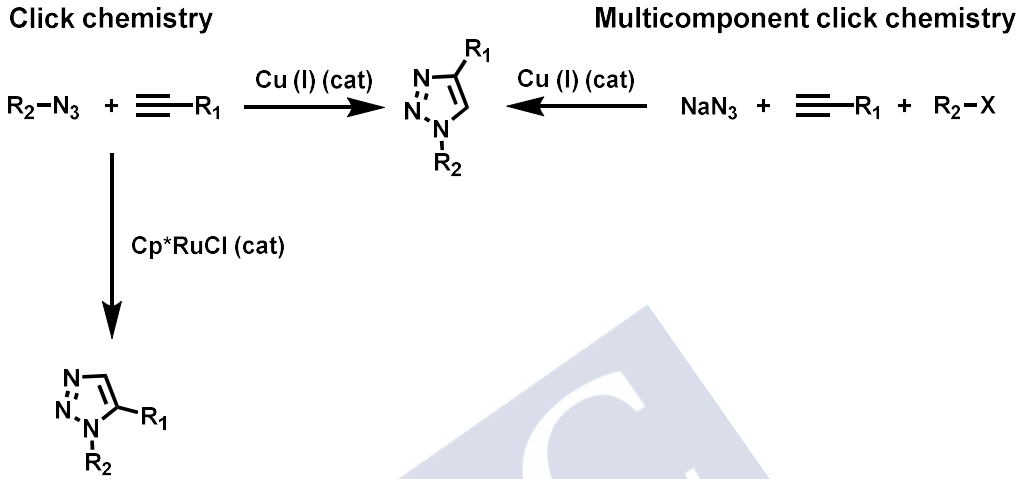

Scheme 1.5: General scheme for click chemistry and the multicomponent variation.

Furthermore, a multicomponent click reaction has emerged recently for the synthesis of 1,4-disubstituted 1,2,3-triazoles and this is catalysed by copper from an *in situ* acidolysis of halides in the presence of alkynes (Scheme 1.5).[77]

The chemistry outlined above has been applied in many different areas, such as organic synthesis, bioconjugation, drug discovery and even polymer and material sciences.[78] The general mechanism for the copper(I)-Catalysed Azide-Alkyne Cycloaddition (CuAAC) is shown in Scheme 1.6.

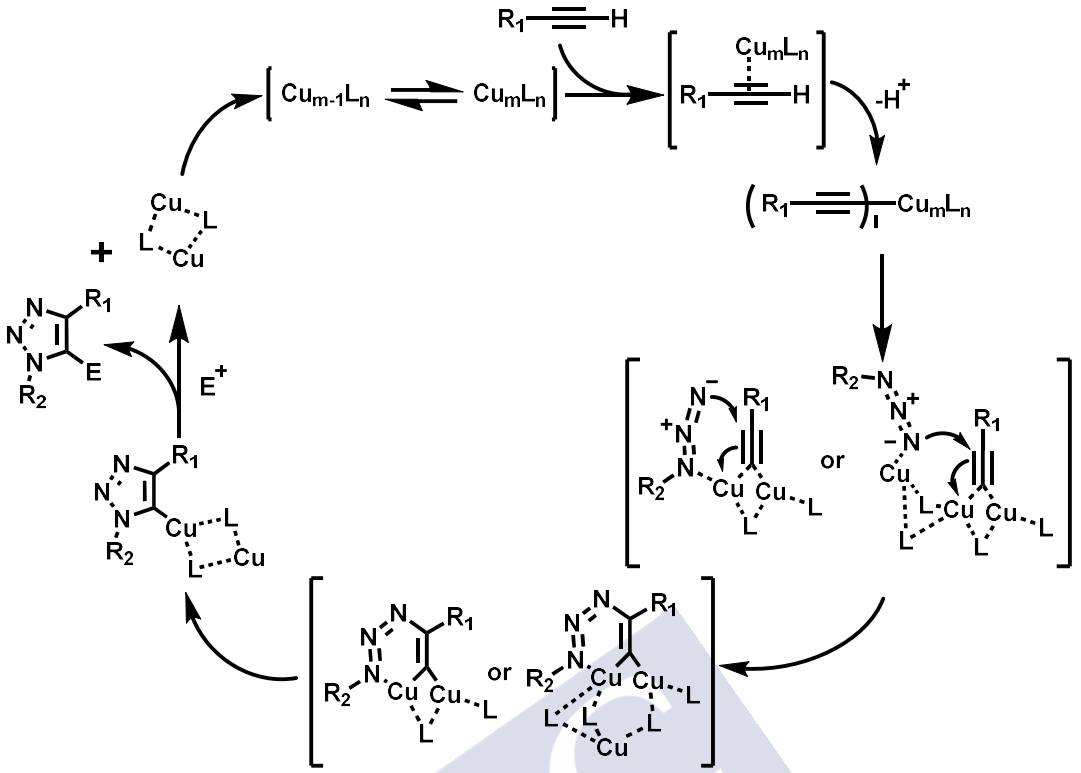

Scheme 1.6: General mechanism for the CuAAC reaction.[79] Reprinted (adapted) with permission from Chem. Rev. 2008, 108, 8, 2952–3015. Copyright (2008) American Chemical Society.

1.2 ADENOSINE RECEPTORS

Adenosine (Figure 1.13) is a ubiquitous purine nucleoside whose importance for human health cannot be neglected, as it regulates the function of every tissue and organ in the body.[80] This compound is structurally and metabolically related to bioactive nucleotides (adenosine triphosphate (ATP), adenosine diphosphate (ADP), adenosine monophosphate (AMP), cAMP, ribonucleic acids (RNA), coenzyme A, nicotinamide adenine dinucleotide (NAD^+), and flavin adenine dinucleotide (FAD)) (Figure 1.13). In addition, adenosine is known to take part in several metabolic pathways and its intracellular concentrations can never be zero, thus it is produced both extra- and intracellularly following the activity of specific enzymes and a certain level of adenosine will be at the extracellular space, even under the most basal conditions (in a range between 20–300 nM).[81]

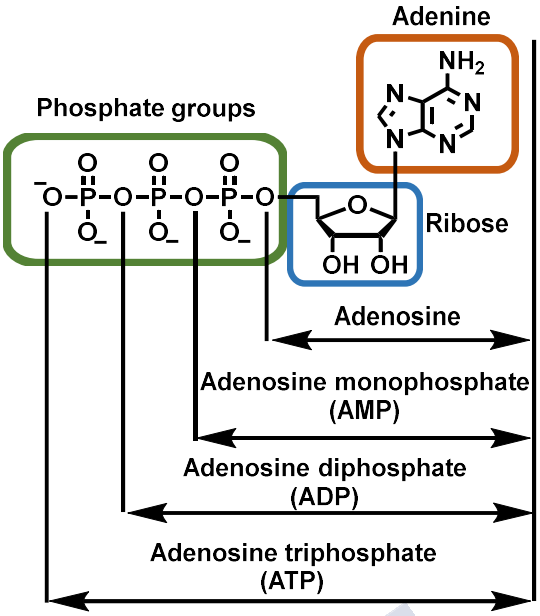

Figure 1.13: Chemical structure of adenosine and its derivatives.

Extracellular adenosine interacts with a family of four cell surface receptors (or GPCRs), namely adenosine receptors (ARs), also called purine P1, which are subdivided into four subtypes[82]: A_1AR, $A_{2A}AR$, $A_{2B}AR$, and A_3AR belonging to the α-Group of Rhodopsin Receptors. Human ARs exhibit high sequence homology; for example, there is 49% of sequence identity between A_1AR and A_3AR and 59% between $A_{2A}AR$ and $A_{2B}AR$.[83] Besides, A_1 and A_3 receptors couple preferentially to G_i protein, which causes inhibition of adenylate cyclase (AC) and hence of the production of cAMP, whereas $A_{2A}AR$ and $A_{2B}AR$ receptors are coupled to G_s or G_o proteins, which stimulate the production of cAMP.[84]

AR activation effects tend to be cytoprotective in several organs and tissues under a wide variety of physiological conditions. Extracellular adenosine levels can increase significantly in response to stress, such as hypoxic stress, and this leads to AR activation that acts to adapt this stress.[85] These receptors are widely expressed in the body and are involved in numerous (not only physiological but also pathological) effects and, for that reason, they are potential drug targets for the treatment of several diseases.[86] However, the persistence of increased adenosine concentrations beyond acute stress can become detrimental to tissues by activating pathways that lead to an immune suppression process. This process has been associated with the generation of an immunosuppressed niche that favours the onset of neoplasia.[87] The immunosuppressive activities of adenosine in cancer are described below.

A summary of several validated therapeutic applications of these receptors is provided in Table 1.1.[85,88]

Table 1.1: Potential therapeutic applications of ARs.

System or process	Receptors				Therapeutic applications
	A_1AR	$A_{2A}AR$	$A_{2B}AR$[89]	A_3AR[90]	
Inflammation		Agonist	Antagonist		Anti-inflammatory
				Antagonist	Antiallergic
		Agonist	Antagonist	Agonist	Antiarthritic
Endocrine system[91]	Antagonist				Improvement of insulin release and effect
Cellular cycle		Antagonist	Antagonist	Agonist	Cell cycle control, tumour growth inhibitor[92]
Vascular system				Antagonist	Antiglaucomatous
Nervous system[93]	Antagonist				Alzheimer, anxiolytic
	Agonist	Antagonist	Antagonist		Analgesic
		Antagonist			Antiparkinsonian
	Agonist	Antagonist		Agonist	Anti-ischemic, neuroprotector
	Agonist	Agonist			Sleep regulation
Respiratory system	Agonist			Agonist	Protector
			Antagonist	Antagonist	Anti-asthmatic, chronic obstructive pulmonary disease
Cardiovascular system	Agonist				Antiarrhythmic
	Agonist			Agonist	Anti-ischemic
			Antagonist	Antagonist	Atherosclerosis prophylaxis[94]
		Agonist	Agonist		Vasodilator
Renal system	Agonist	Agonist		Antagonist	Protector
			Antagonist		Renal interstitial fibrosis[95]
	Antagonist				Diuretic
Hepatic system	Antagonist		Antagonist		Fatty liver formation[96]
Immune system[97]		Antagonist	Antagonist		Experimental autoimmune encephalomyelitis, multiple sclerosis

1.2.1 Adenosine A_{2B} receptor

The first part of this thesis is focused on the optimisation of A_{2B} adenosine receptor (A_{2B}AR) antagonists. It is widely known that A_{2B}AR has the lowest affinity for adenosine, and it requires micromolar concentrations to become functional, while A_1AR, A_{2B}AR and A_3AR receptors only require nanomolar adenosine concentrations to be activated.[98] Hence A_{2B}AR remains silent under resting conditions when extracellular concentrations of adenosine are low, but its role becomes more relevant in pathophysiological conditions when adenosine concentrations are the highest.[98]

A_{2A}AR and A_{2B}AR are the most closely related ARs, with an overall sequence identity of >50%.[86] these receptors are co-expressed in many different cell types and several tissues and organs such as heart, brown and white adipocytes, and many cancers.[99] Moreover, in 2018 Hinz *et al*. demonstrated the existence of A_{2A}AR-A_{2B}AR heteromers in native tissues. In this case, A_{2A}AR is blocked by A_{2B}AR and this explains the altered pharmacology for A_{2A}ARs in tissues where it is co-expressed with A_{2B}AR. [99]

The fact that A_{2B}AR is not stimulated by physiological levels of adenosine suggests that it may play a crucial role in pathophysiological conditions associated with massive adenosine release.[100] An example of these conditions is hypoxia, a phenomenon that occurs in many cancers.[101] The A_{2B}AR and its related transcription factors (hypoxia-inducible transcription factors: HIF-1α and HIF-2α) promote the activation of the adenosine pathway at multiple stages.[102]

There are several pathways involved in the immunosuppressive activities of adenosine in the tumour microenvironment.[103] The immune response regulated by the balance between ATP and adenosine is explained in Figure 1.14.

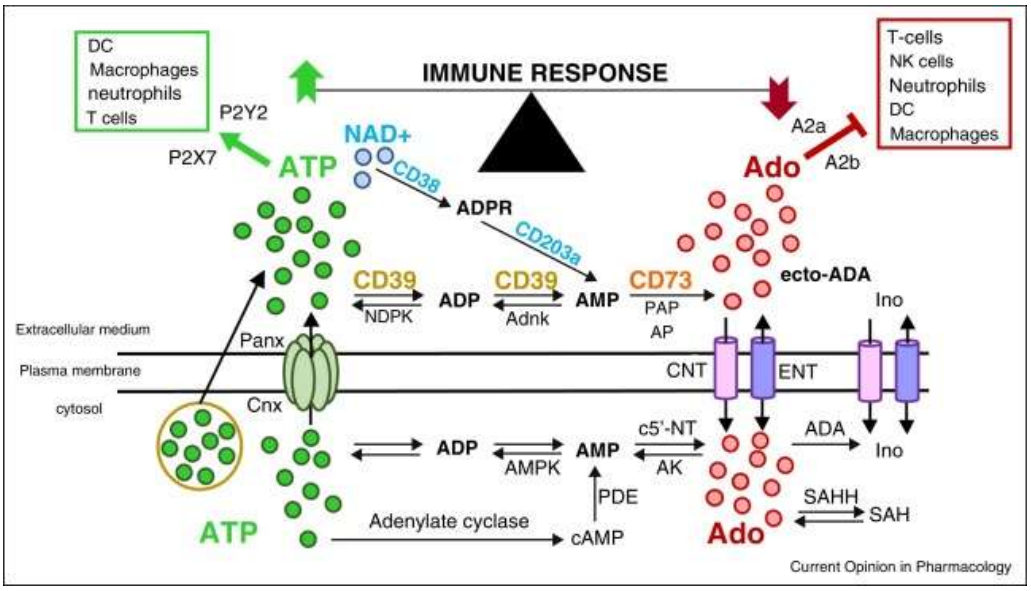

Figure 1.14: The immune response regulated by the balance between ATP and adenosine. Reprinted with permission from Elsevier: Elsevier, Current Opinion in Pharmacology 29 (2016) 7-16, © 2016.

Overexpression of A_{2B}AR has been associated with poor prognosis in patients with several cancer diseases such as triple negative breast cancer (TNBC), multiple myeloma, acute myeloid leukaemia (AML), and liposarcoma.[104] It has been shown that A_{2B}AR signalling can affect the maturation and function of dendritic cells (DCs) during their generation from monocytes, thus leading to the appearance of the DCs peculiar phenotype, which can promote angiogenesis by producing vascular endothelial growth (VEGF).[105] Likewise, this adenosine receptor subtype promotes the expansion of myeloid-derived suppressor cells (MDSCs), which are immunosuppressive cells that develop tumour progression by impairing T-cell responses and/or modulation of angiogenesis, and these produce immunosuppressive and pro-angiogenic mediators (including VEGF) by themselves.[106]

On considering all of the information discussed above, it is worth nothing that the development of A_{2B}AR antagonists may be a useful approach for the suppression of the angiogenesis process that occurs *in vivo* in tumour cells. However, the modulation of this receptor by potent and selective ligands remains challenging. From a structural point of view, A_{2B}AR antagonists are planar heterocyclic compounds that can be classified into two main groups (Figure 1.15): xanthines (appropriately decorated with phenyl/heteroaryl groups at position 8), and nonxanthines, with only a few examples of potent and selective nonxanthine A_{2B}AR antagonists currently known. The structural

elaboration of some of these prototypes has provided potent and selective ligands, some of which have entered clinical trials or preclinical development.[89]

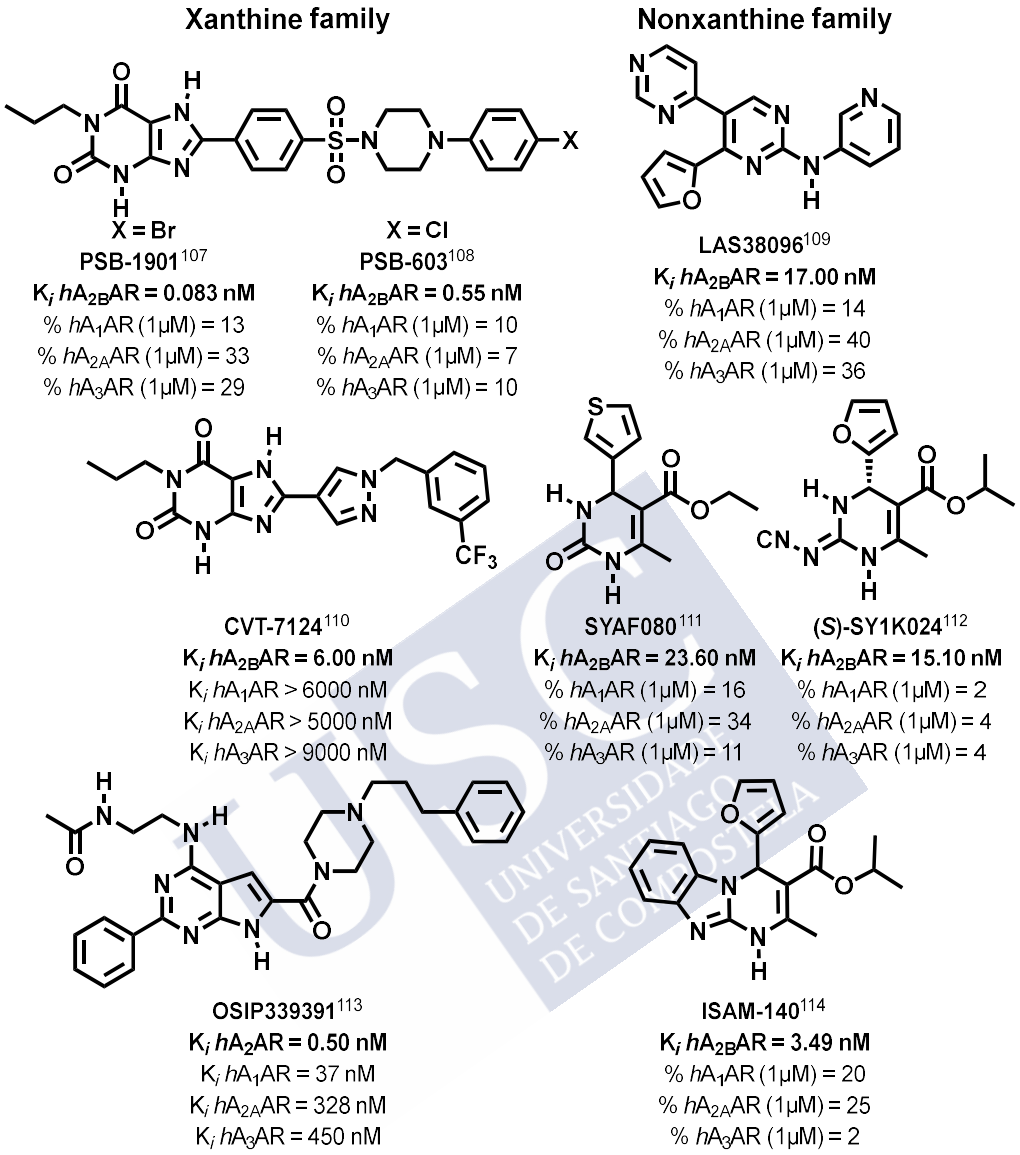

Figure 1.15: Representative structures of A_{2B}AR antagonist families.[107-114]

1.3 DOPAMINE RECEPTORS

Dopamine (DA) is a catecholamine neurotransmitter that is involved in many physiological processes such as motivation, pleasure, cognition, memory, learning, fine motor control, and modulation of endocrine signalling, amongst others, in the central nervous system (CNS).

The dysregulation of dopamine's function has been implicated in the physiopathology of several major human neuropsychiatric disorders such as

schizophrenia, Parkinson's disease, drug addiction, or attention deficit with hyperactivity disorder.[115] This catecholamine interacts with five DA GPCR subtypes (Figure 1.16), which are classified into two families based on their biochemical and pharmacological properties: D_1-like receptors (DRD_1 and DRD_5 subtypes), which are primarily coupled to $G\alpha_{s/olf}$ proteins and stimulate the AC activity and the production of the second messenger cAMP, and D_2-like receptors (DRD_2, DRD_3 and DRD_4), which are coupled to $G\alpha_{i/o}$ proteins to inhibit the production of cAMP (Figure 1.16).[116]

Within the DRD_2 subtype there is another subclassification based on the alternative splicing of 29 amino acids on the third intracellular loop, with distinct physiological signalling and pharmacological properties observed. This gives rise to the isoforms DRD_{2S} (D_2-short receptor) and DRD_{2L} (D_2-long receptor) (Figure 1.16).[116,117]

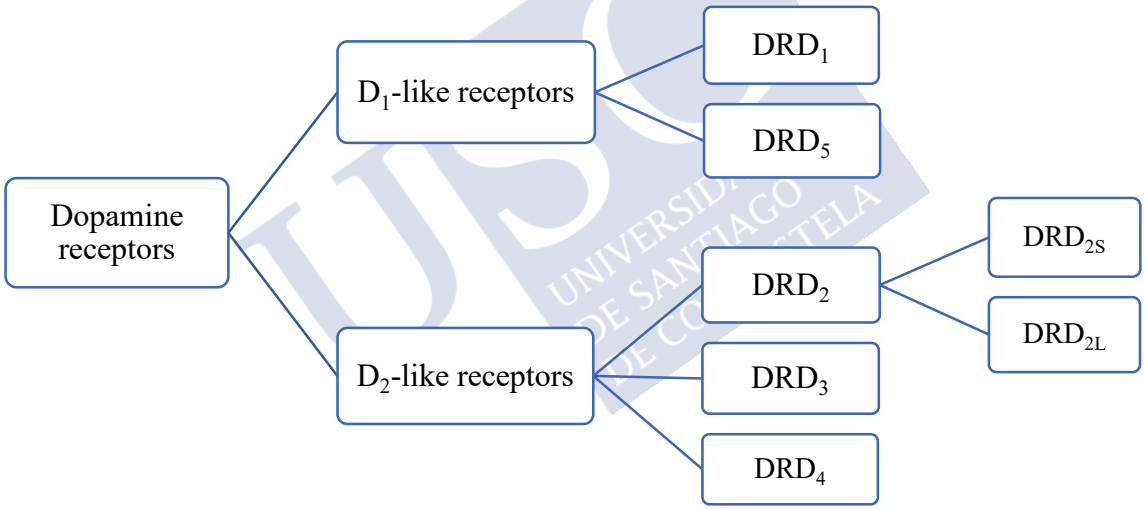

Figure 1.16: General scheme for dopamine receptors.

The most widespread dopamine receptors (DAR), which also have the highest level of expression, are DRD_1 and DRD_2. Most of the DRD_1s are expressed in the cortical plate (CP), nucleus accumbent (Acb), olfactory tubercle (OT), cerebral cortex (Cx), and amygdala.[117] Moreover, this subtype of receptor has been found on the island of Calleja as well as in the subthalamic nucleus. The second member of the D_1-like receptors, DRD_5, is expressed in the hippocampus, lateral mammillary nucleus, and in the thalamus parafascicular nucleus.[117]

Furthermore, DRD_2 has been detected mainly in brain tissues, such as CP, OT, and Acb. DRD_2s are also expressed in the *substantia nigra pars compacta* and in the ventral tegmental area (VTA). Additionally, DRD_2s have been shown outside the brain, in the retina, kidney, pituitary gland, and vascular system.[117]

Meanwhile, DRD_3s are limited to a few brain areas, such as the hypothalamus, few septal nuclei, islands of Calleja, and diverse regions of the thalamus and cerebellum.[117] Finally, DRD_4 seems to be strongly expressed in the amygdala, the olfactory bulb, the frontal cortex, hippocampus, hypothalamus, and mesencephalon.[117]

There is 80% homology between DRD_1 and DRD_5, whilst only 75% and 50% homology is found between DRD_3 and DRD_4, respectively, with respect to DRD_2.[118]

1.3.1 Dopamine D_2 receptor

The second part of this thesis is focused on the discovery of D_2 dopamine receptor ligands. The DRD_2 remains a major target for the development of anti-Parkinson and antipsychotic agents.[119]

Schizophrenia is a complex psychiatric disorder that occurs worldwide and affects around 1% of the world's population. It is characterized by fundamental disturbances in thinking, perception, and emotions.[120] Schizophrenic symptoms are classified into positive (hallucinations, delusions and thought disorder), negative (alogia, anhedonia, avolition, a flat affect and apathy), and cognitive dysfunction (deficit in working memory, executive function, or attention).[121] The dopamine hypothesis of schizophrenia has been one of the most abiding concepts in psychiatry. This hypothesis proposed a mechanism where schizophrenia is characterized by frontal hypodopaminergia resulting in striatal hyperdopaminergia (Figure 1.17). This fact may be due to genetic and environmental risk factors such as markers of social adversity (migration, unemployment, urban upbringing, and childhood abuse), pregnancy/obstetric complications, and the use of psychoactive drugs, amongst others.[122]

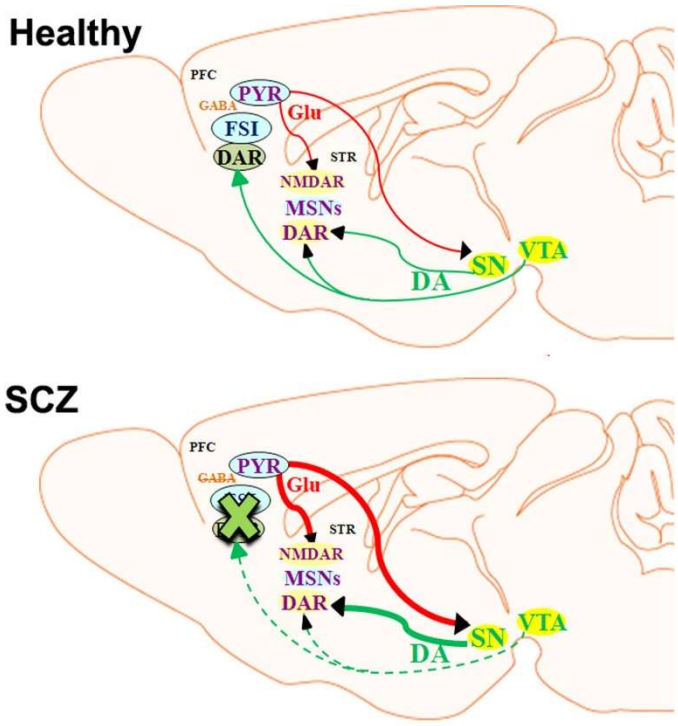

Figure 1.17: Sagittal sections of a mouse brain with a simplified circuit scheme of the dopamine (DA) hypothesis.[123] The first picture shows a healthy mouse brain. DA receptors (DARs) in the prefrontal cortex (PFC) regulate the firing of fast-spiking gamma-aminobutyric acidergic parvalbumin-positive interneurons (FSIs) which control the rhythmic firing of glutamate (Glu) releasing by pyramidal neurons (PYR). It is assumed that the PYR neurons not only regulate the neuronal activity of medium spiny neurons (MSNs) situated in the striatum (MSNs express N-methyl-D-aspartate receptors (NMDAR), and DARs), but also exert an analogous function at neurons located in the midbrain *subtantia nigra pars compacta* (SN), which release DA onto striatal MSNs. Under conditions that mimic the schizophrenia disease (second picture), a decay in levels of dopamine in PFC (hipodopaminergia) or the neuronal activity inhibition of FSIs leads to an enhancement of PYRs excitation. This enriched activity of PYR may trigger enhanced striatal MSNs activity directly or through increased DA release (hyperdopaminergia) in the striatum by SN neurons. Reprinted with permission from Elsevier: Elsevier Biological Psychiatry 81 (2017) 78-85, © 2017.

The pharmacological treatment of this neurological disorder is based on the use of antipsychotic drugs[124] and these are classified as follows:

- Typical antipsychotics, also known as first generation antipsychotics (or FGAs), such as chlorpromazine and haloperidol (Figure 1.18). These drugs are effective in mitigating positive symptoms by blocking the DRD_2 in the mesolimbic dopamine pathway. Nevertheless, the inevitable inhibition of other dopamine pathways triggers some significant adverse effects such as, hyperprolactinemia, tardive dyskinesia (TD), and extrapyramidal symptoms (EPS).[125]

- Atypical antipsychotics, also called second generation antipsychotics (or SGAs). Clozapine was the first drug of this group, followed by risperidone and ziprasidone[126] (Figure 1.18). These compounds act by blocking both serotonin 5-HT_{2A} and dopamine D_2 receptors, thus reducing substantially the presence of EPS and TD side effects. However, their effects on negative symptoms and cognitive dysfunction are still far from ideal, as they have other side effects such as weight gain, hyperlipidemia, and sexual dysfunction.[125]

- Atypical antipsychotics: third generation. Since the discovery of aripiprazole, followed by the breakthrough of cariprazine, a new class of antipsychotics has emerged, namely the third generation antipsychotics (TGAs) has emerged (Figure 1.18). Due to its unique pharmacological profile, aripiprazole is a potent partial agonist at both presynaptic and postsynaptic D_2, and it also acts as a partial agonist at the serotonin 5-HT_{1A} receptor. This drug has a lower propensity to produce motor side effects.[127]

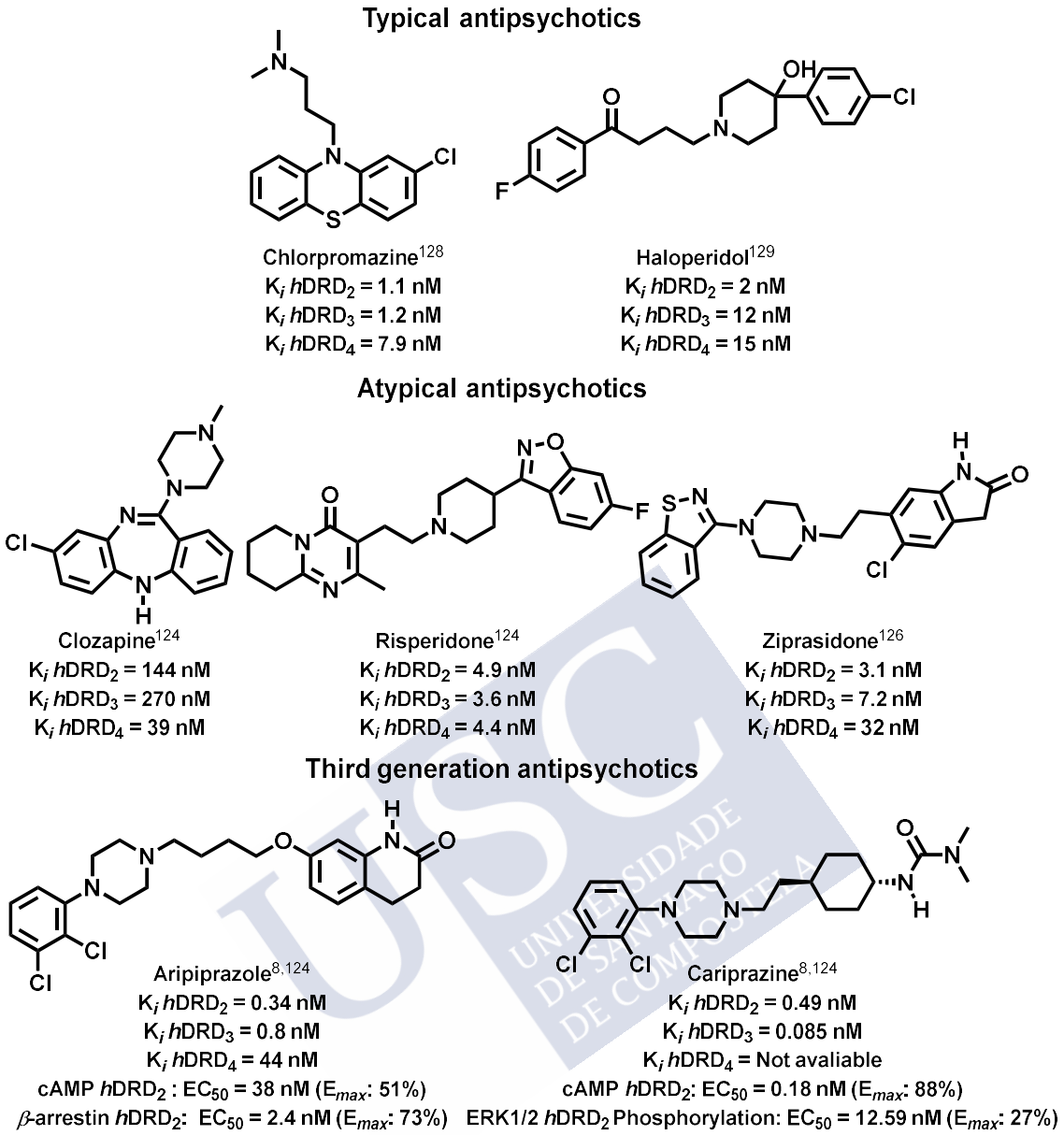

Figure 1.18: Examples of commercial antipsychotic drugs.[8,124,126,128,129]

Nonetheless, after the appearance of phenomena such as 'functional selectivity' or 'biased signalling', and due to the efficacy of pluridimensional signalling, this theory was postulated as the main explanation of the GPCR signaling model (see above). Aripiprazole was classified as a balanced DRD_2 agonist and it can activate a plethora of downstream signalling pathways.[8,130] Therefore, the development of novel biased compounds that increase the functional selectivity for the major signalling arms of the DRD_2 should elucidate their involvement in the therapeutic effects in schizophrenia or other neurological disorders.

1.4 REFERENCES

(1) McCorvy, J. D.; Butler, K. V; Kelly, B.; Rechsteiner, K.; Karpiak, J.; Betz, R. M.; Kormos, B. L.; Shoichet, B. K.; Dror, R. O.; Jin, J.; et al. Structure-Inspired Design of *β*-Arrestin-Biased Ligands for Aminergic GPCRs. *Nat. Chem. Biol.* **2018**, *14* (2), 126–134.

(2) Qu, X.; Wang, D.; Wu, B. Progress in GPCR Structure Determination. *GPCRs* **2020**, 3–22.

(3) Pal, S.; Chattopadhyay, A. Extramembranous Regions in G Protein-Coupled Receptors: Cinderella in Receptor Biology? *J. Membr. Biol.* **2019**, *252* (4–5), 483–497.

(4) Latorraca, N. R.; Venkatakrishnan, A. J.; Dror, R. O. GPCR Dynamics: Structures in Motion. *Chem. Rev*. **2017**, *1*, 139–155.

(5) Durdagi, S.; Dogan, B.; Erol, I.; Kayık, G.; Aksoydan, B. Current Status of Multiscale Simulations on GPCRs. *Curr. Opin. Struct. Biol.* **2019**, *55*, 93–103.

(6) Fredriksson, R.; Lagerström, M. C.; Lundin, L.-G.; Schiöth, H. B. The G-Protein-Coupled Receptors in the Human Genome Form Five Main Families. Phylogenetic Analysis, Paralogon Groups, and Fingerprints. *Mol. Pharmacol.* **2003**, *63* (6), 1256–1272.

(7) Kolakowski, L. F. GCRDb: A G-Protein-Coupled Receptor Database. *Receptors Channels* **1994**, *2* (1), 1–7.

(8) Tan, L.; Yan, W.; McCorvy, J. D.; Cheng, J. Biased Ligands of G Protein-Coupled Receptors (GPCRs): Structure-Functional Selectivity Relationships (SFSRs) and Therapeutic Potential. *J. Med. Chem.* **2018**, *61* (22), 9841–9878.

(9) Lagerström, M. C.; Schiöth, H. B. Structural Diversity of G Protein-Coupled Receptors and Significance for Drug Discovery. *Nat. Rev. Drug Discov.* **2008**, *7* (4), 339–357.

(10) Mannhold, R.; Kubinyi, H.; Folkers, G. *Ligand Design for G Protein-Coupled Receptors*; Wiley, **2006**; Vol. 30.

(11) Culhane, K. J.; Liu, Y.; Cai, Y.; Yan, E. C. Y. Transmembrane Signal

Transduction by Peptide Hormones via Family B G Protein-Coupled Receptors. *Front. Pharmacol.* **2015**, *6*, 264.

(12) Bazarsuren, A.; Grauschopf, U.; Wozny, M.; Reusch, D.; Hoffmann, E.; Schaefer, W.; Panzner, S.; Rudolph, R. In Vitro Folding, Functional Characterization, and Disulfide Pattern of the Extracellular Domain of Human GLP-1 Receptor. *Biophys. Chem.* **2002**, *96* (2–3), 305–318.

(13) Grauschopf, U.; Lilie, H.; Honold, K.; Wozny, M.; Reusch, D.; Esswein, A.; Schäfer, W.; Rücknagel, K. P.; Rudolph, R. The N-Terminal Fragment of Human Parathyroid Hormone Receptor 1 Constitutes a Hormone Binding Domain and Reveals a Distinct Disulfide Pattern. *Biochemistry* **2000**, *39* (30), 8878–8887.

(14) Hamann, J.; Aust, G.; Araç, D.; Engel, F. B.; Formstone, C.; Fredriksson, R.; Hall, R. A.; Harty, B. L.; Kirchhoff, C.; Knapp, B.; et al. International Union of Basic and Clinical Pharmacology. XCIV. Adhesion G Protein–Coupled Receptors. *Pharmacol. Rev.* **2015**, *67* (2), 338–367.

(15) Rondard, P.; Goudet, C.; Kniazeff, J.; Prézeau, L. The Complexity of Their Activation Mechanism Opens New Possibilities for the Modulation of MGlu and GABAB Class C G Protein-Coupled Receptors. *Neuropharmacology* **2011**, *60* (1), 82–92.

(16) Huang, H.-C.; Klein, P. S. The Frizzled Family: Receptors for Multiple Signal Transduction Pathways. *Genome Biol.* **2004**, *5* (7), 234.

(17) Palczewski, K.; Kumasaka, T.; Hori, T.; Behnke, C. A.; Motoshima, H.; Fox, B. A.; Le Trong, I.; Teller, D. C.; Okada, T.; Stenkamp, R. E.; et al. Crystal Structure of Rhodopsin: A G Protein-Coupled Receptor.(Illustration). *Science (80-.).* **2000**, *289* (5480), 739.

(18) Teller, D. C.; Okada, T.; Behnke, C. A.; Palczewski, K.; Stenkamp, R. E. Advances in Determination of a High-Resolution Three-Dimensional Structure of Rhodopsin, a Model of G-Protein-Coupled Receptors (GPCRs). *Biochemistry*. **2001**, *40* (26), 7761–7772.

(19) Gouldson, P. R.; Kidley, N. J.; Bywater, R. P.; Psaroudakis, G.; Brooks, H. D.; Diaz, C.; Shire, D.; Reynolds, C. A. Toward the Active Conformations of

Rhodopsin and the β-Adrenergic Receptor. *Proteins Struct. Funct. Genet.* **2004**, *56* (1), 67–84.

(20) Goncalves, J. A.; Ahuja, S.; Erfani, S.; Eilers, M.; Smith, S. O. Structure and Function of G Protein-Coupled Receptors Using NMR Spectroscopy. *Prog Nucl Magn Reson Spectrosc*. **2010**, *57*, 159–180.

(21) Kahsai, A. W.; Xiao, K.; Ahn, S.; Sun, J.; Oas, T. G.; Lefkowitz, R. J. Multiple Ligand-Specific Conformations of the β_2-Adrenergic Receptor. *Nat. Chem. Biol.* **2011**, *7*, 692-700.

(22) Wacker, D.; Stevens, R. C.; Roth, B. L. How Ligands Illuminate GPCR Molecular Pharmacology. *Cell*, **2017**, *170* (3), 414–427.

(23) Ehlert, F. J.; Suga, H. Quantifying Allosteric Modulation of G Protein-Coupled Receptors. *Neuromethods*. **2011**, pp 273–304.

(24) Gilman, A. G. G Proteins: Transducers of Receptor-Generated Signals. *Annu. Rev. Biochem.* **1987**, *56* (1), 615–649.

(25) Rodbell, M. The Role of Hormone Receptors and GTP-Regulatory Proteins in Membrane Transduction. *Nature* **1980**, *284* (5751), 17–22.

(26) Denis, C.; Saulière, A.; Galandrin, S.; Sénard, J.-M.; Galés, C. Probing Heterotrimeric G Protein Activation: Applications to Biased Ligands. *Curr. Pharm. Des.* **2012**, *18* (2), 128–144.

(27) Oldham, W. M.; Hamm, H. E. Heterotrimeric G Protein Activation by G-Protein-Coupled Receptors. *Nat. Rev. Mol. Cell Biol.* **2008**, *9* (1), 60–71.

(28) Janetopoulos, C.; Jin, T.; Devreotes, P. Receptor-Mediated Activation of Heterotrimeric G-Proteins in Living Cells. *Science* **2001**, *291* (5512), 2408–2411.

(29) Galandrin, S.; Bouvier, M. Distinct Signaling Profiles of β_1 and β_2 Adrenergic Receptor Ligands toward Adenylyl Cyclase and Mitogen-Activated Protein Kinase Reveals the Pluridimensionality of Efficacy. *Mol. Pharmacol.* **2006**, *70* (5), 1575–1584.

(30) Urban, J. D.; Clarke, W. P.; Von Zastrow, M.; Nichols, D. E.; Kobilka, B.; Weinstein, H.; Javitch, J. A.; Roth, B. L.; Christopoulos, A.; Sexton, P. M.; et al.

Functional Selectivity and Classical Concepts of Quantitative Pharmacology. *J Pharmacol Exp Ther*. **2007**, *320* (1), 1–13.

(31) Kenakin, T. Gaddum Memorial Lecture 2014: Receptors as an Evolving Concept: From Switches to Biased Microprocessors. *Br. J. Pharmacol.* **2015**, *172* (17), 4238–4253.

(32) Smith, J. S.; Lefkowitz, R. J.; Rajagopal, S. Biased Signalling: From Simple Switches to Allosteric Microprocessors. *Nat Rev Drug Discov*. **2018**, *17*, 243–260.

(33) Galandrin, S.; Oligny-Longpré, G.; Bouvier, M. The Evasive Nature of Drug Efficacy: Implications for Drug Discovery. *Trends in Pharmacol Sci*. **2007**, *28*, 423–430.

(34) Steen, A.; Larsen, O.; Thiele, S.; Rosenkilde, M. M. Biased and G Protein-Independent Signaling of Chemokine Receptors. *Front Immunol*. **2014**, *5*, 277.

(35) Felker, G. M.; Butler, J.; Collins, S. P.; Cotter, G.; Davison, B. A.; Ezekowitz, J. A.; Filippatos, G.; D., L. P.; Violin, J. D.; Voors, A. A.; et al. Heart Failure Therapeutics on Thebasisofabiased Ligand of Theangiotensin-2 Type 1 Receptor. Rationale and Design of the Blast-Ahf Study (Biased Ligand of the Angiotensin Receptor Study in Acute Heart Failure). *JACC Hear. Fail.* **2015**, *3* (3), 193–201.

(36) Christopoulos, A. Allosteric Binding Sites on Cell-Surface Receptors: Novel Targets for Drug Discovery. *Nat Rev Drug Discov*. **2002**, *1*, 198–210.

(37) Felder, C. C. GPCR Drug Discovery-Moving beyond the Orthosteric to the Allosteric Domain. In *Advances in Pharmacology*; Academic Press Inc., **2019**, *86*, 1-20.

(38) Burford, N. T.; Watson, J.; Bertekap, R.; Alt, A. Strategies for the Identification of Allosteric Modulators of G-Protein-Coupled Receptors. *Biochem Pharmacol*. **2011**, *6*, 691–702.

(39) Burford, N. T.; Clark, M. J.; Wehrman, T. S.; Gerritz, S. W.; Banks, M.; O'Connell, J.; Traynor, J. R.; Alt, A. Discovery of Positive Allosteric Modulators and Silent Allosteric Modulators of the μ-Opioid Receptor. *Proc. Natl. Acad. Sci. U. S. A.* **2013**, *110* (26), 10830–10835.

(40) López-Rodríguez, M. L.; Benhamú, B.; Vázquez-Villa, H. Allosteric Modulators Targeting GPCRs. In *GPCRs*; Elsevier, **2020**; pp 195–241.

(41) Dong, B. J. Cinacalcet: An Oral Calcimimetic Agent for the Management of Hyperparathyroidism. *Clin. Ther.* **2005**, *27* (11), 1725–1751.

(42) Neelanjana, R. Maraviroc in the Treatment of HIV Infection. *Drug Des. Devel. Ther.* **2008**, *2*, 151–161.

(43) DiPersio, J. F.; Uy, G. L.; Yasothan, U.; Kirkpatrick, P. Plerixafor. *Nat. Rev. Drug Discov.* **2009**, *8* (2), 105–107.

(44) Schwyzer, R. ACTH: A SHORT INTRODUCTORY REVIEW. *Ann. N. Y. Acad. Sci.* **1977**, *297*, 3–26.

(45) Mohr, K.; Schmitz, J.; Schrage, R.; Tränkle, C.; Holzgrabe, U. Molecular Alliance-From Orthosteric and Allosteric Ligands to Dualsteric/Bitopic Agonists at G Protein Coupled Receptors. *Angew. Chemie Int. Ed.* **2013**, *52* (2), 508–516.

(46) Lane, J. R.; Sexton, P. M.; Christopoulos, A. Bridging the Gap: Bitopic Ligands of G-Protein-Coupled Receptors. *Trends Pharmacol. Sci.* **2013**, *34* (1), 59–66. https://doi.org/10.1016/j.tips.2012.10.003.

(47) Valant, C.; Gregory, K. J.; Hall, N. E.; Scammells, P. J.; Lew, M. J.; Sexton, P. M.; Christopoulos, A. A Novel Mechanism of G Protein-Coupled Receptor Functional Selectivity MUSCARINIC PARTIAL AGONIST McN-A-343 AS A BITOPIC ORTHOSTERIC/ALLOSTERIC LIGAND. *J. Biol. Chem.* **2008**, *283* (43), 29312-29321.

(48) Percherancier, Y.; Berchiche, Y. A.; Slight, I.; Volkmer-Engert, R.; Tamamura, H.; Fujii, N.; Bouvier, M.; Heveker, N. Bioluminescence Resonance Energy Transfer Reveals Ligand-Induced Conformational Changes in CXCR4 Homo-and Heterodimers* Downloaded From. *J. Biol. Chem.* **2005**, *280* (11), 9895–9903.

(49) Brogi, S.; Tafi, A.; Désaubry, L.; Nebigil, C. G. Discovery of GPCR Ligands for Probing Signal Transduction Pathways. *Front Pharmacol*. **2014**, *5*, 255.

(50) Daniels, D. J.; Lenard, N. R.; Etienne, C. L.; Law, P. Y.; Roerig, S. C.; Portoghese, P. S. Opioid-Induced Tolerance and Dependence in Mice Is Modulated by the Distance between Pharmacophores in a Bivalent Ligand Series.

Proc. Natl. Acad. Sci. U. S. A. **2005**, *102* (52), 19208–19213.

(51) Zhang, Y.; Gilliam, A.; Maitra, R.; Damaj, M. I.; Tajuba, J. M.; Seltzman, H. H.; Thomas, B. F. Synthesis and Biological Evaluation of Bivalent Ligands for the Cannabinoid 1 Receptor. *J. Med. Chem* **2010**, *53*, 7048–7060.

(52) Ruijter, E.; Orru, R. Multicomponent Reactions in Drug Discovery and Medicinal Chemistry. *Drug Discov. Today Technol.* **2018**, *29*, 1–2.

(53) Muñoz-Torrero, D.; Lavilla, R.; Pérez-Areales, F. J.; Ghashghaei, O. Multicomponent Reactions: A Mighty Journey Partner for Infectious Tropical Disease Drug Discovery. In *Annual Reports in Medicinal Chemistry*; Academic Press Inc., **2019**, *53*, 181-217.

(54) Cioc, R. C.; Ruijter, E.; Orru, R. V. A. Multicomponent Reactions: Advanced Tools for Sustainable Organic Synthesis. *Green Chem.* **2014**, *16* (6), 2958–2975.

(55) Anastas, P. T.; Warner, J. C. Green Chemistry: Theory and Practice. *Green Chem. Theory Pract. Oxford Univ. Press. New York* **1998**, 30.

(56) Dömling, A.; Wang, W.; Wang, K. Chemistry and Biology Of Multicomponent Reactions. *Chem. Rev.* **2012**, *112* (6), 3083–3135.

(57) Ruijter, E.; Orru, R. V. A. Multicomponent Reactions – Opportunities for the Pharmaceutical Industry. *Drug Discov. Today Technol.* **2013**, *10* (1), e15–e20.

(58) Strecker, A. Ueber Einen Neuen Aus Aldehyd - Ammoniak Und Blausäure Entstehenden Körper. *Ann. der Chemie und Pharm.* **1854**, *91* (3), 349–351.

(59) Mannich, C.; Krösche, W. Ueber Ein Kondensationsprodukt Aus Formaldehyd, Ammoniak Und Antipyrin. *Arch. Pharm. (Weinheim).* **1912**, *250* (1), 647–667.

(60) Hantzsch, A. Condensationsprodukte Aus Aldehydammoniak Und Ketonartigen Verbindungen. *Berichte der Dtsch. Chem. Gesellschaft* **1881**, *14* (2), 1637–1638.

(61) Petasis, N. A.; Zavialov, I. A. A New and Practical Synthesis of α-Amino Acids from Alkenyl Boronic Acids. *J. Am. Chem. Soc.* **1997**, *119* (2), 445–446.

(62) Passerini, M.; Simone, L. Sopra Gli Isonitrili (I). Composto Del p-Isonitril-Azobenzolo Con Acetone Ed Acido Acetico. *Gazz. Chim. Ital.* **1921**, *51*, 126–129.

(63) Biginelli, P. Derivati Aldeiduredici Degli Eteri Acetile Dossal-Acetico. *Gazz. Chim. Ital.* **1893**, *23*, 360–416.

(64) Ugi, I.; Meyr, R.; Fetzer, U.; Steinbruckner, C. Studies on Isonitriles. *Angew. Chemie* **1959**, *71* (11), 386.

(65) Zhu, J.; Bienaymé, H. *Multicomponent Reactions*; Wiley-VCH, **2005**.

(66) Nagarajaiah, H.; Mukhopadhyay, A.; Moorthy, J. N. Biginelli Reaction: An Overview. *Tetrahedron Lett.* **2016**, *57* (47), 5135–5149.

(67) Suresh; Sandhu, J. S. Past, Present and Future of the Biginelli Reaction: A Critical Perspective. *Arkivoc* **2011**, *2012* (1), 66.

(68) Kaur, R.; Chaudhary, S.; Kumar, K.; Gupta, M. K.; Rawal, R. K. Recent Synthetic and Medicinal Perspectives of Dihydropyrimidinones: A Review. *Eur J Med Chem*. **2017**, *132* (26), 108-134.

(69) Wilk, M.; Brodzka, A.; Koszelewski, D.; Madej, A.; Paprocki, D.; Żądło-Dobrowolska, A.; Ostaszewski, R. The Influence of the Isocyanoesters Structure on the Course of Enzymatic Ugi Reactions. *Bioorg. Chem.* **2019**, *93*, 102817

(70) Azuaje, J. Nuevas Aplicaciones de La Reacción de Ugi En El Descubrimiento de Fármacos., **2012**.

(71) Dömling, A.; Ugi, I. Multicomponent Reactions with Isocyanides. *Angew. Chemie* **2000**, *39* (18), 3168–3210.

(72) Simila, S. T. M.; Martin, S. F. Applications of the Ugi Reaction with Ketones. *Tetrahedron Lett.* **2008**, *49* (29–30), 4501–4504.

(73) Abdelraheem, E. M. M.; Khaksar, S.; Kurpiewska, K.; Kalinowska-Tuścik, J.; Shaabani, S.; Dömling, A. Two-Step Macrocycle Synthesis by Classical Ugi Reaction. *J. Org. Chem.* **2018**, *83* (3), 1441–1447.

(74) Patil, P.; Mishra, B.; Sheombarsing, G.; Kurpiewska, K.; Kalinowska-Tluścik, J.; Dömling, A. Library-to-Library Synthesis of Highly Substituted *α*-Aminomethyl Tetrazoles via Ugi Reaction. *ACS Comb. Sci.* **2018**, *20* (2), 70–74.

(75) Hulme, C.; Gore, V. "Multi-Component Reactions : Emerging Chemistry in Drug Discovery" 'From Xylocain to Crixivan'. *Curr. Med. Chem.* **2005**, *10* (1), 51–80.

(76) Zhang, C. T.; Zhang, X.; Qing, F. L. Ruthenium-Catalyzed 1,3-Dipolar Cycloaddition of Trifluoromethylated Propargylic Alcohols with Azides. *Tetrahedron Lett.* **2008**, *49* (24), 3927–3930.

(77) Velpuri, V. R.; Muralidharan, K. Multicomponent Click Reaction Catalyzed by Organic Surfactant-Free Copper Sulfide (Sf-CuS) Nano/Micro Flowers. *J. Organomet. Chem.* **2019**, *884*, 59–65.

(78) Hou, J.; Liu, X.; Shen, J.; Zhao, G.; Wang, P. G. The Impact of Click Chemistry in Medicinal Chemistry. *Expert Opin. Drug Discov.* **2012**, *7* (6), 489–501.

(79) Meldal, M.; Tornøe, C. W. Cu-Catalyzed Azide−Alkyne Cycloaddition. *Chem. Rev.* **2008**, *108* (8), 2952–3015.

(80) Borea, P. A.; Gessi, S.; Merighi, S.; Varani, K. Adenosine as a Multi-Signalling Guardian Angel in Human Diseases: When, Where and How Does It Exert Its Protective Effects? *Trends in Pharmacol Sci*. **2016**, *6*, 419–434.

(81) Fredholm, B. B.; IJzerman, A. P.; Jacobson, K. A.; Linden, J.; Müller, C. E. International Union of Basic and Clinical Pharmacology. LXXXI. Nomenclature and Classification of Adenosine Receptors - An Update. *Pharmacol Rev*. March **2011**, 63 (1), 1–34.

(82) Abdelrahman, A.; Yerande, S. G.; Namasivayam, V.; Klapschinski, T. A.; Alnouri, M. W.; El-Tayeb, A.; Müller, C. E. Substituted 4-Phenylthiazoles: Development of Potent and Selective A_1, A_3 and Dual A_1/A_3 Adenosine Receptor Antagonists. *Eur. J. Med. Chem.* **2019**, 111879.

(83) Moro, S.; Deflorian, F.; Bacilieri, M.; Spalluto, G. Ligand-Based Homology Modeling as Attractive Tool to Inspect GPCR Structural Plasticity. *Curr. Pharm. Des.* **2006**, *12* (17), 2175–2185.

(84) Varano, F.; Catarzi, D.; Falsini, M.; Dal Ben, D.; Buccioni, M.; Marucci, G.; Volpini, R.; Colotta, V. Novel Human Adenosine Receptor Antagonists Based on the 7-Amino-Thiazolo[5,4-*d*]Pyrimidine Scaffold. Structural Investigations at the 2-, 5- and 7-Positions to Enhance Affinity and Tune Selectivity. *Bioorganic Med. Chem. Lett.* **2019**, *29* (4), 563–569.

(85) Müller, C. E.; Jacobson, K. A. Recent Developments in Adenosine Receptor

Ligands and Their Potential as Novel Drugs. *BBA - Biomembranes*. **2011**, *1808* (5), 1290–1308.

(86) De Filippo, E.; Namasivayam, V.; Zappe, L.; El-Tayeb, A.; Schiedel, A. C.; Müller, C. E. Role of Extracellular Cysteine Residues in the Adenosine A2A Receptor. *Purinergic Signal.* **2016**, *12* (2), 313–329.

(87) Antonioli, L.; Blandizzi, C.; Pacher, P.; Haskó, G. Immunity, Inflammation and Cancer: A Leading Role for Adenosine. *Nat Rev Cancer*. **2013**, *13*, 842–857.

(88) Borea, P. A.; Gessi, S.; Merighi, S.; Vincenzi, F.; Varani, K. Pathological Overproduction: The Bad Side of Adenosine. *Br. J. Pharmacol.* **2017**, *174* (13), 1945–1960.

(89) Müller, C. E.; Baqi, Y.; Hinz, S.; Namasivayam, V. Medicinal Chemistry of A_{2B} Adenosine Receptors. *Receptors* **2018**, *34*, 137–168.

(90) Borea, P. A.; Varani, K.; Vincenzi, F.; Baraldi, P. G.; Tabrizi, M. A.; Merighi, S.; Gessi, S. The A_3 Adenosine Receptor: History and Perspectives. *Pharmacol. Rev.* **2015**, *67* (1), 74–102.

(91) Yang, T.; Gao, X.; Sandberg, M.; Zollbrecht, C.; Zhang, X. M.; Hezel, M.; Liu, M.; Peleli, M.; Lai, E. Y.; Harris, R. A.; et al. Abrogation of Adenosine A_1 Receptor Signalling Improves Metabolic Regulation in Mice by Modulating Oxidative Stress and Inflammatory Responses. *Diabetologia* **2015**, *58* (7), 1610–1620.

(92) Ma, D. F.; Kondo, T.; Nakazawa, T.; Niu, D. F.; Mochizuki, K.; Kawasaki, T.; Yamane, T.; Katoh, R. Hypoxia-Inducible Adenosine A_{2B} Receptor Modulates Proliferation of Colon Carcinoma Cells. *Hum. Pathol.* **2010**, *41* (11), 1550–1557.

(93) Sebastião, A. M.; Ribeiro, J. A. Adenosine Receptors and the Central Nervous System. *Handbook of Experimental Pharmacology*. **2009**, pp 471–534.

(94) Gessi, S.; Fogli, E.; Sacchetto, V.; Merighi, S.; Varani, K.; Preti, D.; Leung, E.; MacLennan, S.; Borea, P. A. Adenosine Modulates HIF-1α, VEGF, IL-8, and Foam Cell Formation in a Human Model of Hypoxic Foam Cells. *Arterioscler. Thromb. Vasc. Biol.* **2010**, *30* (1), 90–97.

(95) Tang, J.; Jiang, X.; Zhou, Y.; Dai, Y. Effects of A_{2B}R on the Biological Behavior

of Mouse Renal Fibroblasts during Hypoxia. *Mol. Med. Rep.* **2015**, *11* (6), 4397–4402.

(96) Peng, Z.; Borea, P. A.; Wilder, T.; Yee, H.; Chiriboga, L.; Blackburn, M. R.; Azzena, G.; Resta, G.; Cronstein, B. N. Adenosine Signaling Contributes to Ethanol-Induced Fatty Liver in Mice. *J. Clin. Invest.* **2009**, *119* (3), 582–594.

(97) Wei, W.; Du, C.; Lv, J.; Zhao, G.; Li, Z.; Wu, Z.; Haskó, G.; Xie, X. Blocking A_{2B} Adenosine Receptor Alleviates Pathogenesis of Experimental Autoimmune Encephalomyelitis via Inhibition of IL-6 Production and Th17 Differentiation . *J. Immunol.* **2013**, *190* (1), 138–146.

(98) Feoktistov, I.; Biaggioni, I. Role of Adenosine A_{2B} Receptors in Inflammation. *Adv. Pharmacol.* **2011**, *61*, 115–144.

(99) Hinz, S.; Navarro, G.; Borroto-Escuela, D.; Seibt, B. F.; Ammon, Y. C.; de Filippo, E.; Danish, A.; Lacher, S. K.; Červinková, B.; Rafehi, M.; et al. Adenosine A_{2A} Receptor Ligand Recognition and Signaling Is Blocked by A_{2B} Receptors. *Oncotarget* **2018**, *9* (17), 13593–13611.

(100) Kasama, H.; Sakamoto, Y.; Kasamatsu, A.; Okamoto, A.; Koyama, T.; Minakawa, Y.; Ogawara, K.; Yokoe, H.; Shiiba, M.; Tanzawa, H.; et al. Adenosine A2b Receptor Promotes Progression of Human Oral Cancer. *BMC Cancer* **2015**, *15*, 563.

(101) Sitkovsky, M. V; Hatfield, S.; Abbott, R.; Belikoff, B.; Lukashev, D.; Ohta, A. Hostile, Hypoxia-A2-Adenosinergic Tumor Biology as the next Barrier to Overcome for Tumor Immunologists. *Cancer immunol res*. **2014**, *2* (7), 598–605.

(102) Hatfield, S. M.; Kjaergaard, J.; Lukashev, D.; Belikoff, B.; Schreiber, T. H.; Sethumadhavan, S.; Abbott, R.; Philbrook, P.; Thayer, M.; Shujia, D.; et al. Systemic Oxygenation Weakens the Hypoxia and Hypoxia Inducible Factor 1α-Dependent and Extracellular Adenosine-Mediated Tumor Protection. *J. Mol. Med.* **2014**, *92* (12), 1283–1292.

(103) Allard, B.; Beavis, P. A.; Darcy, P. K.; Stagg, J. Immunosuppressive Activities of Adenosine in Cancer. *Curr Opin Pharmacol*. **2016**, *29*, 7–16.

(104) Vijayan, D.; Young, A.; Teng, M. W. L.; Smyth, M. J. Targeting

Immunosuppressive Adenosine in Cancer. *Nat Rev Cancer*. **2017**, *17*, 709–724.

(105) Kazemi, M. H.; Raoofi Mohseni, S.; Hojjat-Farsangi, M.; Anvari, E.; Ghalamfarsa, G.; Mohammadi, H.; Jadidi-Niaragh, F. Adenosine and Adenosine Receptors in the Immunopathogenesis and Treatment of Cancer. *J Cell Physiol*. **2018**, *233* (3), 2032–2057.

(106) Morello, S.; Miele, L. Targeting the Adenosine A2b Receptor in the Tumor Microenvironment Overcomes Local Immunosuppression by Myeloid-Derived Suppressor Cells. *Oncoimmunology* **2014**, *3* (2), e27989.

(107) Jiang, J.; Seel, C. J.; Temirak, A.; Namasivayam, V.; Arridu, A.; Schabikowski, J.; Baqi, Y.; Hinz, S.; Hockemeyer, J.; Müller, C. E. A_{2B} Adenosine Receptor Antagonists with Picomolar Potency. *J. Med. Chem.* **2019**, *62* (8), 4032–4055.

(108) Borrmann, T.; Hinz, S.; Bertarelli, D. C. G.; Li, W.; Florin, N. C.; Scheiff, A. B.; Müller, C. E. 1-Alkyl-8-(Piperazine-1-Sulfonyl)Phenylxanthines: Development and Characterization of Adenosine A_{2B} Receptor Antagonists and a New Radioligand with Subnanomolar Affinity and Subtype Specificity. *J. Med. Chem.* **2009**, *52* (13), 3994–4006.

(109) Vidal, B.; Nueda, A.; Esteve, C.; Domenech, T.; Benito, S.; Reinoso, R. F.; Pont, M.; Calbet, M.; López, R.; Cadavid, M. I.; et al. Discovery and Characterization of 4′-(2-Furyl)-*N*-pyridin-3-yl-4, 5′-bipyrimidin-2′-amine (LAS38096), a Potent, Selective, and Efficacious A_{2B} Adenosine Receptor Antagonist. *J. Med. Chem.* **2007**, *50* (11), 2732–2736.

(110) Kalla, R. V.; Elzein, E.; Perry, T.; Li, X.; Gimbel, A.; Yang, M.; Zeng, D.; Zablocki, J. Selective, high affinity A_{2B} adenosine receptor antagonists: N-1 monosubstituted 8-(pyrazol-4-yl)xanthines. *Bioorganic Med. Chem. Lett.* **2008**, *18* (4), 1397–1401.

(111) Crespo, A.; El Maatougui, A.; Biagini, P.; Azuaje, J.; Coelho, A.; Brea, J.; Loza, M. I.; Cadavid, M. I.; García-Mera, X.; Gutiérrez-De-Terán, H.; et al. Discovery of 3,4-Dihydropyrimidin-2(1*H*)-Ones as a Novel Class of Potent and Selective A_{2B} Adenosine Receptor Antagonists. *ACS Med. Chem. Lett.* **2013**, *4* (11), 1031–1036.

(112) Carbajales, C.; Azuaje, J.; Oliveira, A.; Loza, M. I.; Brea, J.; Cadavid, M. I.; Masaguer, C. F.; García-Mera, X.; Gutiérrez-De-Terán, H.; Sotelo, E. Enantiospecific Recognition at the A_{2B} Adenosine Receptor by Alkyl 2-Cyanoimino-4-substituted-6-methyl-1,2,3,4-tetrahydropyrimidine-5-carboxylates. *J. Med. Chem.* **2017**, *60* (8), 3372–3382.

(113) Stewart, M.; Steinig, A. G.; Ma, C.; Song, J. P.; McKibben, B.; Castelhano, A. L.; MacLennan, S. J. [^{3}H]OSIP339391, a Selective, Novel, and High Affinity Antagonist Radioligand for Adenosine A_{2B} Receptors. *Biochem. Pharmacol.* **2004**, *68* (2), 305–312.

(114) El Maatougui, A.; Azuaje, J.; González-Gómez, M.; Miguez, G.; Crespo, A.; Carbajales, C.; Escalante, L.; García-Mera, X.; Gutiérrez-de-Terán, H.; Sotelo, E. Discovery of Potent and Highly Selective A_{2B} Adenosine Receptor Antagonist Chemotypes. *J. Med. Chem.* **2016**, *59* (5), 1967–1983.

(115) Xin, J.; Fan, T.; Guo, P.; Wang, J. Identification of Functional Divergence Sites in Dopamine Receptors of Vertebrates. *Comput. Biol. Chem.* **2019**, *83*.

(116) Beaulieu, J. M.; Espinoza, S.; Gainetdinov, R. R. Dopamine Receptors - IUPHAR Review 13. *Br. J. Pharmacol.* **2015**, *172* (1), 1–23.

(117) Vallone, D.; Picetti, R.; Borrelli, E. Structure and Function of Dopamine Receptors. *Neurosci Biobehav Rev,* **2000**, *24* (1), 125–132.

(118) Beaulieu, J. M.; Gainetdinov, R. R. The Physiology, Signaling, and Pharmacology of Dopamine Receptors. *Pharmacol Rev*. **2011**, 63 (1), 182–217.

(119) Chen, X.; McCorvy, J. D.; Fischer, M. G.; Butler, K. V.; Shen, Y.; Roth, B. L.; Jin, J. Discovery of G Protein-Biased D_2 Dopamine Receptor Partial Agonists. *J. Med. Chem.* **2016**, *59* (23), 10601–10618.

(120) Rössler, W.; Joachim Salize, H.; Van Os, J.; Riecher-Rössler, A. Size of Burden of Schizophrenia and Psychotic Disorders. *Eur. Neuropsychopharmacol.* **2005**, *15* (4), 399–409.

(121) Kehne, J.; Andree, T.; Heinrich, J. D_2 Receptor Partial Agonists: Treatment of CNS Disorders of Dopamine Function. *Curr. Top. Med. Chem.* **2008**, *8* (12), 1068–1088.

(122) Howes, O. D.; Kapur, S. The Dopamine Hypothesis of Schizophrenia: Version III - The Final Common Pathway. *Schizophr Bull*. **2009**, 35 (3), 549–562.

(123) Urs, N. M.; Peterson, S. M.; Caron, M. G. New Concepts in Dopamine D_2 Receptor Biased Signaling and Implications for Schizophrenia Therapy. *Biol Psychiatry*. **2017**, *84* (1), 78–85.

(124) Li, P.; L. Snyder, G.; E. Vanover, K. Dopamine Targeting Drugs for the Treatment of Schizophrenia: Past, Present and Future. *Curr. Top. Med. Chem.* **2016**, *16* (29), 3385–3403.

(125) Xu, M.; Wang, Y.; Yang, F.; Wu, C.; Wang, Z.; Ye, B.; Jiang, X.; Zhao, Q.; Li, J.; Liu, Y.; et al. Synthesis and Biological Evaluation of a Series of Novel Pyridinecarboxamides as Potential Multi-Receptor Antipsychotic Drugs. *Bioorganic Med. Chem. Lett.* **2018**, *28* (4), 606–611.

(126) Schmidt, A. W.; Lebel, L. A.; Howard, H. R.; Zorn, S. H. Ziprasidone: A Novel Antipsychotic Agent with a Unique Human Receptor Binding Profile. *Eur. J. Pharmacol.* **2001**, *425* (3), 197–201.

(127) Szabo, M.; Klein Herenbrink, C.; Christopoulos, A.; Lane, J. R.; Capuano, B. Structure-Activity Relationships of Privileged Structures Lead to the Discovery of Novel Biased Ligands at the Dopamine D_2 Receptor. *J. Med. Chem.* **2014**, *57* (11), 4924–4939.

(128) *The Dopamine Receptors*, Second Edi.; Neve, K. A., Ed.; Springer Science & Business Media, **2009**.

(129) Tyler, M. W.; Zaldivar-Diez, J.; Haggarty, S. J. Classics in Chemical Neuroscience: Haloperidol. *ACS Chem. Neurosci.* **2017**, *8* (3), 444–453.

(130) Bonifazi, A.; Yano, H.; Ellenberger, M. P.; Muller, L.; Kumar, V.; Zou, M. F.; Cai, N. S.; Guerrero, A. M.; Woods, A. S.; Shi, L.; et al. Novel Bivalent Ligands Based on the Sumanirole Pharmacophore Reveal Dopamine D_2 Receptor (D_2R) Biased Agonism. *J. Med. Chem.* **2017**, *60* (7), 2890–2907.

USC
UNIVERSIDADE
DE SANTIAGO
DE COMPOSTELA

2. AIMS AND OUTLINE OF THE THESIS

USC
UNIVERSIDADE
DE SANTIAGO
DE COMPOSTELA

The ComBioMed group has developed a multicomponent-assisted platform for the rapid and efficient discovery and optimization of new drug candidates. During the last ten years, our group has contributed to the discovery of novel drug candidates that target several GPCRs (*e.g.*, adenosine A_{2B}, adenosine A_3, dopamine D_2 serotonin $5HT_{2B}$ and $5HT_{2A}$, and cannabinoid CB_1). These GPCRs are validated targets that allow serious pathologies to be tackled – including Parkinson's disease, cancer, glaucoma, diabetes, schizophrenia, and neuropathic pain.

The present PhD Thesis is focused on the discovery and optimization of novel potent and selective ligands and pharmacological tools that target the A_{2B}AR and the DRD_2R. The herein described research is part of a long-term project aimed at demonstrating the advantages of using of multicomponent reactions in Medicinal Chemistry. The project is divided into three main chapters, each of which has its own context and objectives. A brief summary of the main goals for each chapter is provided below.

Chapter 3.1. deals with the development and optimization of trifluorinated A_{2B}AR ligands (Figure 2.1) as metabolically stable analogues of two prototypic A_{2B}AR antagonists discovered by our research group (**ISAM-140** and **SYAF080**). Additionally, we decided to explore new evidence that supports the stereospecific recognition of these families of pyrimidine-based A_{2B}AR antagonists by using a combination of chiral HPLC, circular dichroism (CD) and X-ray crystallography.

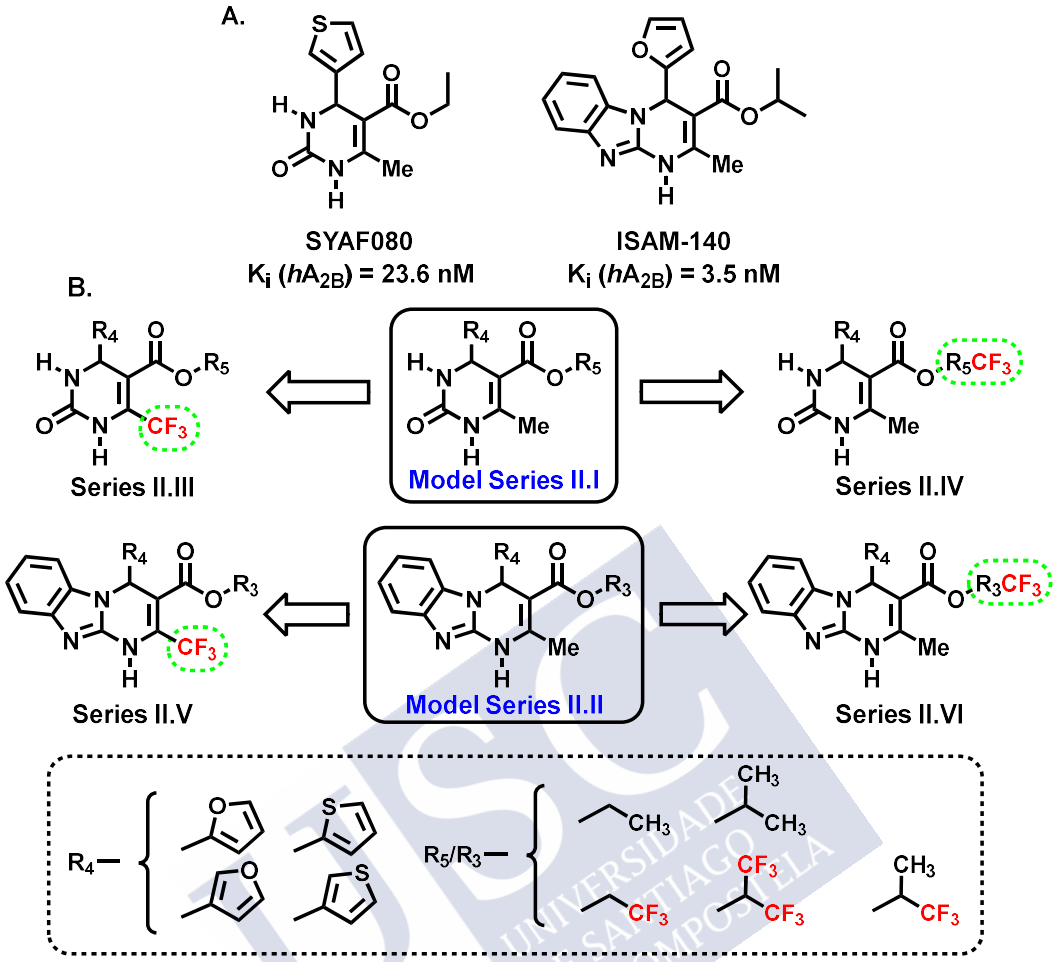

Figure 2.1: A. Pharmacological ligands taken as a model in the first project. B. Design strategy and diversity elements studied in the first part of the thesis.

Chapter 3.2 deals with the further exploration of $A_{2B}AR$ antagonists with improved pharmacokinetic properties (particularly metabolic stability). Using **ISAM-140** as a model ligand, our objective was to identify pentagonal heterocyclic cores that allow replacement of the furan and thiophene cores (which can be considered as toxicophores) by a nitrogen walk approach (Figure 2.2). The aim of the study included not only the characterization of the new ligands in terms of $A_{2B}AR$ potency and selectivity, but also a preliminary *in vitro* evaluation in two highly relevant cytochromes (CYP3A4 and CYP2D6). With the aim of studying the structural determinants that govern the stereospecific recognition of these series it was decided to separate and evaluate the enantiomers of the most attractive ligand identified.

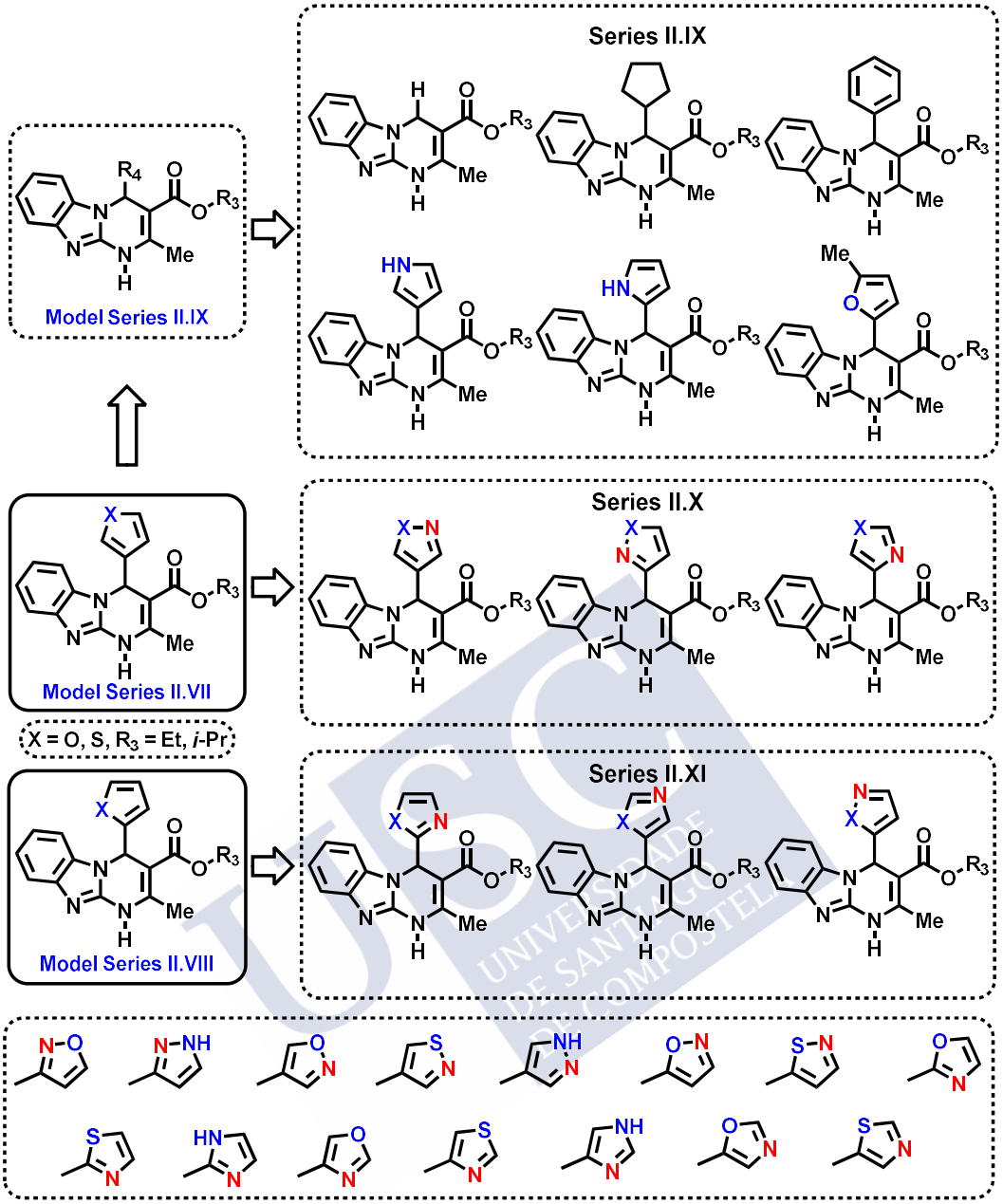

Figure 2.2: Design strategy and diversity elements studied during the second part of the thesis.

Chapter 3.3. deals with the discovery of novel antipsychotic drugs, with particular emphasis on novel aripiprazol-inspired DRD_2 partial agonists (Figure 2.3). During the planning of this chapter, we highlighted two main goals: 1) the identification of robust DRD_2 partial agonists that simultaneously exhibit biased signalling and subtype selectivity and, 2) to explore the advantages of multicomponent reactions as synthetic tools to generate unexplored diversity in a pharmacophoric model, in this case by expanding the diversity of the secondary pharmacophore region.

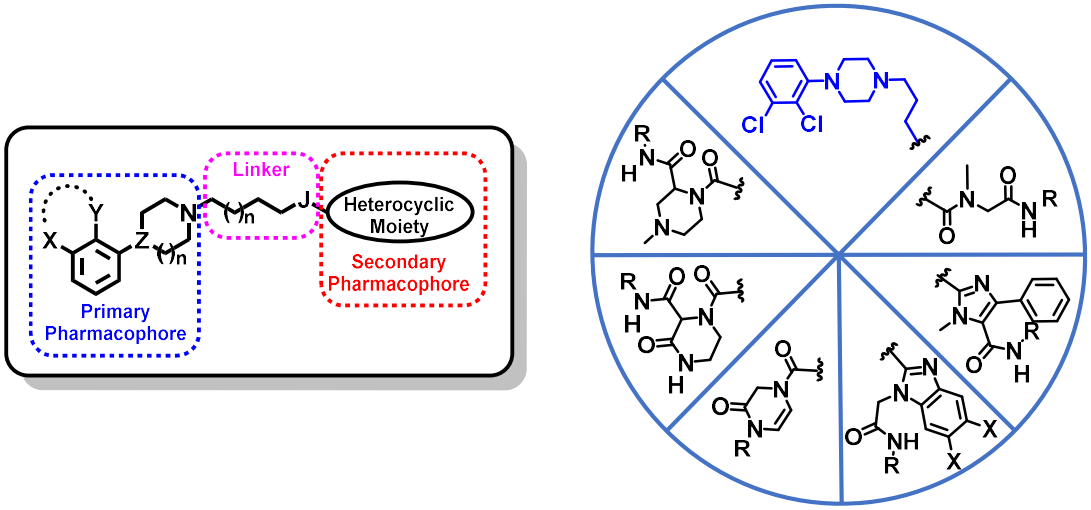

Figure 2.3: Pharmacophoric model of DRD_2 biased ligands and the novel series described herein.

As a complement of these chapters, **Appendix 1** provides details of a study carried out during my research stay at the Research Institute for Medicines, Universidade de Lisboa (iMed.Ulisboa), under the supervision of Professor Doutor Rui Moreira. This study is based on the development of quenched activity-based probes (qABPs), with a *β*-lactam warhead oriented toward the ubiquitin-proteasome system.

3. RESULTS

USC
UNIVERSIDADE
DE SANTIAGO
DE COMPOSTELA

3.1 TRIFLUORINATED PYRIMIDINE-BASED A_{2B} ANTAGONISTS: OPTIMIZATION AND EVIDENCES OF STEREOSPECIFIC RECOGNITION

DOI: https://doi.org/10.1021/acs.jmedchem.9b01340

3.2 NITROGEN-WALK APPROACH TO EXPLORE BIOISOSTERIC REPLACEMENTS IN A SERIES OF POTENT A_{2B} ADENOSINE RECEPTOR ANTAGONISTS

DOI: https://doi.org/10.1021/acs.jmedchem.0c00564

3.3 POTENT AND SUBTYPE-SELECTIVE DOPAMINE D_2 RECEPTOR BIASED PARTIAL AGONISTS DISCOVERED VIA AN UGI-BASED APPROACH

DOI: https://doi.org/10.1021/acs.jmedchem.1c00704

USC
UNIVERSIDADE
DE SANTIAGO
DE COMPOSTELA

4. DISCUSSION

USC
UNIVERSIDADE
DE SANTIAGO
DE COMPOSTELA

4.1 METHODOLOGY AND DISCUSSION OF THE SYNTHETIC APPROACH

The present work deals with the development of novel pharmacologically active compounds for the treatment of several important pathologies by modulating two GPCRs (*e.g.*, $A_{2B}AR$ and DRD_2). Although the three chapters (**3.1-3.3**) differ in their aims, receptor subtypes (*e.g.*, $A_{2B}AR$ and DRD_2) and scaffolds, all of them have in common the use of MCR (Biginelli and Ugi reactions) as a methodological approach that allows to achieve the main aim proposed in each chapter.

Chapter 3.1 documents novel series of $A_{2B}AR$ antagonists bearing CF_3 groups at positions 6 or 5 of the pyrimidin-2-one or the positions 2 or 3 of the tricyclic dihydrobenzo[4,5]imidazo[1,2-*a*]pyrimidine scaffold. These series were conceived by structural modifications of model ligands (**ISAM-140** and **SYAF080**) previously discovered in our group. The synthesis of these novel derivatives (series **IV.I-IV.IV**) was accomplished by using the corresponding trifluoromethyl ketoesters (**4.3**) under modified conditions of the Biginelli reaction as shown in Scheme 4.1.

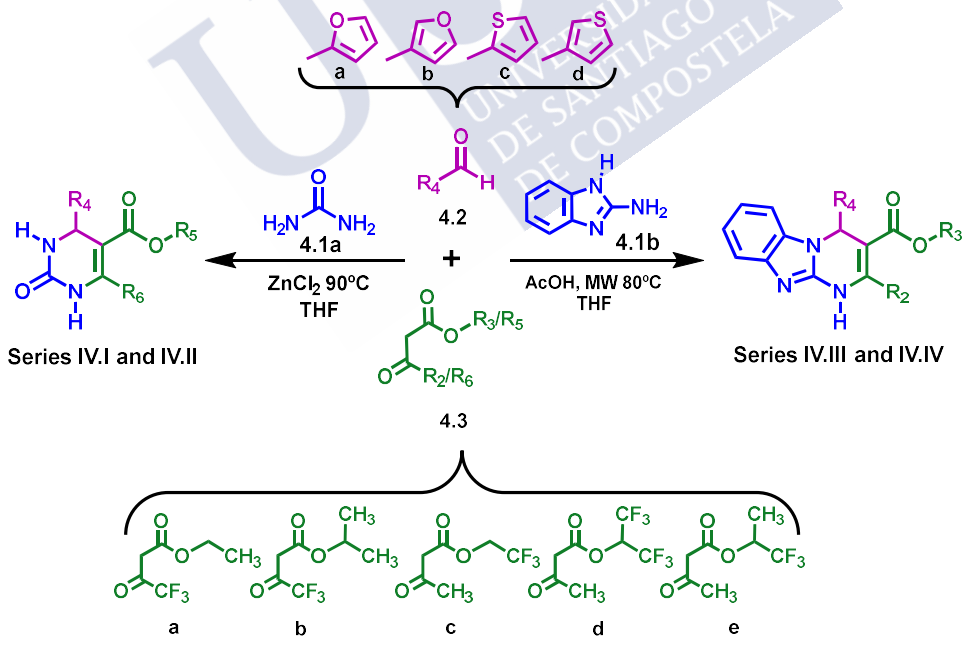

Scheme.4.1: General synthetic strategy for all compounds of the first objective.

During the synthesis of ligands of series **IV.II** and **IV.IV** (bearing a CF_3 at position 6 and 2, respectively, Figure 4.2) it was observed that instead of the desired Biginelli products (Scheme 4.2, series **IV.II** and **IV.IV**), the isolated products were the

corresponding adducts bearing a hydroxy group at position 6 or 2 respectively (**4.4**, **4.5**, Scheme 4.2). Once the structure of the isolated adducts had been identified and to obtain the targeted ligands, it was decided to treat the reaction mixtures with 1.5 equivalents of *p*-toluenesulfonic acid (TsOH) to promote the elimination reaction that finally rendered the targeted structures (Scheme 4.2).

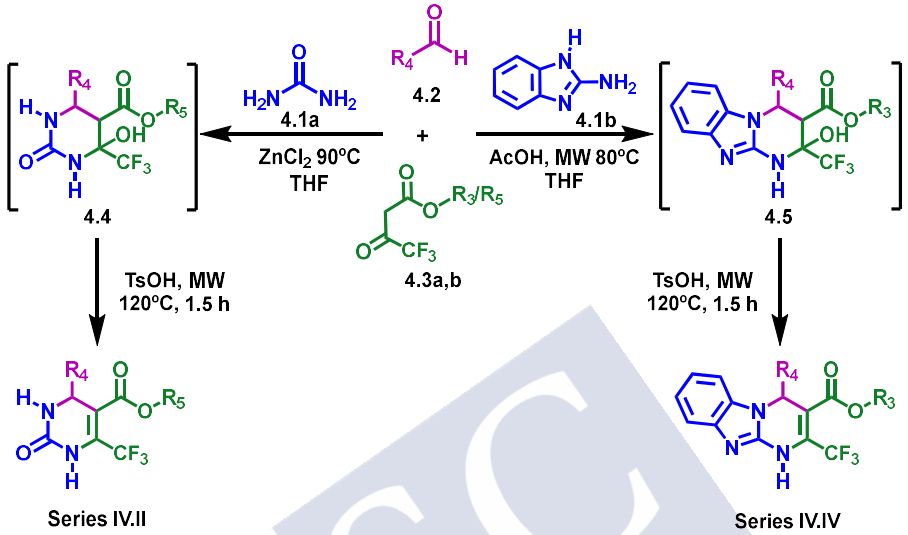

Scheme 4.2: Additional step in the one-pot synthesis to assist the elimination reaction thus obtaining the desired compound.

All the A_{2B}AR antagonists described in **Chapters 3.1** and **3.2** contain a chiral centre at position 4. In the case of series **IV.I** and **IV.III**, they contain an additional stereocenter at the alkyl residue of the ester function (1,1,1-trifluoro-2-methylpropane). Column chromatography allowed the isolation of 3,4-dihydropyrimidin-2-(1*H*)-ones as pairs of diastereomers without knowing the assignment of the natural stereocenter in each of the compounds. However, the diastereomeric separation of the tricyclic series was unsuccessful. Due to the promising affinity of the racemic mixture and the impossibility of a diastereomeric separation by chiral HPLC, a diastereoselective reaction for compound **4.6i** was carried out. To do so, enantiopure forms of the *β*-ketoester **4.3e** [(*R*)-**4.3e** and [(*S*)-**4.3e**] were employed to develop the following synthesis (Scheme 4.3).

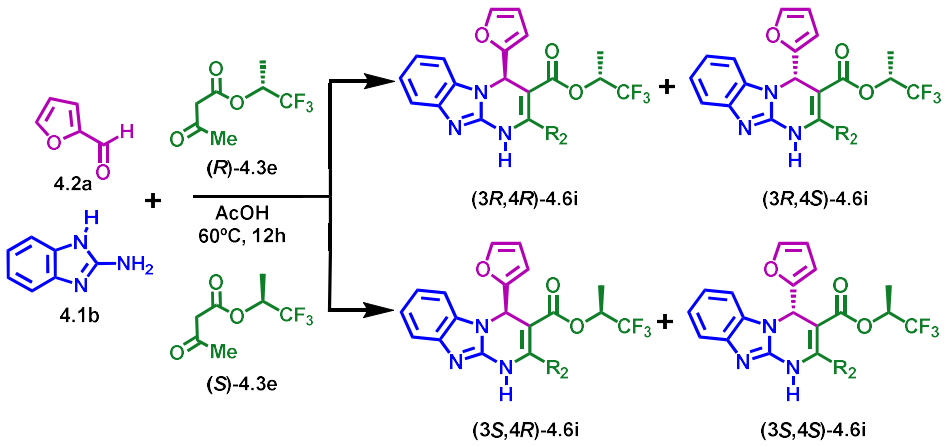

Scheme 4.3: Diastereoselective Biginelli-based synthesis from the enantiopure forms of *β*-ketoester **4.3e** giving rise of tricyclic derivatives **4.6i**.

Chapter 3.2 is dealt with the identification of unexplored pentagonal cores enabling to substitute the furan and thiophene rings at position 4 of the dihydrobenzo[4,5]imidazo[1,2-*a*]pyrimidine scaffold. These heterocyclic rings have been associated with suboptimal metabolic stability profiles in other systems, so it was decided to explore alternatives for potency, selectivity and metabolic stability of new series bearing different azole rings at position 4. By taking this point as the chapter goal, the Biginelli reaction (Scheme 4.4) has been recursed by employing 1*H*-benzo[*d*]imidazol-2-amine (**4.1b**), *β*-ketoesters **4.3** and a collection of fifteen highly diverse aldehydes (**4.2**). All reactions were performed in a microwave organic synthesiser at 80 ºC in THF and using chloroacetic acid as catalyst.

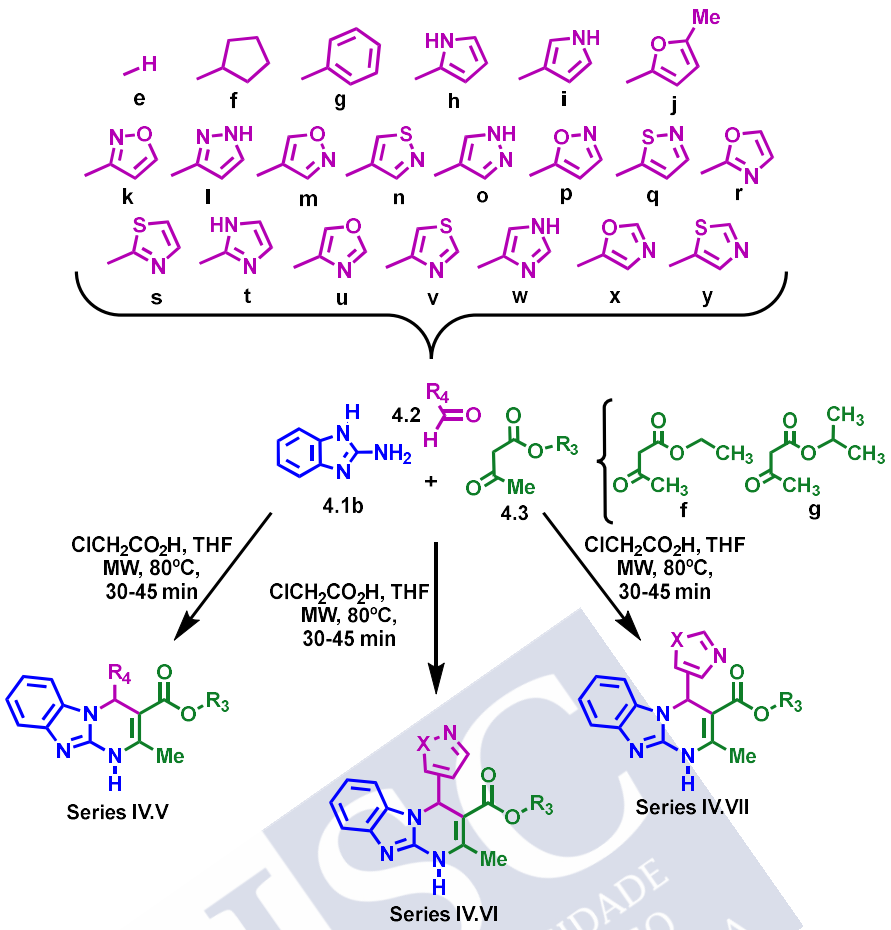

Scheme 4.4: General synthetic strategy for all compounds of the second objective.

Finally, **Chapter 3.3** dealt with the discovered of subtype selective biased DRD_2 partial agonists. In this case, it has been decided to explore the performance of a highly divergent and diversity oriented Ugi-based synthetic approach to identify novel moieties that would provide novel binding modes and selectivity profiles. The synthetic strategy is documented in Scheme 4.5 and take advantage of the reactivity of the readily available carboxylic acid **4.7**. Combination of **4.7** with different subsets of amines (**4.1**), aldehydes (**4.2**) and isocyanides (**4.8**) rapidly provided different Ugi adducts that are either final compounds (series **IV.VIII**, **IV.XII**) or reactive intermediates (**4.9-4.12**). The manupulation structural elaboration of the functional groups (*e.g.*, protecting groups) present at the Ugi adducts using the Ugi-deprotection-cyclization (UDC) strategy, enabled the rapid generation of diverse motifs in a time- and cost-efficient manner (series **IV.IX**, **IV.X**, **IV.XI**, **IV.XIII**).

The functional evaluation of the obtained collection enabled to identify novel molecular probes exhibiting high affinity and previously undisclosed selectivity profiles.

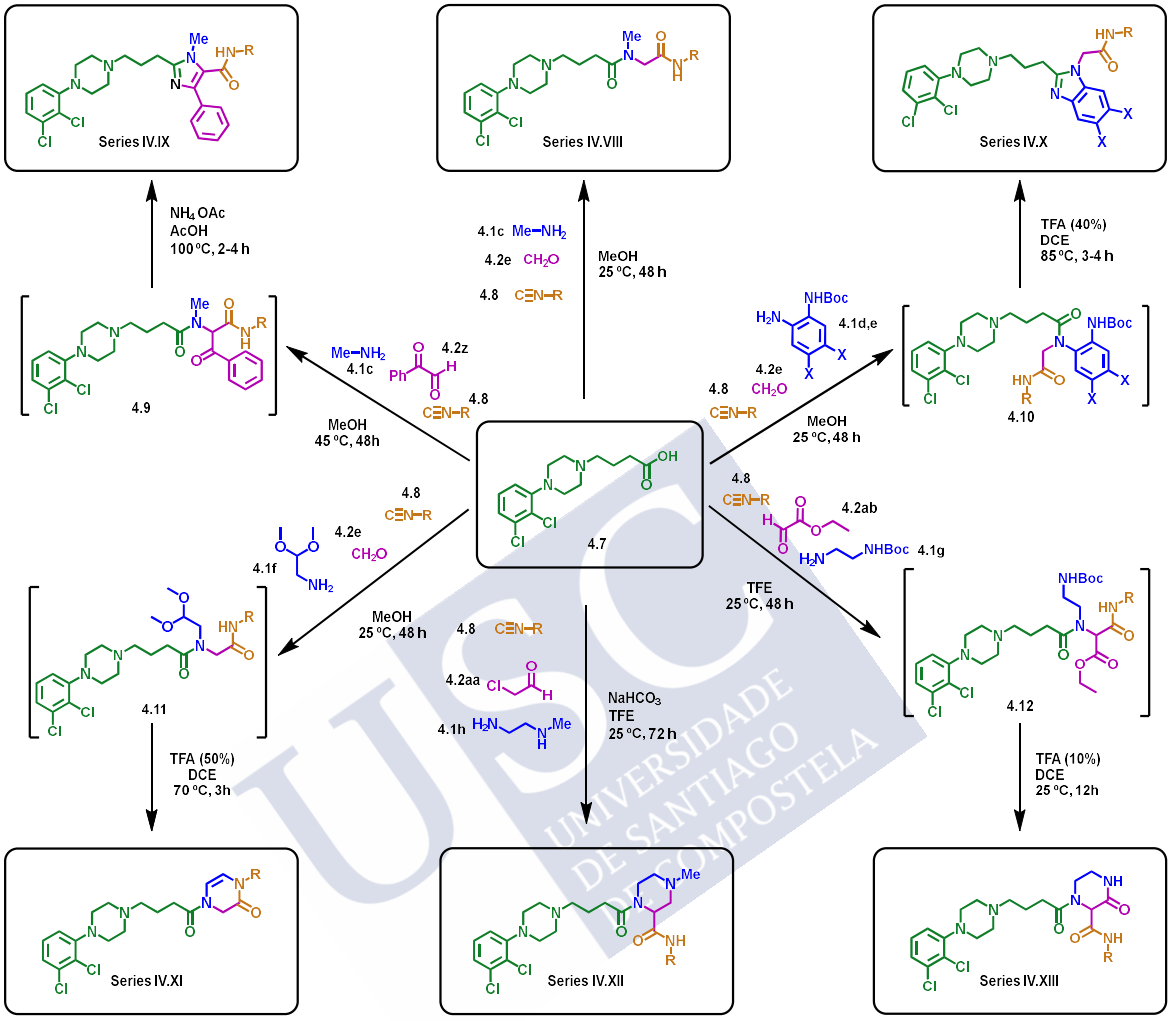

Scheme 4.5: Ugi-based assembly of the target compounds.

4.2 GENERAL DISCUSSION OF THE RESULTS

All compounds synthesized in this thesis were developed using multicomponent reactions (see above) to target two GPCRs ($A_{2B}AR$ and DRD_2). The compounds shown in the first and second chapters were obtained through Biginelli reaction to target $A_{2B}AR$, while those developed in the third chapter, were obtained with Ugi reaction to target DRD_2.

The design of compounds targeting $A_{2B}AR$, was inspired considering several representative structures of $A_{2B}AR$ antagonists previously described (Figure 4.1).

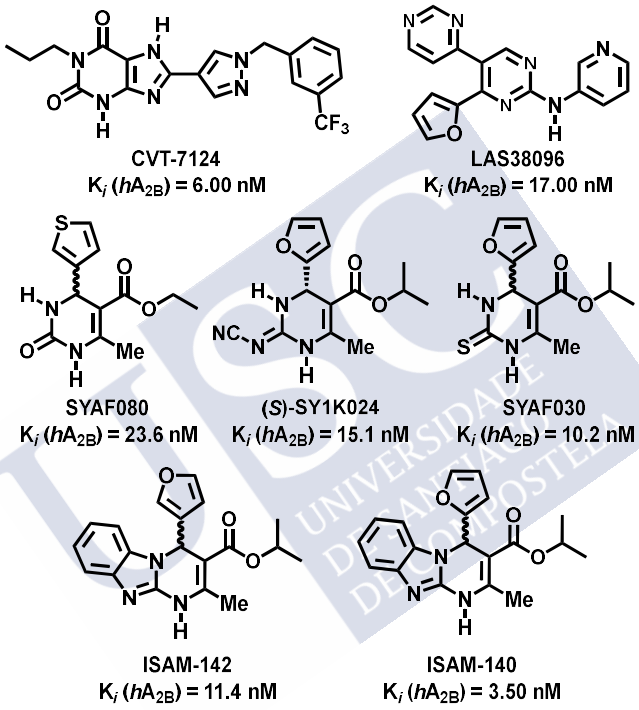

Figure 4.1: Several representative structures of Chapter 3.1 and Chapter 3.2.

In the first case, research was focused on the development of novel fluorinated compounds that replace hydrogen atoms by fluorine at active prototypes (Figure 4.2). This modification can exert a significant effect on diverse structural, pharmacodynamic, and pharmacokinetic parameters, leading to improved metabolic stability or optimized ligand efficiency. Furthermore, fluorinated ligands have become highly valued molecular probes during research programs employing positron emission tomography (PET). Being aware that the impact of fluorination on binding affinity can be scaffold-dependent, two representative Biginelli-based $A_{2B}AR$ antagonist chemotypes were selected for the study (Figure 4.2).

The second chapter is focused on the fact that the electron-rich nature of heterocyclic cores (such as furan or thiophene) means that some of these scaffolds can be classified as putative structural alerts. The early identification of structural elements that have the potential to become structural alerts constitutes a key issue during early drug discovery. Five-membered hetereoarenes are one example of such elements, which are ubiquitous scaffolds in the structures of adenosine antagonists (Figure 4.2).

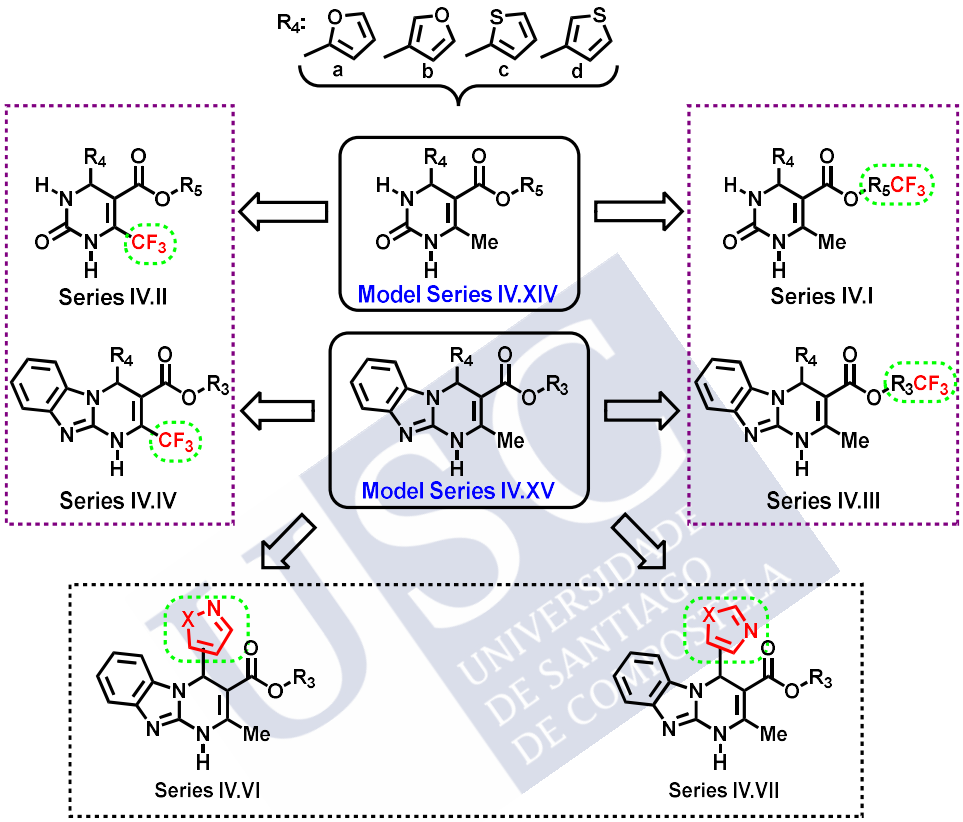

Figure 4.2: General structures of the designed compounds with their modifications (red).

The affinity and selectivity profiles of the compounds of both chapters were studied *in vitro*, by radioligand binding assays, at the four human ARs subtypes, using experimental protocols described in **Chapters 3.1** and **3.2**. Most ligands of both chapters were reported and tested as racemic mixtures.

Human ARs expressed in transfected CHO (A_1AR), HeLa (A_{2A}AR and A_{3A}R), and HEK-293 (A_{2B}AR) cells were employed for both chapters. [^{3}H]1,3-Dipropyl-8-cyclopentylxanthine ([^{3}H]DPCPX) for A_1AR and A_{2B}AR, [^{3}H]ZM241385 for A_{2A}AR, and [^{3}H]NECA for A_{3A}R were assessed as radioligands. The biological data are expressed as K_i ± SEM (nM, n = 3) or as percentage inhibition of specific binding at 1 μM (n = 2, average) for those compounds that did not fully displace the radioligand. K_i

values were obtained by fitting the data with nonlinear regression using Prism 5.0 software (GraphPad, San Diego, CA). For those compounds that showed either little affinity or poor solubility a percentage inhibition of specific binding is reported. Results are the mean of three experiments, each performed in duplicate. For comparative purposes, three structurally diverse and well-known adenosine antagonists (**DPCPX**, **ISAM-140**, and **ZM241385**) were tested under these conditions and their binding data included in the tables.

The pharmacological data and the Structure-Activity Relationship (SAR) analysis of the fluorinated compounds are presented below. Table 4.1 shows the parent series, published in previous articles of the group, while Tables 4.2−4.5 contain the new data obtained in this study.

Table 4.1: Structure and Adenosine Receptor Affinities of the 3,4-Dihydropyrimidin-2(1*H*)-ones (Series **IV.XIV**, Cpds **4.13a-h**) and 1,4-Dihydrobenzo[4,5]imidazo[1,2-*a*]pyrimidine-3-carboxylates (Series **IV.XV**, Cpds **4.14a-h**).

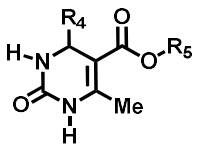

Model Series IV.XIV (Cpds 4.13a-h)

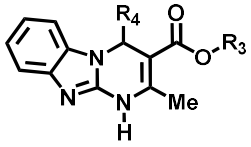

Model Series IV.XV (Cpds 4.14a-h)

			K_i (nM) or % at 1 μM			
Compound	**R_4**	**R_5**	*h*A_1[a]	*h*A_{2A}[b]	*h*A_{2B}[c]	*h*A_3[d]
4.13a	2-furyl	-CH_2-CH_3	18%	41%	585 ± 61	2%
4.13b	3-furyl	-CH_2-CH_3	21%	39%	39.6 ± 3	1%
4.13c	2-thienyl	-CH_2-CH_3	1%	33%	44%	1%
4.13d	3-thienyl	-CH_2-CH_3	22%	39%	23.6 ± 1	24%
4.13e	2-furyl	-$CH(CH_3)_2$	20%	30%	40.8 ± 3	1%
4.13f	3-furyl	-$CH(CH_3)_2$	25%	26%	1486 ± 41	3%
4.13g	2-thienyl	-$CH(CH_3)_2$	37%	19%	44%	14%
4.13h	3-thienyl	-$CH(CH_3)_2$	26%	25%	56.7 ± 3	1%
4.14a (ISAM-134)	2-furyl	-CH_2-CH_3	5%	14%	12.03 ± 2	1%
4.14b (ISAM-141)	3-furyl	-CH_2-CH_3	7%	11%	20.60 ± 1	1%
4.14c	2-thienyl	-CH_2-CH_3	8%	16%	484.6 ± 17	1%
4.14d	3-thienyl	-CH_2-CH_3	3%	10%	29.71 ± 3	2%
4.14e (ISAM-140)	2-furyl	-$CH(CH_3)_2$	20%	28%	3.49 ± 0.2	2%
4.14f (ISAM-142)	3-furyl	-$CH(CH_3)_2$	12%	23%	11.40 ± 1	2%
4.14g	2-thienyl	-$CH(CH_3)_2$	1%	17%	371.2 ± 8	3%
4.14h	3-thienyl	-$CH(CH_3)_2$	11%	3%	29.34 ± 1	21%
DPCPX	-	-	2.2 ± 0.2	157 ± 3	73.2 ± 2	1722 ± 11
ZM241385	-	-	683 ± 4	1.9 ± 0.1	65.7 ± 1.7	863 ± 4

[a]Displacement of specific [^{3}H]DPCPX binding in human CHO cells expressed as K_i ± SEM in nM (n = 3) or percentage displacement of specific binding at a concentration of 1 μM (n = 2). [b]Displacement of specific [^{3}H]4-(2-[7-amino-2-(2-furyl)[1,2,4]triazolo[2,3-*a*][1,3,5]triazin-5-ylamino]ethyl)phenol binding in human HeLa cells expressed as K_i ± SEM in nM (n = 3) or percentage displacement of specific binding at a concentration of 1 μM (n = 2). [c]Displacement of specific [^{3}H]DPCPX binding in human HEK-293 cells expressed as K_i ± SEM in nM (n = 3) or percentage displacement of specific binding at a concentration of 1 μM (n = 2). [d]Displacement of specific [^{3}H]NECA binding in human HeLa cells expressed as K_i ± SEM in nM (n = 3) or percentage displacement of specific binding at a concentration of 1 μM (n = 2).

Table 4.2: Structure and Adenosine Receptor Affinities of the 5-Alcoxy-Fluorinated Carbonyl 3,4-Dihydropyrimidin-2(1*H*)-ones (Series **IV.I**, Cpds **4.15a-l**).

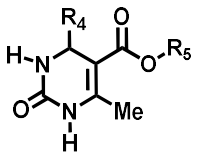

			K_i (nM) or % at 1 μM			
Compound	**R_4**	**R_5**	*h*A_1[a]	*h*A_{2A}[b]	*h*A_{2B}[c]	*h*A_3[d]
4.15a	2-furyl	-CH_2-CF_3	10%	1%	157 ± 3	1%
4.15b	3-furyl	-CH_2-CF_3	13%	9%	588 ± 15	1%
4.15c	2-thienyl	-CH_2-CF_3	3%	3%	1%	1%
4.15d	3-thienyl	-CH_2-CF_3	2%	1%	24%	1%
4.15e	2-furyl	-$CH(CF_3)_2$	6%	1%	1%	2%
4.15f	3-furyl	-$CH(CF_3)_2$	7%	22%	2%	1%
4.15g	2-thienyl	-$CH(CF_3)_2$	9%	1%	1%	1%
4.15h	3-thienyl	-$CH(CF_3)_2$	17%	1%	1%	8%
4.15i-D_1[&]	2-furyl	-CH(Me)CF_3	1%	3%	61.50 ± 2	11%
4.15i-D_2[&]	2-furyl	-CH(Me)CF_3	1%	1%	303 ± 3	7%
4.15j-D_1[&]	3-furyl	-CH(Me)CF_3	10%	1%	234 ± 2	12%
4.15j-D_2[&]	3-furyl	-CH(Me)CF_3	1%	1%	23%	5%
4.15k-D_1[&]	2-thienyl	-CH(Me)CF_3	12%	2%	4%	3%
4.15k-D_2[&]	2-thienyl	-CH(Me)CF_3	16%	1%	1%	3%
4.15l-D_1[&]	3-thienyl	-CH(Me)CF_3	3%	2%	643 ± 10	2%
4.15l-D_2[&]	3-thienyl	-CH(Me)CF_3	3%	2%	1%	1%
ISAM-140	2-furyl	-$CH(CH_3)_2$	20%	28%	3.49 ± 0.2	2%
DPCPX	-	-	2.2 ± 0.2	157 ± 3	73.2 ± 2	1722 ± 11
ZM241385	-	-	683 ± 4	1.9 ± 0.1	65.7 ± 1.7	863 ± 4

[&]Tested as a diastereomer pair. [a]Displacement of specific [^{3}H]DPCPX binding in human CHO cells expressed as K_i ± SEM in nM (n = 3) or percentage displacement of specific binding at a concentration of 1 μM (n = 2). [b]Displacement of specific [^{3}H]4-(2-[7-amino-2-(2-furyl)[1,2,4]triazolo[2,3-*a*][1,3,5]triazin-5-ylamino]ethyl)-phenol binding in human HeLa cells expressed as K_i ± SEM in nM (n = 3) or percentage displacement of specific binding at a concentration of 1 μM (n = 2). [c]Displacement of specific [^{3}H]DPCPX binding in human HEK-293 cells expressed as K_i ± SEM in nM (n = 3) or percentage displacement of specific binding at a concentration of 1 μM (n = 2). [d]Displacement of specific [^{3}H]NECA binding in human HeLa cells expressed as K_i ± SEM in nM (n = 3) or percentage displacement of specific binding at a concentration of 1 μM (n = 2).

Table 4.3: Structure and Adenosine Receptor Affinities of the 6-Trifluoromethyl-5-alcoxycarbonyl 3,4-dihydro-pyrimidin-2(1*H*)-ones (Series **IV.II**, Cpds **4.16a-h**).

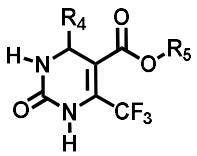

			K_i (nM) or % at 1 μM			
Compound	**R_4**	**X**	*h*A_1[a]	*h*A_{2A}[b]	*h*A_{2B}[c]	*h*A_3[d]
4.16a	2-furyl	-CH_2-CH_3	15%	32%	2%	2%
4.16b	3-furyl	-CH_2-CH_3	37%	55%	521 ± 7	1%
4.16c	2-thienyl	-CH_2-CH_3	28%	20%	16%	1%
4.16d	3-thienyl	-CH_2-CH_3	32%	46%	575 ± 9	3%
4.16e	2-furyl	-$CH(CH_3)_2$	11%	24%	238 ± 4	5%
4.16f	3-furyl	-$CH(CH_3)_2$	27%	21%	37%	1%
4.16g	2-thienyl	-$CH(CH_3)_2$	8%	13%	19%	7%
4.16h	3-thienyl	-$CH(CH_3)_2$	23%	9%	651 ± 8	3%
ISAM-140	2-furyl	-$CH(CH_3)_2$	20%	28%	3.49 ± 0.2	2%
DPCPX	-	-	2.2 ± 0.2	157 ± 3	73.2 ± 2	1722 ± 11
ZM241385	-	-	683 ± 4	1.9 ± 0.1	65.7 ± 1.7	863 ± 4

[a]Displacement of specific [^{3}H]DPCPX binding in human CHO cells expressed as K_i ± SEM in nM (n = 3) or percentage displacement of specific binding at a concentration of 1 μM (n = 2). [b]Displacement of specific [^{3}H]4-(2-[7-amino-2-(2-furyl)[1,2,4]triazolo[2,3-*a*][1,3,5]triazin-5-ylamino]ethyl)phenol binding in human HeLa cells expressed as K_i ± SEM in nM (n = 3) or percentage displacement of specific binding at a concentration of 1 μM (n = 2). [c]Displacement of specific [^{3}H]DPCPX binding in human HEK-293 cells expressed as K_i ± SEM in nM (n = 3) or percentage displacement of specific binding at a concentration of 1 μM (n = 2). [d]Displacement of specific [^{3}H]NECA binding in human HeLa cells expressed as K_i ± SEM in nM (n = 3) or percentage displacement of specific binding at a concentration of 1 μM (n = 2).

Table 4.4: Structure and Adenosine Receptor Affinities of the Alkyl 4-Heteroaryl-2-methyl-1,4-dihydrobenzo[4,5]imidazo[1,2-*a*]pyrimidine-3-carboxylates (Series **IV.III**, Cpds **4.6a-l**).

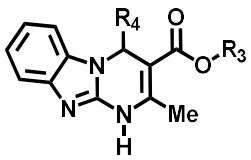

			K_i (nM) or % at 1 μM			
Compound	**R_4**	**R_3**	*h*A_1[a]	*h*A_{2A}[b]	*h*A_{2B}[c]	*h*A_3[d]
4.6a	2-furyl	-CH_2-CF_3	16%	7%	27.03 ± 1	23%
4.6b	3-furyl	-CH_2-CF_3	14%	11%	42.10 ± 2	1%
4.6c	2-thienyl	-CH_2-CF_3	1%	7%	6%	2%
4.6d	3-thienyl	-CH_2-CF_3	7%	17%	30%	2%
4.6e	2-furyl	-$CH(CF_3)_2$	16%	2%	16%	24%
4.6f	3-furyl	-$CH(CF_3)_2$	24%	10%	21%	6%
4.6g	2-thienyl	-$CH(CF_3)_2$	11%	10%	7%	19%
4.6h	3-thienyl	-$CH(CF_3)_2$	3%	15%	1%	1%
4.6i	2-furyl	-CH(Me)CF_3	3%	4%	29.60 ± 2	18%
4.6j	3-furyl	-CH(Me)CF_3	2%	3%	52.27 ± 2	3%
4.6k	2-thienyl	-CH(Me)CF_3	34%	2%	27%	4%
4.6l	3-thienyl	-CH(Me)CF_3	2%	24%	47%	2%
ISAM-140	2-furyl	-$CH(CH_3)_2$	20%	28%	3.49 ± 0.2	2%
DPCPX	-	-	2.2 ± 0.2	157 ± 3	73.2 ± 2	1722 ± 11
ZM241385	-	-	683 ± 4	1.9 ± 0.1	65.7 ± 1.7	863 ± 4

[a]Displacement of specific [^{3}H]DPCPX binding in human CHO cells expressed as K_i ± SEM in nM (n = 3) or percentage displacement of specific binding at a concentration of 1 μM (n = 2). [b]Displacement of specific [^{3}H]4-(2-[7-amino-2-(2-furyl)[1,2,4]triazolo[2,3-*a*][1,3,5]triazin-5-ylamino]ethyl)phenol binding in human HeLa cells expressed as K_i ± SEM in nM (n = 3) or percentage displacement of specific binding at a concentration of 1 μM (n = 2). [c]Displacement of specific [^{3}H]DPCPX binding in human HEK-293 cells expressed as K_i ± SEM in nM (n = 3) or percentage displacement of specific binding at a concentration of 1 μM (n = 2). [d]Displacement of specific [^{3}H]NECA binding in human HeLa cells expressed as K_i ± SEM in nM (n = 3) or percentage displacement of specific binding at a concentration of 1 μM (n = 2).

Table 4.5: Structure and Adenosine Receptor Affinities of the Alkyl 4-Heteroaryl-2-trifluoro-methyl-1,4-dihydrobenzo[4,5]imidazo[1,2-*a*]pyrimidine-3-carboxylates (Series **IV.IV**, Cpds **4.17a-h**).

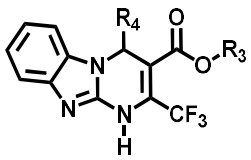

			K_i (nM) or % at 1 μM			
Compound	**R_4**	**R_3**	*h*A_1[a]	*h*A_{2A}[b]	*h*A_{2B}[c]	*h*A_3[d]
4.17a	2-furyl	-CH_2-CH_3	11%	4%	731 ± 11	20%
4.17b	3-furyl	-CH_2-CH_3	9%	18%	37.42 ± 3	6%
4.17c	2-thienyl	-CH_2-CH_3	7%	4%	38%	19%
4.17d	3-thienyl	-CH_2-CH_3	16%	13%	117.8 ± 9	29%
4.17e	2-furyl	-$CH(CH_3)_2$	3%	10%	39%	5%
4.17f	3-furyl	-$CH(CH_3)_2$	8%	23%	49.20 ± 3	23%
4.17g	2-thienyl	-$CH(CH_3)_2$	4%	1%	17%	1%
4.17h	3-thienyl	-$CH(CH_3)_2$	10%	3%	48%	2%
ISAM-140	2-furyl	-$CH(CH_3)_2$	20%	28%	3.49 ± 0.2	2%
DPCPX	-	-	2.2 ± 0.2	157 ± 3	73.2 ± 2	1722 ± 11
ZM241385	-	-	683 ± 4	1.9 ± 0.1	65.7 ± 1.7	863 ± 4

[a]Displacement of specific [^{3}H]DPCPX binding in human CHO cells expressed as K_i ± SEM in nM (n = 3) or percentage displacement of specific binding at a concentration of 1 μM (n = 2). [b]Displacement of specific [^{3}H]4-(2-[7-amino-2-(2-furyl)[1,2,4]triazolo[2,3-*a*][1,3,5]triazin-5-ylamino]ethyl)phenol binding in human HeLa cells expressed as K_i ± SEM in nM (n = 3) or percentage displacement of specific binding at a concentration of 1 μM (n = 2). [c]Displacement of specific [^{3}H]DPCPX binding in human HEK-293 cells expressed as K_i ± SEM in nM (n = 3) or percentage displacement of specific binding at a concentration of 1 μM (n = 2). [d]Displacement of specific [^{3}H]NECA binding in human HeLa cells expressed as K_i ± SEM in nM (n = 3) or percentage displacement of specific binding at a concentration of 1 μM (n = 2).

As shown in Tables 4.2–4.5, the binding affinity data obtained for series **IV.I**–**IV.IV** revealed the identification of ligands with attractive affinity and selectivity profiles, in some cases comparable to the values of model series **IV.XIV** and **IV.XV**. In addition, some compounds of series **IV.III** (**4.6a**, **4.6b**, **4.6i**, and **4.6j**; see Table 4.4) and **IV.IV** (such as **4.17b**, **4.17f**, Table 4.5) combine high affinity (< 50 nM) and exquisite selectivity (>1000-fold) for the A_{2B}AR. A direct comparison of the affinity data between each new series related to their respective model scaffolds (i.e., series **IV.XIV** and **IV.XV** in Table 4.1) shows two main tendencies: (1) the introduction of trifluoromethyl groups generally affects the affinity of *h*A_{2B}AR detrimentally. There is a clear exception to these trend, fluorination of the ethyl residue at the ester group for the

4.13a/**4.15a** pair, where there is a gain in affinity; (2) the effect of trifluorination is scaffold-dependent.

Since all these compounds have one (or even two) stereogenic centers, the three most potent ligands (**4.6a**, **4.6i**, and **4.17b**) were separated into their diastereoisomers and evaluated at the four human adenosine receptor subtypes in its enantio- or diastereopure forms, respectively, to determine the affinity role of stereoselectivity on the synthesized compounds. The tricyclic compounds selected were **4.6a**, and **4.6i** (from series **IV.III**, bearing a trifluoromethyl group at the ethyl or isopropyl residues of the ester group, respectively, which creates an additional stereogenic center), and **4.17b** (from series **IV.IV**, which is trifluoromethylated at position 2).

A combination of chiral HPLC, circular dichroism (CD) spectroscopy, and X-ray crystallography was employed to separate and unequivocally assign the configuration of the heterocyclic stereocenter in each stereoisomer. Semipreparative HPLC separation of (4*R*/4*S*)-**4.6a** and (4*R*/4*S*)-**4.17b** on a chiral stationary phase provided the expected four enantiomers with excellent stereochemical purity (*e.g.*, 97−99%).

As reported in the literature for structurally related 3,4-dihydropyrimidin-2-ones, the characteristic CD activity of the enamide chromophore (300−350 nm) allowed the unambiguous assignment of the absolute configuration of each enantiomer (Figure 4.3). The assignment was developed by comparison with the reported CD data for enantiopure 3,4-dihydropyrimidin-2(1*H*)-ones of known configuration. At 300−350 nm, enantiomers showing a positive Cotton effect (blue line) contain the backward furan ring (and correspond to (4*S*)-**4.6a** and (4*R*)-**4.17b**, respectively), whereas stereoisomers giving a negative Cotton effect (red line) contain the forward pentagonal heterocycle (which are (4*R*)-**4.6a** and (4*S*)-**4.17b**, respectively). Structural analysis of monocrystals of (4*S*)-**4.6a**, (4*R*)-**4.6a**, (4*S*)-**4.17b**, and (4*R*)-**4.17b**, through X-ray crystallography provided additional experimental data corroborating the CD-assisted stereochemical assignment. All these data can be found at Figure 4.3.

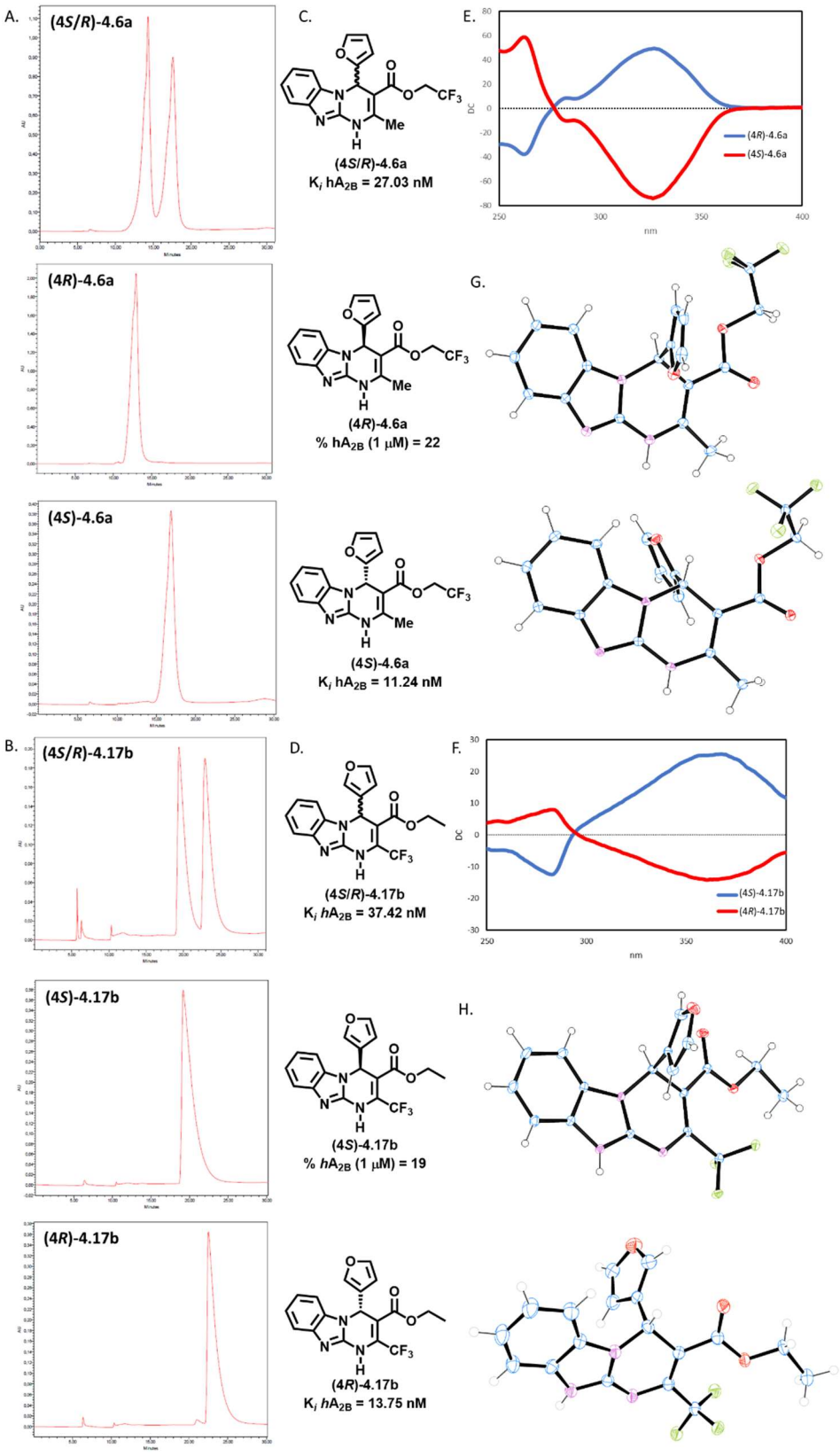

Figure 4.3: (A, B) Chiral HPLC traces; (C, D) absolute configuration and biological data; (E, F) circular dichroism spectra and (G, H) crystal structure of compounds **4.6a** (top) and **4.17b** (bottom).

Nevertheless, as opposed to the successful separation of the previous compounds, all efforts to isolate the four diastereomers of **4.6i** by preparative chiral HPLC were unsuccessful, even after extensive exploration of diverse chiral stationary phases, mobile phases, or other experimental conditions. Moreover, the unequivocal assignment of the exocyclic chiral center configuration in **4.6i** would not be achievable by CD spectroscopy, which motivated the design of a diastereoselective synthetic pathway for these compounds. The synthetic approach can be seen above (**Chapter 4.1**).

Once the **4.6i** diastereomers were synthesized, the two pairs were successfully resolved into single diastereomers, with excellent stereochemical purity (97−99%), using semipreparative chiral HPLC. As for the previous stereoisomers, the unambiguous assignment of the absolute configuration of the heterocyclic stereocenter was established by CD spectroscopy, using the sign of the Cotton effect at 300 nm as a reference (Figure 4.4).

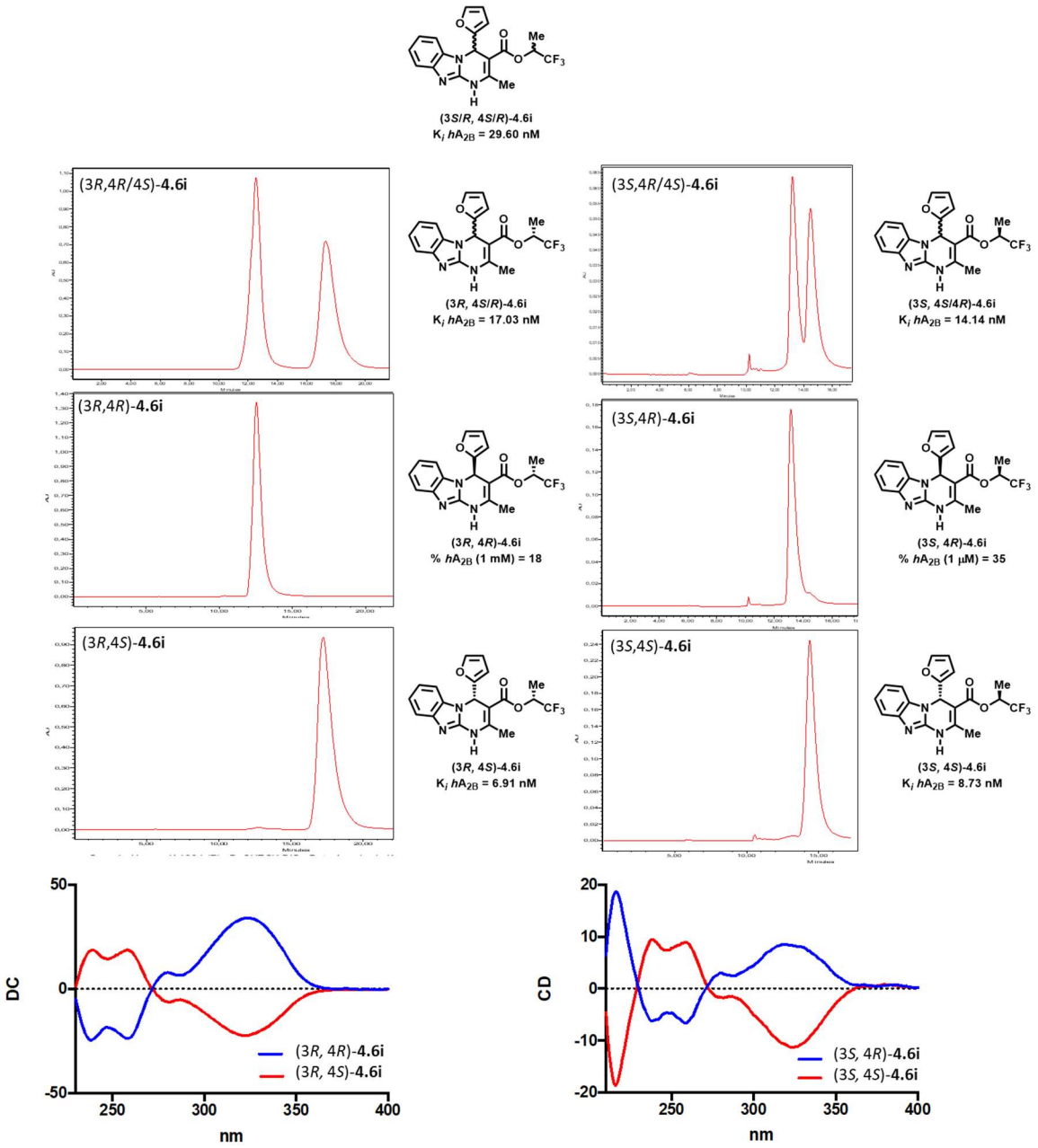

Figure 4.4: Chiral HPLC traces, absolute configuration and hA_{2B} affinity and circular dichroism spectra of the diastereoisomers of **4.6i**.

The results of the pharmacological evaluation of the different stereoisomers isolated and identified in this study are depicted in the Table 4.6

Table 4.6: Affinity Binding Data for the Different Stereoisomers of Compounds **4.6a**, **4.6i**, and **4.17b** at the Human Adenosine Receptors (structural details in Figures 4.3 and 4.4).

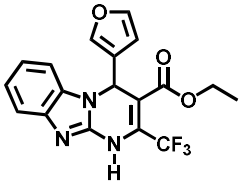

4.17b

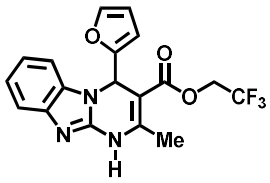

4.6a

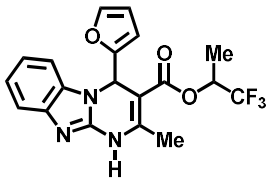

4.6i

	K_i (nM) or % at 1 μM			
Compound	hA_1[a]	hA_{2A}[b]	hA_{2B}[c]	hA_3[d]
(**4*R*/4*S*)-4.17b**	9%	18%	37.42 ± 3	6%
(4*R*)-4.17b	11%	9%	13.75 ± 1	3%
(4*S*)-4.17b	10%	17%	19%	3%
(**4*R*/4*S*)-4.6a**	16%	7%	27.03 ± 1	23%
(4*R*)-4.6a	12%	3%	22%	8%
(4*S*)-4.6a	9%	1%	11.24 ± 1	7%
(3*R*/*S*,4*R*/*S*)-4.6i	3%	4%	29.60 ± 2	18%
(3*R*,4*R*/*S*)-4.6i	12%	11%	17.03 ± 1	23%
(3*R*,4*R*)-4.6i	2%	2%	18%	1%
(3*R*,4*S*)-4.6i	12%	1%	6.91± 0.5	14%
(3*S*,4*R*/*S*)-4.6i	26%	1%	15.14 ± 1	7%
(3*S*,4*R*)-4.6i	7%	19%	35%	9%
(3*S*,4*S*)-4.6i	22%	5%	8.73 ± 0.7	21%
ISAM-140	20 ± 1	28 ± 5	3.49 ± 0.2	2 ± 5
DPCPX	2.2 ± 0.2	157 ± 3	73.2 ± 2	1722 ± 11
ZM241385	683 ± 4	1.9 ± 0.1	65.7 ± 1.7	863 ± 4

[a]Displacement of specific [^{3}H]DPCPX binding in human CHO cells expressed as K_i ± SEM in nM (n = 3) or percentage displacement of specific binding at a concentration of 1 μM (n = 2). [b]Displacement of specific [^{3}H]4-(2-[7-amino-2-(2-furyl)[1,2,4]triazolo[2,3-*a*][1,3,5]triazin-5-ylamino]ethyl)phenol binding in human HeLa cells expressed as K_i ± SEM in nM (n = 3) or percentage displacement of specific binding at a concentration of 1 μM (n = 2). [c]Displacement of specific [^{3}H]DPCPX binding in human HEK-293 cells expressed as K_i ± SEM in nM (n = 3) or percentage displacement of specific binding at a concentration of 1 μM (n = 2). [d]Displacement of specific [^{3}H]NECA binding in human HeLa cells expressed as K_i ± SEM in nM (n = 3) or percentage displacement of specific binding at a concentration of 1 μM (n = 2).

Functional experiments were performed with the aim of providing further evidence for the pharmacological functionality of this novel series of fluorinated A_{2B}AR ligands. The three compounds with the most attractive affinity/selectivity profiles (**4.6a**, **4.6i**, and **4.17b**) were tested in cAMP assays to evaluate their ability to inhibit NECA-stimulated (10 μM) cAMP production. This study demonstrated that all ligands inhibit cAMP accumulation, validating the A_{2B}AR antagonistic profile of the new fluorinated derivatives. Comparison of affinity and functional data showed excellent correlation (**4.6a**, K_i = 27.03 nM and K_B = 83.22 nM; **4.6i**, K_i = 29.60 nM and K_B = 105.63 nM; **4.17b**, K_i = 37.42 nM and K_B = 79.41 nM).

The aim of **Chapter 3.2** was to identify novel heteroarene cores to be introduced at position 4 of the 4-heteroaryl-2-methyl-1,4-dihydrobenzo[4,5]imidazo[1,2-*a*]pyrimidine-3-carboxylate scaffold. The first subset (series **IV.V**, Table 4.7), which was conceived to expand the diversity elements at position 4 of the model series **IV.XV** (Table 4.1), demonstrates the importance of the pentagonal core, and facilitates an exhaustive exploration of the effect of nitrogen introduction, therefore allowing a comparative analysis within the aza-analogues (Tables 4.8 and 4.9). Thus, 12 additional ligands (**4.18a−l**) were synthesized and evaluated, all containing hydrogen, cyclopentyl, and phenyl or 3-pyrrolyl, 2-pyrrolyl, and 5-methylfuran-2-yl residues at position 4 of the 1,4-dihydrobenzo-[4,5]-imidazo[1,2-*a*]pyrimidine-3-carboxylate scaffold.

On the other hand, novel series (**IV.VI** and **IV.VII**) were designed according to bioisosteric replacement criteria, applying 'the nitrogen-walk approach'. This method consists of the systematic introduction of a nitrogen atom in different positions of the pentagonal core in parent series **IV.XV.** This approach is widely recognized as a classical bioisosteric replacement. The substitution of a CH group for a nitrogen atom in heteroaromatic systems often has important consequences during multiparametric optimization. Even though the effects of these seemingly trivial modifications (such as the replacement of a CH group with a N atom) on basicity, lipophilicity, polar surface area, and hydrogen-bonding capacity are relatively predictable, their impact on receptor recognition and binding affinity, solubility, active transport, and metabolic stability can be more troublesome.

Since previous studies on structurally related scaffolds reported that the introduction of hexagonal aryl and heteroaryl scaffolds completely abolished the affinity

of A_{2B}AR, this work has focused on pentagonal scaffolds. A subset of 15 azole scaffolds (series **IV.VI** and **IV.VII**) was used to expand the structural diversity at position 4 of the original tricyclic scaffold (series **IV.XV**).

The carboxaldehydes used during this chapter can be classified into two subsets (1,2-azoles and 1,3-azoles). It should be noted that both differ not only in the heteroatoms but also in the position of the formyl group within the heterocycle (2-, 3-, 4-, or 5-position). To our knowledge, this is the first study in which the real impact of bioisosteric replacement of furan/thiophene cores in terms of binding affinity and selectivity for a prototypic series of potent A_2BAR antagonists has been comprehensively explored. In order to obtain a broad overview of the effect of bioisosteric replacement, and to maintain consistency with the SAR from the model series, the libraries synthesized in this study (series **IV.V**−**IV.VII**) retained the two alkoxy residues at position 3 that were previously associated with high A_{2B}AR affinity (*e.g.*, ethyl or isopropyl groups).

The adenosinergic (affinity and selectivity) profile of the 42 novel ligands was evaluated *in vitro* using radioligand binding assays (for the four human AR subtypes). Tables 4.7−4.9 contain the binding data for the three novel series reported in the second chapter. In the case of the most potent compound (**4.20g**), the enantiomers were separated, identified, and tested for the four human AR subtypes in its enantiopure forms (Table 4.11). These data were employed to complement the SAR study and to evaluate the importance of the configuration of the stereogenic center on affinity. The whole set was evaluated *in silico*, using the PAINS filter in RDkit, to rule out these ligands being promiscuous pan-assay interference compounds (PAINS).

All the binding data were evaluated and measured as mentioned above, using the same transfected cells as in the previous study, as well as the same radioligands.

Table 4.7: Structure and Affinity Binding Data for the Alkyl 4-Substituted-2-methyl-1,4-dihydrobenzo[4,5] imidazo[1,2-*a*]pyrimidine-3-carboxylates **4.18a-l** at the Human ARs.

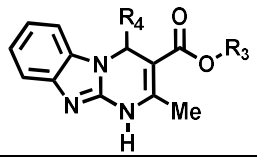

			K_i (nM) or % at 1 μM			
Compound	**R_4**	**R_3**	*h*A_1[a]	*h*A_{2A}[b]	*h*A_{2B}[c]	*h*A_3[d]
4.18a	H	Et	34%	11%	32%	9%
4.18b		*i*-Pr	31%	4%	19%	13%
4.18c		Et	11%	10%	33%	17%
4.18d		*i*-Pr	14%	2%	38%	23%
4.18e		Et	12%	9%	8%	15%
4.18f		*i*-Pr	9%	3%	11%	9%
4.18g	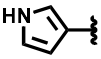	Et	26%	7%	449.30 ± 3	1%
4.18h		*i*-Pr	19%	1%	517.10 ± 4	2%
4.18i		Et	45%	2%	49.60 ± 2.5	9%
4.18j		*i*-Pr	38%	19%	31.30 ± 1.9	1%
4.18k	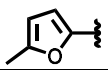	Et	14%	1%	17%	3%
4.18l		*i*-Pr	14%	3%	9%	1%
DPCPX	-	-	2.20 ± 0.2	157 ± 2.9	73.24 ± 1.4	1722 ± 11
ZM241385	-	-	683 ± 4.1	1.9 ± 0.1	65.70 ± 1.1	863 ± 4.0
ISAM-140	-	-	20%	28%	3.49 ± 0.2	2%

[a]Displacement of specific [^{3}H]DPCPX binding in human CHO cells expressed as K_i ± SEM in nM (n = 3) or percentage displacement of specific binding at a concentration of 1 μM (n = 2). [b]Displacement of specific [^{3}H]4-(2-[7-amino-2-(2-furyl)[1,2,4]triazolo[2,3-*a*][1,3,5]triazin-5-ylamino]ethyl)phenol binding in human HeLa cells expressed as K_i ± SEM in nM (n = 3) or percentage displacement of specific binding at a concentration of 1 μM (n = 2). [c]Displacement of specific [^{3}H]DPCPX binding in human HEK-293 cells expressed as K_i ± SEM in nM (n = 3) or percentage displacement of specific binding at a concentration of 1 μM (n = 2). [d]Displacement of specific [^{3}H]NECA binding in human HeLa cells expressed as K_i ± SEM in nM (n = 3) or percentage displacement of specific binding at a concentration of 1 μM (n = 2).

Table 4.8: Structure and Affinity Binding Data for the Alkyl 4-Substituted-2-methyl-1,4-dihydrobenzo[4,5] imidazo[1,2-*a*]pyrimidine-3-carboxylates **4.19a-n** at the Human ARs.

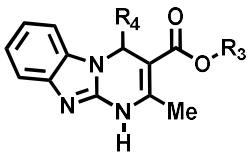

			K_i (nM) or % at 1 μM			
Compound	**R_4**	**R_3**	*h*A_1[a]	*h*A_{2A}[b]	*h*A_{2B}[c]	*h*A_3[d]
4.19a	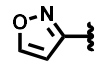	Et	2%	1%	789 ± 35	3%
4.19b		*i*-Pr	1%	2%	721 ± 31	4%
4.19c	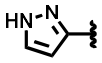	Et	8%	11%	707 ± 42	1%
4.19d		*i*-Pr	1%	7%	1104 ± 103	2%
4.19e (ISAM-A344)		Et	21%	30%	23.40 ± 1.2	13%
4.19f (ISAM-A275)		*i*-Pr	1%	2%	29.60 ± 1.4	5%
4.19g		Et	20%	11%	1%	14%
4.19h		*i*-Pr	9%	11%	278 ± 14	14%
4.19i	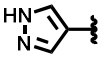	Et	14.80 ± 0.9	28%	92.60 ± 4.8	1%
4.19j		*i*-Pr	8.30 ± 0.5	40%	340 ± 29	6%
4.19k		Et	1%	1%	714 ± 46	11%
4.19l		*i*-Pr	37%	7%	1031 ± 112	1%
4.19m		Et	20.20 ± 1.2	7%	98.70 ± 1.1	8%
4.19n		*i*-Pr	24%	18%	175 ± 16	4%
DPCPX	-	-	2.20 ± 0.2	157 ± 2.9	73.24 ± 1.4	1722 ± 11
ZM241385	-	-	683 ± 4.1	1.9 ± 0.1	65.7 ± 1.1	863 ± 4.0
ISAM-140	-	-	20%	25%	3.49 ± 0.2	2%

[a]Displacement of specific [^{3}H]DPCPX binding in human CHO cells expressed as K_i ± SEM in nM (n = 3) or percentage displacement of specific binding at a concentration of 1 μM (n = 2). [b]Displacement of specific [^{3}H]4-(2-[7-amino-2-(2-furyl)[1,2,4]triazolo[2,3-*a*][1,3,5]triazin-5-ylamino]ethyl)phenol binding in human HeLa cells expressed as K_i ± SEM in nM (n = 3) or percentage displacement of specific binding at a concentration of 1 μM (n = 2). [c]Displacement of specific [^{3}H]DPCPX binding in human HEK-293 cells expressed as K_i ± SEM in nM (n = 3) or percentage displacement of specific binding at a concentration of 1 μM (n = 2). [d]Displacement of specific [^{3}H]NECA binding in human HeLa cells expressed as K_i ± SEM in nM (n = 3) or percentage displacement of specific binding at a concentration of 1 μM (n = 2).

Table 4.9: Structure and Affinity Binding Data for the Alkyl 4-Substituted-2-methyl-1,4-dihydrobenzo[4,5] imidazo[1,2-*a*]pyrimidine-3-carboxylates **4.20a-p** at the Human ARs.

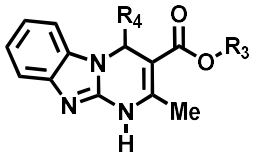

			K_i (nM) or % at 1 μM			
Compound	**R_4**	**R_3**	*h*A_1[a]	*h*A_{2A}[b]	*h*A_{2B}[c]	*h*A_3[d]
4.20a		Et	8%	2	769 ± 41	10%
4. 20b		*i*-Pr	1%	1	708 ± 38	10%
4. 20c		Et	3%	3	388 ± 24	1%
4. 20d		*i*-Pr	5%	4%	753 ± 39	20%
4. 20e		Et	6%	5	402 ± 25	1%
4. 20f		*i*-Pr	2%	4%	45%	2%
4. 20g (ISAM-C032)		Et	5%	11%	8.10 ± 0.5	7%
4. 20h		*i*-Pr	7%	19%	43.41 ± 1.3	16%
4. 20i		Et	1%	1%	8%	2%
4. 20j		*i*-Pr	1%	3%	7%	18%
4. 20k	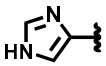	Et	7%	16%	4%	3%
4. 20l		*i*-Pr	5%	4%	5%	8%
4. 20m		Et	233 ± 17	282 ± 2	508 ± 27	418 ± 21
4. 20n		*i*-Pr	301 ± 13	38%	4%	39%
4. 20o		Et	32%	1%	215 ± 29	1%
4. 20p		*i*-Pr	2%	3%	68.30 ± 3.3	5%
DPCPX	-	-	2.20 ± 0.2	157 ± 2.9	73.24 ± 1.4	1722 ± 11
ZM241385	-	-	683 ± 4.1	1.9 ± 0.1	65.7 ± 1.1	863 ± 4.0
ISAM-140	-	-	20%	25%	3.49 ± 0.2	2%

[a]Displacement of specific [^{3}H]DPCPX binding in human CHO cells expressed as K_i ± SEM in nM (n = 3) or percentage displacement of specific binding at a concentration of 1 μM (n = 2). [b]Displacement of specific [^{3}H]4-(2-[7-amino-2-(2-furyl)[1,2,4]triazolo[2,3-*a*][1,3,5]triazin-5-ylamino]ethyl)phenol binding in human HeLa cells expressed as K_i ± SEM in nM (n = 3) or percentage displacement of specific binding at a concentration of 1 μM (n = 2). [c]Displacement of specific [^{3}H]DPCPX binding in human HEK-293 cells expressed as K_i ± SEM in nM (n = 3) or percentage displacement of specific binding at a concentration of 1 μM (n = 2). [d]Displacement of specific [^{3}H]NECA binding in human HeLa cells expressed as K_i ± SEM in nM (n = 3) or percentage displacement of specific binding at a concentration of 1 μM (n = 2).

The binding data obtained for the novel compounds (Tables 4.7−4.9) reveal several interesting features of the effect of variability at position 4 (R_4), while allowing the identification of four potent (K_i < 50 nM) and highly selective A_{2B}AR ligands, **4.19e** and **4.19f** (Table 4.8) and **4.20g** and **4.20h** (Table 4.9). The data reported in Table 4.7 highlight the crucial role of the pentagonal heterocycle at position R_4 of the tricyclic scaffold for interaction with A_{2B}AR. Therefore, ligands with a 5-methyl-2-furyl group or containing cyclopentyl or phenyl residues at position 4 are inactive (Table 4.7). Nevertheless, ligands bearing a pentagonal heterocycle bind A_{2B}AR with affinities ranging from moderate to high.

As mentioned above, ligands **4.18g−l** (Table 4.7) were included in the study with two aims: (i) to expand the diversity of the former series and (ii) to better understand the biological impact of the CH/N bioisosteric replacement. While the pyrrole core is also classified as a structural alert by several published works (see Chapter 3.2), it is known that the introduction of a methyl group in the furan core generally increases the metabolic stability. Two compelling observations emerge from the analysis of the binding data obtained for this subset (Table 4.7, **4.18g−l**). Firstly, in clear contrast to structural analogues of this pharmacophore, the introduction of a pyrrole core at position 4 produces ligands with moderate (**4.18g** and **4.18h**) to high (**4.18i** and **4.18j**) A_{2B}AR affinity. Although the 2-pyrrolyl derivatives **4.18i** and **4.18j** exhibit attractive affinities (K_i = 49.60 and 31.30 nM, respectively), they do not share the exceptional selectivity profiles characteristic of this series, with incipient affinity for A_1AR (Table 4.7).

Secondly, the high affinities measured for ligands bearing a 2-furyl group (Table 4.1, compounds **4.14a** and **4.14e**, K_i = 12.03 and 3.49 nM, respectively) are completely abolished when a methyl group is introduced at position 5 of the furan ring (Table 4.7, compounds **4.18k** and **4.18l**). This effect could be explained as this methyl group would create steric repulsion with the tight pocket of the receptor. The same effect was noticed for derivatives bearing carbocycles at R_4 *(e.g.*, **4.18c−f**), which were completely inactive irrespectively of the ring size or topology. A closer inspection of the affinity data reveals that, in most cases, the introduction of heterocycles with two heteroatoms within the tricyclic system (Tables 4.8 and 4.9) diminishes the affinity compared to the former series (Tables 4.1 and 4.7).

Some aza-derivatives of the former 2-thienyl (**4.19m** and **4.19n**), 3-pyrrolyl (**4.19i** and **4.19j**), and 3-furyl (**4.19e−f** and **4.20g−h**) derivatives seem to be exceptions to this trend. For example, the weak A_{2B}AR affinities observed for **4.14c** and **4.14g** (K_i = 484 and 371 nM, respectively) increased substantially (4/5-fold) when a N atom was introduced at position 4 or 5 of the original thiophene core (Table 4.8, compounds **4.19m−n**; Table 4.9, compounds **4.20o−p**). The improvement in affinity is particularly remarked for 5-thiazolyl derivatives **4.20p** (K_i = 68.30 nM) and **4.19m** (K_i = 98.70 nM). While compound **4.20p** remains A_{2B}AR-selective, a high-affinity profile for A_1AR (K_i = 20.20 nM) is observed for **4.19m**. As for preceding examples, the effect of introducing a second nitrogen atom in ligands bearing a 3-pyrrolyl residue (**4.18g** and **4.18h**) proved to be highly dependent on the position where the nitrogen was inserted (Table 4.7), as it affects the azole substitution pattern. Hence, the poor A_{2B}AR affinity measured for **4.18g** and **4.18h** (K_i = 449 and 517 nM, respectively) is improved in derivatives **4.19i** and **4.19j** (K_i = 92.6 and 340 nM), which experienced a reversal of their selectivity profile in favor of A_1AR (K_i = 14.80 and 8.30 nM), while affinity is diminished (**4.19c** and **4.19d**) or abolished (**4.20k** and **4.20l**) in other aza-derivatives.

These data suggest that the double pattern of H-bond donor and acceptor present in imidazolyl and pyrazolyl units is important for a favorable A_{2B}AR affinity and selectivity profiles. It should be noted that, because of the prototropic annular tautomerism present in 4(5)-substituted imidazoles, ligands **4.20k** and **4.20l** (Table 4.9) can be considered as aza-analogues of both **4.18g−h** and **4.18i−j** (Table 4.7). Four of the six aza-derivatives (**4.19e−f** and **4.20g−h**) obtained by CH/N bioisosteric replacements in the 3-furyl moiety at position 4 of the 1,4-dihydrobenzo[4,5]-imidazo[1,2-*a*]pyrimidine derivatives, retain (**4.19e−f**) or improve (**4.20g−h**) the outstanding affinity and selectivity profiles observed in the original ligands (**4.14b,f** and **4.14a,e**, respectively).

These series provide new evidence for the relevance of the relative position of the nitrogen atom in the pentagonal core for effective A_{2B}AR binding. Therefore, while optimal A_{2B}AR affinity is observed for derivatives **4.19e−f** and **4.20g−h**, which contain different azole cores (*e.g.*, 1,2-oxazole vs 1,3-oxazole), a sharp drop in potency is observed for its isomers of **4.19a−b**. The 4-oxazolyl derivative **4.20g** constitutes the most appealing A_{2B}AR antagonist (K_i = 8.10 nM) identified in this study, while its close analogue **4.20h** exhibited a 5-fold decrease in A_{2B}AR affinity (K_i = 43.41 nM).

Considering all the data, it seems that the bioisosteric replacement of the original 3-furyl group by oxazole can affect the resulting molecule in two ways: (i) by increasing the electronegativity and polar surface of the pentagonal scaffold and (ii) by affecting access to the preferred bioactive conformation, due to a combination of the H-bond pattern offered to the receptor and internal H-bonds within the molecule.

Since an early understanding of the ADME profile of novel prototypical chemical entities is crucial for improving quality during preliminary drug discovery programs, the effect of the more promising compounds at two cytochrome P450 (CYP) isoforms, CYP2D6 and CYP3A4, has been characterized in **Chapter 3.2**. In an effort to identify potential metabolic liabilities within the series documented here, some representative A_{2B}AR antagonists were selected to assess the likelihood of side effects in the liver and to explore the propensity for drug−drug interactions by a joint theoretical and experimental approach.

A subset consisting of six assorted A_{2B}AR antagonists obtained herein (**4.14e**, **4.14f**, **4.19e**, **4.20e**, **4.20g**, and **4.20h**; Table 4.10) was experimentally tested for CYP3A4 and CYP2D6 inhibitory activity as a complement to the *in silico* screening, where three different computational tools have been used. All experiments were performed in duplicate using fluorescence detection, employing ketoconazole (IC_{50} = 0.027 μM) and quinidine (IC_{50} = 0.0073 μM) as reference compounds for CYP3A4 and CYP2D6, respectively.

Table 4.10: Inhibition Data of Selected A_{2B}AR Antagonists on CYP3A4 and CYP2D6.

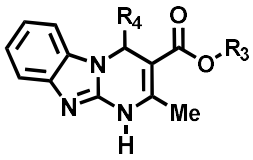

Compound	R_4	R_3	CYP3A4 IC_{50} (μM)	CYP2D6 % Inhib. or IC_{50} (μM) (1 μM)	(10 μM)
4.14e		*i*-Pr	2.90 ± 0.37	5%	35%
4.14f		*i*-Pr	2.68 ± 0.53	8%	31%
4.19e		Et	4.92 ± 0.46	6%	37%
4.20e		*i*-Pr	4.54 ± 1.16	8%	18%
4.20g		Et	6.41 ± 0.73	13%	19%
4.20h		*i*-Pr	5.92 ± 0.68	23%	43%
Ketoconazole			0.027 ± 0.003	-	-
Quinidine			-	0.0073 ± 0.005	

Data are the mean±SD of three (n=3) determinations. Due to the low activity showed at CYP2D6, the percentage of inhibition at 1 and 10 μM is reported.

As can be observed (Table 4.10), most of the tested ligands exhibit a moderate to weak CYP3A4 inhibitory activity, with IC_{50} values ranging from 2.7 to 6.4 μM. In particular, the 4-oxazolyl derivatives **4.20g** and **4.20h** and the 2-imidazolyl ligand **4.20e** exhibited the best CYP3A4 inhibitory profiles (IC_{50} 6.41, 5.92, and 4.54 μM respectively). In clear contrast to CYP3A4, the selected ligands do not show significant interaction with CYP2D6, which usually exhibits preference for basic ligands.

A more systematic study (*e.g.*, including other relevant CYP subfamilies) would be required to draw definitive conclusions, but two observations emerge from the available data. While the observed CYP3A4 inhibitory profiles could be considered as suboptimal, it should be noted that, for the most potent A_{2B}AR antagonists developed in the present study, the IC_{50} value is more than 800 times higher than the determined K_i value. A comparison of the obtained data for selected ligands (*e.g.*, **4.14f** vs **4.19e**, **4.20g**, and **4.20h**) corroborates that introduction of the nitrogen atom enhances approximately 2-fold IC_{50}.

Further studies are now in progress to evaluate the inhibitory potential of representative ligands in a broader CYP panel (CYP1A2, CYP2C9) and also to study the time-dependent inhibition profiles (TDI) and stability in liver microsomes. The *in vitro* ADME profile of the most promising compound (**4.20g**) was completed by studying its solubility and microsomal stability. The compound showed high microsomal stability with just 5.62% metabolization after 60 min of exposure to human microsomes and solubility at pH 7 in PBS higher than 20 μM.

Moreover, the most promising compound (**4.20g**) was resolved into its enantiopure forms and these were evaluated at the four human AR subtypes to determine the role of the stereochemistry of the synthesized compounds plays in their interaction with A_{2B}AR. The selected compound, which was evaluated as a racemate, exhibited promising affinity (K_i = 8.10 nM) and selectivity profiles (Table 4.11).

As in the previous chapter, a combination of chiral high-performance liquid chromatography (HPLC) and circular dichroism (CD) spectroscopy has again been used to separate and unequivocally assign the configuration of the heterocyclic stereocenter in each stereoisomer. Semipreparative HPLC separation of (4*R*/4*S*)-**4.20g** on a chiral stationary phase provided the expected enantiomers (Figure 4.5) with excellent stereochemical purity (>97%). Once again, the characteristic CD activity of the enamide chromophore (300−350 nm) allowed the unambiguous assignment of the absolute configuration of each enantiomer (Figure 4.5) by comparison with the reported CD data for enantiopure 3,4-dihydropyrimidin-2(1*H*)-ones of known configuration.

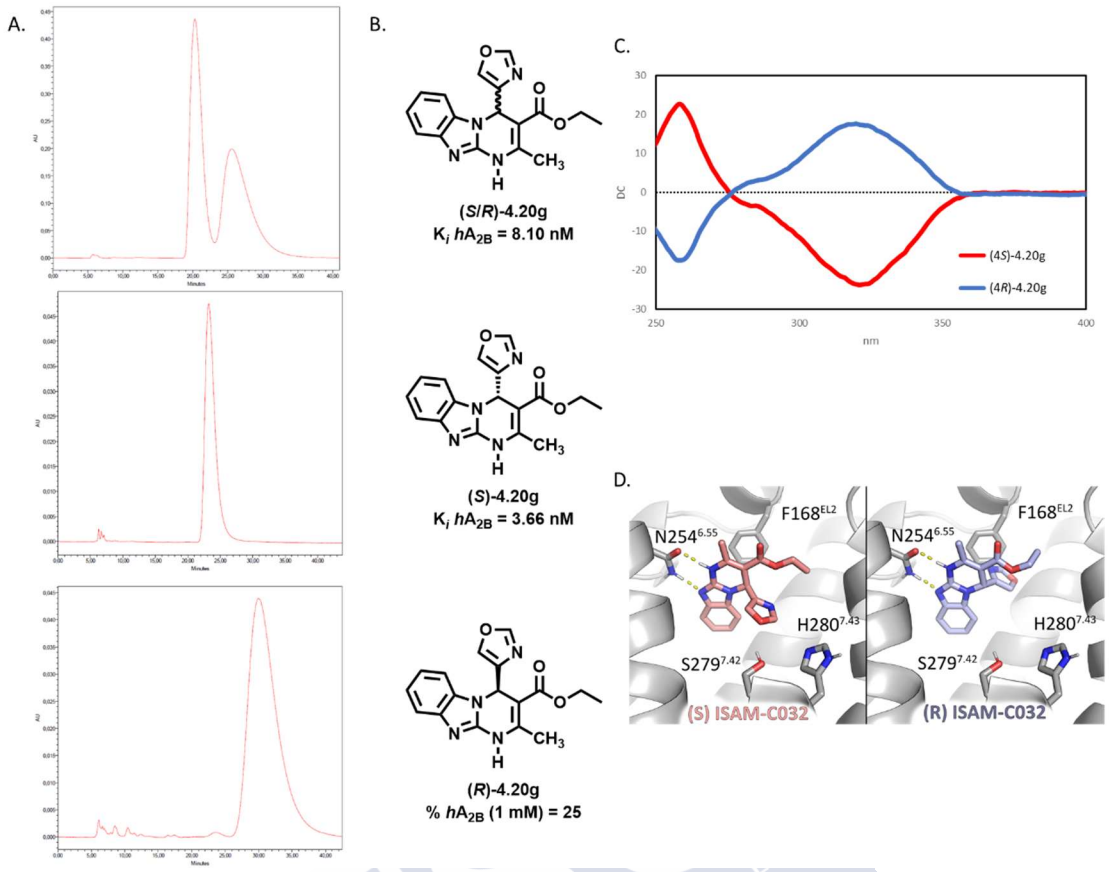

Figure 4.5: A. Chiral HPLC traces, B. absolute configuration, C. circular dichroism spectra, and D. proposed binding modes of the enantiomers of **4.20g** (**ISAM-C032**).

As can be shown in Figure 4.5, enantiomers showing a negative Cotton effect (red line) contain the oxazole ring pointing backward, corresponding to (4*S*)-**4.20g**, while the stereoisomers giving positive Cotton effect (blue line) contain the pentagonal heterocycle pointing forward, corresponding to (4*R*)-**4.20g**. These results were validated by comparing the data obtained for the structural analogues by X-ray crystallography from the previous hapter.

The affinities of the enantiomers of **4.20g** [(4*R*)-**4.20g** and (4*S*)-**4.20g**] were evaluated at the four human ARs. The results are presented in Table 4.11 for the four ARs, and these allowed the identification of one stereoisomer with excellent A_{2B}AR affinity (K_i = 3.66 nM, Figure 4.6A) and selectivity (>1000-fold compared to any other AR).

Table 4.11: Structure and Affinity Binding Data for the Enantiomers of the Ethyl 4-(oxazol-4-yl)-2-methyl-1,4-dihydrobenzo[4,5]imidazo[1,2-*a*]pyrimidine-3-carboxylate **4.20g** at the Human ARs.

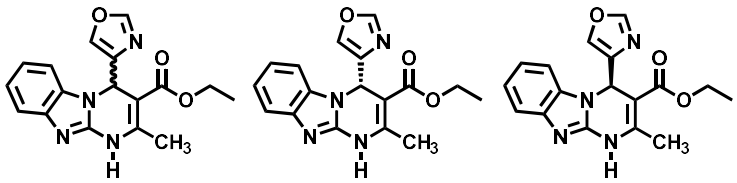

(*S*/*R*)-4.20g (*S*)-4.20g (*R*)-4.20g

	K_i (nM) or % at 1 μM			
Compound	*h*A_1[a]	*h*A_{2A}[b]	*h*A_{2B}[c]	*h*A_3[d]
(±)-4.20g	5%	11%	8.10 ± 0.5	7%
(*S*)-4.20g	1%	20%	3.66 ± 0.2	18%
(*R*)-4.20g	3%	4%	25%	6%

[a]Displacement of specific [^{3}H]DPCPX binding in human CHO cells expressed as K_i ± SEM in nM (n = 3) or percentage displacement of specific binding at a concentration of 1 μM (n = 2). [b]Displacement of specific [^{3}H]4-(2-[7-amino-2-(2-furyl)[1,2,4]triazolo[2,3-*a*][1,3,5]triazin-5-ylamino]ethyl)phenol binding in human HeLa cells expressed as K_i ± SEM in nM (n = 3) or percentage displacement of specific binding at a concentration of 1 μM (n = 2). [c]Displacement of specific [^{3}H]DPCPX binding in human HEK-293 cells expressed as K_i ± SEM in nM (n = 3) or percentage displacement of specific binding at a concentration of 1 μM (n = 2). [d]Displacement of specific [^{3}H]NECA binding in human HeLa cells expressed as K_i ± SEM in nM (n = 3) or percentage displacement of specific binding at a concentration of 1 μM (n = 2).

Furthermore, the compound that exhibited the best affinity/selectivity profile [(*S*)-**4.20g**] was tested in cAMP assays to assess its ability to inhibit NECA stimulated (10 μM) cAMP production to obtain more information about the pharmacological action of this novel series of A_{2B}AR ligands. The results of this study demonstrated that (*S*)-**4.20g** inhibits cAMP accumulation (K_B = 26.6 nM, Figure 4.6B), thus unequivocally validating its A_{2B}AR antagonistic profile.

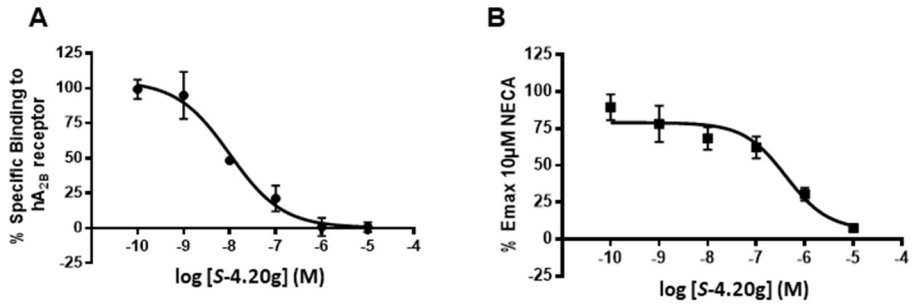

Figure 4.6: A. Radioligand binding competition curve of *S*-**4.20g** at human A_{2B}AR labelled with [^{3}H]DPCPX. B. Concentration-response curve of *S*-**4.20g** in functional assays at human A_{2B}AR measuring 10 μM NECA-induced cAMP accumulation. Points represent the mean ± SD (vertical bars) of three independent experiments.

Chapter 3.3 was focused on the development of novel potent and subtype selective DRD_2 biased partial agonists. For this purpose, aripiprazole was selected as a model compound.

Aripiprazole and cariprazine, two representative third generation atypical antipsychotics, contain three well-defined regions: (1) the primary pharmacophore (PP) [commonly referred to as the left-hand side (LHS) or head group], which consists of a mono- or disubstituted phenyl-piperazine scaffold, (2) the central linker, which is usually of variable length and nature (*e.g.*, acyclic or cyclic), and (3) the secondary (or allosteric) pharmacophore (SP) [commonly referred to as the right-hand side (RHS) or tail group], which generally consists of a heterocyclic core.

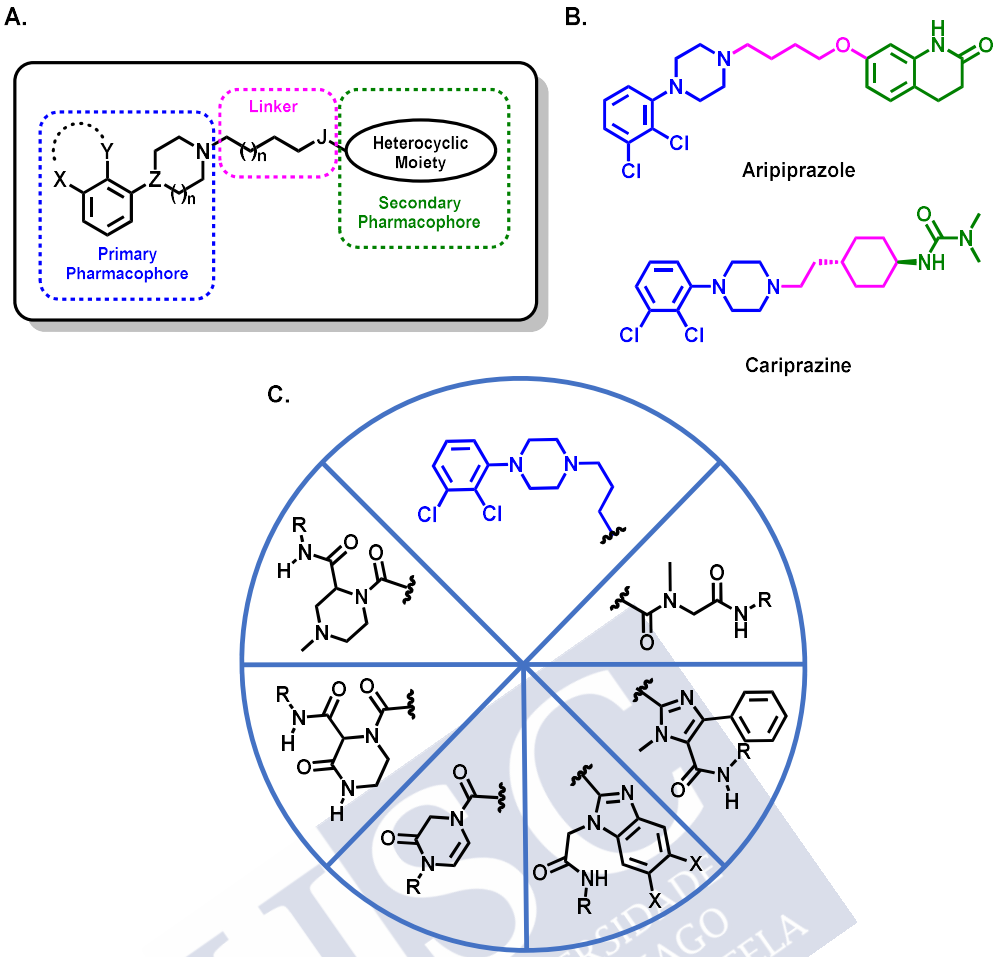

Figure 4.7: A. General structure of the pharmacophore. B. Structure of the model compounds. C. General structure of the ligands described in this chapter. Blue: common (primary) pharmacophore of the series, Black: structure of the scaffolds explored in the secondary pharmacophore.

In **Chapter 3.3**, it was decided to mantain the primary pharmacophore unaltered (Figure 4.7), selecting the 1-(2,3-dichlorophenyl)piperazine moiety (present in aripiprazole and cariprazine), and a shorter than usual (four atoms) linear linker.

Six previously unexplored secondary pharmacophoric (SP) groups (Table 4.12) were conceived to examine the effect of these structural modifications on subtype selectivity (DRD_2, DRD_3, DRD_4), and also their effect on the DRD_2 functional selectivity profile of novel ligands. The selected SP frameworks provide novel features and alternative binding modes that should enable the capture of diverse conformational states within the receptor. Performing an in-depth structural analysis, the five heterocyclic cores explored in this study as secondary pharmacophore groups (series **IV.IX-IV-XIII**) revealed that they can be considered conformationally restricted analogues of the early acyclic series **IV.VIII**, with differences in structure, topology,

physicochemical descriptors, and complexity. Furthermore, some of the proposed SP fragments bear a stereogenic center within the heterocyclic framework, thus introducing a stereochemical diversity that would allow future investigation of scarcely explored stereoselective interactions within the SP region.

In this chapter, all newly synthesized ligands were initially tested in cAMP inhibition assays with three dopamine receptor subtypes (DRD_2, DRD_3, and DRD_4), i.e., DRD_2-like receptors, to evaluate their functional behavior and selectivity profile (Table 4.12). All experiments were performed *in vitro* on transfected HEK-293T cells, evaluating the efficacy (E_{max}) and half maximum inhibitory concentration (IC_{50}) for the cAMP assays. Quinpirole was used as a control and reference drug during these studies. Series **IV.XII** and **IV.XIII** were tested as racemic mixtures.

Based on its DRD_2 potency ($pIC_{50} > 8$) and subtype selectivity criteria, seven ligands (**4.21a**, **4.21b**, **4.22a**, **4.25a**, **4.25b**, **4.26a**, and **4.26c**) were selected for further pharmacological characterization of DRD_2-mediated potency (EC_{50}) and efficacy (E_{max}) for *β*-arrestin-2 recruitment (Table 4.13). Because of its excellent DRD_2 potency ($pIC_{50} = 8.66$), although it did not exhibit selectivity toward DRD_4, ligand **4.23d** was also included in the set of compounds selected for bias characterization.

The *β*-arrestin-2 recruitment study involved BRET experiments and was performed on transfected HEK-293T cells. During the development of these studies, aripiprazole and quinpirole were employed as controls.

Table 4.12: Structures and Pharmacological Data at the D_2 Receptor Family for the Ligands.

Cmpd	SP	R	X	cAMP Functional data at the D_2-like receptor family[a,b]					
				*h*D$_2$		*h*D$_3$		*h*D$_4$	
				pIC_{50}	$\%E_{max}$	pIC_{50}	$\%E_{max}$	pIC_{50}	$\%E_{max}$
4.21a	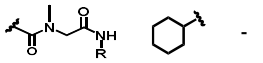		-	8.34 ± 0.60	55 ± 4	5.24 ± 0.50	125 ± 5	6.79 ± 0.45	48 ± 10
4.21b			-	8.54 ± 0.42	45 ± 4	4.91 ± 1.37	128 ± 5	5.13 ± 0.81	82 ± 6
4.21c			-	5.81 ± 0.45	65 ± 5	5.64 ± 0.55	65 ± 4	4.86 ± 1.41	109 ± 6
4.22a	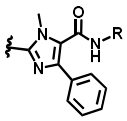		-	8.30 ± 0.38	60 ± 5	5.63 ± 0.33	98 ± 3	5.46 ± 0.72	101 ± 7
4.22b			-	5.76 ± 0.43	83 ± 8	6.11 ± 0.26	86 ± 8	5.64 ± 0.27	103 ± 10
4.22c			-	6.79 ± 0.56	73 ± 5	5.72 ± 0.42	80 ± 5	8.24 ± 0.50	72 ± 4
4.23a	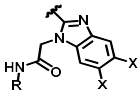		H	4.87 ± 0.69	164 ± 4	4.42 ± 0.10	288 ± 5	5.00 ± 0.51	148 ± 3
4.23b			H	5.04 ± 0.88	92 ± 3	7.94 ± 0.42	20 ± 9	4.80 ± 1.20	93 ± 10
4.23c			H	6.43 ± 0.41	55 ± 8	6.40 ± 0.21	65 ± 6	8.10 ± 0.36	53 ± 9
4.23d			Br	8.66 ± 0.63	55 ± 5	4.63 ± 0.56	214 ± 3	8.01 ± 0.41	65 ± 6
4.23e			Br	5.42 ± 0.57	104 ± 3	5.64 ± 0.28	82 ± 3	6.89 ± 0.30	65 ± 8
4.23f			Br	6.35 ± 0.50	66 ± 5	5.59 ± 0.37	107 ± 3	5.58 ± 0.38	120 ± 4
4.24a	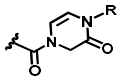		-	5.86 ± 0.26	88 ± 7	5.43 ± 0.26	111 ± 6	5.24 ± 1.25	95 ± 6
4.24b			-	6.96 ± 0.23	68 ± 8	5.49 ± 0.46	97 ± 7	5.89 ± 0.60	55 ± 5
4.24c			-	5.76 ± 0.30	113 ± 7	8.47 ± 1.26	66 ± 4	5.94 ± 0.13	80 ± 10
4.25a	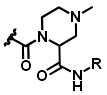		-	8.96 ± 1.37	47 ± 4	4.80 ± 0.80	171 ± 8	5.04 ± 0.51	109 ± 8
4.25b			-	8.78 ± 0.79	60 ± 5	5.83 ± 0.57	93 ± 5	5.22 ± 1.40	54 ± 5
4.25c			-	5.83 ± 0.49	77 ± 9	5.25 ± 0.92	73 ± 7	5.26 ± 0.24	68 ± 9
4.26a	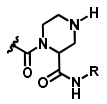		-	8.94 ± 1.16	62 ± 9	6.30 ± 0.42	86 ± 4	6.06 ± 0.42	53 ± 8
4.26b			-	5.48 ± 0.52	104 ± 3	4.57 ± 0.17	290 ± 4	5.16 ± 0.20	155 ± 3
4.26c			-	8.42 ± 0.85	58 ± 5	5.22 ± 0.21	146 ± 5	5.18 ± 0.53	83 ± 8
Quinpirole				8.58 ± 0.11	100 ± 5	7.57 ± 0.14	100 ± 3	7.48 ± 0.07	100 ± 6

[a]pIC_{50} and E_{max} values are the average of five experiments, each performed in duplicate with ± SEM values that are three-times lower than the average. E_{max} relative to the effect of the reference agonist quinpirole. [b]Tested using the experimental protocols described in the experimental part.

As part of the exhaustive pharmacological characterization of the novel series documented in this chapter, the most promising ligands (Table 4.13, **4.21a**, **4.21b**, **4.22a**, **4.23d**, **4.25a**, **4.25b**, **4.26a**, and **4.26c**) were evaluated in antagonist mode. In this case, cells were pretreated with the selected compounds prior to treatment with the agonist quinpirole. As can be observed in Figure 4.8A, there were no significant variations in the efficacy between each of the compounds tested with quinpirole compared to the quinpirole tested alone. These results allow us to discard a potential antagonistic behavior for the studied compounds. In addition, Figure 4.8B shows a comparative profile of the cAMP dose-response curves obtained for ligands **4.22a** and **4.23d** and quinpirole at DRD_2, DRD_3, and DRD_4, the ligands showing the best bias factor by the G protein-dependent pathway.

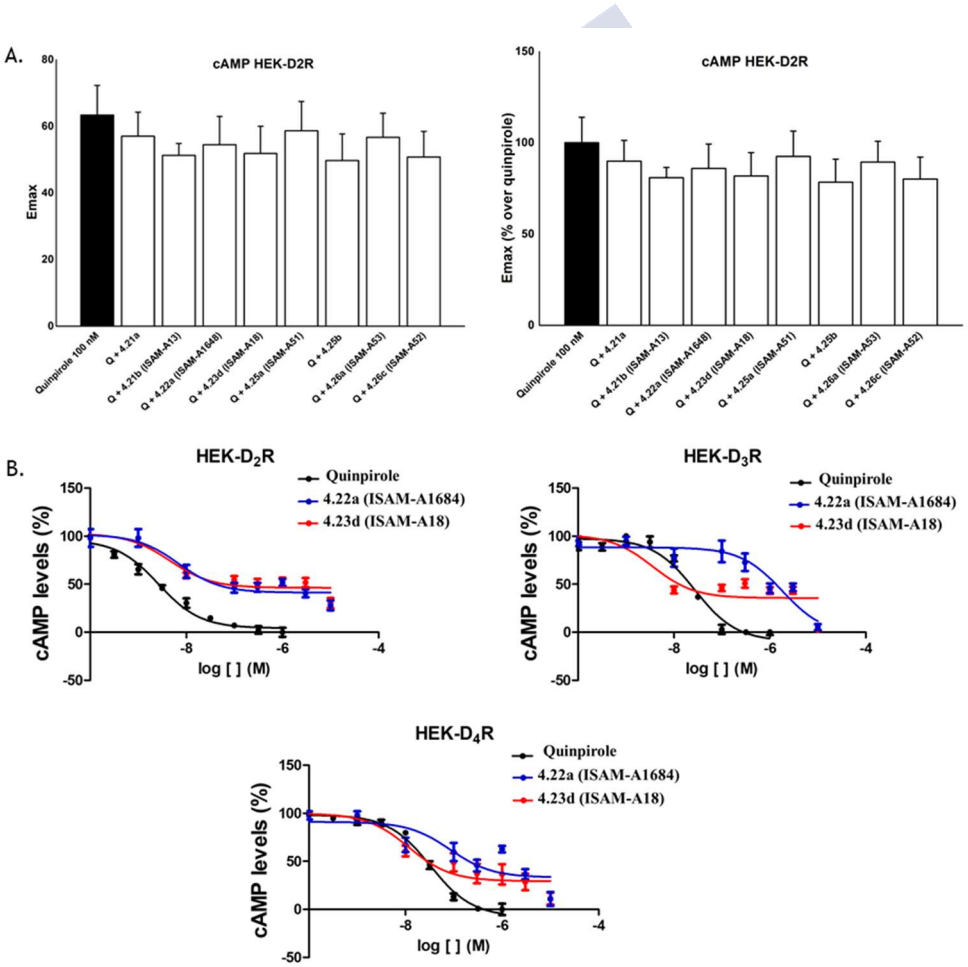

Figure 4.8: A. E_{max} values for 100 nM quinpirole in cAMP assays performed in HEK-293T cells expressing DRD_2, pretreated or not (reference black column) with 100 nM of the selected compounds. Data are normalized (right) to the effect of quinpirole alone (100%) B. HEK-293T cells expressing human DRD_2, DRD_3 or DRD_4 were treated with the indicated compounds. The effect of the compounds on the decrease of 500 nM-induced cAMP levels was determined as described in Chapter 3.3. Data are given relative to the value of forskolin alone, and then normalized to the effect of quinpirole.

The cAMP functional data obtained for the novel compounds (Table 4.12) reveal that some of them behave as DRD_2 selective partial agonists. Analysis of the reported data allowed the identification of eight novel and highly potent ($pIC_{50} > 8$) DRD_2 ligands (*e.g.*, **4.21a**, **4.21b**, **4.22a**, **4.23d**, **4.25a**, **4.25b**, **4.26a**, and **4.26c**), six of which demonstrate remarkable selectivity (>1000-fold) toward DRD_3 and DRD_4. Furthermore, some potent and selective ligands were identified for DRD_3 (i.e., **4.23b** and **4.24c** pIC_{50} = 7.94 and 8.47, respectively) or DRD_4 (i.e., **4.22c** and **4.23c** pIC_{50} = 8.24 and 8.10, respectively).

In order to obtain a more immediate and efficient analysis of the variation of both affinity and selectivity, the pIC_{50} values at DRD_2 (*X* axis) versus DRD_3 (*Y* axis, top panel) and DRD_4 (*Y* axis, bottom panel) are provided as independent scatter plots using the same scale and range for both axes (square plot). Each subset was represented in a different color and shape to facilitate a more comprehensive analysis of both potency and selectivity within a series. In both plots, the DRD_2 selective compounds appear below the diagonal (lower right zone). Therefore, as the distance from the diagonal is proportional to the degree of selectivity, it is confirmed that the identified DRD_2 partial agonists also show a high degree of selectivity versus DRD_3/DRD_4. This subset was selected for further pharmacological characterization (blue circle, Figure 4.9).

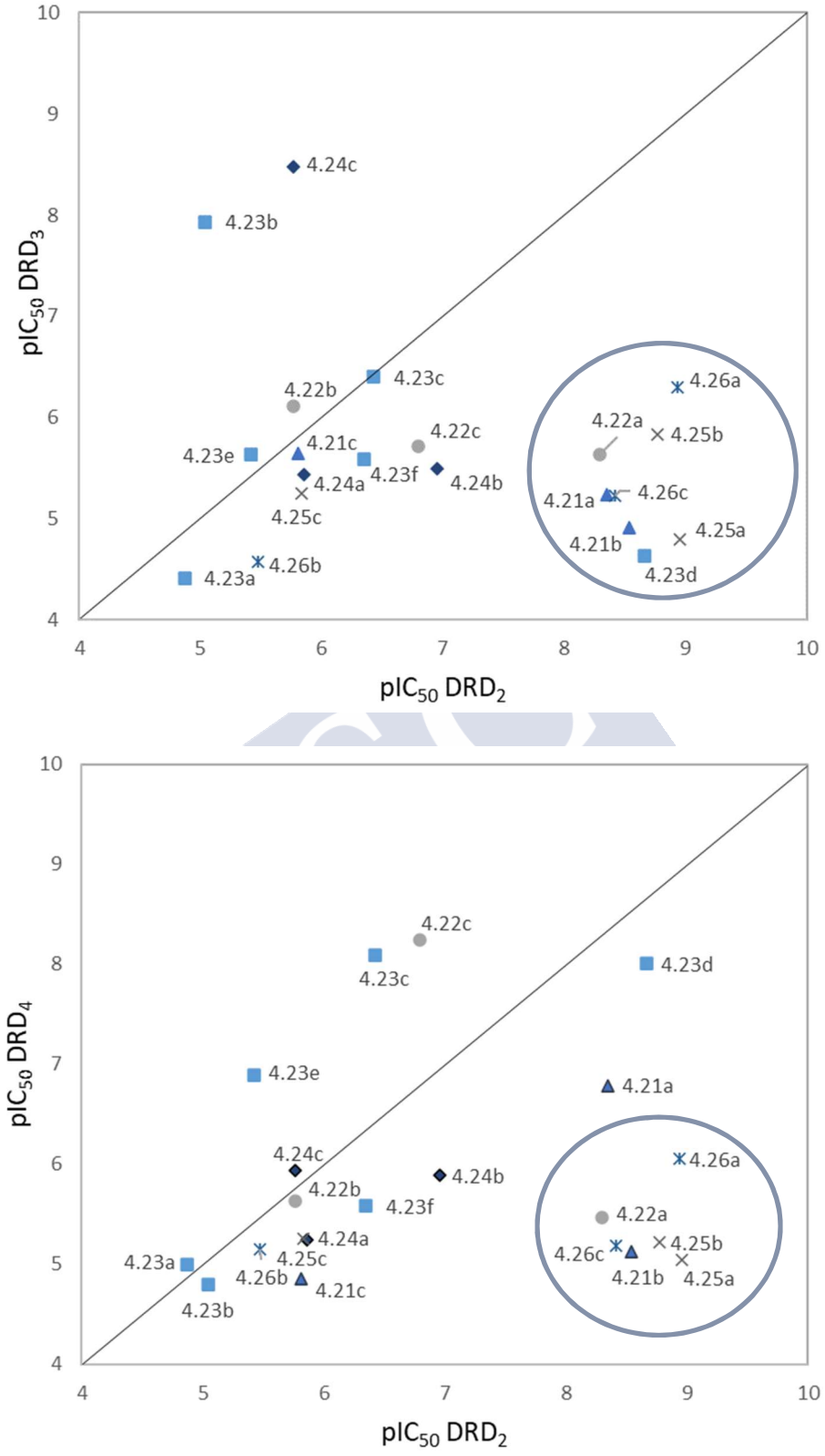

Figure 4.9: Potency-selectivity DRD_3-DRD_2 and DRD_4-DRD_2 plots.

The functional data presented in Table 4.12 highlight the relevance of the amide group in the secondary pharmacophore for an effective interaction within DRD_2. The only subset that did not provide potent DRD_2 ligands (series **IV.XI**) has this amide group embedded within the heterocyclic core, meaning that they lacked the polar hydrogen and had a conformational restraint, while the rest of the series provided at least one ligand with significant DRD_2 potency. In contrast to the low affinity on the DRD_2, series **IV.XI** provided compound **4.24c**, a novel, highly potent (pIC_{50} = 8.47) and selective (>300-fold) DRD_3 partial agonist.

Series **IV.VIII**, **IV.XII**, and **IV.XIII** generally produced potent and subtype-selective DRD_2 partial agonists and these included the most attractive ligands identified in this study (Table 4.12, Figure 4.9). In these series, compounds bearing a benzyl group on the amide moiety (**4.21a**, **4.25a**, and **4.26a**) systematically exhibited low nanomolar potency (pIC_{50} = 8.34, 8.96 and 8.94, respectively). Nevertheless, the cyclohexyl group seems to be well tolerated only in acyl-aminoamides (**4.21b**) and the *N*-methylpiperazines (**4.25b**). Conversely, compounds containing a *tert*-butyl residue generated ligands (**4.21c** and **4.25c**) that systematically exhibited micromolar potency apart from **4.26c**, suggesting that this group could not facilitate optimal complementarity within DRD_2. Although most ligands with imidazole- or benzimidazole-based SP groups (Table 4.12, series **IV.IX** and **IV.X**) show low potency at DRD_2, the pIC_{50} values determined for ligands **4.22a** and **4.23d** (pIC_{50} = 8.30 and 8.66, respectively) reveal that these scaffolds, when appropriately decorated on the exocyclic amide group (i.e., with a benzyl group), can provide potent and selective DRD_2 partial agonists.

As previously discussed, 1-acyl-*N*-methylpiperazine-2-carboxamides **IV.XII** and 1-acyl-*N*-methyl-3-oxopiperazine-2-carboxamides **IV.XIII** can be considered conformationally restricted analogues of the acyl-aminoamides **IV.VIII**. Thus, their similar biological profile (potency and selectivity) could be a consequence of the close structural similarity of these three series. Despite the structural analogy, the cyclic constrained analogues (piperazine-2-carboxamides **IV.XII** and 3-oxopiperazine-2-carboxamides **IV.XIII**) exhibited slightly superior potency (Table 4.12) compared to the acyclic series (**IV.VIII**). This trend suggests that the cyclic derivatives are more similar to the bioactive conformation. As observed in the early series, and except for

4.26c (pIC_{50} = 8.42), ligands bearing the *tert*-butyl group in the exocyclic amide afforded the weakest potency (pIC_{50} = 5.76–6.79).

Another interesting structural feature of the conformationally restricted series **IV.XII** and **IV.XIII** is the presence of a stereogenic center at position 2 of the heterocyclic core. Although these compounds were tested as racemates, it is reasonable to expect diverse pharmacological profiles for the different enantiomers. Therefore, the potential influence of the absolute configuration of the stereogenic center in these series will be explored in future work.

DRD_2-mediated signaling events are initiated by G protein dependent (G protein-coupled) and/or independent (β-arrestin recruitment) pathways. The ability of a (partial) agonist to selectively activate one of these specific signaling pathways is a pharmacological phenomenon known as functional bias (or functional selectivity). Hence, the seven derivatives (**4.21a**, **4.21b**, **4.22a**, **.4.25a**, **4.25b**, **4.26a**, and **4.26c**) that exhibited the highest cAMP potency (pIC_{50} > 8) and optimal DRD_2 selectivity (Table 4.12) were selected to perform a β-arrestin-2 recruitment BRET assay in transfected HEK-293T cells, which determines the potency and efficacy for β-arrestin-2 recruitment.

Although it was not selective (DRD_4, pIC_{50} = 8.01), the benzimidazole derivative **4.23d** was included in this study due to its excellent DRD_2 potency (pIC_{50} = 8.66). Aripiprazole, a known biased ligand, was used as a reference ligand and quinpirole (a full agonist of DRD_2) was used as positive control in both cAMP and β-arrestin-2 recruitment BRET assays.

Comparative cAMP and β-arrestin-2 data are presented in Table 4.13. To identify rapidly functional bias, a bias factor was calculated using the Black and Leff operational model with respect to quinpirole (see **Chapter 3.3**). Most of the evaluated ligands exhibited excellent efficacy in the β-arrestin recruitment pathway (E_{max} over quinpirole in the range 68–142%, see Table 4.13), thus behaving as full agonists for this pathway.

Table 4.13: Ligands and Structure-Selectivity Relationship (SSR) Data for Selected Ligands.[a,b]

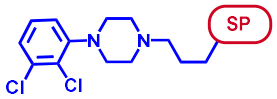

Compd	Secondary Pharmacophore (SP)	D_2 cAMP Inhibition		D_3 cAMP Inhibition		D_4 cAMP Inhibition		D_2 β-Arrestin		Bias factor[c] cAMP - β-Arr
		pIC_{50} ± SEM	E_{max} ± SEM (%)	pIC_{50} ± SEM	E_{max} ± SEM (%)	pIC_{50} ± SEM	E_{max} ± SEM (%)	pEC_{50} ± SEM	E_{max} ± SEM (%)	$\Delta\Delta\log(\tau/K_A)$
4.21a	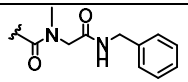	8.34 ± 0.60	55 ± 4	5.24 ± 0.50	125 ± 5	6.79 ± 0.45	48 ± 10	8.49 ± 0.30	122 ± 2	**-0.446**
4.21b (ISAM-A13)	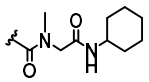	8.54 ± 0.42	45 ± 4	4.91 ± 1.37	128 ± 5	5.13 ± 0.81	82 ± 6	8.63 ± 0.31	129 ± 2	**-0.508**
4.22a (ISAM-A1684)	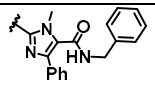	8.30 ± 0.38	60 ± 5	5.63 ± 0.33	98 ± 3	5.46 ± 0.72	101 ± 7	5.30 ± 1.05	*	**2.223**
4.23d (ISAM-A18)	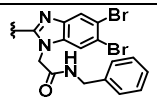	8.66 ± 0.69	55 ± 5	4.63 ± 0.56	214 ± 3	8.01 ± 0.41	65 ± 6	5.50 ± 1.46	*	**2.768**
4.25a (ISAM-A51)	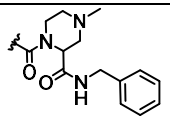	8.96 ± 1.37	47 ± 4	4.80 ± 0.80	171 ± 8	5.04 ± 0.51	109 ± 8	9.67 ± 0.62	93 ± 1	**-0.977**
4.25b	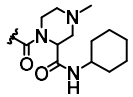	8.78 ± 0.79	60 ± 5	5.83 ± 0.57	93 ± 5	5.22 ± 1.94	54 ± 5	8.44 ± 0.25	120 ± 1	0.079
4.26a (ISAM-A53)	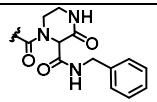	8.94 ± 1.16	62 ± 9	6.30 ± 0.42	86 ± 4	6.06 ± 0.42	53 ± 8	8.12 ± 0.20	142 ± 1	**0.502**
4.26c (ISAM-A52)	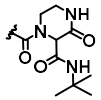	8.42 ± 0.85	58 ± 5	5.22 ± 0.21	146 ± 5	5.18 ± 0.53	83 ± 8	9.43 ± 0.57	68 ± 2	**-1.043**
Aripiprazole	-	7.42 ± 0.17	74 ± 4	7.09 ± 0.17	115 ± 4	5.93 ± 0.46	151 ± 3	9.00 ± 0.30	128 ± 2	**-1.774**
Quinpirole	-	8.75 ± 0.11	100 ± 5	7.57 ± 0.14	100 ± 3	7.48 ± 0.07	100 ± 6	8.61 ± 0.12	100 ± 1	0.000

[a]EC_{50}, IC_{50} and E_{max} values are the average of five experiments, each performed in duplicate with ± SEM values that are 3-fold less than the average. E_{max} relative to the effect of the reference agonist quinpirole. [b]Tested using the experimental protocols described in the experimental part. [c]Bias factors were quantified by the operational model using quinpirole as a positive control (see experimental part). Ligand bias values > 0 indicate preference for the cAMP pathway, < 0 indicate preference for the β-arrestin signaling pathway. Values above 0.5 are considered significant and are highlighted. *E_{max} is not shown due to low affinity of the ligand.

The most salient data emerging from *β*-arrestin recruitment assays evidenced two pairs of ligands that elicit opposite signaling profiles. Therefore, while ligands **4.25a** and **4.26c** exhibit a very attractive subnanomolar profile in the *β*-arrestin recruitment assay (pIC_{50} = 9.67 and 9.43, respectively), derivatives **4.22a** and **4.23d** showed only weak potency (micromolar range). The availability of ligands bearing different groups on the exocyclic amide in series **IV.VIII**, **IV.XII**, and **IV.XIII** provided evidence of the key role of the alkyl group (benzyl, cyclohexyl or *tert*-butyl) in the *β*-arrestin recruitment potency. Interestingly, the compounds that elicited the poorest *β*-arrestin recruitment potency (**4.22a** and **4.23d**) contain an aromatic heterocyclic core with an *N*-benzyl group within the secondary pharmacophore.

Six of the ligands (**4.21b**,**4.22a**, **4.23d**, **4.25a**, **4.26a**, and **4.26c**) showed a clear functional selectivity profile (biased agonism) according to the bias factor parameter (Table 4.13), where a positive value indicates a preference for the cAMP pathway and a negative value denotes that *β*-arrestin recruitment is dominant. As expected, the weak potency in the *β*-arrestin recruitment assay and excellent cAMP data mean that ligands **4.22a** (Figure 4.10B) and **4.23d** show a significant bias toward cAMP [$\Delta\Delta\log(\tau/K_A)$ = 2.223 and $\Delta\Delta\log(\tau/K_A)$ = 2.768, respectively], representing 167-fold and 586-fold bias, respectively, toward the cAMP pathway. Furthermore, compound **4.26a** also shows a moderate [$\Delta\Delta\log(\tau/K_A)$ = 0.502] 3-fold bias toward cAMP inhibition.

On the other hand, ligands **4.25a** and **4.26c** (Figure 4.10B), due to their subnanomolar effect and excellent efficacy in the *β*-arrestin pathway (pEC_{50} = 9.67 and 9.43, respectively) and its potency and moderate efficacy in the cAMP pathway, showed 10- and 11-fold *β*-arrestin biased agonism. Compound **4.23d**, besides being one of the most potent binders at DRD_2 and, in fact, the partial agonist with the strongest bias toward the cAMP pathway (Table 4.13), lacks the required D_2/D_4 selectivity profile (Table 4.12) to warrant further characterization of this compound. In any case, compound **4.23d** was used as a tool to understand the molecular basis of its bias profile.

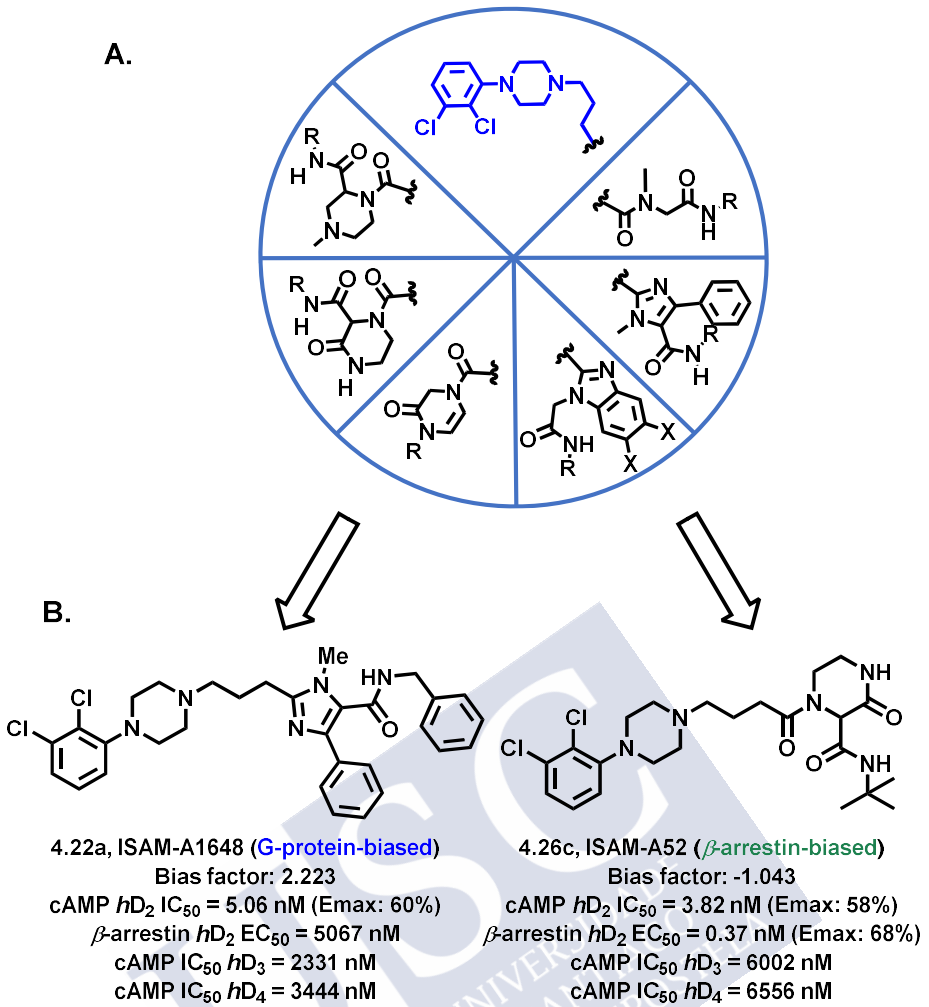

Figure 4.10: A. General structure of the ligands described in this chapter. Blue: common (primary) pharmacophore of the series, Black: structure of the scaffolds explored in the secondary pharmacophore. B. Structure of the most attractive biased agonist identified during this study.

5. CONCLUSIONS

USC
UNIVERSIDADE
DE SANTIAGO
DE COMPOSTELA

- Herein, the first examples of trifluorinated A_{2B}AR antagonists have been reported. The optimized ligands exhibit excellent *h*A_{2B}AR affinity (K_i < 15 nM) and remarkable selectivity toward the other three adenosine receptors.

- In the frame of this project unequivocal evidence supporting the stereospecific interaction between the *h*A_{2B}AR and some of the trifluorinated stereoisomers has been obtained. Previously stated evidence was established through the synergistic use of different experimental techniques (*e.g.*, chiral HPLC, circular dichroism, diastereoselective synthesis, and X-ray crystallography).

- The nitrogen-walk approach (*e.g.*, bioisosteric replacements for the furan and thiophene rings) enabled to identify metabolically stable ligands in a series of potent A_{2B}AR antagonists.

- Several new ligands combining remarkable affinity (K_i < 30 nM) and exquisite selectivity (> 1000-fold) were identified by introducing 18 different pentagonal heterocyclic frameworks at position 4 of the 1,4-dihydrobenzo[4,5]imidazo[1,2-*a*]pyrimidine scaffold.

- The antagonistic behaviour of the lead compound and its eutomer was corroborated through functional cAMP experiments and joint analysis of the current and previous series allowed a comprehensive understanding of the binding mode and SARs within the series.

- The microsomal stability and the inhibitory effect on cytochromes CYP3A4 and CYP2D6 were evaluated for the most appealing ligands. These studies demonstrated negligible inhibitory activity and excellent microsomal stability of evaluated A_{2B}AR antagonists.

- A combination of chiral HPLC and circular dichroism provided experimental support to the stereospecific interaction between the (4*S*) stereoisomers of the most attractive bioisosteres obtained and the human A_{2B}AR.

- Herein a previously unexplored, efficient, and versatile multicomponent-based diversification strategy that enables the rapid generation of novel subtype-selective DRD_2 biased ligands is documented. The optimized strategy exemplifies the

importance of discovering diverse and previously unexplored RHS groups but also highlights their critical role in modulating the functional selectivity profile.

- The pharmacological characterization of the new series of compounds enabled the identification of several ligands that elicit excellent DRD_2 selectivity and remarkable functional selectivity by either the cAMP or β-arrestin signaling pathways. The binding modes of these novel biased ligands was interpreted in the context of a molecular modeling based on the recently published DRD_2 crystal structure.

- The functional data of some of the biased ligands obtained suggest the configuration of the stereocenter within the RHS of the ligand could play a role in the recognition at the DRD_2. Accordingly, further studies are now in progress in our laboratory to establish the role of stereochemistry in the observed biased profiles.

- Jointly, the herein documented results highlight the synthetic potential of multicomponent reactions to accelerate the discovery, optimization, and profiling of new prototypes in Medicinal Chemistry.

6. APPENDIX

USC
UNIVERSIDADE
DE SANTIAGO
DE COMPOSTELA

The following chapter was developed in Research Institute for Medicines, at Universidade de Lisboa (iMed.Ulisboa), under the supervision of Professor Doutor Rui Moreira during a three-months research stay. This study is based on the development of quenched activity-based probes (qABPs), with a β-lactam warhead oriented toward the ubiquitin-proteasome system.

6.1 INTRODUCTION

6.1.1 The ubiquitin proteasome pathway

The ubiquitin proteasome pathway (UPP) is the most important eukaryotic system for the regulation of protein degradation, and it plays an essential role in maintaining homeostasis and regulating cellular function.[1] More than 80% of cellular proteins are degraded through UPP, including those involved in processes like cell cycle, apoptosis, transcription, DNA repair, protein quality control, and antigen presentation.[2]

When proteins are degraded through the ubiquitin proteasome system, they follow two distinct and successive steps: The ubiquitin tagged covalently by a polyubiquitin chain to the protein which will be degraded and then, the degradation of the labeled protein by proteasome happens.

During the ubiquitin tagging, three enzymes are involved. First of all, the ubiquitin-activating enzyme, also known as E1, is responsible for activating ubiquitin with the formation of an ATP-dependent thiol ester bond.[3] Later, the E1-ubiquitin thiol ester is recognized by multiple ubiquitin-conjugation enzymes or E2s and ubiquitin is transferred to them.[4] Then, the E2-ubiquitin complex could pass ubiquitin to the E3s enzyme (ubiquitin ligase) or it could cooperate with E3 enzymes for substrate selectivity and directly add ubiquitin to the target.[5] In successive reactions, a polyubiquitin chain associated with a Lys residue (the most common is Lys48) is synthesized and the whole acts as a signal to target proteins for subsequent degradation in the 26S proteasome[6] (Figure 6.1).

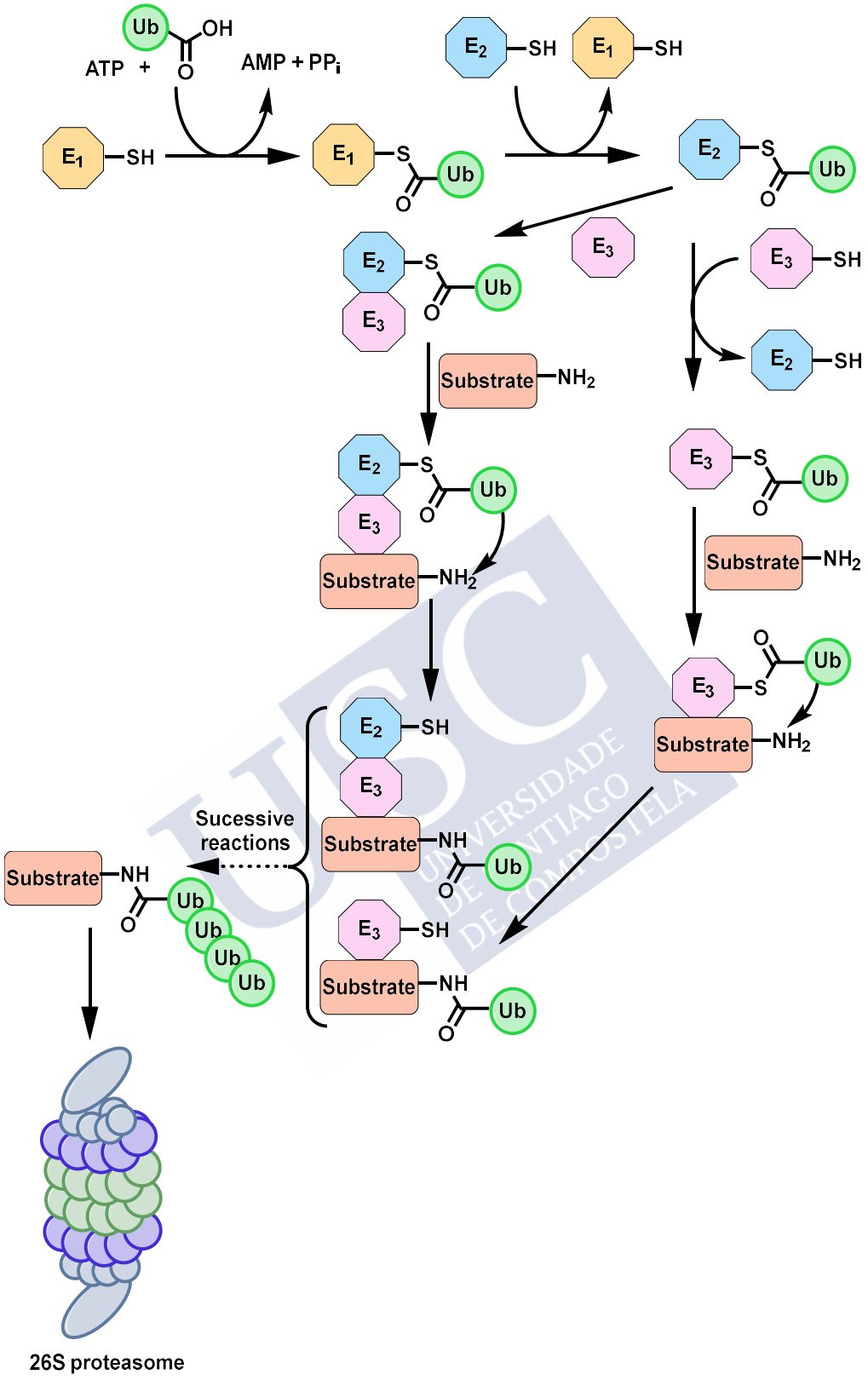

Figure 6.1:Ubiquitin-tagged process.[7]

6.1.1.1 Proteasome structure and function

26S proteasome can be found in the cytosol and nucleus of all eukaryotic cells.[8] It is formed by the core particle (CP) or proteolytic chamber (20S proteasome), and two caps at the ends of the proteolytic chamber, called 19S proteasome. 19S regulatory complexes are responsible for various activities such as ATPase, recognizing poly-Ub chains, ubiquitin-binding, deubiquitinating and the substrate translocation into the CP, among others.[4,9–11]

The 20S proteasome is a cylinder-shaped structure composed of 28 protein subunits arranged in 4 stacked rings in the order of α-β-β-α with C2 symmetry. Both α-rings are located at the ends of the CP and consist of 7 different subunits each.[12] Their function is predominantly structural, but they also regulate access to the substrate through the N-terminal extensions.[13] Furthermore, β-rings are located at the barrel-shaped internal proteasome site. Among their 7 different β subunits per β-ring, three of them (β_1, β_2 and β_5) comprise the catalytic site. Since there are two β-rings in each 20S proteasome, the latter has six proteolytic sites[13,14] (Figure 6.2).

In the case of β_1, the activity of this subunit is caspase-like (C-L) that cleaves after acidic residues and branched chain amino acid preferring (BrAAP). β_2 has threonine-like (T-L) activity which cleaves after basic residues, while the activity of β_5 is chymotrypsin-like (CT-L) that cleaves hydrophobic amino acids, also BrAAP and small neutral amino acid preferring (SNAAP). All its active sites are substrate specific and contain a N-terminal threonine, and its function is to be a nucleophile in peptide bond hydrolysis.[13,14]

In addition to the constitutive proteasome, if cells are exposed to some stimuli such as interferon-γ (INF- γ), tumor necrosis factor-α (TNF- α) or bacterial lipopolysaccharides they will induce the synthesis of an alternative proteasome form known as immunoproteasome.[2] In this case, the proteolytic chamber is called 20S immunoproteasome or i20S and the constitutive subunits β_1, β_2 and β_5 are replaced by immune β_i-subunits, β_{1i} (LMP2), β_{2i} (MECL1) and β_{5i} (LMP7).[15] This i20S is preferentially expressed in lymphoid origin cells and performs a role in major histocompatibility complex class one (MHC-I) antigen processing and presentation.[16]

As previously mentioned, all the active centers have a N-terminal threonine, but the answer to why β subunit is specific to its substrate and no other is because of the

composition of the substrate binding pocket. Each pocket site is called 'nonprimed' (S_1, S_2, S_3, S_4…S_n) or 'primed' (S_1', S_2', S_3', S_4'…S_n') depending on the closeness of the active site. Finally, substrate residues that interact with nonprimed and primed sites are termed P_1, P_2, P_3, P_4…P_n and P_1', P_2', P_3', P_4'…P_n', respectively[17] (Figure 6.2).

Modifications at the residue 45 of the proteasomal S_1 (which interacts with the residue of the amino acid that leads to the formation of the cleaved peptide C-terminal end) determine the cleavage preference of the active sites.[18] Several examples are Arg45 at β_1 subunit or Gly45 at β_2 that confer different properties to the active site.

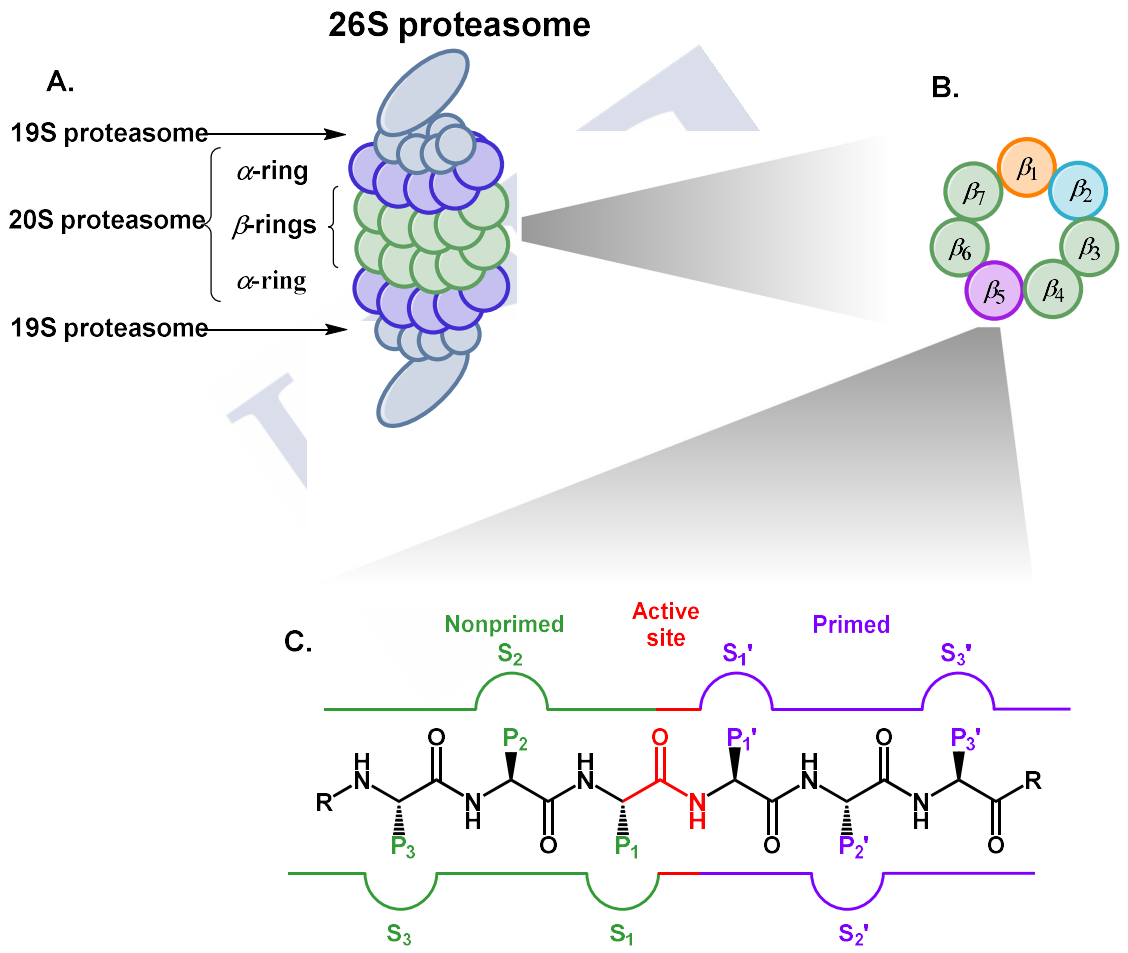

Figure 6.2: A. General structure of the 26S proteasome. B. Structure of a *β*-ring. C. General structure of substrate binding pocket.

The role of the proteasome is to degrade misfolded proteins to peptides with 8-12 amino acids and the catalytic mechanism of their hydrolysis will be described below.

Thanks to the 1995 elucidation of the crystal structure of the archaebacterial *T. acidophilum* CP in complex with the calpain inhibitor I (competitive inhibitor *N*-Acetyl-Leu-Leu-norleucinal), the catalytic mechanism of substrate hydrolysis could be understood.[19] The aldehyde group of calpain inhibitor I was covalently attached by a hemiacetal bond to the threonine γ hydroxyl group (Thr1Oγ) and the threonine N-terminus (Thr1NH_2) acted as a proton acceptor (Scheme 6.1). This fact confirmed that the N-terminal threonine from each β-subunit is essential for the proteolytic active sites in the proteasome.

Further mutagenic and structural studies assigned the major important catalytic residues to Thr1, Asp/Glu 17 and Lys33.[20] Also, Ser129, Asp 166 and Ser169 which are close to the active site, contribute to both structural integrity and catalysis.[20] Thr1Oγ forms hydrogen bonds with Lys33N^{ζ}; whereas Thr1NH_2 is hydrogen bonding to Ser129O^{γ}, Asp168O and Ser169O^{γ}.[17]

Subsequently, it is important to mention a catalytic water molecule, called 'NUK', since it is important in several steps in the catalytic process.[21]

The mechanism of peptide bond cleavage takes place between the substrate P1 and P1´ residues (Figure 6.2). Thr1NH_2 catalyzes, the nucleophilic addition of Thr1Oγ to the substrate peptide bond, thanks to NUK, as it acts as proton shuttle, making up a tetrahedral adduct transition state. The rearrangement of this intermediate leads to the formation of an acyl-enzyme adduct followed by the diacylation of Thr1Oγ catalyzed, again, by Thr1NH_2 and NUK. (Scheme 6.1).[21]

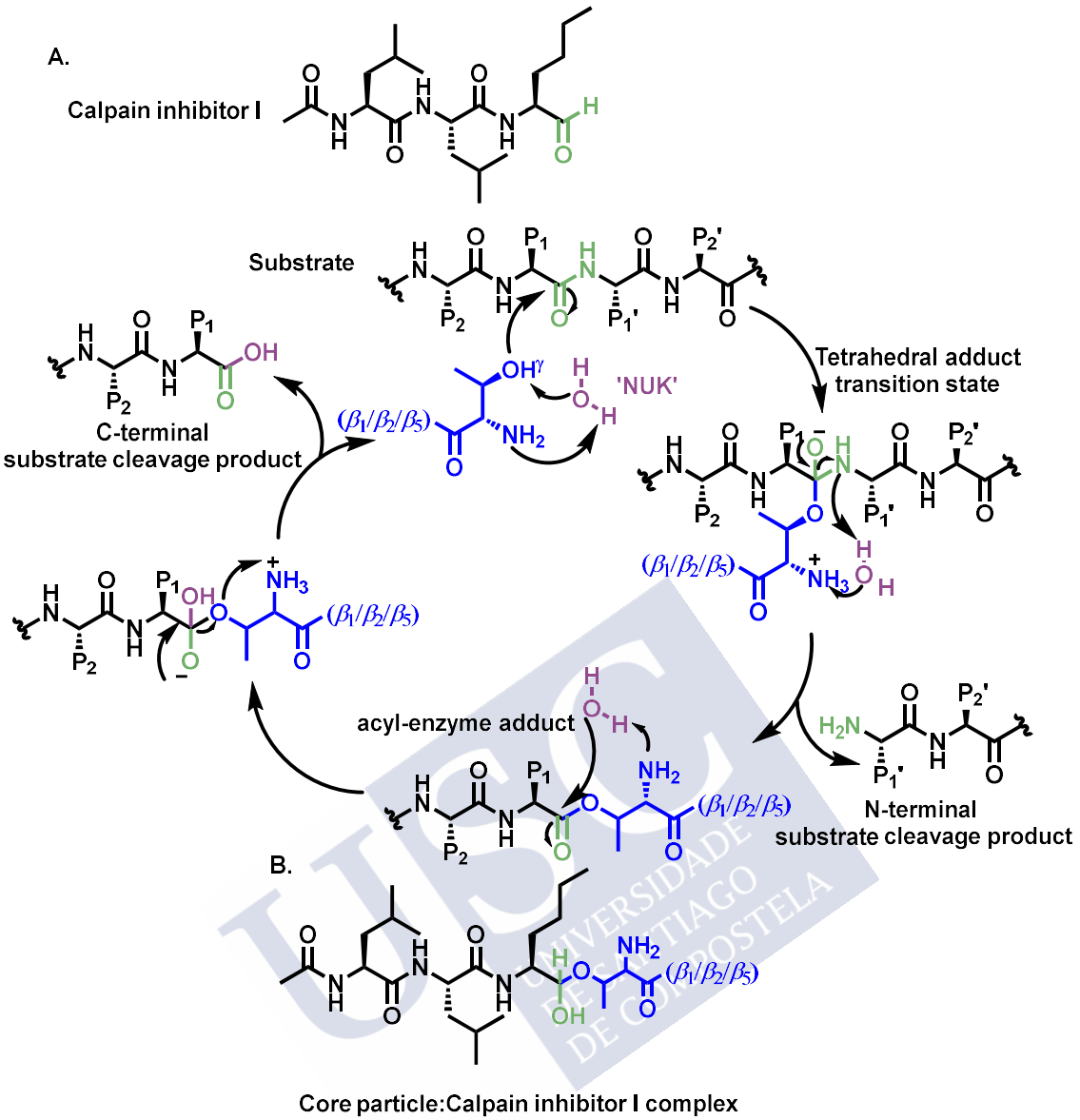

Scheme 6.1: A. Proteolytic mechanism of 20S proteasome. B. Hemiacetal binding of the Calpain inhibitor I with the core particle.[23]

6.1.2 Proteasome inhibitors

It has become evident that deregulations in the ubiquitin proteasome pathway are involved in many diseases such as, cancer (multiple myeloma, Waldenström macroglobulinemia, mantle cell lymphoma), treatment of acute allograft rejection in transplant patients, autoimmune and inflammatory diseases (lupus, lupus nephritis, myasthenia gravis, multiple sclerosis, streptococcal cell-wall induced polyarthritis, rheumatoid arthritis, psoriasis, asthma and colitis), among others.[22,23] They are useful as anti-infectives in *M. tuberculosis*, *P. falciparum*, *T. brucei* and *T. cruzi* too.[24,25] Due to

these defects in the UPP, many proteasome inhibitors have been developed as a rational therapeutic approach.

Proteasome inhibitors (PI) could be classified attending to their structures, binding mode characteristics, specificity to the catalytic active site and reversibility of binding.[17]

Considering all these classifications, in 2012, Kisselev *et al.* separated PI in two large groups, depending on whether the compound binds covalently or not.[23] Non-covalent proteasome inhibitors have been investigated as reversible inhibitors that could reduce the cytotoxicity and adverse effects of covalent inhibitors. Nevertheless, this family has been less studied due to their weak bond to the CP. They are classified in natural compounds, synthetic 'pseudopeptides' (synthetic modified peptides) and synthetic non-peptidic inhibitors.[26]

On the other hand, covalent proteasome inhibitors could be separated into eight main groups that will be described below (Figure 6.3).

- **Peptide aldehydes**: Mimic the natural proteasome substrate and, as previously mentioned with calpain inhibitor I, form a covalent binding to Thr1.[27]
- **Peptide vinyl sulfones**: Their electrophilic pharmacophore act as a Michael acceptor that leads to an irreversible covalent bond with Thr1Oγ.[28] Another peptide-based Michael acceptor family is **syrbactins**, they are peptidyl natural and synthetic products whose pharmacophore binds to the β_5 subunit with an irreversible covalent bond by a typical Michael 1,4-addition mechanism.[28–30]
- **Peptide α'β'-epoxyketones**: Irreversible inhibitors whose mechanism of action forms a morpholino ring with Thr1.[31] The most representative proteasome inhibitor of this family is carfilzomib, known as Kyprolis®, approved by US FDA as the second-in-class PI in 2012.[32] This compound inhibits the β_5 subunit at low-doses and both β_5 and β_2 subunits at high-doses.[22] Then, **peptide α-ketoaldehydes** (glyoxals) are cell-permeable inhibitors described as a group that could act with a mechanism of action similar to α'β'-epoxyketones, the proposed one is through six-membered ring formation, but they selectively inhibit the β_5 subunit in a reversible way.[33]
- **Peptide boronates**: This group contains a boronate electrophilic group that increases the specificity for the proteasome and reacts better to the hydroxyl group

of Thr proteases.[34] Nowadays, there are two boronate compounds in the market, bortezomib, and ixazomib.

Bortezomib (Velcade®)[35] is the first proteasome inhibitor approved by US FDA in 2003.[32] This PI reversibly inhibits the β_5 subunit and, to a lesser extent, β_1 subunit of the proteasome. It is used as the first-in-class PI drug for hematologic and solid tumor malignancies, in particular, human multiple myeloma (MM) cells.[32] This drug not only inhibits the nuclear factor κB (NF-κB), a protein complex that is part of many tumor-related processes (anti-apoptotic effect, induction of angiogenesis, migration, and proliferation) as also activates various inflammatory and immune pathways;[36] but is also a strong activator of three defined apoptotic pathways in MM cells. These are the intrinsic pathway that is mediated by the activation of caspase-9; the extrinsic pathway is mediated by another caspase, caspase-8 and, by the activation of death receptors (DR) and, finally, the activation of endoplasmic reticulum stress pathway involving caspase-2.[37] Moreover, bortezomib induces apoptosis in replicating cells by blocking cell cycle at G2/M phase as well as the inhibition of angiogenesis in MM cells.[38,39]

The second peptide boronate approved in 2015 by the US FDA is ixazomib, also known as Ninlaro®, and it is the only oral proteasome inhibitor so far.[32] Besides, it is a reversible inhibitor that binds to the β_5 subunit and to the β_1 subunit at higher concentrations.[40] This drug is used in combination with dexamethasone and lenalidomide for the treatment of relapsed and refractory multiple myeloma.[41]

- **Bacteria-specific oxathiazol-2-ones**: These compounds showed an irreversible potential inhibition of mycobacterial proteasomes, having a trypanocidal effect and killing *P. falciparum* parasite, responsible for Malaria disease.[23]

- ***β*-lactones**: The interest of the development of these types of natural proteasome inhibitors as possible second-generation candidates has increased since the discovery of resistance to bortezomib in multiple myeloma.[42]

The first compound of this family to be discovered was lactacystin from *Streptomyces sp.*, and it has a γ-lactam core with a N-acetylated cysteine residue. Studies showed that at pH 8 aqueous solutions, lactacystin undergoes a spontaneous intramolecular reaction that loses N-acetylcysteine to form a new proteasome

inhibitor with a fused β-lactone ring called 'clasto-lactacystin-β-lactone' or 'omuralide'.[43] This new finding leads to the development of new non-peptide proteasome inhibitors with a β-lactone-γ-lactams cores.

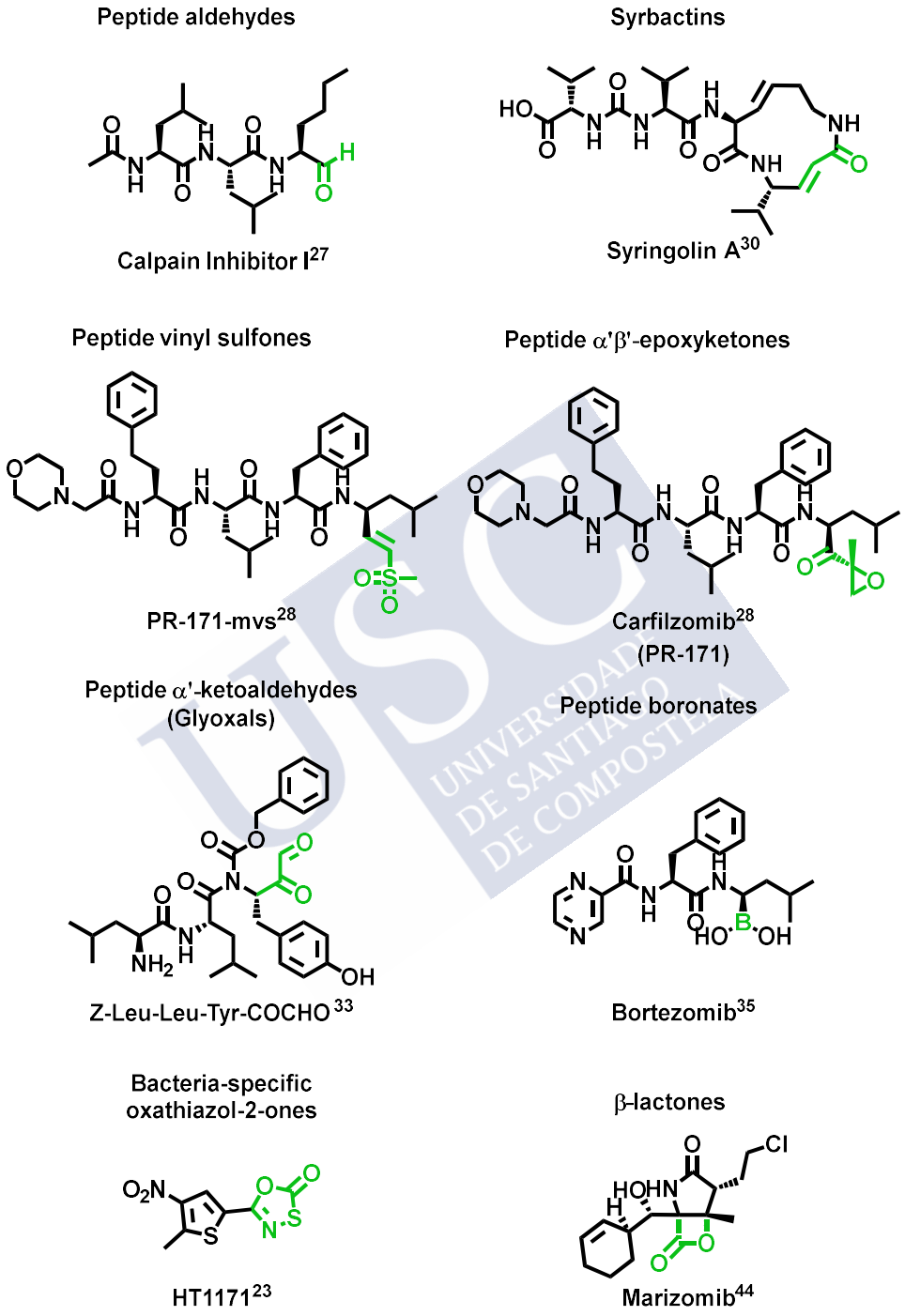

Figure 6.3: Covalent proteasome inhibitors.[23,27,28,30,33,35,44]

6.1.2.1 β-lactone-γ-lactam: Omuralide and marizomib

As previously mentioned, omuralide is an *in situ* cyclization of lactacistine. This compound binds to the catalytic site of the β_5 subunit. Specifically, its mechanism of

action is based on an opening reaction of the nucleophilic β-lactone ring with the N-terminal Thr1Oγ to form an acyl-enzyme product. To restore the proteasome inhibitor, this product could be removed with ester hydrolysis mediated by Thr1NH_2 and NUK (Scheme 6.2).[45,46] Many publications consider that covalent omuralide bond is irreversible, but taking into account the marizomib binding, it is more appropriate to refer to it as 'slowly reversible'.[46,47]

Thanks to the crystal structure of the yeast CP with omuralide it has been found that the isopropyl group in C-6 position is important for the β_5 binding capacity, this residue makes hydrophobic interactions to the Met45 present at the proteasome S_1 substrate-binding pocket and also, the methyl group in C-2 position points toward proteasome S_2 substrate-binding poket.[46,47]

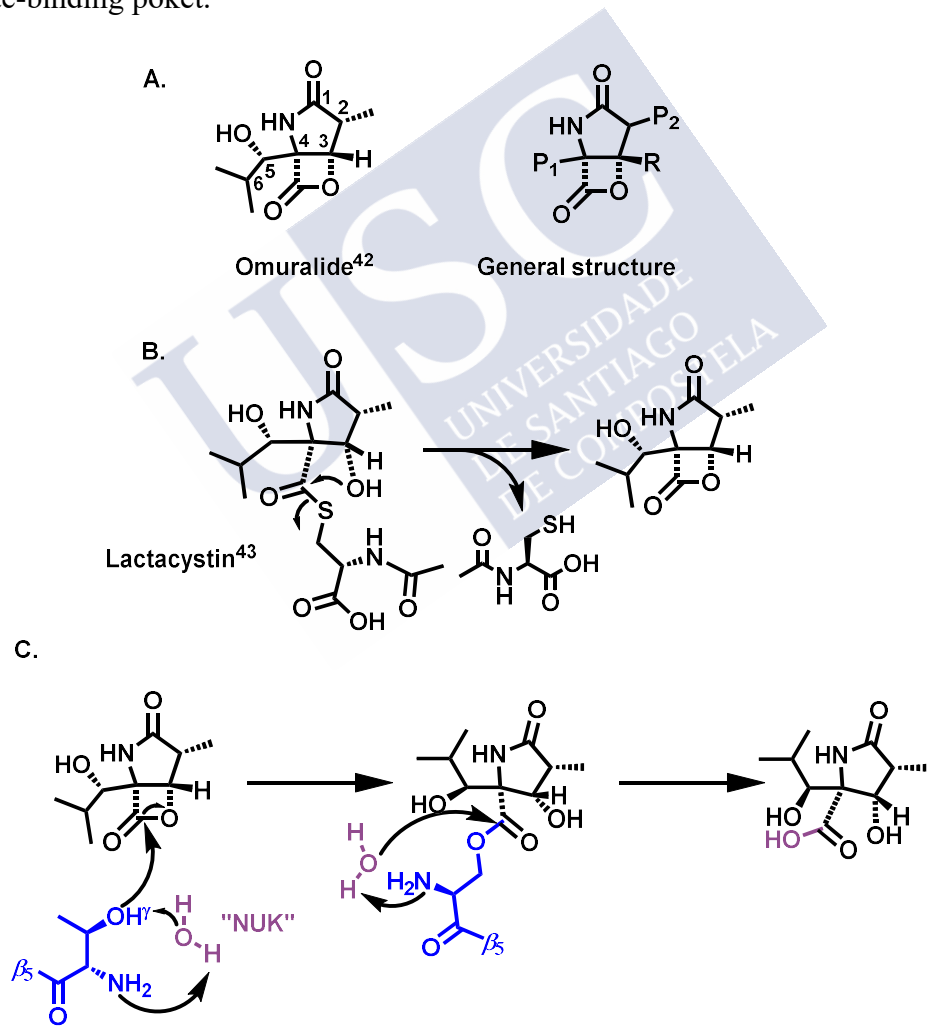

Scheme 6.2: A. Structure of omuralide and general *B*-lactone-*y*-lactam structure. P_1 and P_2 are moieties interacted with S_1 and S_2, respectively.[42,43] B. Spontaneous intramolecular reaction of lactacystin to form omuralide. C. Mechanism of inhibition of the omuralide at subunit β_5.

Although clinical essays of omuralide were dropped due to its high off-target activities, another natural β-lactone-γ-lactam compound named salinosporamide A or marizomib is currently in clinical trials.[45]

Marizomib has been isolated as a second metabolite of marine actinomycete *Salinispora tropica*. This compound is the first of its class, produced by a saline fermentation of an obligate marine actinomycete, used as a clinical candidate.[48] In this case, marizomib not only inhibits irreversibly the β_5 subunit, but also β_1 and β_2 subunits due to the cyclohexene ring at position C-6. This residue makes enough favorable interactions with the three S1 substrate-binding pockets despite of their preferences (positively and negatively charged residues and hydrophobic residues). Nonetheless, enzyme inhibition kinetics confirmed that the binding affinity is higher by β_5, then by β_2 and finally by β_1.[49]

Moreover, it is relevant to mention the chloroethyl group in C-2 position since it plays an important role in the marizomib mechanism of inhibition. This moiety, as methyl omuralide residue, points toward proteasome S_2 substrate-binding pocket. This pocket is commonly described as an open space, suggesting that all the CP active binding sites should be able to accept space-demanding residues.[46]

The mechanism of irreversible inhibition has been characterized by detailed kinetic studies and crystal structures of marizomib in complex with the 20S CP. Binding begins with the recognition of cyclohexene ring to the S1 substrate-binding pocket. Once linked, the N-terminal Thr1Oγ present at the catalytic site opens the β-lactone ring and forms an ester bond. Such reaction is followed by the formation of a tetrahydrofuran (THF) ring thanks to the displacement of chloride catalyzed by Thr1NH_2.[50] This ligand could only be removed when the formation of THF is slow enough to perform the ester hydrolysis catalyzed by Thr1NH_2 via NUK.[46] In the case of marizomib, the most favored pathway is the irreversible one, while the reversible pathway will prevail for marizomib analogues with a weak leaving group, for example, fluorine (Scheme 6.3). This inhibition leads to a higher potent activation of apoptosis by a caspase-8 dependent mechanism than the one caused by the inhibition of bortezomib in leukemia and MM cells.[44,51,52]

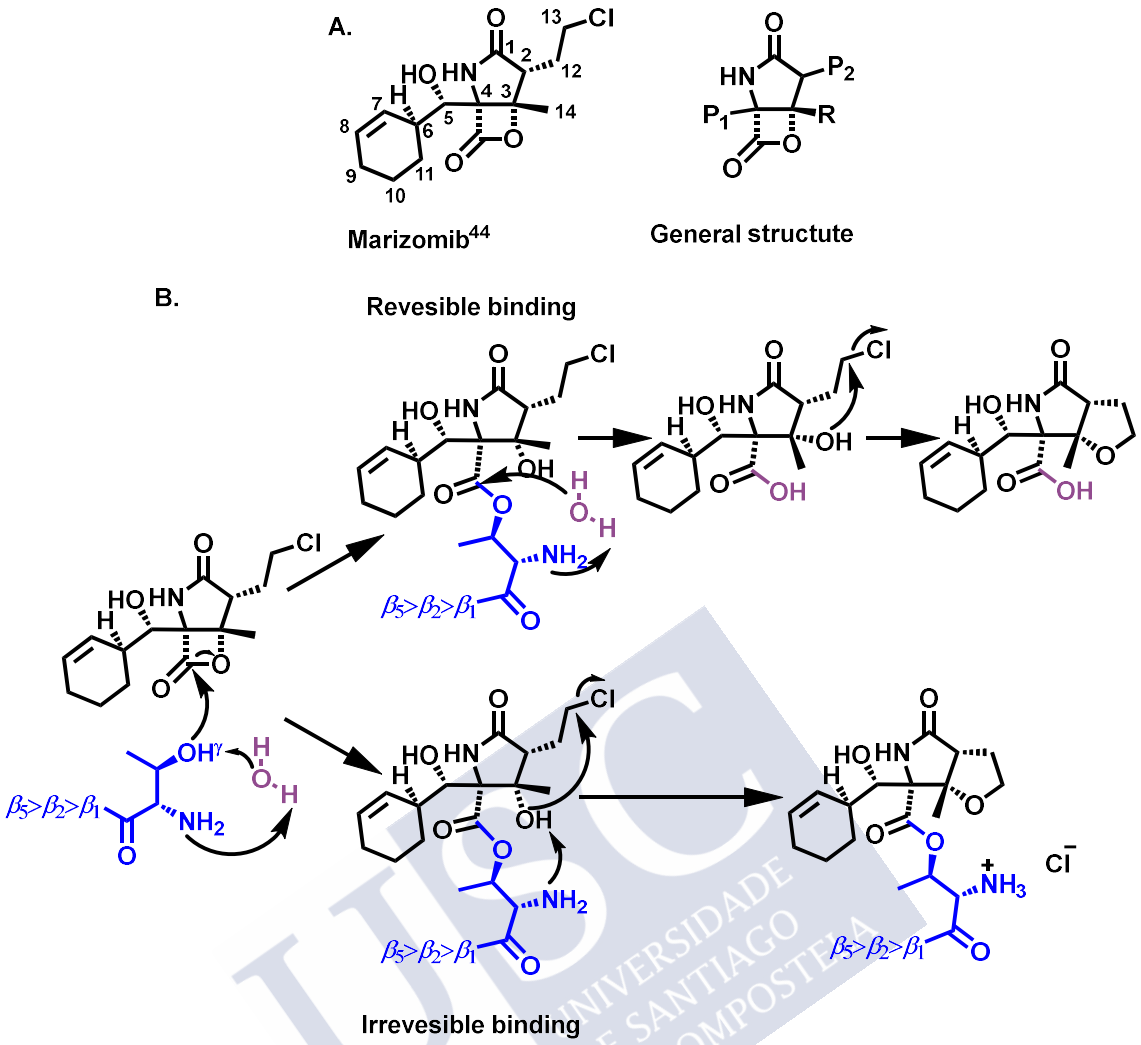

Scheme 6.3: A. Structure of marizomib and general *β*-lactone-γ-lactam structure. P_1 and P_2 are moieties interact with S_1 and S_2, respectively.[44] B. Mechanism of irreversible and reversible inhibition of marizomib at proteasome.

Further SAR studies demonstrated the importance of hydroxyl group at position C-5. Epimerization, oxidation to ketone or the absent of this moiety do not show any proteasomal inhibition or a decrease of potency.[53] Crystal structures of marizomib or salinosporamide B prove that this hydroxyl group stabilizes those ligands by a hydrogen bond with Thr21NH.[54]

In context of preclinical studies, marizomib has been shown to be a potential ligand to treat, alone or in combination with other agents, a broad spectrum of hematologic cancers such as MM, mantle cell lymphoma (MCL) and Hodgkin's lymphoma, Waldenstrom's macroglobulinemia and acute and chronic lymphocytic leukemia. Besides that, there are also preclinical studies that associated marizomib with the treatment of solid tumors such as colorectal and pancreatic carcinoma, and glioma.[50]

6.1.3 Quenched activity-based probes (qABPs)

Fluorescence imaging provides a fundamental way to detect and monitor biological targets in complex and dynamic intracellular environments.[55] Activity-based probes (ABPs) are small compounds that covalently bind and modify a defined set of active catalytic residues.[56]

Specifically, chemical 26S proteasome ABPs have been developed to identify and control the activity of the catalytic subunit active site as opposed to non-covalent interacting peptide-based substrates. In this case, proteasome ABPs are formed by three parts: a reactive group (warhead), responsible for binding to the active catalytic subunits of the 20S CP, a linker, and a tag region that allows the detection (*e.g.*, a fluorophore) or isolation (Figure 6.4A).[57]

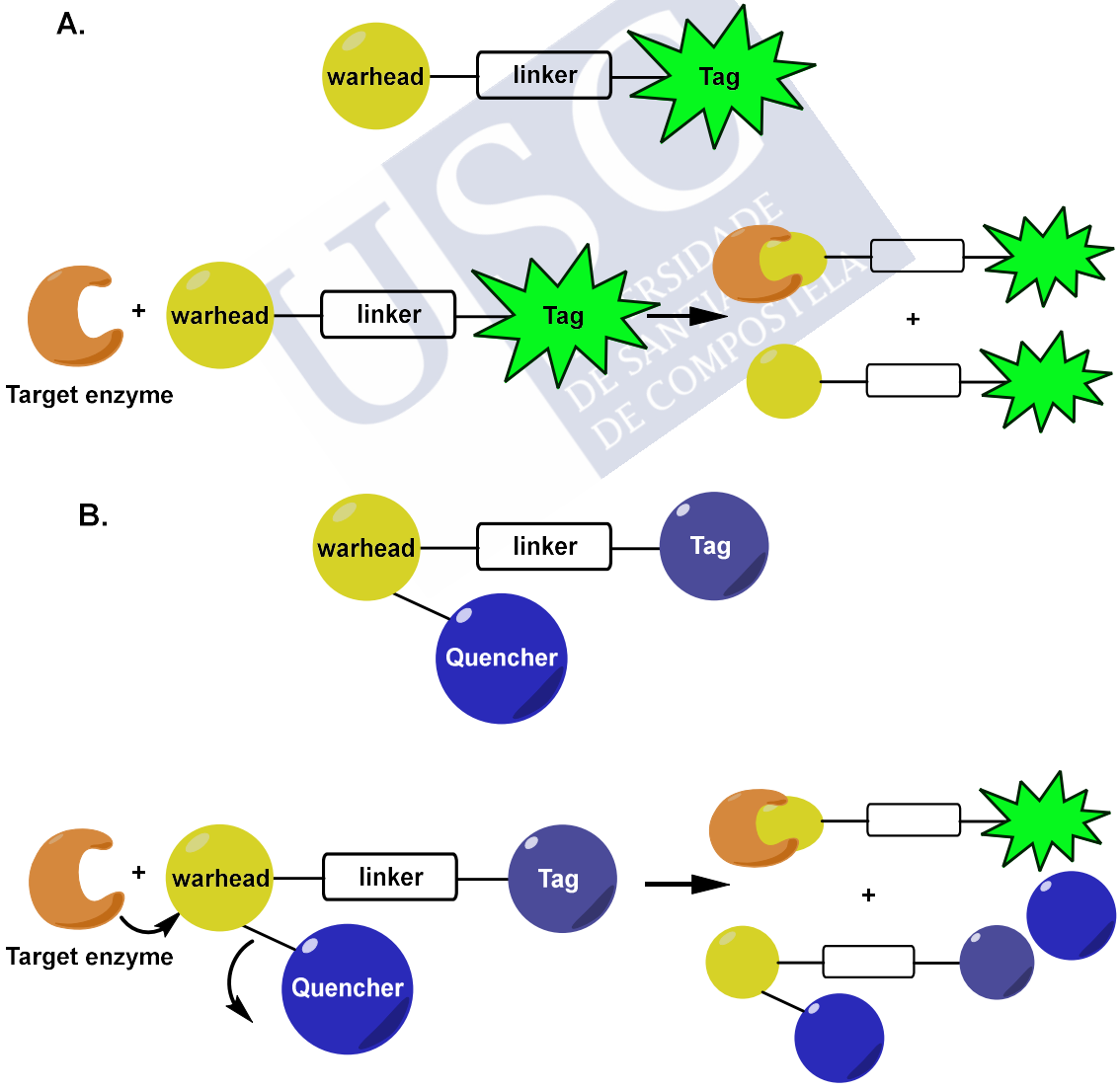

Figure 6.4: A. General structure of ABPs and their biological binding reaction. B. General structure of qABPs and their biological binding reaction.

However, the main limitation of this technique is that these ligands are fluorescent, not only when they are binding to the target enzyme, but also when they are free in the solution (Figure 6.4A). To overcome this limitation quenched activity-based probes (qABPs) were developed, and these only become fluorescent after their covalent binding to the target enzyme (Figure 6.4B).[56,58]

These probes, unlike the previous ones, are designed to contain a fluorescent donor and acceptor (also known as quencher) so, in their native state, they will not be fluorescents.[59] The quencher is part of the leaving group so, when this ligand covalently binds to the target enzyme to form the enzyme-probe complex, the quencher is released and causes the probe to fluoresce brightly (Figure 6.4B).[59,60] Several studies were developed with these types of probes targeting different enzymes such as cysteine cathepsins[61], kinases[62] and serine proteases[63], among others.

6.1.4 Click chemistry

Click chemistry is one of various synthetic approaches (such as multicomponent reactions mentioned in previous chapters) that can accelerate and simplify the discovery of novel and promising compounds. This is a powerful reaction to make heteroatoms link (carbon-heteroatom-carbon bonds) in an aqueous environment. It has broad chemical and biological applications in different fields such as biomedical research, ranging from lead discovery and optimization to tagging of biological systems (proteins, nucleotides or even a whole organism).[64–66]

Generally, the advantages of click reactions are that they are modular, wide in scope, have high yields, generate only inoffensive byproducts that can be removed by nonchromatographic methods and are stereospecific (but not necessarily enantioselective).[67] Several main characteristics of these types of reactions include simple reaction conditions (they should be insensitive to oxygen and water in ideal situations), starting material and reagents ready to use. Further common properties are the use of no-solvent, a 'benign' solvent (for example water) or an easily removed solvent, and simple product isolation.[66]

Among all the types of reactions that involved click chemistry, Huisgen's 1,3-dipolar cycloaddition of alkynes and azides to give triazoles is the most characteristic one.[65] Initially, this cycloaddition required high temperature and the reaction usually gives a mixture of 1,4 and 1,5-disubstituted regioisomers, but thanks to the copper(I)-

Catalyzed Azide-Alkyne Cycloaddition (CuAAC), the 1,4-disubstituted 1,2,3-triazoles is obtained specifically.[68]

CuAAC is an extraordinarily robust click reaction in which Cu(II) is reduced to Cu(I). It could be performed under a wide variety of conditions and, the most important factor seems to be the maintenance of high levels of Cu (I) concentration during the reaction.[69] That is why Cu(II) source in presence of a large excess of reducing agent makes the reaction less susceptible to oxygen.[69]

6.2 OBJECTIVE

Taking all this background as a starting point, the aim of this thesis chapter is the development of a novel 20S proteasome quenched activity-based probe (qABP) to improve the understanding of this complex regulatory system and its associated pathways.

To do so, a general structure of qABP inhibitors has been designed by using the *β*-lactone family as a model, but for this project the chosen pharmacophore was a *β*-lactam ring, a bioisostere of *β*-lactones (Figure 6.5).

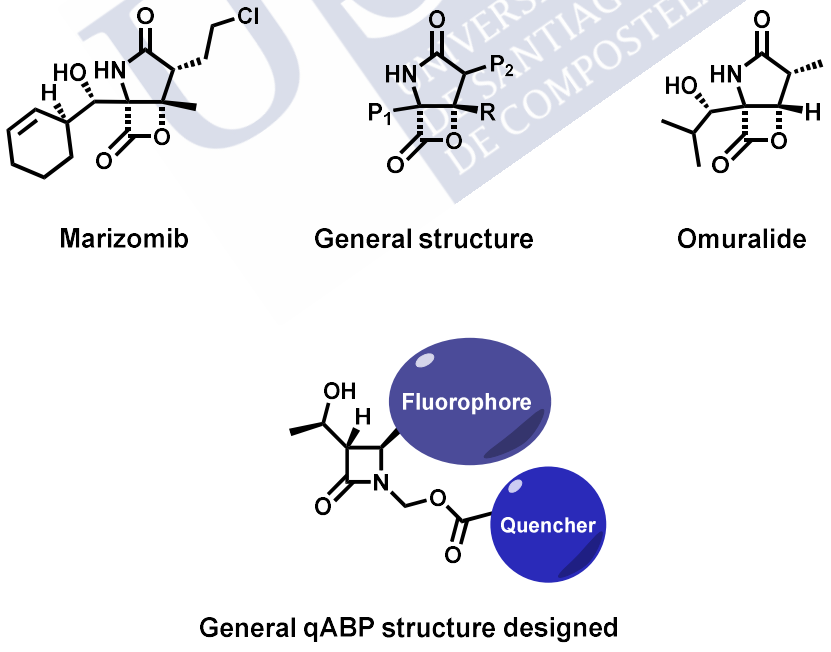

Figure 6.5: General structure of *β*-lactone-*γ*-lactam family with the most important ligands compared to the general structure of the designed qABP inhibitors.

Therefore, a qAPB was developed having a *β*-lactam core as reactive group, carboxy acid blue 40 (cAB40) as broad spectrum quencher (Q) and Cyanine 5 (Cy5) as

fluorescence donor (F). In addition, the theoretical mechanism of action of this qABP is to act as irreversible suicide inhibitor at the β_5 subunit of the proteasome 20S CP. The N-terminal Thr1Oγ present at the catalytic active site opens the β-lactam ring, the quencher is released, and an ester bond is formed. Subsequently, an imine group is formed, and it will react with a nucleophilic enzyme forming a covalent bond (Scheme 6.4).

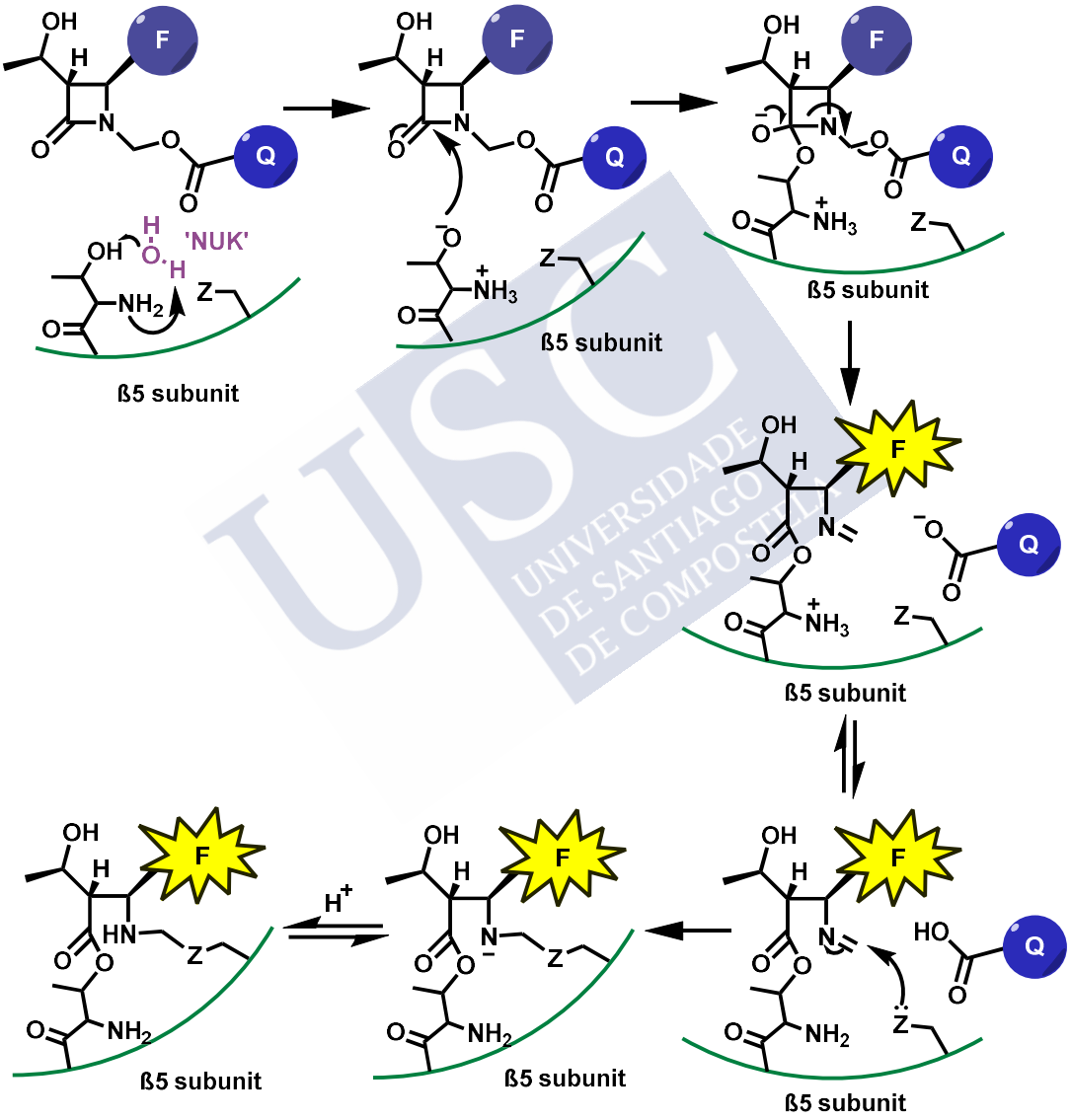

Scheme 6.4: Proposed mechanism of action of designed qABPs.

6.3 RESULTS AND DISCUSSION

To achieve the goal, an appropriate strategy was designed for the development of the qABP, which is shown in Scheme 6.5.

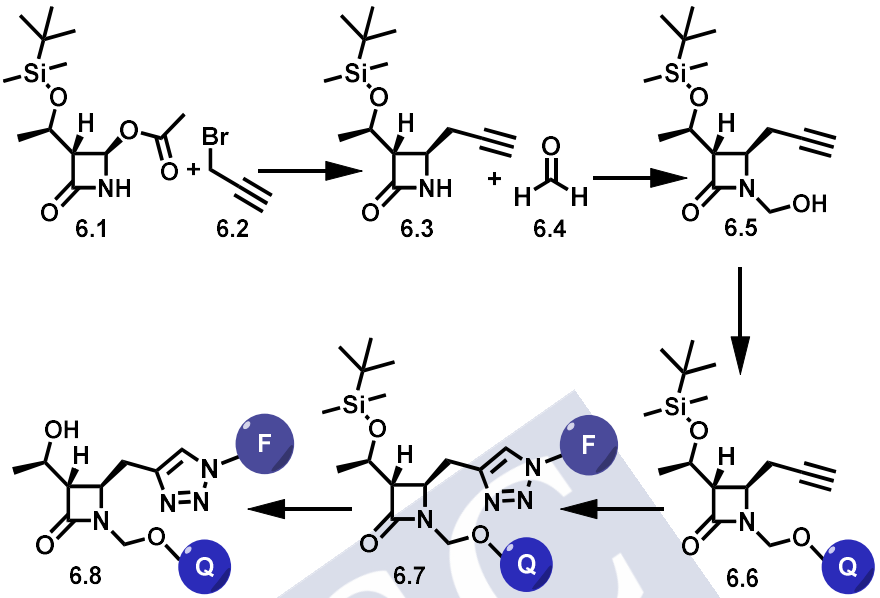

Scheme 6.5: General procedure of qABP synthesis.

The first synthetic step has already been described by P. Lee *et al*. and the yield obtained was almost the same as the one mentioned in the article, 73%.[70]

The most important point of this reaction is whether the product maintains the stereochemistry or not. To find out if this had happened, NMR characterization was performed on both reagent **6.1** and product **6.3** to compare the coupling constant.

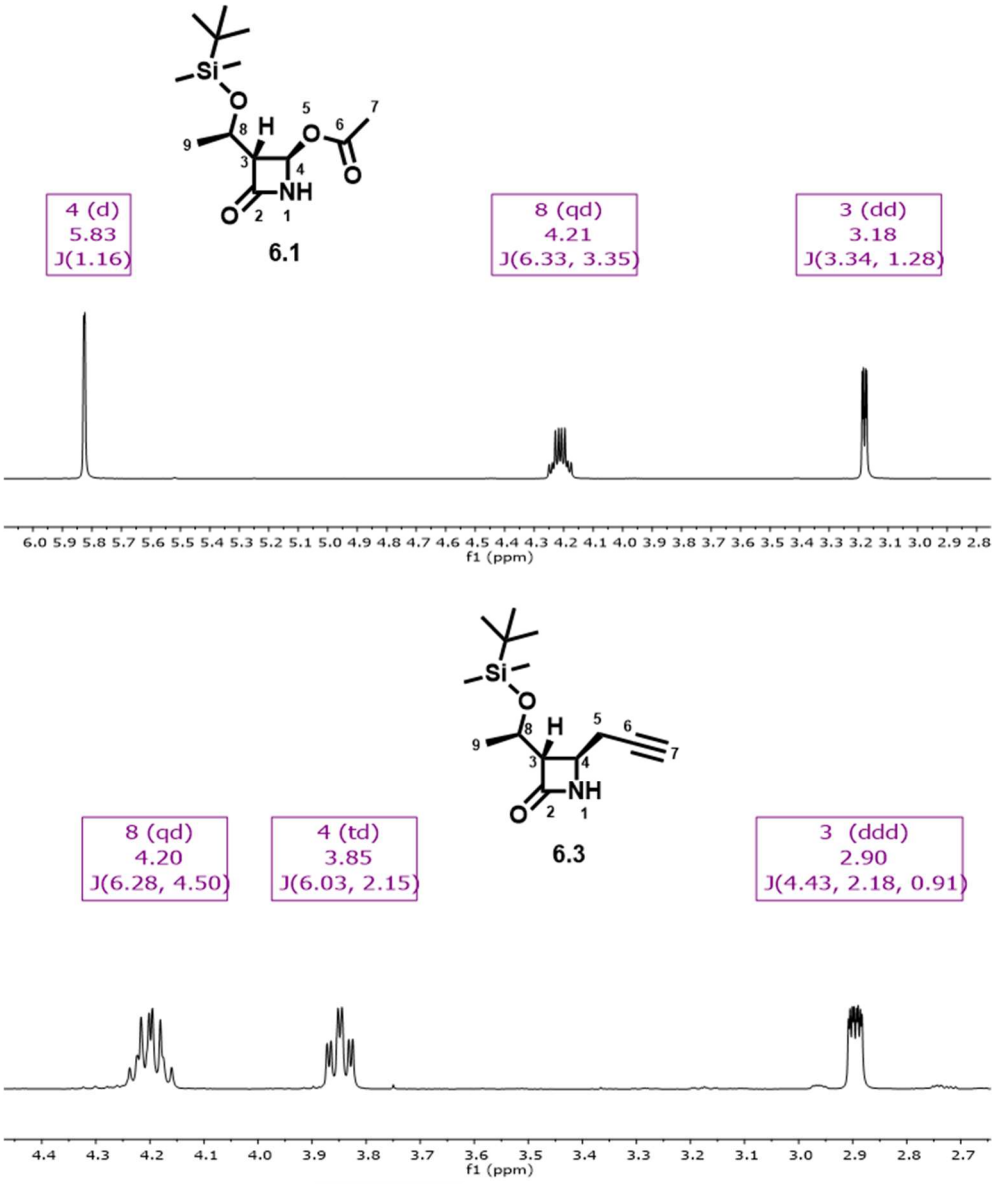

Figure 6.6: ^{1}H-RMN extensions of protons at positions 3, 4, and 8 of compounds 6.1 and 6.3.

^{1}H-NMR of compound **6.1** shows that the proton at position 4 has a coupling constant (*J*) of 1,2 Hz with proton at position 3 and between protons at positions 3 and 8, *J* is 3,4 Hz. Once the reaction was performed, the protons coupling constant between positions 4 and 3, as well as 3 and 8 is 2,2 Hz and 4,5 Hz, respectively (Figure 6.6). In both cases, the variation of *J* is around 1 Hz.

Furthermore, several previous studies made with the same *β*-lactam core show that the coupling constant for the *trans* conformation between protons at positions 3 and 4 is approximately 2 Hz while for the same protons in the *cis* conformation, *J* is around 5.5 Hz.[71,72]

These data confirm that the dihedral angle between the proton is not significantly different and corresponds to the *trans* conformation.

Once compound **6.3** was obtained, the optimization study of second step reaction conditions was developed taking the reaction conditions of H. Nagai *et al.* as reference (Scheme 6.6).[73]

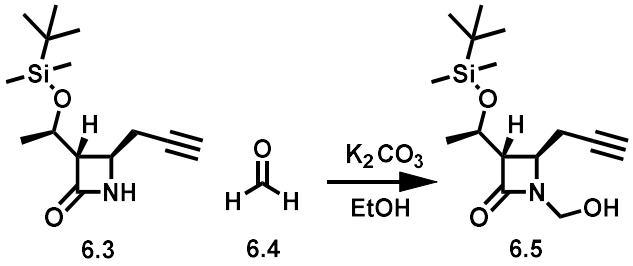

6.3 6.4 6.5

Scheme 6.6: Synthesis of compound **6.5**.

Table 6.1: Synthetic optimization of Scheme 6.6.

Entry	Formaldehyde (35% aq)	K_2CO_3	Solvent	T (ºC)	Time (h)	Yield (%)
1	2.5 + 1.25[a] equiv	0.32 + 0.16[a] equiv	EtOH	90 → 25	1→ 17[a]	52
2	3.75 equiv	0.5 equiv	EtOH	90 → 25	1 → 12	91

[a]After 12 h. at 25 ºC, 1.25 equiv of formaldehyde and 0.16 equiv of K_2CO_3 were added. The reaction was stirred for 5 h at 25 ºC.

In the first attempt, the reaction was performed using the conditions described. After 12 hours it was not completed, so 1.25 equiv of formaldehyde and 0.16 equiv of K_2CO_3 were added, and the reaction was finished after 5 hours.

Meanwhile, in the second attempt, the reaction was performed using the total equivalents previously employed and was completed after 12 hours. The yield increased from 52% to 91%.

6.3.1 Quencher synthesis and coupling

As previously mentioned, carboxy acid blue 40 (cAB40) was synthetized as quencher for this project. This is an anthraquinone-based fluorescent quencher that is used for fluorophores throughout visible spectrum and near IR.[74] The quencher was obtained through a one-step synthesis described by F. Jenigan *et al.*[74] (Scheme 6.7).

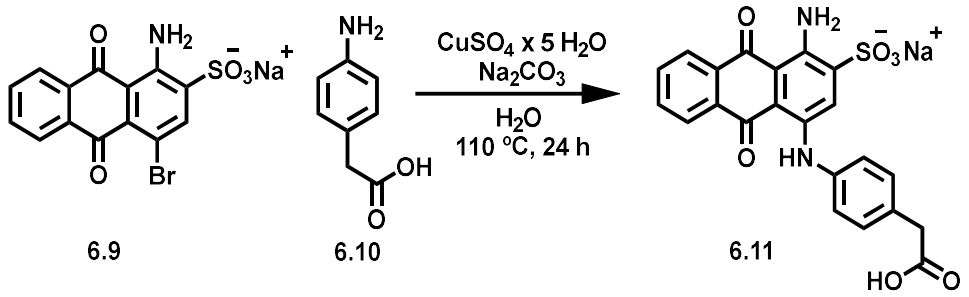

Scheme 6.7: Synthesis of cAB40.

This nucleophilic aromatic substitution was developed with bromaminic acid sodium salt **6.9** (1-Amino-4-bromo-9,10-dihydro-9,10-dioxo-2-anthracenesulfonic acid sodium salt), 4-aminophenylacetic acid **6.10**, copper (II) sulfate pentahydrate and sodium carbonate in water under reflux for 24 hours. After purification, product **6.11** was obtained with 30% yield.

Before the quencher coupling with the pharmacophore, the hydroxyl reactivity was tested through the reaction and conditions presented in Scheme 6.8 and Table 6.2, respectively.

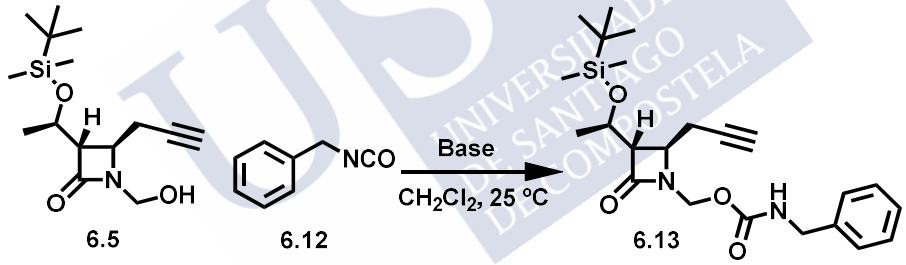

Scheme 6.8: Synthesis of compound **6.13**.

Table 6.2: Hydroxyl reactivity test.

Entry	Benzyl isocyanate (6.12)	Base	Time (h)	Yield %
1	2.2 equiv	-	24	67
2	2.2 equiv	TEA (0.5 equiv)	1.5	70

From the results of Table 6.2, it can be concluded that the presence of base is necessary for the reaction to be carried out in a short period of time, and the hydroxyl group has enough reactivity to be modified with a good yield. Once this test was performed, the quencher coupling reaction was optimized (Scheme 6.9 and Table 6.3).

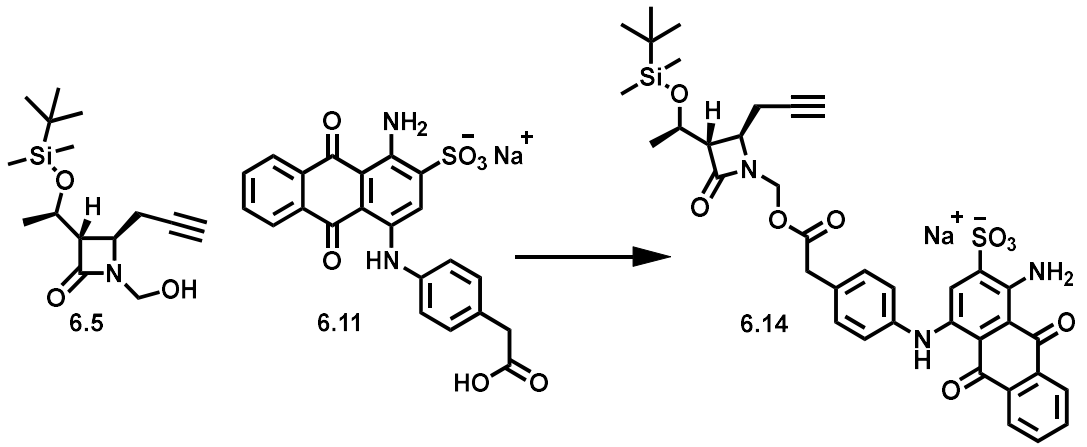

Scheme 6.9: Synthesis of compound **6.14**.

Table 6.3: Synthetic optimization of cAB40 coupling.

Entry	cAB40 (6.11)	Coupling reagent	Base	Solvent	T (ºC)	Time (h)	Yield (%)
1	1.1 equiv	HATU (1.6 equiv)	DIPEA (2.1 equiv)	DMF[a]	0 → 25	12	0
2	1 equiv	EDC (1.68 equiv)	DIPEA (2.1 equiv)	DMF[b]	0 → 25	12	11
3	1.1 equiv	HATU (1.6 equiv)	DIPEA (2.1 equiv)	DMF[b]	0 → 25	12	Traces
4	1 equiv	DCC (1 equiv)	DIPEA (1 equiv)	DMF[b]	0 → 25	12	Traces
5	1 equiv	TBTU (1.2 + 1[c] equiv)/HOBt (1.2 equiv)	DIPEA (3 + 1[c] equiv)	DMF[b]	0 → 25[c]	17	45
6	1 equiv	TBTU (2.2 equiv)/HOBt (1.2 equiv)	DIPEA (4 equiv)	DMF[b]	0 →25	12	65

[a]Concentration 0.01 M. [b]Concentration 0.1 M. [c]After 12 h. at 25 ºC, 1 equiv of TBTU and 1 equiv of DIPEA were added at 0 ºC. The reaction was stirred for 5 h at 25 ºC.

The optimization process to obtain compound **6.14** started with the test of different coupling agents (entries from 1 to 4). In these cases, only in entry 2, the product was isolated with 11% yield, and in entries 3 and 4, traces of **6.14** were detected in the reaction crude.

For the sake of improving the yield and the efficacy of the reaction, a conjugation of two different coupling agents (TBTU and HOBt) were tested following the conditions described in the PhD thesis of Dr. A. Ressurreição.[75] In the first attempt (entry 5), the reaction was not completed after 12 hours. Therefore, 1 equiv of TBTU and DIPEA were added and, after 5 hours, the reaction was completed, obtaining a yield of 45%.

Finally, in entry 6, the reaction was completed after 12 hours by using the equivalents corresponding to entry 5, and the compound was isolated with a yield of 65%.

6.3.2 Fluorophore coupling, click chemistry

After quencher coupling, a click reaction was performed to couple the fluorophore to the pharmacophore. At this point, it can be observed how the bind of the pharmacophore with the fluorophore turns off its fluorescence. In this project, the fluorophores used will be nitrobenzoxadiazole (NBD) **6.15** and Cy5 (**6.19**).

The aim of the first click reaction was to evaluate the following synthetic route steps. NBD azide **6.15** was used as an easy handle fluorophore to start with, and the compound **6.16** was obtain as described in Scheme 6.10.

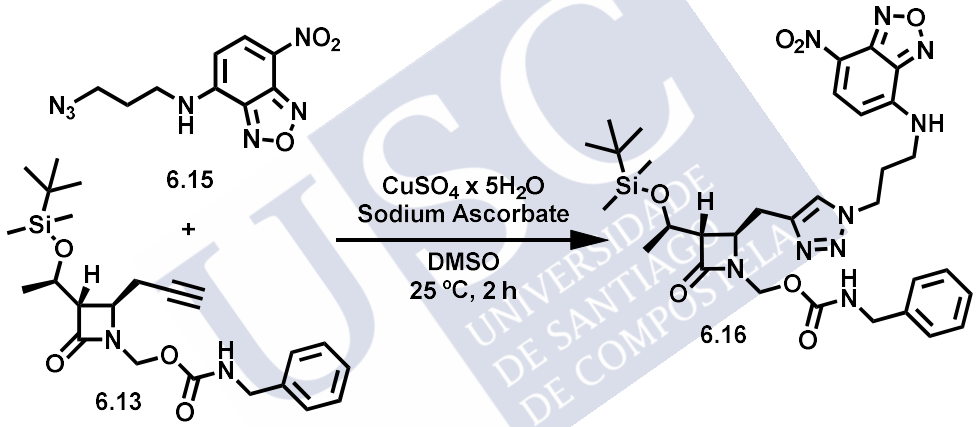

Scheme 6.10: Coupling reaction of NBD with hydroxyl group protected.

The reaction had a satisfactory yield, 59%. However, the biological importance of the hydroxyl group was described before. Moreover, it is relevant to understand how the presence or absence of the protecting group in the hydroxyl group affects the efficacy of the click reaction. Hence, a deprotected pharmacophore (deprotection reactions will be discussed below) was used to test the click reaction in the same conditions. (Scheme 6.11).

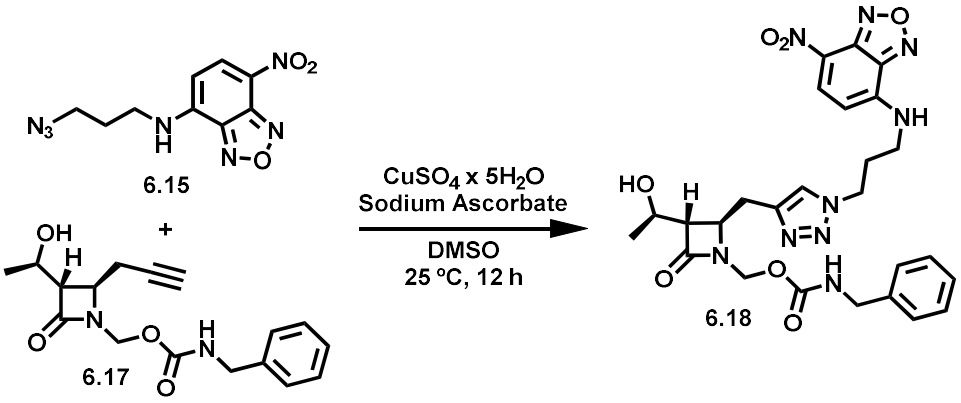

Scheme 6.11: Coupling reaction of NBD with hydroxyl group unprotected.

In this case, the reaction seems to be slower and presented a lower yield than the previous one (31%), so in this particular case, it would be better to do the fluorophore coupling before the deprotection reaction.

In order to obtain the proposed qABP, a click reaction between **6.14** and Cyanine 5 (Cy5) azide **6.19** was performed using the conditions presented in Scheme 6.12.

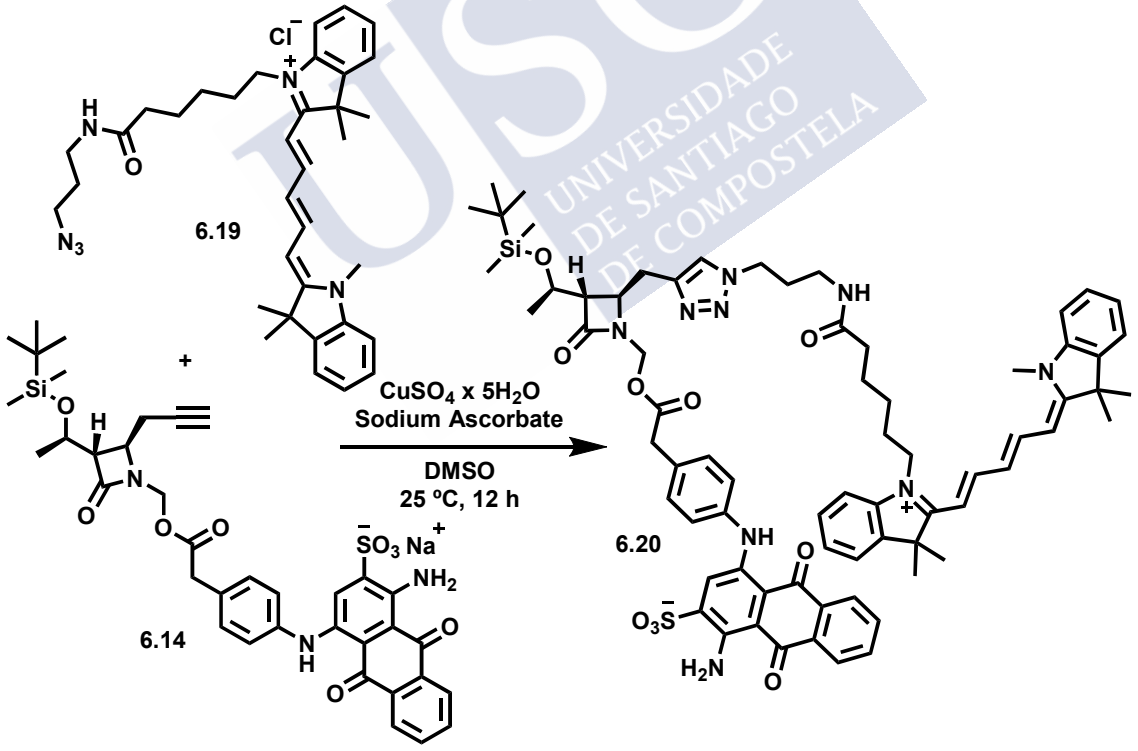

Scheme 6.12: Coupling reaction of Cy5.

This reaction was successful. The results coming from the NMR spectroscopy indicated that the product could have been obtained and this was confirmed by MS. Since the purification of the product was not completed, it was not possible to calculate

the yield. The purification and optimization of the reaction will be carried out in future projects.

6.3.3 Deprotection reaction

Considering the biological importance of the hydroxyl group, it is a crucial part of this work to optimize the deprotection step. The optimization was performed with compound **6.13** since it is easier to handle (Scheme 6.13). The optimization conditions are presented in Table 6.4.

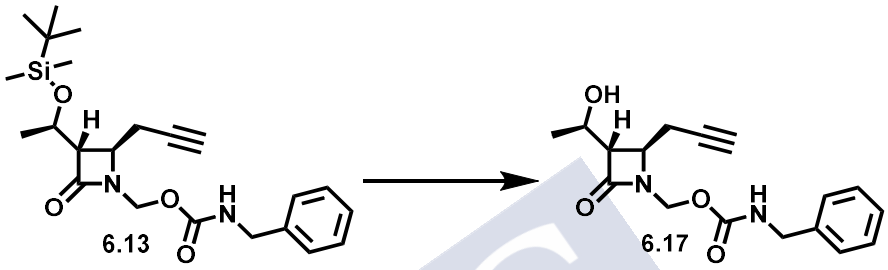

Scheme 6.13: Deprotection tests.

Table 6.4: Synthetic optimization for the deprotection reaction.

Entry	Acid	Base	Solvent	T (ºC)	Time (h)	Yield (%)
1[a]	$TiCl_4$/AcOET 1:1 (2.4 equiv)	-	CH_2Cl_2	0	4	0
2	HCl (1M) (1.2 equiv)	-	CH_3CN	25	1	0
3[a]	AcOH (10 equiv)	TBAF (1M) (3.5 equiv)	THF	25	48	43
4[a]	AcOH (40 equiv)	TBAF (1M) (14 equiv)	THF	25	72	76

[a]Under inert atmosphere.

To the optimization of this reaction, several procedures of the literature were tested and adapted. Although all the starting compound was consumed in entries 1 and 2, the product obtained was the resulting of the quencher moiety elimination. Therefore, a different approach was used by adapting a method of patent CA 0243207674 where is described that a fluorinated base, in this case, tetra-*N*-butylammonium fluoride (TBAF), is necessary to displace tert-butyldimethylsilyl group.[76] The reaction was not completed in entry 3, but the product was successfully isolated with a yield of 43%.

Besides, to improve the efficiency of the reaction, acid and base equivalents were increased 4-fold, obtaining the complete reaction after 3 days with a yield of 76%.

In order to understand if the deprotection step needs to be preferentially performed at a specific point of the synthetic route, compounds **6.5** and **6.17** were also deprotected. (Scheme 6.14 and Scheme 6.15)

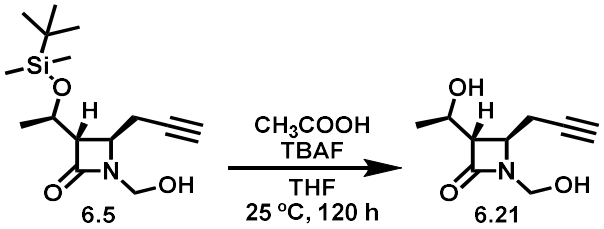

Scheme 6.14: Deprotection of compound **6.5**.

In the particular case of this reaction, it was understood that probably the reaction time could be important since the yield of this reaction (21%) is almost 4-fold lower than the previous one. This fact might be due to the lower stability of compound **6.21**, which may decompose in solution over time.

Further optimizations of this synthetic step and the following route reactions will be carried out in the future to corroborate whether this change will improve the whole synthetic route yield.

Finally, compound **6.16**, with NBD fluorophore, was successfully deprotected with the optimized condition of Table 6.4 with a promising yield (82%).

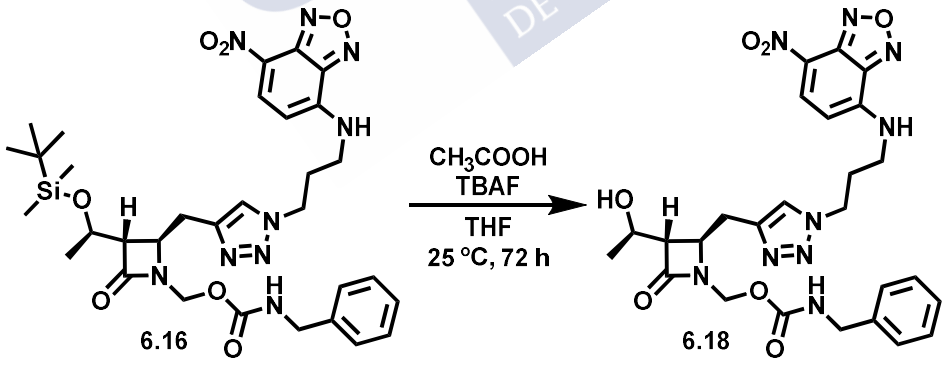

Scheme 6.15: Deprotection of compound **6.16**.

6.4 CONCLUSIONS AND FUTURE PERSPECTIVES

This work has been developed in a three-months research stay; from September 10 to December 21, 2018. During that period, a novel and promising synthetic route of proteasome qABPs has been developed to better understand how the UPP works and where exactly it is located.

This synthetic route consists in five synthetic steps with the aid of click chemistry to accelerate these processes. Several steps were optimized in this work, obtaining considerable route yield. Future studies will reveal whether the deprotected and click reactions could be altered in order to increase the overall synthetic route yield.

Two main compounds, **6.18** and **6.20**, were obtained during this period. Compound **6.18** has been developed as a proof of the synthetic concept and could be tested as a potential proteasome fluorescent probe. Nonetheless, compound **6.20**, requires further purifications. Moreover, it also needs to be unprotected and will be tested as the first proteasome quenched activity-based probe so far.

Furthermore, it is relevant to remark that, although only two compounds were synthesized, this route could be considered an excellent starting point to develop several qABPs, not only to upgrade our understanding of the UPP, but also to enhance the knowledge of other targets.

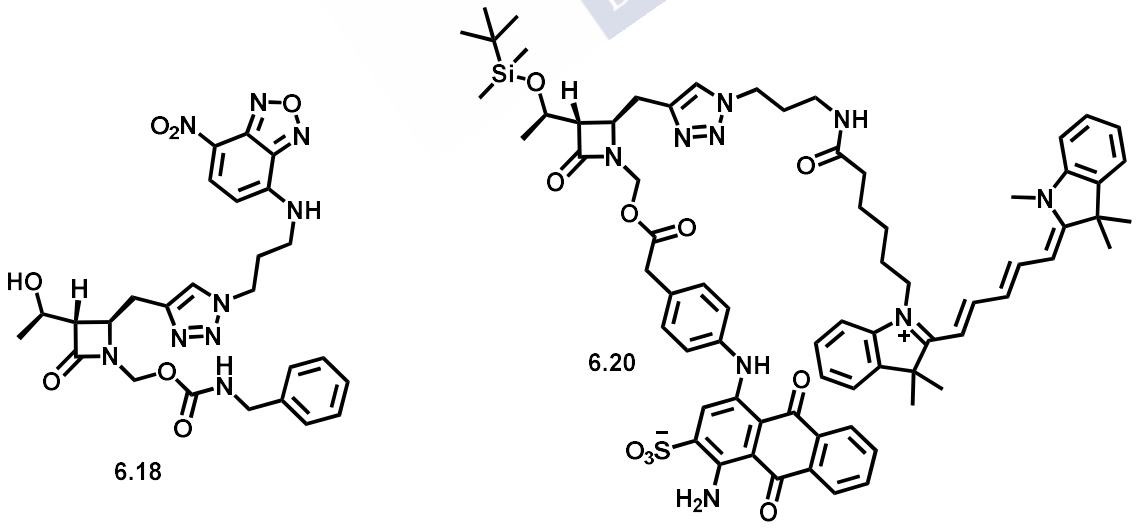

Figure 6.7: The most promising compounds of this research stay.

6.5 EXPERIMENTAL PART

6.5.1 General considerations

Commercially available starting materials, reagents and solvents were purchased from Sigma-Aldrich/Merck, Fluorochem or Lumiprobe, and used without further purification.

Solvents were previously dried before used and moisture sensitive reactions were performed under an inert atmosphere using nitrogen gas.

The reactions were monitored by thin-layer chromatography (TLC) with 2.5 mm Merck aluminum backed sheets coated with 60 F254 silica gel and/or Merck aluminum backed sheets coated with 60 RP-18 F254S, and the purified compounds each showed a single spot; unless stated otherwise, UV light and/or potassium permanganate acid solution were used for detection of compounds.

LRMS and NMR spectra are described below. The NMR spectra were recorded on Bruker Avance 300 spectrometer. Chemical shifts are given as δ and *J* values are given in Hz with the following splitting abbreviations: s = singlet, bs = broad singlet, d = doublet, dd = doublet of doublets, qd = quartet of doublets, ddd = doublet of doublet of doublets, td = triplet of doublets, t = triplet, dt = doublet of triplets, q = quartet, m = multiplet. Low-resolution mass spectra were obtained on a Micromass Quattro Micro API mass spectrometer, using electrospray ionization. A detailed description of synthetic methodologies as well as analytical and spectroscopic data for all described compounds is described below.

6.5.2 Chemistry

Synthesis of (3*S*,4*R*) 3-((*R*)-1-((*tert*-butyldimethylsilyl)oxy)ethyl)-4-(prop-2-yn-1-yl)azetidin-2-one (6.3):

3-Bromoprop-1-yne **6.2** (5.46 mmol, 3 equiv), indium powder (3.64 mmol, 2 equiv) and anhydrous potassium iodide (5.46 mmol, 3 equiv) in DMF (0.26 M, 7 ml) were added in a reaction flask under inert atmosphere and the reaction was stirred during 1 h at 30 ºC. Compound **6.1** (1.82 mmol, 1 equiv) was added to the reaction mixture and it was stirred for 3 h. Saturated ammonium chloride solution (20 ml) was added to the reaction mixture and extracted with EtOAc (6 × 20 ml). The organic layer was washed with brine (4 × 20 ml), dried over anhydrous Na_2SO_4, filtered and concentrated under

reduced pressure. The obtained residue was purified by flash chromatography using EtOAc/Hex (starting with EtOAc/Hex 1:8 and ending with 1:5) to yield a white solid (341 mg, 73%).

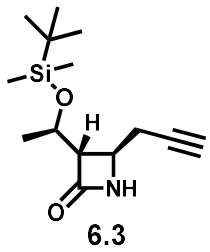

6.3

^{1}H-NMR (300 MHz, $CDCl_3$) δ (ppm): 6.03 (bs, 1H), 4.20 (qd, *J* = 6.3, 4.5 Hz, 1H), 3.85 (td, *J* = 6.2, 2.2 Hz, 1H), 2.90 (ddd, *J* = 4.4, 2.2, 0.9 Hz, 1H), 2.62 – 2.43 (m, 2H), 2.05 (t, *J* = 2.6 Hz, 1H), 1.23 (d, *J* = 6.2 Hz, 3H), 0.87 (s, 9H), 0.07 (s, 3H), 0.07 (s, 3H). ^{13}C-NMR (75 MHz, $CDCl_3$) δ (ppm):168.0, 79.6,70.9, 65.0, 63.9, 48.8, 25.7, 24.6, 22.6, 17.9, -4.3, -5.1. LRMS (ESI) *m/z* calcd. for $C_{14}H_{26}NO_2Si$ $[M+H]^+$: 268.2 found: 268.3.

Synthesis of (3*S*,4*R*) 3-((*R*)-1-((tert-butyldimethylsilyl)oxy)ethyl)-1-(hydroxy-methyl)-4-(prop-2-yn-1-yl)azetidin-2-one (6.5):

A solution of **6.3** (0.04 mmol, 1 equiv), 35% aqueous formaldehyde (0.15 mmol, 3.75 equiv) and potassium carbonate (0.02 mmol, 0.5 equiv) in ethanol (0.01 M, 4 ml) was stirred under reflux for 1 h. Then, the reaction was stirred overnight at room temperature. The reaction mixture was filtered, and the filtrate was concentrated under reduced pressure. CH_2Cl_2 (20 ml) was added to the resulting residue, washed with brine (2 × 20 ml), dried over anhydrous Na_2SO_4, filtered and concentrated *in vacuo*. The obtained residue was purified by flash chromatography using EtOAc/Hex (starting with EtOAc/Hex 1:7 and ending with 2:1) to yield a white solid (203.4 mg, 91%).

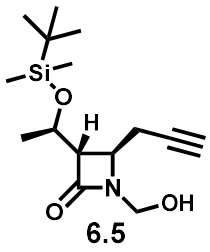

6.5

^{1}H-NMR (300 MHz, $CDCl_3$) δ (ppm): 4.75 (d, *J* = 11.6 Hz, 1H), 4.64 (d, *J* = 11.6 Hz, 1H), 4.19 (qd, *J* = 6.2, 4.4 Hz, 1H), 3.93 (td, *J* = 5.5, 2.2 Hz, 1H), 2.94 (dd, *J* = 4.4, 2.2 Hz, 1H), 2.63 (dd, *J* = 5.6, 2.6 Hz, 2H), 2.08 (t, *J* = 2.6 Hz, 1H), 1.21 (d, *J* = 6.3 Hz, 3H), 0.85 (s, 9H), 0.06 (s, 3H), 0.04 (s, 3H). ^{13}C-NMR (75 MHz, $CDCl_3$) δ (ppm): 167.7, 79.9, 71.4, 65.1, 64.2, 63.1, 52.1, 25.8, 23.1, 22.8, 18.0, -4.2, -4.9. LRMS (ESI) *m/z* calcd. for $C_{15}H_{28}NO_3Si$ $[M+H]^+$: 298.2 found: 298.

Synthesis of cAB40, sodium 1-amino-4-((4-(carboxymethyl)phenyl)amino)-9,10-dioxo-9,10-dihydroanthracene-2-sulfonate (6.11):

A solution of bromaminic acid sodium salt **6.9** (1.12 mmol, 1.12 equiv), 2-(4-aminophenyl)acetic acid **6.10** (1 mmol, 1 equiv), copper (II) sulfate pentahydrate (0.16 mmol, 0.16 equiv) and sodium carbonate (1.44 mmol, 1.44 equiv) in water (0.02 M, 50 ml) was stirred under reflux for 24 h. While the reaction was going on, it was possible to observe a color change from red to purple/dark blue. The reaction mixture was washed with CH_2Cl_2 (3 × 50 ml) and the aqueous layer was evaporated under reduced pressure. The resulting dark solid was dissolved in methanol, filtered and the methanol solution was evaporated *in vacuo*. The obtained residue was purified by reverse-phase column chromatography using only 3% acetonitrile/water to yield a dark blue solid (219 mg, 30%).

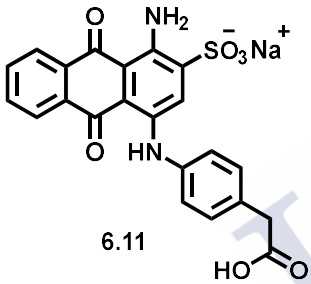

6.11

^{1}H-NMR (300 MHz, DMSO-d_6) δ (ppm): 12.14 (s, 1H), 10.16 (bs, 1H), 8.34 – 8.20 (m, 2H), 7.99 (s, 1H), 7.91 – 7.78 (m, 2H), 7.48 (bs, 1H), 7.31 (d, J = 8.3 Hz, 2H), 7.14 (d, J = 8.3 Hz, 2H), 3.27 (s, 2H). ^{13}C-NMR (75 MHz, DMSO-d_6) δ (ppm): 182.0, 181.7, 144.2, 142.9, 141.7, 136.7, 135.9, 134.1, 133.6, 133.0, 132.7, 130.4, 126.0, 125.9, 122.9, 122.6, 110.7, 109.0, 52.6. LRMS (ESI) *m/z* calcd. for $C_{22}H_{15}N_2O_7S^-$ [M-Na]$^-$: 451.1 found: 451.1.

Synthesis of (3*S*,4*R*) (3-((*R*)-1-((tert-butyldimethylsilyl)oxy)ethyl)-2-oxo-4-(prop-2-yn-1-yl)azetidin-1-yl)methyl benzylcarbamate (6.13):

To a solution of **6.5** (0.01 mmol, 1 equiv), TEA (0,005 mmol, 0.5 equiv) in dry CH_2Cl_2 (0.2 M, 0.5 ml), benzyl isocyanate (0.02 mmol, 2.2 equiv) was added and the reaction was stirred at room temperature under inert atmosphere for 1.5 h. The reaction mixture was concentrated under reduced pressure and was purified by flash chromatography using EtOAc/Hex (starting with EtOAc/Hex 1:5 and ending with 1:3) to yield a yellow oil (117 mg, 70%).

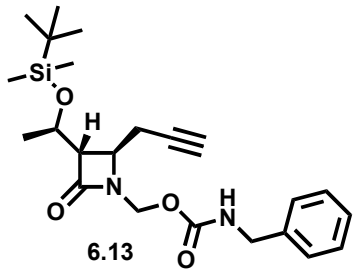

6.13

^{1}H-NMR (300 MHz, $CDCl_3$) δ (ppm): 7.34 – 7.17 (m, 5H), 5.13-5.02 (m, 3H), 4.43 – 4.09 (m, 3H), 3.95 (dt, *J* = 5.3, 3.7 Hz, 1H), 3.04 – 2.99 (m, 1H), 2.67 (qdd, *J* = 17.3, 5.3, 2.7 Hz, 2H), 1.96 (t, *J* = 2.7 Hz, 1H), 1.15 (d, *J* = 6.3 Hz, 3H), 0.80 (s, 9H), 0.01 (s, 3H), 0.00 (s, 3H).

Synthesis of (3*S*,4*R*) sodium 1-amino-4-((4-(2-((3-((*R*) -1-((tert-butyldimethylsilyl)oxy)ethyl)-2-oxo-4-(prop-2-yn-1-yl)azetidin-1-yl)methoxy)-2-oxoethyl)phenyl)amino)-9,10-dioxo-9,10-dihydroanthracene- 2-sulfonate (6.14):

To a solution of cAB40 **6.11** (0.067 mmol, 1 equiv), TBTU (0.146 mmol, 2.2 equiv), HOBt (0.08 mmol, 1.2 equiv) and DIPEA (0.27 mmol, 4 equiv) in dry DMF (0.1 M, 0.665 ml), compound **6.5** (0.067 mmol, 1 equiv) was added under inert atmosphere at 0 ºC. The reaction was stirred for 1 h at 0 ºC and room temperature overnight. The mixture was evaporated *in vacuo* and purified by flash reverse-phase column chromatography using acetone/water (starting with acetone/water 5% and ending with 80%) to yield a dark blue solid (32 mg, 65%).

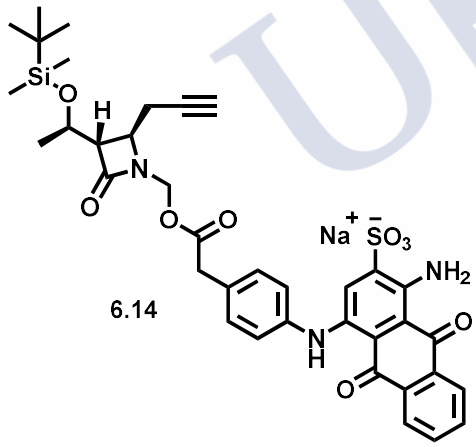

6.14

The resulting product was not completely purified, so the ^{1}H-NMR was not conclusive. LRMS (ESI) *m/z* calcd. for $C_{37}H_{40}N_3O_9SSi^-$ $[M-Na]^-$: 730.2 found: 730.

Synthesis of (2*R*,3*S*) (3-((*R*)-1-((tert-butyldimethylsilyl)oxy)ethyl)-2-((1-(3-((7-nitrobenzo[*c*][1,2,5]oxadiazol-4-yl)amino)propyl)-1*H*-1,2,3-triazol-4-yl)methyl)-4-oxoazetidin-1-yl)methyl benzylcarbamate (6.16):

A solution of **6.13** (0.07 mmol, 1 equiv), copper (II) sulfate aqueous solution (0.077 ml, 0.1 M, 0.11 equiv) and sodium ascorbate aqueous solution (0.084 ml, 0.2 M, 0.24 equiv) in DMSO (0.14 M, 0.5 ml) was stirred for 10 min. Then, nitrobenzoxadiazole (NBD) azide **6.15** (0.077 mmol, 1.1 equiv) was added and the reaction was stirred at room temperature for 2 h. The reaction mixture was diluted with water (10 ml) and

extracted with EtOAc (3 × 10 ml). The organic layer was concentrated under reduced pressure. The obtained residue was purified by flash chromatography using EtOAc/Hex (starting with of EtOAc/Hex 4:1 and ending with 6:1) to yield an orange solid (28 mg, 59%).

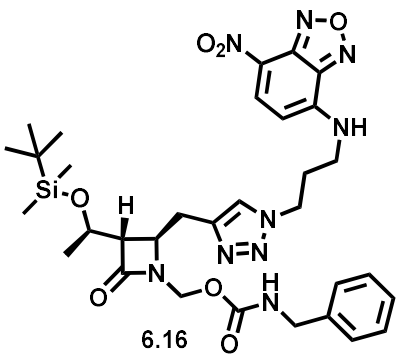

6.16

^{1}H-NMR (300 MHz, $CDCl_3$) δ (ppm): 8.42 (d, *J* = 8.7 Hz, 1H), 7.47 (s, 1H), 7.33 – 7.19 (m, 5H), 7.13 (s, 1H), 6.13 (d, *J* = 8.7 Hz, 1H), 5.33 – 5.24 (m, 1H), 5.12 (s, 2H), 4.53 – 4.40 (m, 2H), 4.34 (dd, *J* = 17.3, 6.0 Hz, 2H), 4.23 – 4.10 (m, 2H), 3.57 – 3.42 (m, 2H), 3.30 – 3.12 (m, 2H), 2.99 – 2.91 (m, 1H), 2.45-2.26 (m, 2H), 1.02 (d, *J* = 6.3 Hz, 3H), 0.84 (s, 9H), 0.04 (s, 3H), 0.03 (s, 3H). ^{13}C-NMR (75 MHz, $CDCl_3$) δ (ppm): 168.7, 156.3, 144.4, 144.0, 143.5, 140.6, 138.0, 136.6, 130.1, 128.8, 127.7, 127.3, 124.0, 99.0, 64.9, 63.9, 62.7, 53.6, 47.3, 45.1, 40.8, 28.9, 28.5, 25.8, 22.4, 18.0, -4.2, -5.0. LRMS (ESI) *m/z* calcd. for $C_{32}H_{42}N_9O_7Si$ $[M-H]^-$: 692.3 found: 693.

Synthesis of (3*S*,4*R*) (3-((*R*)-1-hydroxyethyl)-2-oxo-4-(prop-2-yn-1-yl)azetidin-1-yl)methyl benzylcarbamate (6.17):

To a solution of **6.13** (0.13 mmol, 1 eqUIV) in THF (0.25 M, 0.516 ml), acetic acid (5,16 mmol, 40 equiv) was added dropwise. Then, a solution of TBAF in THF (1.81 ml, 1 M, 14 equiv) was also added dropwise and stirred under inert atmosphere for 72 h. The reaction was diluted in EtOAc (10 ml) and cold saturated sodium hydrogen carbonated solution (10 ml) was added. The mixture was extracted with EtOAc (3 × 10 ml) and the organic layer was washed with brine (2 × 10 ml), dried over anhydrous Na_2SO_4, filtered and concentrated under reduced pressure. The obtained residue was purified by flash chromatography using EtOAc/Hex (starting with EtOAc/Hex 1:4 and ending with 1:1) to yield a yellow oil (31 mg, 76%).

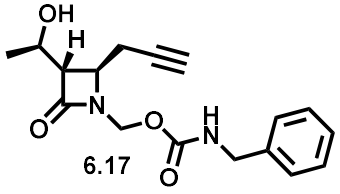

6.17

^{1}H-NMR (300 MHz, $CDCl_3$) δ (ppm): 7.39 – 7.24 (m, 5H), 5.45 (t, *J* = 5.8 Hz, 1H), 5.18 (d, *J* = 11.6 Hz, 1H), 5.10 (d, *J* = 11.6 Hz, 1H), 4.40 – 4.29 (m, 2H), 4.25 – 4.15 (m, 1H), 3.97 (td, *J* = 5.0, 2.4 Hz, 1H), 3.11 (dd, *J* = 5.0, 2.5 Hz, 1H), 2.81 – 2.63 (m, 2H), 2.04 (t, *J* = 2.5 Hz, 1H), 1.29 (d, *J* = 6.4 Hz, 3H). ^{13}C-NMR (75 MHz, $CDCl_3$) δ (ppm):168.4,

156.2, 138.2, 128.8, 127.7, 127.6, 78.8, 71.7, 64.5, 63.4, 62.4, 52.7, 45.1, 22.0, 21.6.

Synthesis of (2*R*,3*S*) (3-((*R*)-1-hydroxyethyl)-2-((1-(3-((7-nitrobenzo[*c*][1,2,5]-oxadiazol-4-yl)amino)propyl)-1*H*-1,2,3-triazol-4-yl)methyl)-4-oxoazetidin-1-yl)methyl benzylcarbamate (6.18):

From **Scheme 6.11**: A solution of **6.17** (0.015 mmol, 1 equiv), copper (II) sulfate aqueous solution (0.037 ml, 0.1 M, 0.24 equiv) and sodium ascorbate aqueous solution (0.037 ml, 0.2 M, 0.48 equiv) in DMSO (0.14 M, 0.11 ml) was stirred for 10 min. Then, nitrobenzoxadiazole (NBD) azide **6.15** (0.017 mmol, 1.1 equiv) was added and the reaction was stirred at room temperature overnight. The reaction mixture was diluted with water (10 ml) and extracted with EtOAc (3 × 10 ml). The organic layer was concentrated under reduced pressure. The obtained residue was purified by flash chromatography using EtOAc/Hex (starting with EtOAc/Hex 7:1 and ending with 10:1) to yield an orange solid (2.8 mg, 31%).

From **Scheme 6.15**: To a solution of **6.16** (0.01 mmol, 1 equiv) in THF (0.25 M, 0.04 ml), acetic acid (0.4 mmol, 40 equiv) was added dropwise. Then, a solution of TBAF in THF (0.14 ml, 1 M, 14 equiv) was also added dropwise and stirred under inert atmosphere for 72 h. The reaction was diluted in EtOAc (10 ml) and cold saturated sodium hydrogen carbonated solution (10 ml) was added. The mixture was extracted with EtOAc (3 × 10 ml) and the organic layer was washed with brine (2 × 10 ml), dried over anhydrous Na_2SO_4, filtered and concentrated under reduced pressure. The obtained residue was purified by flash chromatography using EtOAc/Hex 12:1 to yield an orange solid (4.6 mg, 82%).

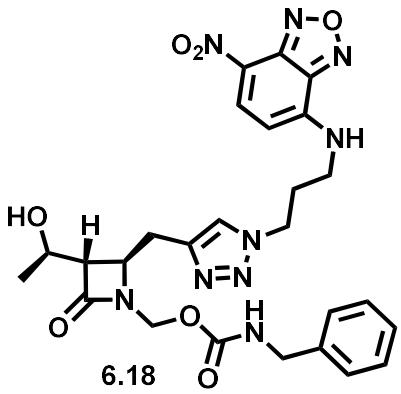

6.18

^{1}H-NMR (300 MHz, $(CD_3)_2CO$) δ (ppm): 8.52 (d, *J* = 8.8 Hz, 1H), 8.29 (bs, 1H), 7.91 (s, 1H), 7.33 – 7.16 (m, 5H), 6.93 (bs, 1H), 6.43 (d, *J* = 8.8 Hz, 1H), 5.17 (d, *J* = 11.5 Hz, 1H), 5.09 (d, *J* = 11.5 Hz, 1H) , 4.62 (t, *J* = 6.8 Hz, 2H), 4.41 – 4.27 (m, 2H), 4.09 – 3.92 (m, 2H), 3.77 – 3.65 (m, 2H), 3.37 – 3.26 (m, 1H), 3.06 – 2.91 (m, 2H), 2.46 (p, *J* = 6.8 Hz, 2H), 1.11 (d, *J* = 6.3 Hz, 3H). LRMS (ESI) *m/z* calcd. for $C_{26}H_{28}N_9O_7$ $[M-H]^-$: 578.2 found: 578.3.

Synthesis of 1-amino-4-((4-(2-(((2*R*,3*S*)-3-((*R*)-1-((tert-butyldimethylsilyl)oxy)-ethyl)-2-((1-(3-(6-(3,3-dimethyl-2-((1*E*,3*E*)-5-((*Z*)-1,3,3-trimethylindolin-2-ylidene)-penta-1,3-dien-1-yl)-3*H*-indol-1-ium-1-yl)hexanamido)propyl)-1*H*-1,2,3-triazol-4-yl)methyl)-4-oxoazetidin-1-yl)methoxy)-2-oxoethyl)phenyl)amino)-9,10-dioxo-9,10-dihydroanthracene-2-sulfonate (6.20):

A solution of compound **6.14** (0.015 mmol, 1 equiv), copper (II) sulfate aqueous solution (0.037 ml, 0.1 M, 0.24 equiv) and sodium ascorbate aqueous solution (0.037 ml, 0.2 M, 0.48 equiv) in DMSO (0.14 M, 0.11 ml) was stirred for 10 min. Then, Cyanine 5 azide **6.19** (0.016 mmol, 1.1 equiv) was added and the reaction was stirred at room temperature overnight. The reaction mixture was filtered through reverse-phase silica and concentrated under reduced pressure. The obtained residue was purified by preparative thin layer chromatography using 5:1 methanol/EtOAc.

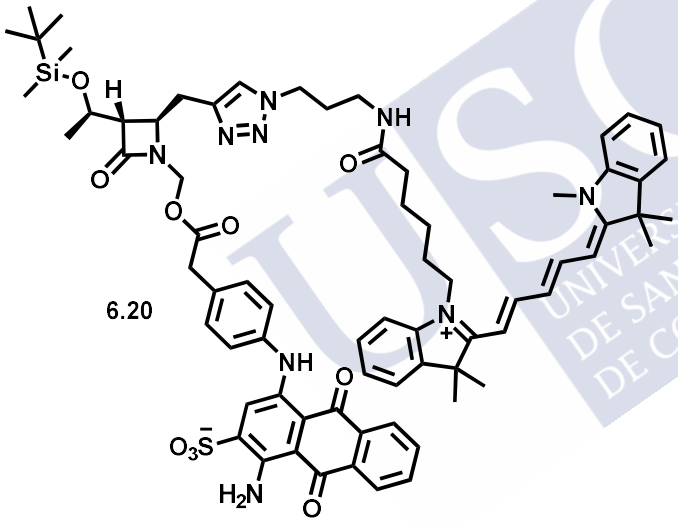

6.20

The resulting product was not completely purified so, the ^{1}H-NMR was not conclusive. LRMS (ESI) *m/z* calcd. for $C_{72}H_{86}N_9O_{10}SSi$ [M-H]$^-$: 1294.6 found: 1296.2.

Synthesis of (3*S*,4*R*) 3-((*R*)-1-hydroxyethyl)-1-(hydroxymethyl)-4-(prop-2-yn-1-yl)azetidin-2-one (6.21):

To a solution of protected compound **6.5** (0.067 mmol, 1 equiv) in THF (0.25 M, 0.268 ml), acetic acid (2.68 mmol, 40 equiv) was added dropwise. Then, a solution of TBAF in THF (0.94 ml, 1 M, 14 equiv) was also added dropwise and stirred under inert atmosphere for 120 h. The reaction was diluted in EtOAc (10 ml) and cold saturated sodium hydrogen carbonated solution (10 ml) was added. The mixture was extracted with EtOAc (3 × 10 ml) and the organic layer was washed with brine (2 × 10 ml), dried over anhydrous Na_2SO_4, filtered and concentrated under reduced pressure. The obtained

residue was purified by flash chromatography using EtOAc/hex (starting with EtOAc/Hex 1:3 and ending with 2:1) to yield a yellow oil (3 mg, 21%).

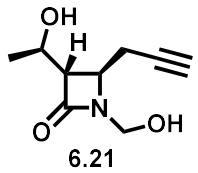

6.21

^{1}H-NMR (300 MHz, $CDCl_3$) δ (ppm): 4.94 (d, *J* = 11.6 Hz, 1H), 4.46 (d, *J* = 11.6 Hz, 1H), 4.35 – 4.18 (m, 1H), 4.08 (td, *J* = 5.6, 2.2 Hz, 1H), 3.42 (bs, 1H), 3.07 – 2.98 (m, 1H), 2.60 (ddd, *J* = 21.0, 5.6, 2.7 Hz, 2H), 2.08 (t, *J* = 2.7 Hz, 1H), 1.29 (d, *J* = 6.5 Hz, 3H).

6.6 REFERENCES

(1) Jones, C. L.; Njomen, E.; Sjögren, B.; Dexheimer, T. S.; Tepe, J. J. Small Molecule Enhancement of 20S Proteasome Activity Targets Intrinsically Disordered Proteins. *ACS Chem. Biol.* **2017**, *12* (9), 2240–2247.

(2) Crawford, L. J.; Walker, B.; Irvine, A. E. Proteasome Inhibitors in Cancer Therapy. *J. Cell Commun. Signal.* **2011**, *5* (2), 101–110.

(3) Abramson, H. N. The Multiple Myeloma Drug Pipeline—2018: A Review of Small Molecules and Their Therapeutic Targets. *Clin. Lymphoma Myeloma Leuk.* **2018**, *18* (9), 611–627.

(4) Nandi, D.; Tahiliani, P.; Kumar, A.; Chandu, D. The Ubiquitin-Proteasome System. *J. Biosci.* **2006**, *31* (1), 137–155.

(5) Nagy, V.; Dikic, I. Ubiquitin Ligase Complexes: From Substrate Selectivity to Conjugational Specificity. *Biol Chem*. **2010**, *391*, 163–169.

(6) Kwon, Y. T.; Ciechanover, A. The Ubiquitin Code in the Ubiquitin-Proteasome System and Autophagy. *Trends Biochem. Sci.* **2017**, *42* (11), 873–886.

(7) Ciechanover, A. The Ubiquitin Proteolytic System: From a Vague Idea, through Basic Mechanisms, and onto Human Diseases and Drug Targeting. *Neurology*; **2006**, *66* (1 suppl 1), S7–S19.

(8) Ogorevc, E.; Schiffrer, E. S.; Sosič, I.; Gobec, S. A Patent Review of Immunoproteasome Inhibitors. *Expert Opin. Ther. Pat.* **2018**, *28* (7), 517–540.

(9) Sharon, M.; Taverner, T.; Ambroggio, X. I.; Deshaies, R. J.; Robinson, C. V. Structural Organization of the 19S Proteasome Lid: Insights from MS of Intact Complexes. *PLoS Biol.* **2006**, *4* (8), e267.

(10) Mofers, A.; Pellegrini, P.; Linder, S.; D'Arcy, P. Proteasome-Associated Deubiquitinases and Cancer. *Cancer Metastasis Rev.* **2017**, *36* (4), 635–653.

(11) Seo, H. D.; Choi, Y.; Kim, M.; Kang, K.; Urano, T.; Lee, D. The 19S Proteasome Is Directly Involved in the Regulation of Heterochromatin Spreading in Fission Yeast. *J. Biol. Chem.* **2017**, *292* (41), 17144–17155.

(12) Jung, T.; Grune, T. The Proteasome and the Degradation of Oxidized Proteins: Part I—Structure of Proteasomes. *Redox Biol.* **2013**, *1* (1), 178–182.

(13) Budenholzer, L.; Cheng, C. L.; Li, Y.; Hochstrasser, M. Proteasome Structure and Assembly. *J. Mol. Biol.* **2017**, *429* (22), 3500–3524.

(14) Harshbarger, W.; Miller, C.; Diedrich, C.; Sacchettini, J. Crystal Structure of the Human 20S Proteasome in Complex with Carfilzomib. *Structure* **2015**, *23* (2), 418–424.

(15) Huber, E. M.; Basler, M.; Schwab, R.; Heinemeyer, W.; Kirk, C. J.; Groettrup, M.; Groll, M. Immuno- and Constitutive Proteasome Crystal Structures Reveal Differences in Substrate and Inhibitor Specificity. *Cell* **2012**, *148* (4), 727–738.

(16) Rivett, A. J.; Hearn, A. R. Proteasome Function in Antigen Presentation: Immunoproteasome Complexes, Peptide Production, and Interactions with Viral Proteins. *Curr. Protein Pept. Sci.* **2004**, *5* (3), 153–161.

(17) Borissenko, L.; Groll, M. 20S Proteasome and Its Inhibitors: Crystallographic Knowledge for Drug Development. *Chem Rev*. **2007**, *107*, 687–717.

(18) Vigneron, N.; Stroobant, V.; Ferrari, V.; Abi Habib, J.; Van den Eynde, B. J. Production of Spliced Peptides by the Proteasome. *Mol. Immunol.* **2018**, *113*, 93-102.

(19) Löwe, J.; Stock, D.; Jap, B.; Zwickl, P.; Baumeister, W.; Huber, R. Crystal Structure of the 20S Proteasome from the Archaeon T. Acidophilum at 3.4 A Resolution. *Science* **1995**, *268* (5210), 533–539.

(20) Guedes, R.; Serra, P.; Salvador, J.; Guedes, R. Computational Approaches for the Discovery of Human Proteasome Inhibitors: An Overview. *Molecules* **2016**, *21* (7), 927.

(21) Groll, M.; Bochtler, M.; Brandstetter, H.; Clausen, T.; Huber, R. Molecular Machines for Protein Degradation. *ChemBioChem* **2005**, *6* (2), 222–256.

(22) Besse, A.; Besse, L.; Kraus, M.; Mendez-Lopez, M.; Bader, J.; Xin, B.-T.; de Bruin, G.; Maurits, E.; Overkleeft, H. S.; Driessen, C. Proteasome Inhibition in Multiple Myeloma: Head-to-Head Comparison of Currently Available Proteasome Inhibitors. *Cell Chem. Biol.* **2019**, *26* (3), 340-351.

(23) Kisselev, A. F.; van der Linden, W. A.; Overkleeft, H. S. Proteasome Inhibitors: An Expanding Army Attacking a Unique Target. *Chem. Biol.* **2012**, *19* (1), 99–115.

(24) Moura, D. M. N.; de Melo Neto, O. P.; Carrington, M. A New Reporter Cell Line for Studies with Proteasome Inhibitors in Trypanosoma Brucei. *Mol. Biochem. Parasitol.* **2019**, *227*, 15–18.

(25) Li, H.; O'Donoghue, A. J.; van der Linden, W. A.; Xie, S. C.; Yoo, E.; Foe, I. T.; Tilley, L.; Craik, C. S.; da Fonseca, P. C. A.; Bogyo, M. Structure- and Function-Based Design of Plasmodium-Selective Proteasome Inhibitors. *Nature* **2016**, *530* (7589), 233–236.

(26) Kaffy, J.; Bernadat, G.; Ongeri, S. Non-Covalent Proteasome Inhibitors. *Curr. Pharm. Des.* **2013**, *19* (22), 4115–4130.

(27) Hines, J.; Groll, M.; Fahnestock, M.; Crews, C. M. Proteasome Inhibition by Fellutamide B Induces Nerve Growth Factor Synthesis. *Chem. Biol.* **2008**, *15* (5), 501–512.

(28) Micale, N.; Scarbaci, K.; Troiano, V.; Ettari, R.; Grasso, S.; Zappalà, M. Peptide-Based Proteasome Inhibitors in Anticancer Drug Design. *Med. Res. Rev.* **2014**, *34* (5), 1001–1069.

(29) Anshu, A.; Thomas, S.; Agarwal, P.; Ibarra-Rivera, T. R.; Pirrung, M. C.; Schönthal, A. H. Novel Proteasome-Inhibitory Syrbactin x Inducing Endoplasmic Reticulum Stress and Apoptosis in Hematological Tumor Cell Lines. *Biochem. Pharmacol.* **2011**, *82* (6), 600–609.

(30) Groll, M.; Schellenberg, B.; Bachmann, A. S.; Archer, C. R.; Huber, R.; Powell, T. K.; Lindow, S.; Kaiser, M.; Dudler, R. A Plant Pathogen Virulence Factor

Inhibits the Eukaryotic Proteasome by a Novel Mechanism. *Nature* **2008**, *452* (7188), 755–758.

(31) Groll, M.; Kim, K. B.; Kairies, N.; Huber, R.; Crews, C. M. Crystal Structure of Epoxomicin:20S Proteasome Reveals a Molecular Basis for Selectivity of α',β'-Epoxyketone Proteasome Inhibitors. *J Am Chem Soc*. **2000**, *122* (6), 1237–1238.

(32) Park, J. E.; Miller, Z.; Jun, Y.; Lee, W.; Kim, K. B. Next-Generation Proteasome Inhibitors for Cancer Therapy. *Transl. Res.* **2018**, *198*, 1–16.

(33) Gräwert, M. A.; Gallastegui, N.; Stein, M.; Schmidt, B.; Kloetzel, P.-M.; Huber, R.; Groll, M. Elucidation of the α-Keto-Aldehyde Binding Mechanism: A Lead Structure Motif for Proteasome Inhibition. *Angew. Chemie Int. Ed.* **2011**, *50* (2), 542–544.

(34) de Bettignies, G.; Coux, O. Proteasome Inhibitors: Dozens of Molecules and Still Counting. *Biochimie* **2010**, *92* (11), 1530–1545.

(35) Adams, J.; Kauffman, M. Development of the Proteasome Inhibitor Velcade™ (Bortezomib). *Cancer Invest.* **2004**, *22* (2), 304–311.

(36) Hideshima, T.; Chauhan, D.; Richardson, P.; Mitsiades, C.; Mitsiades, N.; Hayashi, T.; Munshi, N.; Dang, L.; Castro, A.; Palombella, V.; et al. NF-KB as a Therapeutic Target in Multiple Myeloma. *J. Biol. Chem.* **2002**, *277* (19), 16639–16647.

(37) Kubiczkova, L.; Pour, L.; Sedlarikova, L.; Hajek, R.; Sevcikova, S. Proteasome Inhibitors - Molecular Basis and Current Perspectives in Multiple Myeloma. *J. Cell. Mol. Med.* **2014**, *18* (6), 947–961.

(38) Ling, Y.-H.; Liebes, L.; Jiang, J.-D.; Holland, J. F.; Elliott, P. J.; Adams, J.; Muggia, F. M.; Perez-Soler, R. Mechanisms of Proteasome Inhibitor PS-341-Induced G(2)-M-Phase Arrest and Apoptosis in Human Non-Small Cell Lung Cancer Cell Lines. *Clin. Cancer Res.* **2003**, *9* (3), 1145–1154.

(39) Roccaro, A. M.; Hideshima, T.; Raje, N.; Kumar, S.; Ishitsuka, K.; Yasui, H.; Shiraishi, N.; Ribatti, D.; Nico, B.; Vacca, A.; et al. Bortezomib Mediates Antiangiogenesis in Multiple Myeloma via Direct and Indirect Effects on Endothelial Cells. *Cancer Res.* **2006**, *66* (1), 184–191.

(40) Okazuka, K.; Ishida, T. Proteasome Inhibitors for Multiple Myeloma. *Jpn. J. Clin. Oncol.* **2018**, *48* (9), 785–793.

(41) Nunes, A. T.; Annunziata, C. M. Proteasome Inhibitors: Structure and Function. *Semin. Oncol.* **2017**, *44* (6), 377–380.

(42) Moore, B. S.; Eustáquio, A. S.; McGlinchey, R. P. Advances in and Applications of Proteasome Inhibitors. *Curr. Opin. Chem. Biol.* **2008**, *12* (4), 434–440.

(43) Gulder, T. A. M.; Moore, B. S. Salinosporamide Natural Products: Potent 20 S Proteasome Inhibitors as Promising Cancer Chemotherapeutics. *Angew. Chemie Int. Ed.* **2010**, *49* (49), 9346–9367.

(44) Allegra, A.; Alonci, A.; Gerace, D.; Russo, S.; Innao, V.; Calabrò, L.; Musolino, C. New Orally Active Proteasome Inhibitors in Multiple Myeloma. *Leuk. Res.* **2014**, *38* (1), 1–9.

(45) Stein, M. L.; Groll, M. Applied Techniques for Mining Natural Proteasome Inhibitors. *Biochim. Biophys. Acta - Mol. Cell Res.* **2014**, *1843* (1), 26–38.

(46) Groll, M.; C. Potts, B. Proteasome Structure, Function, and Lessons Learned from Beta-Lactone Inhibitors. *Curr. Top. Med. Chem.* **2011**, *11* (23), 2850–2878.

(47) Groll, M.; Huber, R. Inhibitors of the Eukaryotic 20S Proteasome Core Particle: A Structural Approach. *Biochim. Biophys. Acta - Mol. Cell Res.* **2004**, *1695* (1–3), 33–44.

(48) Subramani, R.; Aalbersberg, W. Marine Actinomycetes: An Ongoing Source of Novel Bioactive Metabolites. *Microbiol. Res.* **2012**, *167* (10), 571–580.

(49) Lam, K. S.; Lloyd, G. K.; Neuteboom, S. T. C.; Palladino, M. A.; Sethna, K. M.; Spear, M. A.; Potts, B. C. Chapter 12. From Natural Product to Clinical Trials: NPI-0052 (Salinosporamide A), a Marine Actinomycete-Derived Anticancer Agent, *Natural Product Chemistry for Drug Discovery* **2009**, 355–373.

(50) Potts, B. C.; Albitar, M. X.; Anderson, K. C.; Baritaki, S.; Berkers, C.; Bonavida, B.; Chandra, J.; Chauhan, D.; Cusack, J. C.; Fenical, W.; et al. Marizomib, a Proteasome Inhibitor for All Seasons: Preclinical Profile and a Framework for Clinical Trials. *Curr. Cancer Drug Targets* **2011**, *11* (3), 254–284.

(51) Miller, C. P.; Ban, K.; Dujka, M. E.; McConkey, D. J.; Munsell, M.; Palladino, M.; Chandra, J.; McConkey, D. J. NPI-0052, a Novel Proteasome Inhibitor, Induces Caspase-8 and ROS-Dependent Apoptosis Alone and in Combination with HDAC Inhibitors in Leukemia Cells. *Blood* **2007**, *110* (1), 267–277.

(52) Chauhan, D.; Catley, L.; Li, G.; Podar, K.; Hideshima, T.; Velankar, M.; Mitsiades, C.; Mitsiades, N.; Yasui, H.; Letai, A.; et al. A Novel Orally Active Proteasome Inhibitor Induces Apoptosis in Multiple Myeloma Cells with Mechanisms Distinct from Bortezomib. *Cancer Cell* **2005**, *8* (5), 407–419.

(53) Macherla, V. R.; Mitchell, S. S.; Manam, R. R.; Reed, K. A.; Chao, T. H.; Nicholson, B.; Deyanat-Yazdi, G.; Mai, B.; Jensen, P. R.; Fenical, W. F.; et al. Structure-Activity Relationship Studies of Salinosporamide A (NPI-0052), a Novel Marine Derived Proteasome Inhibitor. *J. Med. Chem.* **2005**, *48* (11), 3684–3687.

(54) Groll, M.; Huber, R.; Potts, B. C. M. Crystal Structures of Salinosporamide A (NPI-0052) and B (NPI-0047) in Complex with the 20S Proteasome Reveal Important Consequences of β-Lactone Ring Opening and a Mechanism for Irreversible Binding. *J. Am. Chem. Soc.* **2006**, *128* (15), 5136–5141.

(55) Hu, M.; Li, L.; Wu, H.; Su, Y.; Yang, P.-Y.; Uttamchandani, M.; Xu, Q.-H.; Yao, S. Q. Multicolor, One- and Two-Photon Imaging of Enzymatic Activities in Live Cells with Fluorescently Quenched Activity-Based Probes (QABPs). *J. Am. Chem. Soc.* **2011**, *133* (31), 12009–12020.

(56) Blum, G.; Mullins, S. R.; Keren, K.; Fonovič, M.; Jedeszko, C.; Rice, M. J.; Sloane, B. F.; Bogyo, M. Dynamic Imaging of Protease Activity with Fluorescently Quenched Activity-Based Probes. *Nat. Chem. Biol.* **2005**, *1* (4), 203–209.

(57) Leestemaker, Y.; Ovaa, H. Tools to Investigate the Ubiquitin Proteasome System. *Drug Discov. Today Technol.* **2017**, *26*, 25–31.

(58) Fonovic, M.; Bogyo, M. Activity Based Probes for Proteases: Applications to Biomarker Discovery,Molecular Imaging and Drug Screening. *Curr. Pharm. Des.* **2007**, *13* (3), 253–261.

(59) Lee, S.; Park, K.; Kim, K.; Choi, K.; Kwon, I. C. Activatable Imaging Probes

with Amplified Fluorescent Signals. *Chem. Commun.* **2008**, No. 36, 4250.

(60) van Rooden, E. J.; Kohsiek, M.; Kreekel, R.; van Esbroeck, A. C. M.; van den Nieuwendijk, A. M. C. H.; Janssen, A. P. A.; van den Berg, R. J. B. H. N.; Overkleeft, H. S.; van der Stelt, M. Design and Synthesis of Quenched Activity-Based Probes for Diacylglycerol Lipase and *α,β*-Hydrolase Domain Containing Protein 6. *Chem. - An Asian J.* **2018**, *13* (22), 3491–3500.

(61) Verdoes, M.; Edgington, L. E.; Scheeren, F. A.; Leyva, M.; Blum, G.; Weiskopf, K.; Bachmann, M. H.; Ellman, J. A.; Bogyo, M. A Nonpeptidic Cathepsin S Activity-Based Probe for Noninvasive Optical Imaging of Tumor-Associated Macrophages. *Chem. Biol.* **2012**, *19* (5), 619–628.

(62) Zhang, Q.; Liu, H.; Pan, Z. A General Approach for the Development of Fluorogenic Probes Suitable for No-Wash Imaging of Kinases in Live Cells. *Chem. Commun.* **2014**, *50* (97), 15319–15322.

(63) Serim, S.; Baer, P.; Verhelst, S. H. L. Mixed Alkyl Aryl Phosphonate Esters as Quenched Fluorescent Activity-Based Probes for Serine Proteases. *Org. Biomol. Chem.* **2015**, *13* (8), 2293–2299.

(64) Kolb, H. C.; Sharpless, K. B. The Growing Impact of Click Chemistry on Drug Discovery. *Drug Discov. Today* **2003**, *8* (24), 1128–1137.

(65) Hou, J.; Liu, X.; Shen, J.; Zhao, G.; Wang, P. G. The Impact of Click Chemistry in Medicinal Chemistry. *Expert Opin. Drug Discov.* **2012**, *7* (6), 489–501.

(66) Thirumurugan, P.; Matosiuk, D.; Jozwiak, K. Click Chemistry for Drug Development and Diverse Chemical–Biology Applications. *Chem. Rev.* **2013**, *113* (7), 4905–4979.

(67) Kolb, H. C.; Finn, M. G.; Sharpless, K. B. Click Chemistry: Diverse Chemical Function from a Few Good Reactions. *Angew. Chemie Int. Ed.* **2001**, *40* (11), 2004–2021.

(68) Rostovtsev, V. V.; Green, L. G.; Fokin, V. V.; Sharpless, K. B. A Stepwise Huisgen Cycloaddition Process: Copper(I)-Catalyzed Regioselective "Ligation" of Azides and Terminal Alkynes. *Angew. Chemie Int. Ed.* **2002**, *41* (14), 2596–2599.

(69) Meldal, M.; Tornøe, C. W. Cu-Catalyzed Azide−Alkyne Cycloaddition. *Chem. Rev.* **2008**, *108* (8), 2952–3015.

(70) Lee, P. H.; Kim, H.; Lee, K.; Kim, M.; Noh, K.; Kim, H.; Seomoon, D. The Indium-Mediated Selective Introduction of Allenyl and Propargyl Groups at the C4-Position of 2-Azetidinones and the AuCl3-Catalyzed Cyclization of 4-Allenyl-2-Azetidinones. *Angew. Chemie Int. Ed.* **2005**, *44* (12), 1840–1843.

(71) Deng, B. L.; Demillequand, M.; Laurent, M.; Touillaux, R.; Belmans, M.; Kemps, L.; Cérésiat, M.; Marchand-Brynaert, J. Preparation of (3S,4S)-1-Benzhydryl-3-[(5R)-1'-Hydroxyethyl]-4-Acyl-2- Azetidinones from (2R,3R)-Epoxybutyramide Precursors. *Tetrahedron* **2000**, *56* (20), 3209–3217.

(72) Shiozaki, M.; Ishida, N.; Maruyama, H. Short-Step Synthesis of a Chiral 3-(1-Hydroxyethyl)-4-Cyanoazetidin-2-One Derivative. *Agric. Biol. Chem.* **1986**, *50* (9), 2353–2356.

(73) Nagai, H.; Shiozawa, T.; Achiwa, K.; Terao, Y. Convenient Syntheses of Optically Active .BETA.-Lactams by Enzymatic Resolution. *Chem. Pharm. Bull. (Tokyo).* **1993**, *41* (11), 1933–1938.

(74) Jernigan, F. E.; Lawrence, D. S. A Broad Spectrum Dark Quencher: Construction of Multiple Colour Protease and Photolytic Sensors. *Chem. Commun. (Camb).* **2013**, *49* (60), 6728–6730.

(75) Ressurreição, A. S. Synthesis, Conformational Analysis and Biological Evaluation of Peptidomimetics Acting as *β*-Sheet Inducers, **2008**.

(76) Sunagawa, M.; Sasaki, A. CA 2432076, NOVEL ANTIBACTERIAL CARBAPENEM COMPOUNDS, **2003**.

USC
UNIVERSIDADE
DE SANTIAGO
DE COMPOSTELA

SUPPLEMENTARY INFORMATION

Chapter 3.1 Reprinted (adapted) with permission from (Ana Mallo-Abreu, María Majellaro, Willem Jespers, Jhonny Azuaje, Olga Caamaño, Xerardo García-Mera, José M. Brea, María I. Loza, Hugo Gutiérrez-de-Terán, and Eddy Sotelo *Journal of Medicinal Chemistry* **2019** *62* (20), 9315-9330) Copyright (2019) American Chemical Society. DOI: https://doi.org/10.1021/acs.jmedchem.9b01340 I. F.: 6,205. Print Edition ISSN: 0022-2623 Web Edition ISSN: 1520-4804.

Ana Mallo-Abreu,[1,2] María Majellaro,[1,2] Willem Jespers, [4] Jhonny Azuaje,[1,2] Olga Caamaño,[2] Xerardo García-Mera,[2] José M. Brea,[3] María I. Loza,[3] Hugo Gutiérrez-de-Terán[4*] and Eddy Sotelo[1,2]

[1]Centro Singular de Investigación en Química Biolóxica e Materiais Moleculares (CIQUS), [2]Departamento de Química Orgánica, Facultade de Farmacia. Universidade de Santiago de Compostela, 15782. Santiago de Compostela, Spain. [3]Centro Singular de Investigación en Medicina Molecular y Enfermedades Crónicas (CIMUS). Universidade de Santiago de Compostela, 15782. Santiago de Compostela, Spain. [4]Department of Cell and Molecular Biology, Uppsala University, Uppsala SE-75124.

Chapter 3.2 Reprinted (adapted) with permission from (Ana Mallo-Abreu, Rubén Prieto-Díaz, Willem Jespers, Jhonny Azuaje, Maria Majellaro, Carmen Velando, Xerardo García-Mera, Olga Caamaño, José Brea, María I. Loza, Hugo Gutiérrez-de-Terán, and Eddy Sotelo *Journal of Medicinal Chemistry*, **2020**, *63* (14), 7721-7739) Copyright (2020) American Chemical Society. DOI: https://doi.org/10.1021/acs.jmedchem.0c00564 I. F.: 7,446. Print Edition ISSN: 0022-2623 Web Edition ISSN: 1520-4804.

Ana Mallo-Abreu,[1,2] Rubén Prieto-Díaz,[1,2] Willem Jespers,[3] Jhonny Azuaje,[1,2] Maria Majellaro,[1,2] Carmen Velando,[1] Xerardo García-Mera,[2] Olga Caamaño,[2] José Brea,[4*] María I. Loza,[4] Hugo Gutiérrez-de-Terán[3] and Eddy Sotelo[1,2]

[1]Centro Singular de Investigación en Química Biolóxica y Materiais Moleculares (CIQUS), [2]Departamento de Química Orgánica, Facultade de Farmacia, Universidade de Santiago de Compostela, 15782 Santiago de Compostela, Spain. [3]Department of Cell and Molecular Biology, Uppsala University, Uppsala SE-75124. [4]Centro Singular de Investigación en Medicina Molecular y Enfermedades Crónicas (CIMUS), Universidade de Santiago de Compostela, 15782 Santiago de Compostela, Spain.

Chapter 3.3 Reprinted (adapted) with permission from (Ana Mallo-Abreu, Irene Reyes-Resina, Jhonny Azuaje, Rafael Franco, Aitor García-Rey, Maria Majellaro, Darío Miranda-Pastoriza, Xerardo García-Mera, Willem Jespers, Hugo Gutiérrez-de-Terán, Gemma Navarro, and Eddy Sotelo *Journal of Medicinal Chemistry* **2021** *64* (12), 8710-8726) Copyright (2021) American Chemical Society. DOI: https://doi.org/10.1021/acs.jmedchem.1c00704 I. F.: 7,446. Print Edition ISSN: 0022-2623 Web Edition ISSN: 1520-4804.

Ana Mallo-Abreu,[1,2] Irene Reyes-Resina,[3,5] Jhonny Azuaje,[1,2] Rafael Franco,[4,5] Aitor García-Rey,[1,2] Maria Majellaro,[1,2] Darío Miranda-Pastoriza,[1,2] Xerardo García-Mera,[2] Willem Jespers,[6] Hugo Gutiérrez-de-Terán,[6] Gemma Navarro,[3,4*] and Eddy Sotelo[1,2]

[1]Centro Singular de Investigación en Química Biolóxica e Materiais Moleculares (CIQUS) and [2]Departamento de Química Orgánica, Facultade de Farmacia, Universidade de Santiago de Compostela, 15782 Santiago de Compostela, Spain. [3]Department of Biochemistry and Physiology, Faculty of Pharmacy and Food Science, [4]Faculty of Chemistry, University of Barcelona, 08028 Barcelona, Spain. [5]Centro de Investigación Biomédica en Red Enfermedades Neurodegenerativas (CIBERNED), 28031 Madrid, Spain. [6]Department of Cell and Molecular Biology, Uppsala University, Uppsala SE-75124.

The doctoral candidate declares no conflicts of interest related to her thesis.